Vol. 192 No. 2, January 31, 1987
Completing Vol. 192

ISSN 0003-2670

ANALYTICA CHIMICA ACTA

International journal devoted to all branches of analytical chemistry

ELSEVIER

ANALYTICA CHIMICA ACTA

International journal devoted to all branches of analytical chemistry
Revue internationale consacrée à tous les domaines de la chimie analytique
Internationale Zeitschrift für alle Gebiete der analytischen Chemie

PUBLICATION SCHEDULE FOR 1987

	J	F	M	A	M	J	J	A	S	O	N	D
Analytica Chimica Acta	192	193	194	195	196	197	198	199	200	201	202	203

Scope. *Analytica Chimica Acta* publishes original papers, short communications, and reviews dealing with every aspect of modern chemical analysis both fundamental and applied.

Submission of Papers. Manuscripts (three copies) should be submitted as designated below for rapid and efficient handling:

Papers from the Americas to: Professor Harry L. Pardue, Department of Chemistry, Purdue University, West Lafayette, IN 47907, U.S.A.

Papers from all other countries to: Dr. A. M. G. Macdonald, Department of Chemistry, The University, P.O. Box 363, Birmingham B15 2TT, England. Papers dealing particularly with computer techniques to: Professor J. T. Clerc, Universität Bern, Pharmazeutisches Institut, Baltzerstrasse 5, CH-3012 Bern, Switzerland.

Submission of an article is understood to imply that the article is original and unpublished and is not being considered for publication elsewhere. Upon acceptance of an article by the journal, authors will be asked to transfer the copyright of the article to the publisher. This transfer will ensure the widest possible dissemination of information.

Information for Authors. Papers in English, French and German are published. There are no page charges. Manuscripts should conform in layout and style to the papers published in this Volume. Authors should consult Vol. 190 for detailed information. Reprints of this information are available from the Editors or from: Elsevier Editorial Services Ltd., Mayfield House, 256 Banbury Road, Oxford OX2 7DH (Great Britain).

Reprints. Fifty reprints will be supplied free of charge. Additional reprints (minimum 100) can be ordered. An order form containing price quotations will be sent to the authors together with the proofs of their article.

Advertisements. Advertisement rates are available from the publisher.

Subscriptions. Subscriptions should be sent to: Elsevier Science Publishers B.V., Journals Department, P.O. Box 211, 1000 AE Amsterdam, The Netherlands. Tel: 5803 911, Telex: 18582.

Publication. *Analytica Chimica Acta* appears in 12 volumes in 1987. The subscription for 1987 (Vols. 192–203) is Dfl. 2700.00 plus Dfl. 300.00 (p.p.h.) (total approx. US $1333.30). All earlier volumes (Vols. 1–191) except Vols. 23 and 28 are available at Dfl. 231.00 (US $102.70), plus Dfl. 17.00 (US $7.60) p.p.h., per volume.

Our p.p.h. (postage, packing and handling) charge includes surface delivery of all issues, except to subscribers in the U.S.A., Canada, Japan, Australia, New Zealand, P.R. China, India, Israel, South Africa, Malaysia, Thailand, Singapore, South Korea, Taiwan, Pakistan, Hong Kong, Brazil, Argentina and Mexico, who receive all issues by air delivery (S.A.L. — Surface Air Lifted) at no extra cost. For the rest of the world, airmail and S.A.L. charges are available upon request.

Claims for issues not received should be made within three months of publication of the issues. If not they cannot be honoured free of charge.

For further information, or a free sample copy of this or any other Elsevier Science Publishers journal, readers in the U.S.A. and Canada can contact the following address: Elsevier Science Publishing Co. Inc., Journal Information Center, 52 Vanderbilt Avenue, New York, NY 10017, U.S.A., Tel: (212) 916-1250.

0003-2670/87/$03.50

Printed in The Netherlands

Analytica Chimica Acta, 192 (1987) 133—143
Elsevier Science Publishers B.V., Amsterdam — Printed in The Netherlands

SELECTIVE DETERMINATION OF IRON BY FLUORESCENCE QUENCHING OF A NATURALLY OCCURRING PIGMENT

RONALD A. ASKELAND[a] and R. K. SKOGERBOE*

Department of Chemistry, Colorado State University, Fort Collins, Colorado 80523 (U.S.A.)

(Received 21st April 1986)

SUMMARY

A fluorescent pigment produced by *Pseudomonas fluorescens* is isolated and partially characterized. It is verified that the pigment reacts with iron(III) and iron(II) with respective conditional formation constants of 1.1×10^{26} and 5.3×10^{23} at pH 8 and that the reaction results in quenching of the pigment fluorescence. The quenching effect permits the measurement of iron with a detection limit of 5×10^{-9} M (0.3 $\mu g\ l^{-1}$). Examination of 21 common constituents in water as potential interferents for the iron measurement indicates that a combination buffer solution can be used to mask those that deleteriously affect the measurement. The general accuracy of the procedure is confirmed with reference water samples.

Many micro-organisms produce compounds that bind iron and function as transport agents for it. These compounds, called siderophores, are of two general types; the phenolates are typically amino acid conjugates of 2,3-dihydroxybenzoic acid while the others contain hydroxamate groups (R—CO—NOH—R). Both classes are weak acids and bind iron through the oxygen atoms [1].

The *Pseudomonas* species is well known for production of hydroxamate siderophores which occur as fluorescent pigments [2]. *Pseudomonas* (*P.*) *fluorescens* produces hydroxamate pigments in a biosynthetic process that is enhanced by the incubation temperature and suppressed by increasing iron in the growth medium [2, 3]. Indeed, siderophore production is typically suppressed by increasing iron which apparently represses one or more enzymes involved in the biosynthetic process [1]. Meyer and Abdallah [4] reported that *P. fluorescens* produces a water-soluble fluorescent pigment when grown in iron-deficient media. Only one form of the pigment was produced having a molecular weight of 1500 ± 75. The pigment was alkaline labile, formed a stable 1:1 Fe(III) complex with a stability constant approximating 10^{32}. The iron-free pigment was yellow-green in color and

---

[a]Present address: Hewlett-Packard, San Diego Division, 16399 West Bernardo Drive, San Diego, CA 92127, U.S.A.

0003-2670/87/$03.50

highly fluorescent while the iron complex was red-brown and its formation caused static fluorescence quenching [4].

The intense fluorescence observed for the *P. fluorescens* pigment, the high value of the stability constant for the iron complex, and the ready suppression of fluorescence by iron collectively suggested that this siderophore might be used as an uncommonly effective reagent for the determination of iron. The results of an investigation of this possibility show that iron can be selectively determined by the fluorescence quenching induced when it interacts with the pigment.

EXPERIMENTAL

Instrumentation and reagents

The fluorescence spectrometer (Perkin-Elmer, Model MPF-44B) used was interfaced to a desk-top computer (Hewlett-Packard, Model 9825A) and an X-Y plotter (Houston Instruments, Model 2000). The interface used a 12-bit A/D converter (Datel Systems, Model MDAS-16), a 16-bit parallel duplex interface (Hewlett-Packard, Model 980-32A) and two 12-bit D/A converters (Burr-Brown, Model DAC 80-CBI-V).

Fluorescence excitation spectra were obtained by using excitation and emission spectral bandpasses of 1 and 15 nm, respectively, while emission spectra were obtained with respective bandpasses of 5 and 1 nm. Fixed-wavelength measurements relied on excitation at 405 nm with a 3-nm bandpass and an emission wavelength of 455 nm with a 10-nm bandpass. All spectra were corrected by conventional techniques [5].

All reagents were prepared from materials of analytical-reagent grade or higher purity. The phosphate and histidine buffers (Micro Essential Laboratory, Brooklyn, NY) were treated with a chelating resin to remove trace amounts of iron prior to use. A 5-g quantity of Chelex-100 (Bio-Rad Laboratories, Richmond, CA) was added to a 1-l volume of buffer which was magnetically stirred for at least 4 h and decanted to remove the resin.

Pigment preparation

Cultures of *Pseudomonas fluorescens*, strain 13525, (American Type Culture Collection, Rockville, MD) were inoculated in 1-l volumes of trypticase soy broth (TSB; Benton-Dickenson and Co., Cockeysville, MD). These were incubated in 4-l Erlenmeyer flasks at 20°C for 48 h with magnetic stirring and an additional 96 h without stirring. Five such cultures were pooled and centrifuged at 14,000*g* for 20 min; the supernatant liquid was drawn off, concentrated to 250 ml under reduced pressure at 35° C, saturated with sodium chloride and centrifuged again at 14,000*g* for 20 min. The supernatant liquid was then extracted with 125 ml of 1:1 (v/w) chloroform/phenol; the chloroform layer was treated with 250 ml of diethyl ether and 25 ml of distilled water and the water layer was extracted three times with 100-ml volumes of diethyl ether. After these clean-up steps [4], the aqueous

extract was applied to a CM-25 Sephadex (Pharmacia Fine Chemicals, Uppsala, Sweden) column (2.5 × 125 cm) and eluted with pH 6.5 phosphate buffer (0.02 M) at 3 ml min^{-1}. Fluorescence measurements indicated that two fluorescent fractions representative of the pigment were obtained but the second fraction was selected as the pigment (see below). This fraction was concentrated under reduced pressure to 30 ml, applied to a 2.5 × 125-cm column of G-25 Sephadex, and eluted with distilled water at 3 ml min^{-1}. Fluorescence monitoring was used to collect the purified pigment fraction which was subsequently stored at 4°C.

Pigment characterization

The iron-equivalent concentration per liter of the pigment fraction (IE/L) was measured by titration with iron using fluorescence quenching as the monitor. Aliquots (25 μl) of the pigment fraction were added to 2.0 ml of pH 7 phosphate buffer (0.05 M) and these solutions were titrated by stepwise addition of 25-μl volumes of a 1.0×10^{-4} M iron standard. The amount of iron required to reduce the fluorescence to zero was taken as the iron equivalent concentration.

Absorption spectra of the iron-free pigment were obtained by adding 25 μl of the pigment stock to 2.5 ml of 0.05 M phosphate buffer adjusted to the required pH. The absorption spectrum of the FeP complex was obtained by adding sufficient iron to the above solutions to reduce the fluorescence intensity by half. The same solutions diluted 10-fold were used to obtain the fluorescence spectra.

Reverse-phase, high-pressure liquid chromatographic (h.p.l.c.) examination of the pigment stock was done using absorbance detection at 254 nm and fluorescence detection with excitation at 340 nm and emission at 425 nm; these conditions were imposed by the limitations of the h.p.l.c. instrument available. A 20-μl aliquot of the fraction was applied to a C-18 bonded phase silica column (Partisil P × 5 5/25, Whatman, Inc., Clifton, NJ) and eluted with 15% methanol—85% water at 1 ml min^{-1}.

General procedure

A pigment concentration of 2.5×10^{-7} iron equivalent per liter was added to the pH 8 combination buffer (see below). Sample aliquots, 200 μl, were added to 2.0 ml of this solution and the fluorescence was monitored to assure the attainment of temporal equilibrium prior to measurement under the conditions stipulated above. Typically, this was attained in a few minutes.

RESULTS AND DISCUSSION

Characterization of the pigment

Initial studies focused on isolation and characterization of the pigment. Five cultures of *P. fluorescens* were pooled, concentrated, and extracted as

described above. The chromatographic separation followed that of Meyer and Abdallah [4] except that the pigment was not saturated with iron(III). The separation process produced two fluorescent peaks as observed earlier [4]; the second exhibited the higher fluorescence intensity and the greater sensitivity to fluorescence quenching by iron. It was concluded that the first peak was due to pigment fragmentation products while the second was due to the intact pigment [4]. Titration of an aliquot of the intact pigment fraction with iron(III) while monitoring its fluorescence indicated a pigment concentration of 5.0×10^{-4} iron equivalents per liter of pigment solution (IE l^{-1}).

Measurement of the absorption spectra of the iron-free pigment at pH values of 5—8 indicated partially resolved double maxima (365 and 378 nm) at pH 5 which became single maxima at 380, 398, and 400 nm for pH 6, 7 and 8, respectively. Addition of a half-equivalent amount of Fe(III) at pH 7 resulted in a reduction in the absorbance at 398 nm and the appearance of a broader absorption band at 450—470 nm; the color change was yellow to red-brown [4].

The effects of pH on the fluorescence excitation and emission spectra are shown in Fig. 1. The spectra show that pH shifts do not cause significant shifts in the positions of the band maxima. Fluorescent intensity as a function of pigment concentration was also measured at each pH shown in Fig. 1. Linear relationships were obtained for pigment concentrations up to 1.5×10^{-6} IE l^{-1}; the slopes decreased thereafter.

With the fluorescence characteristics in hand, the purity of the pigment fraction was examined via the h.p.l.c. procedure described above. The data presented in Fig. 2 show six or seven distinct components exhibiting absorbance at 254 nm while only one of those components, i.e., the pigment, exhibited fluorescence at the excitation/emission wavelengths monitored. Although this illustrated that several unknown impurities were present in the pigment fraction, it was shown that they do not absorb or fluoresce at measurable levels in the 300—600-nm region and should therefore not interfere with pigment fluorescence measurements.

The fluorescent intensity was used to examine the acid—base characteristics of the pigment fraction. The data shown in Fig. 3 imply that fluorescence is associated with the loss of a proton ($pK \approx 6.1$) and that subsequent loss of a second proton ($pK \approx 10.6$) produces a nonfluorescent entity. Alternatively, the pigment undergoes alkaline degradation at the higher pH levels resulting in fluorescence reduction. Of primary significance is the apparent stability of the siderophore at pH levels up to 9 and the occurrence of fluorescence in the pH range most typical of aquatic samples.

Fluorescence quenching by iron

Quenching of fluorescence by iron(III) was investigated at four pH levels (Fig. 4). At pH 5, the addition of iron had virtually no effect. As the pH increased and the degree of dissociation of the pigment increased (Fig. 3),

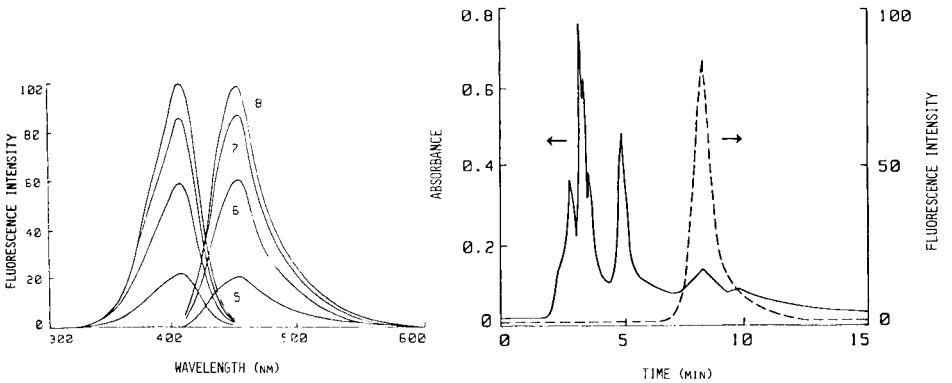

Fig. 1. Corrected fluorescence excitation (left) and emission (right) spectra of the iron-free pigment at pH values of 5—8.

Fig. 2. Reverse-phase h.p.l.c. data for the fluorescent pigment fraction: (——) ultraviolet absorption detection; (- - - -) fluorescence detection.

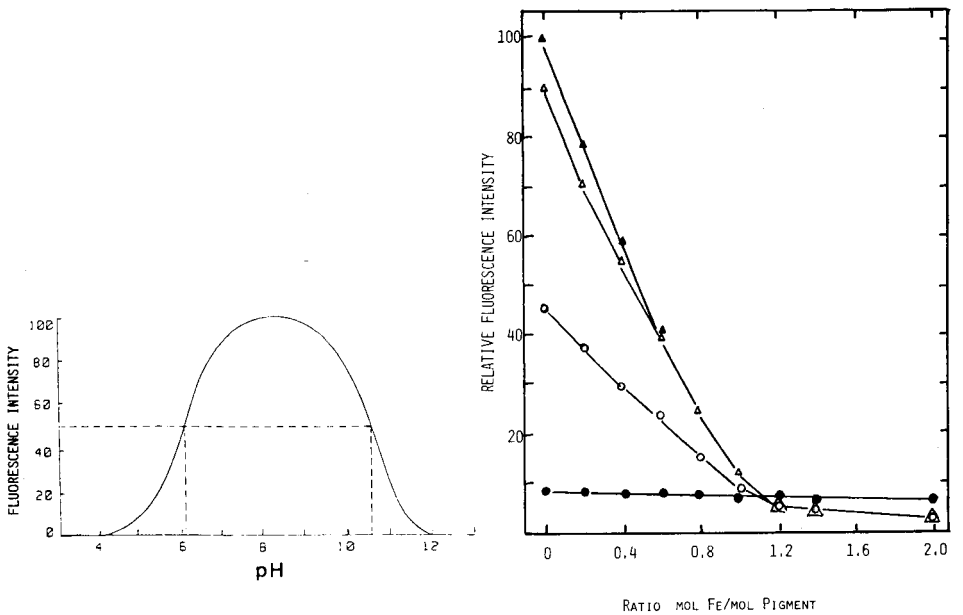

Fig. 3. Estimation of the acid dissociation characteristics of the pigment by fluorescence measurements.

Fig. 4. Curves for the estimation of iron by fluorescence quenching at pH values of 5—8: (●) 5, (○) 6, (△) 7, (▲) 8.

the fluorescence quenching observed was affected by the iron concentration. The curves shown in Fig. 4 are generally representative of the Stern-Volmer type of relationship expected for static quenching. Analogous results were obtained when iron(II) was introduced. These data confirmed the general potential of the pigment for determining Fe(II) and Fe(III) and indicated that fluorescence intensity measurements could be used to estimate conditional formation constants for the iron complexes.

Estimates of the conditional formation constants for the Fe(III) pigment (FeP) complex were based on the use of EDTA as a competitive chelator for iron(III) [6, 7]. The competitive reaction is

$$\text{FeEDTA} + \text{P} \rightleftharpoons \text{FeP} + \text{EDTA} \quad (1)$$

and the overall equilibrium constant is $K = [\text{FeP}][\text{EDTA}]/[\text{P}][\text{FeEDTA}]$, where brackets denote concentrations. Because the conditional formation constants for FeEDTA are known [7], measurement of these concentration terms allows estimation of the conditional formation constants for the present pigment complexes. In the competitive experiments, the total concentrations of pigment, iron(III), and EDTA in each solution were known; fluorescent intensity was used to estimate the iron-free pigment concentration. Other concentrations were estimated from

$$[\text{FeP}] = [\text{P}]_{\text{total}} - [\text{P}] \quad (2)$$

$$[\text{FeEDTA}] = [\text{Fe}]_{\text{total}} - [\text{FeP}] \quad (3)$$

$$[\text{EDTA}] = [\text{EDTA}]_{\text{total}} - [\text{FeEDTA}] \quad (4)$$

The concentrations of Fe^{3+} and hydrolyzed iron species were ignored in Eqn. 3 because they were negligible compared to the other species. To ensure that equilibrium was attained in the estimation of K, experiments were run in which iron-free pigment was added to an FeEDTA solution and in which EDTA was added to an FeP solution. In approaching the equilibrium from both directions, it was noted that the fluorescent intensity was the same (±5%) in each case and two determinations per reaction pH were obtained. All fluorescence measurements were recorded after the intensity had stabilized (>48 h), indicating that equilibrium had been reached.

The results of the conditional formation constant measurements are summarized in Table 1 where they are compared with those for FeEDTA for information purposes. The FeP estimates shown are expressed in terms of the iron equivalent concentration of pigment rather than through the use of a molecular weight estimate for the pigment. Nevertheless, it is clear that the pigment can preferentially complex iron even in the presence of EDTA. Additional measurements at pH 8 with iron(II) using 1,10-phenanthroline [8] as the competitive chelator provided a conditional constant of 5.3×10^{23} for the Fe(II)P complex. Hence the reaction of the pigment with iron(III) is favored over that for iron(II) by more than two orders of magnitude.

TABLE 1

Comparison of Fe(III)P conditional formation constants with those for FeEDTA

pH	Conditional formation constants	
	FeEDTA [7]	FeP[a]
5	4.41×10^{18}	3.3×10^{13}
6	2.77×10^{20}	4.0×10^{18}
7	6.04×10^{21}	8.7×10^{22}
8	6.80×10^{22}	1.1×10^{26}

[a]Degree of ionization of P estimated from Fig. 3. See text for units.

Determination of iron

In view of the favorable nature of the above results, a fluorescence-quenching procedure for determinations of iron was developed. A pigment concentration of 2.5×10^{-7} IE l^{-1} was selected as within the linear fluorescence response range while offering a fluorescence signal near its intensity plateau for the present system. Iron was added in varying amounts to this concentration of pigment in pH 8 combination buffer; the fluorescence-quenching response changed systematically (Fig. 4) up to the pigment concentration of 2×10^{-7} M but this could be extended by increasing this concentration. The detection limit, defined as 3 times the standard deviation of the blank ($3\ s_b$), was 5×10^{-9} M (0.3 μg l^{-1}) while the determination limit ($10 s_b$) was 1.5×10^{-8} M (0.8 μg l^{-1}). Such capabilities are competitive with those available with electrothermal-atomization atomic absorption spectrometry [9].

Twelve cations and nine anions common to water samples were evaluated as potential interferences for the present procedure (see Table 2). These were selected on the basis of the report by Kopp and Kroner [10] which indicated typical concentration ranges of common impurities in U.S. rivers and lakes. The pigment concentration used was 2×10^{-7} IE l^{-1} while the iron concentration used was 1×10^{-7} M and the concomitants were added at concentrations that were typically 10—100-fold above this. Because components of buffer solutions used to regulate pH could interact with some of the concomitants and affect the interference effects, the studies were initially done with both histidine (pH 8) and phosphate (pH 7) buffers.

Two types of interference effects were evident from the data summarized in Table 2. Only aluminum(III) produced a negative effect; it was apparently bound by the pigment in preference to iron and did not quench fluorescence. In other cases, the concomitants appeared to interact with the pigment to increase the degree of quenching. Such interferences observed for Co(II), Cu(II), Ni(II), and Zn(II) in the phosphate buffer were absent in the histidine buffer. Because the formation constants for the complexation of these cations by histidine are in excess of 10^{12} [8], it appears that this buffer at the concentration used served as a masking agent by binding these

TABLE 2

Summary of interference studies

Ion added	Molar ratio: Ion/Fe(III)	Error (%) in indicated buffer[b]		
		0.01 M Histidine	0.02 M Phosphate	Combination
Al^{3+}	100	−137	−134	*
Co^{2+}	100	*	+35	*
Cr^{3+}	100	*	*	−19
	10	*	*	*
Cu^{2+}	100	*	+82	*
Mn^{2+}	100	+42	+20	+17
	10	—	—	+8
	1	—	—	*
Ni^{2+}	100	*	+42	*
Pb^{2+}	100	+52	*	*
Zn^{2+}	100	*	+13	*

[a]In addition to the elements listed, AsO_4^{3-}, BO_3^{3-}, Cd^{2+}, Cl^-, ClO_4^-, CN^-, $Cr_2O_7^{2-}$, K^+, Mg^{2+}, Na^+, NO_3^-, SeO_4^{2+} and SO_4^{2+} were tested at 100:1 molar ratios without measurable effects in any of the buffer media.

[b](*) Not significant; (—) not tested.

cations to prevent their reaction with the pigment. The formation constant for the lead/histidine complex was inadequate for this, while that for the lead/phosphate complex [8] was such that phosphate functioned as an effective masking agent for Pb(II). Neither buffer provided adequate masking for manganese(II).

In view of these observations, a combination buffer for pH 8 was developed; this contained a higher concentration of histidine (0.06 M) to mask Co, Cu, Ni and Zn, phosphate (0.02 M) to mask lead, and 0.4 M sodium fluoride to mask Al(III) through the formation of AlF_6^{3-} ($K = 5 \times 10^{19}$ [8]). The data obtained for this buffer (Table 2) show that only Cr(III) and Mn(II) interfered with the iron determination. Because these ions are typically found at levels below that of iron in water samples, rather than at the levels used in the present tests [10], the significance of their effects is expected to be negligible for most samples.

To test the general accuracy of this method, three reference water samples provided by the U.S. Environmental Protection Agency (EPA) and which covered a wide-compositional range were examined using the combination buffer. The results obtained by the present method (Table 3) agree with the expected concentrations within the precision limits of the triplicate measurements, indicating that accurate measurements can be expected for many types of water samples.

Although quenching measurements typically indicated the attainment of equilibrium in a few minutes, the EDTA competition experiments used to estimate formation constants indicated that nominally a 48-h period was

TABLE 3

Results for iron in EPA samples

Sample number	Fe concentration (mg l^{-1})	
	EPA	Present method[a]
I	18	16.9 (6.0)
II	402	417 (3.1)
III	769	793 (2.7)

[a]Values given are averages and relative standard deviations for 3 replicate measurements.

required to achieve equilibrium. Because other iron complexing agents, e.g., humic materials, may be present in samples and cause kinetically and/or thermodynamically limited interferences in the iron determination, experiments were done to delineate such possibilities. Four complexing agents covering a range of conditional formation constants were chosen as models for comparative evaluation; i.e., citrate, ethylenediaminetetraacetic acid (EDTA), cyclohexane-1,2-diaminotetraacetic acid (CDTA), and hydroxyethylethylenediaminetriacetic acid (HEEDTA). Fluorescence quenching kinetics were examined at pH 8 by adding iron complexes that had 1:1 molar ratio of Fe(III)/complexing agent to an iron-free pigment solution. The final concentrations of the pigment and Fe(III) were 2×10^{-7} and 1×10^{-7} M, respectively; in the absence of other complexing agents this would result in nominally 50% quenching. The results shown in Fig. 5 indicate that the quenching reaction attains completion in 10 min or less when the only iron complexing reactions competing with the pigment were hydroxy species. However, as the conditional formation constants of the competing complexes approached that of the pigment complex, the rate of ligand exchange decreased with a concomitant reduction in the rate of fluorescence quenching. The results summarized in Table 4 indicate that total iron can be measured provided that the formation constants of the competing ligands are less than that for the pigment complex and that adequate time is allowed for equilibration. This would be the case for iron/humic matter complexes [8]. The data also show that fluorescence quenching measurements made after 1- and 48-h periods could be used to obtain reasonable estimates of operationally defined classes of iron, e.g., the amount reacting in 1 h might be considered readily available while the amount reacting in the 1—48-h interval could be classed as moderately available. The difference between the total iron measured by another technique (e.g., atomic absorption) and the amount in the above classes could be further defined as unavailable. To explore the possible use of this type of kinetic differentiation on a preliminary basis, the following experiments were performed.

Iron solutions of EDTA/citrate, CDTA/citrate, and EDTA/CDTA were

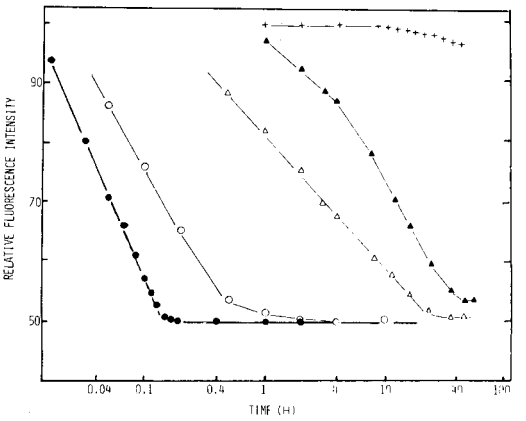

Fig. 5. Effects of ligand competition on the rate of fluorescence quenching: (●) pigment alone; (○) citrate; (△) HEEDTA; (▲) EDTA; (+) CDTA.

prepared so that the distribution of iron would be 50/50 for each of the ligands present. Fluorescence measurements were made at 1 and 48 h to estimate the readily and moderately available classes while the unavailable iron was calculated from mass balance. The results summarized in Table 5 indicate that the measurements were generally accurate within experimental error and imply that kinetic differentiation between stability classes of iron complexes is possible.

Conclusions

The present results have shown that a fluorescent siderophore pigment produced by *Pseudomonas fluorescens* can be conveniently isolated and used for iron determination by fluorescence quenching. Because the pigment has affinity for other cations, the use of a buffer medium containing constit-

TABLE 4

Effects of ligand competition on fluorescence quenching

Complexing agent	Conditional formation constant	Time to completion[a] (h)
Pigment[b]	1.1×10^{26}	0.15
Citrate	1.0×10^{15} [c]	1.0
HEEDTA	9.6×10^{17} [c]	24–30
EDTA	6.8×10^{22} [c]	40–48
CDTA	4.9×10^{25} [c]	>48

[a]Time required for quenching to reach 97–98% of equilibrium value. [b]At pH 8, the iron hydroxy species expected to be prominent is $Fe(OH)_2^+$ with a formation constant of ca. 10^{11} [7]. [c]Conditional values for pH 8 from ref. 7.

TABLE 5

Estimation of iron availability[a] by fluorescence quenching

Iron complexes	Expected availability (%)			Measured availability (%)		
	Readily	Moderately	Unavailable	Readily	Moderately	Unavailable
EDTA/Citrate	50	50	0	51	47	2
CDTA/Citrate	50	0	50	54	<2	46
EDTA/CDTA	0	50	50	2	53	45

[a]See definitions of availability in text.

uents that selectively mask those entities by complexation is required to achieve interference-free measurements of iron. The sensitivity of the present procedure is such that measurements of iron are possible at low concentration levels that often dictate measurements by electrothermal atomic absorption spectrometry [9]. The procedure may consequently find use as an independent method for determining iron when high sensitivity is required; it may also find use for differentiating between iron complexes of varying stability.

It is generally well known that many biological entities have developed reasonably selective chemical mechanisms for acquiring those elements or compounds essential to their survival. The iron-selective fluorescent pigment used herein is only one of what may be thousands of such naturally-produced selective chemical reagents. One cannot help suggesting that nature may hold the key to the nirvana described by Lundell [11], i.e., a shelf of reagents, one for each element and each specific for that element.

REFERENCES

1 J. B. Neilands, in G. L. Eichhorn (Ed.), Inorganic Biochemistry, Elsevier, New York, 1973, Chap. 5.
2 J. A. Garibaldi, J. Bacteriol., 105 (1971) 1036.
3 B. Maurer, A. Muller, W. Keller-Schierlein and H. Zahner, Arch. Mikrobiol., 60 (1968) 326.
4 J. M. Meyer and M. A. Abdallah, J. Gen. Microbiol., 107 (1978) 319.
5 R. F. Chen, Anal. Biochem., 20 (1967) 339.
6 F. J. C. Rossotti and H. Rossotti, The Determination of Stability Constants, McGraw-Hill, New York, 1961.
7 D. A. Skoog and D. M. West, Fundamentals of Analytical Chemistry, Holt, Rinehart and Winston, New York, 1976.
8 L. G. Sillén and A. E. Martell, Stability Constants of Metal-Ion Complexes, The Chemical Society, London, 1964.
9 C. W. Fuller, Electrothermal Atomization for Atomic Absorption Spectrometry, The Chemical Society, London, 1977.
10 J. F. Kopp and R. C. Kroner, Trace Metals in Waters of the United States, Federal Water Pollution Control Admin., Cincinnati, OH, 1967.
11 G. E. F. Lundell, Indust. Engin. Chem., Anal. Ed., 5 (1933) 221.

Analytica Chimica Acta, 192 (1987) 145—153
Elsevier Science Publishers B.V., Amsterdam — Printed in The Netherlands

TIME-RESOLVED FLUORESCENCE WITH AN OPTICAL-FIBER PROBE

G. H. VICKERS, R. M. MILLER[a] and G. M. HIEFTJE*
Department of Chemistry, Indiana University, Bloomington, IN 47405 (U.S.A.)
(Received 19th June 1986)

SUMMARY

Time-resolved fluorescence measurements are made with an optical-fiber probe approximately 16 m long. Fluorescence lifetimes for 1.00 μM solutions of rhodamine-B and rose bengal in ethanol were found to be 2.78 ± 0.04 ns and 0.77 ± 0.07 ns, respectively, similar in accuracy and precision to values obtained with conventional techniques. Calculations are used to investigate the limitations in remote determinations caused by temporal broadening. Results indicate that fiber lengths approaching 1 km can be used without significant loss in accuracy or precision.

Time-resolved fluorescence has found wide application in the study of excited-state lifetimes of both atoms and molecules. The information provided by time resolution can be used to characterize spectroscopic states, energy-transfer processes, molecular structure, and dynamics in fields as diverse as solid-state physics and molecular biology [1]. Time resolution can be used also in quantitative methods if the steady-state fluorescence intensity is not sufficient to allow unambiguous characterization of the sample. For example, the individual contributions from fluorophores with strongly overlapping fluorescence spectra, but different lifetimes, can often be determined by using the measured fluorescence decay curve [2, 3], or by simultaneously monitoring the fluorescence with respect to time and wavelength [4]. Time resolution can assist also in the correction of errors in fluorescence intensity caused by scattered light [5] or the presence of quenching agents [6].

Most time-resolved fluorescence measurements are done on samples which can be conveniently handled in the laboratory, and numerous instruments and methods have been devised for the study of such samples [1, 7]. However, there are occasions when it is either desirable or essential that the sample remains remote from the measurement instrumentation. For example, the sample itself might be too hazardous to be allowed into a normal spectroscopic laboratory, or may be part of a continuous sample stream in an environment which is inimical to delicate optical and electronic instrumentation. It might be necessary to make in-situ measurements in locations with

[a]Present address: Unilever Research, Port Sunlight Laboratory, Wirral, Merseyside, L63 3JW, Great Britain.

0003-2670/87/$03.50

restricted access, or where a number of sample sites must be examined in succession. Any of these requirements would make the use of conventional optical instrumentation difficult if not impossible. In an attempt to provide a solution to such problems, the use of optical fibers to transmit light between the optical instrumentation and the sample has been studied.

Optical fibers have many desirable properties for the remote measurement of fluorescence lifetimes. They are physically small and flexible, and can therefore be introduced into tight spaces where access is difficult. Once light has been focussed into the fiber, propagation losses are small and the sample can be a considerable distance from the light source and detection system without substantial reduction in sensitivity. Also, because the volume that is sampled will depend on the entry and exit geometries of the fiber and the optical characteristics of the sample, there is no need for a cell or cuvette at the sampling end of the fiber probe. These properties have already attracted the attention of other workers in the chemical-sensing field, and optical fibers have been used for a variety of remote spectroscopic measurements. Examples include reflectance [8], absorbance [9], Raman scattering [10], and steady-state fluorescence [11].

A drawback of optical fibers which is unique to the application of time-dependent measurements is the phenomenon of temporal broadening. There are basically two mechanisms for temporal broadening in optical fibers, the first being from the infinite number of paths by which light can be transmitted. Each of these paths has an optical pathlength associated with it, so that a bundle of light traverses a range of distances and produces a range of transit times. The effect of this distribution of transit times is to cause temporal broadening of initially short optical pulses. The problem becomes more severe as the length of the fibers and the effective numerical aperture increase. In the application of fibers to time-resolved fluorescence, broadening from this mechanism will decrease the temporal resolution of the instrument.

The second mechanism for temporal broadening in optical fibers occurs because the refractive index of the fiber core material is a function of wavelength. Therefore, the transit time (dispersion) through the fiber is related also to wavelength. As with the first mechanism, broadening becomes more severe as the fiber length increases, but also as the spectral bandwidth is increased. This phenomenon has been used in a time-of-flight optical spectrometer [12].

One might assume that use of a laser source would eliminate the influence of spectral dispersion because the light is essentially monochromatic. However, molecular fluorescence spectra are broad; if a significant region of the fluorescence spectrum is collected, the measured fluorescence decay curve will be temporally broadened. Consequently, dispersive broadening has a greater effect on a fluorescence signal than on scattered laser light. As the length of an optical fiber increases, it then becomes necessary to reduce the detected spectral bandwidth and sacrifice sensitivity so that erroneously high values are not obtained for the fluorescence lifetimes.

In this paper, the first time-resolved fluorescence investigation with sub-nanosecond resolution using an optical-fiber probe is reported. The instrument has been theoretically modelled to establish the dependence of its performance on experimental parameters, so the effects of temporal broadening can be reduced, and reliable fluorescence decay curves and accurate lifetimes obtained. The results demonstrate that it is possible to make remote measurements of fluorescence lifetimes using optical fibers as a medium to transport the optical signals. By appropriate selection of parameters, it should be possible to reach reasonably distant locations and still maintain the same degree of accuracy.

EXPERIMENTAL

A block diagram of the apparatus used in these experiments is shown in Fig. 1. The light source is a mode-locked argon-ion laser (Model 171-06 argon-ion laser, Model 342 mode locker with Model 452 mode-locker driver; Spectra-Physics, Mountain View, CA) operating at 514.5 nm, with pulse width and inter-pulse separation of approximately 200 ps (FWHM) and 12 ns, respectively. The train of pulses is modulated at a low frequency with a mechanical chopper. The exact frequency of the chopper is monitored by an internal, optical reference. The main beam is then focussed onto the polished end of the source fiber.

For these initial experiments, a simple dual optical-fiber probe was used. The probe is constructed from two sections of 240-μm core, fused silica, multi-mode optical fiber approximately 16 m in length. One end of each

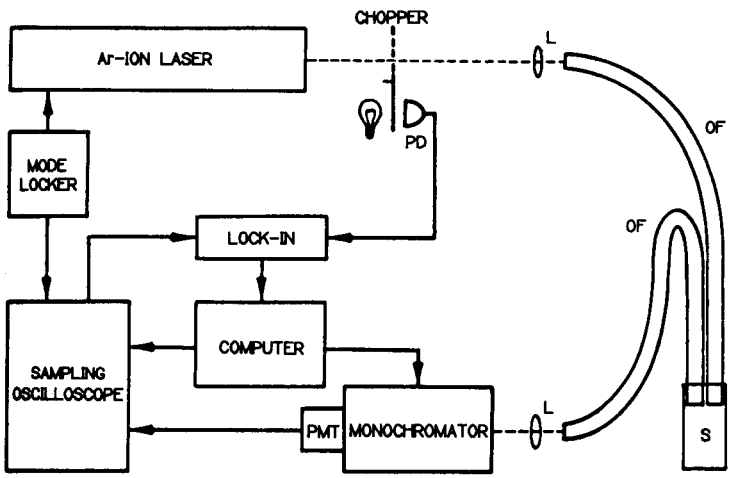

Fig. 1. Block diagram of the apparatus used to measure fluorescence lifetimes with the optical-fiber probe: PD, photodiode; L, lens; OF, optical fiber; S, sample; PMT, photomultiplier tube.

fiber is fixed with epoxy resin into a standard bulkhead connector, while at the distal end, the two fibers are held together with epoxy resin in a 2.5-cm long segment of capillary glass tubing. The three ends of the probe are then trimmed and polished to a smooth finish.

To couple light from the laser into the source fiber of the probe, a lens with an effective *f*-number of about *f*/20 is used. This design ensures that the cone of radiation that is focussed onto the end of the fiber is well within the acceptance angle and that broadening caused by multiple transmission paths is minimized. The light from the laser that is collected by the source fiber is transmitted along its length and illuminates the volume of the sample within its exit cone at the probe tip. Fluorescence from this excitation volume which falls within the entrance cone of the detector fiber is then collected and carried to the optical detection system. Because of the close proximity of the ends of the source and detector fibers at the probe tip, their fields of view overlap so that a fraction of the generated fluorescence is collected.

The collected fluorescence is focused onto the entrance aperture of a monochromator, by a lens that matches the exit geometry of the fiber (approximately *f*/1) with the entrance aperture of the monochromator (*f*/4). Because molecular fluorescence spectra are typically broad, the entrance and exit slits of the monochromator are opened to increase sensitivity. The resulting spectral resolution is 9.00 nm.

After spectral sorting, the signal is detected by a fast photomultiplier tube (PMT, Model C31024; RCA, Lancaster, PA) that is operated with a bias voltage of −3500 V and has a response time of 1.1 ns (FWHM). The output from the PMT is connected to a sampling oscilloscope (Model 7844 oscilloscope mainframe, Model 7T11 sampling time base, and Model 7S11 sampling unit with Model S4 sampling head; Tektronix, Beaverton, OR) for signal recovery. Triggering for the sampling oscilloscope is provided by a reference output from the mode-locker driver, and the time base for the output of the sampling unit is driven with an external ramp generated by the digital-to-analog converter of a laboratory computer (MINC 11/23; Digital Equipment Corporation, Marlboro, MA). With a time-base setting of 2 ns per division, and a digital-to-analog converter resolution of 4096, the maximum temporal resolution that can be obtained is approximately 5 ps.

The output of the sampling unit is connected to a lock-in amplifier (Model 5101; EG&G Princeton Applied Research, Princeton, NJ), as is the chopper reference signal. The lock-in amplifier removes the background dark current generated by the PMT and discriminates effectively against the random and flicker noise in the detection system. The lock-in amplifier is necessary also to amplify the signal so the highest resolution can be maintained in the analog-to-digital converter of the computer, where the signal is ultimately recorded.

As a means of validating the results obtained using the optical-fiber probe, experiments were done with the same experimental apparatus but with direct laser excitation. In this arrangement, a sample-cell holder is fixed to

the entrance aperture of the monochromator. The laser is then redirected by means of a beam translator to excite the sample.

For this initial investigation, stock solutions of rhodamine-B (Exciton Chemical Co., Dayton, OH) and rose bengal (Eastman Kodak Co., Rochester, NY) at 1.00 mM were prepared in ethanol. To increase the scattering signal used as an internal instrument response function, latex particles (0.220-μm diameter with 0.0065 μm standard deviation; Dow Diagnostics, Indianapolis, IN) were added to the solutions. From these stock solutions, samples were prepared at 1.00 μM in 1.00-cm pathlength cuvettes, and deaerated with nitrogen for 15 min prior to measurement. The probe tip was then lowered into the cuvette (or the cuvette placed into the cell holder) with a laser intensity of approximately 40 mW average power incident on the sample. The scattering signal was measured with the monochromator centered on the laser wavelength at 514.5 nm, while fluorescence decays were detected at 565 nm. Finally, scans of the decay curve were collected and signal-averaged for 1 min to collect the scatter, or 10 min for the fluorescence, until an adequate signal-to-noise ratio was obtained.

RESULTS AND DISCUSSION

Typical results obtained for a 1.00-μM solution of rhodamine-B are displayed in Fig. 2. When the monochromator is set at 514.5 nm, the predominant signal arises from laser light which is scattered by particles in the solution and by the walls of the cuvette. Because scattering is an instantaneous process and the width of the mode-locked laser pulses is extremely

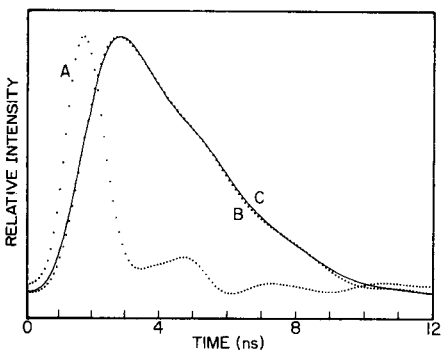

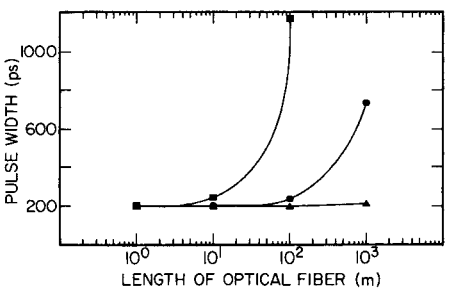

Fig. 2. Experimental and calculated decay curves for a 1.00 μM solution of rhodamine-B in ethanol obtained with the optical-fiber probe: (A) instrument response function; (B) fluorescence response function; (C) calculated response function (lifetime = 2.78 ns).

Fig. 3. Theoretical results for the temporal broadening of a 200-ps pulse as a function of optical-fiber length for several fiber input apertures: (■) $f/5$; (●) $f/20$; (▲) $f/100$.

narrow, the time response of the signal is ultimately dependent on the response characteristics of the PMT and its associated electronics. This curve (trace A) therefore represents the instrument response function.

When the monochromator is scanned to the spectral region near 565 nm, there is an effective discrimination in favor of the rhodamine-B fluorescence over the scattered laser light. The longer decay time of the curve, the fluorescence response function (trace B), arises from the rate coefficient that controls the rhodamine-B fluorescence process.

To evaluate the fluorescence lifetime from the collected decay curves, it is necessary to deconvolute the instrument response function from the fluorescence response function. Because most fluorophores exhibit first-order excited-state decay kinetics, the result will ideally be a first-order exponential with a rate coefficient equal to that for the fluorescence process. Unfortunately, performing a direct deconvolution in the time domain is difficult; therefore, it is necessary to adopt an alternative approach [1]. The method that was used for the results presented in this paper is a convolute-and-compare procedure. Simply, this routine convolutes the instrument response function with a series of exponential decays and compares the result to the fluorescence response function by means of a weighted chi-squared test. The rate coefficient of the exponential is then adjusted, as is the position of the fluorescence response function in the 12-ns time window, until the calculated response function with the best fit is obtained (trace C). It is necessary to shift the fluorescence response function because of the difference between the transit times for the scattered light and the fluorescence through the detector fiber. By taking the reciprocal of the optimal rate coefficient, the fluorescence lifetime is determined. For rhodamine-B with the optical-fiber probe, this value is 2.78 ns.

Table 1 summarizes the results obtained in this investigation for 1.00 μM solutions of rhodamine-B and rose bengal. For both fluorophores, the agreement between the lifetimes and the precisions obtained through the optical fiber and by direct laser excitation is excellent. Similarly, these values are in good agreement with those that have been reported in the literature, indicating that there is no loss in accuracy or precision with the optical-fiber probe.

The instrument response functions that were collected with and without the optical fiber probe are virtually identical, indicating that no detectable temporal broadening occurs over the length of the fibers used for these studies. However, at greater fiber lengths, severe temporal broadening can occur because of the multiple paths by which a photon can be transmitted. It is possible to simulate this process by adding the curves which correspond to these different paths. Figure 3 shows the theoretical broadening of a monochromatic, Gaussian, 200-ps (FWHM) pulse as a function of fiber length for several input apertures. The pulse approximates those which are obtained from the mode-locked argon-ion laser. From these results, it is obvious that as the pulse is transmitted over longer distances, it suffers

TABLE 1

Comparison of fluorescence lifetimes obtained with the optical-fiber probe and direct laser excitation with literature values

Fluorophore	Lifetimes (ns)[a]		
	Optical fiber probe	Direct laser excitation	Literature
Rhodamine-B	2.78 ± 0.04	2.73 ± 0.04	2.72 ± 0.13 [13] 2.79 ± 0.09 [14] 2.94 ± 0.45 [14]
Rose Bengal	0.77 ± 0.07	0.79 ± 0.11	0.83 ± 0.02 [13] 0.70 ± 0.02 [14] 0.78 ± 0.17 [14]

[a]Average of 4 replicates.

more broadening. However, if the pulses are focussed into the fiber with a smaller aperture, the effect of broadening can be decreased greatly. Preliminary experimental results suggest that nanosecond resolution can be maintained for transmission distances up to 1 km in a typical, multimode optical fiber such as that used in this study [15].

Although a light pulse might undergo significant broadening during transmission through an optical fiber, the critical factor is whether or not the broadening is detectable. Typically, PMT's used as detection devices in time-resolved fluorescence have a characteristic response time which limits the minimum detectable pulse width. Using the difference between two exponentials as the response function of a PMT [1], and convoluting this difference curve with the 200-ps pulse, one can simulate the optical detection system and obtain an overall response time of 1.0 ns (FWHM). If the same calculation is done for a fiber input aperture of $f/20$, another curve is generated which represents the detected pulse width as a function of fiber length. These results are displayed in Fig. 4. Again, conditions were selected which represent those of the actual experiments. These curves show that not only the relative, but also the absolute pulse broadening (as reflected in the FWHM) is less significant after detection by the PMT, indicating that in practice the maximum usable fiber length can be longer than suggested by Fig. 3.

These calculations can be used to evaluate the overall effect of temporal broadening on a measured fluorescence lifetime. First, the instrument response function is calculated as described above. The initial laser pulse is assumed to pass through a selected fiber length, and then through the same length again, before being convoluted with the PMT response. This computation accounts for the round trip from source to detector.

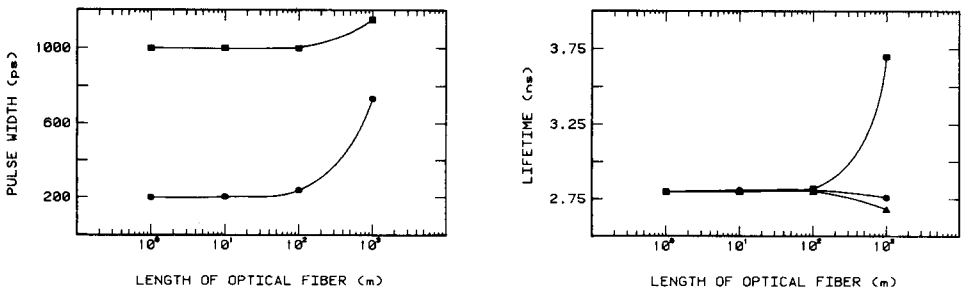

Fig. 4. Comparison of theoretical results for the detection of a 200-ps pulse, with and without the effect of the PMT response time, as a function of optical-fiber length with an input aperture of $f/20$: (■) with PMT response; (●) without PMT response.

Fig. 5. Theoretical values for the computed fluorescence lifetime as a function of optical-fiber length for several monochromator bandwidths: (▲) 0.45 nm; (●) 2.25 nm; (■) 9.00 nm.

In the modelling of the fluorescence response function, the excitation pulse is first viewed as passing through the input fiber; the effect of the fluorescence decay is included by convolution with an exponential having a lifetime of 2.80 ns. The result is then modelled to travel through the return fiber. Because the monochromator passes a finite band of the fluorescence, dispersion (change in the refractive index with wavelength) in the fiber results in additional broadening of the detected decay curve. The equation describing dispersion in fused silica [16] and the dispersion equation itself [12] can be used to find the final pulse width by summing the curves at different wavelengths. This final decay curve is convoluted with the PMT response to yield the theoretical photometric pulse.

To evaluate the fluorescence lifetime from the modelled curves, the instrument response function and the fluorescence response function are subjected to the same convolute-and-compare procedure used for the experimental data. This computation has been done as a function of the optical-fiber length and at several spectral bandwidths; results are shown in Fig. 5.

For modelled bandwidths of 0.45 and 2.25 nm, a surprising decrease in the calculated fluorescence lifetime occurs as the length of the fiber increases. This effect is more severe for the narrower bandwidth. The cause of these errors is a systematic inaccuracy in the curve-comparison process when the response functions are broadened substantially. In contrast, when the bandwidth is 9.00 nm, there is an increase in lifetime with length, because of spectral dispersion. Significantly, the experimental conditions used in this study correspond to a section of the theoretical curves where the degree of accuracy is high; it is therefore not surprising that the experimental results are accurate.

The authors thank The Office of Naval Research, The National Science Foundation, The Royal Society of London, and The Upjohn Company for support of this project.

REFERENCES

1 J. N. Demas, Excited-State Lifetime Measurements, Academic Press, New York, 1983.
2 L. J. Cline-Love and L. M. Upton, Anal. Chem., 52 (1980) 496.
3 F. V. Bright, G. H. Vickers and G. M. Hieftje, Anal. Chem., 58 (1986) 1225.
4 D. A. Wilson, G. H. Vickers and G. M. Hieftje, Anal. Instrum., 14 (1985) 483.
5 R. E. Russo and G. M. Hieftje, Anal. Chim. Acta, 134 (1982) 13.
6 G. M. Hieftje and G. R. Haugen, Anal. Chim. Acta, 123 (1981) 255.
7 F. V. Bright, G. H. Vickers and G. M. Hieftje, in press (1987).
8 G. F. Kirkbright, R. Narayanaswamy and N. A. Welti, Analyst, 109 (1984) 1025.
9 J. T. Coleman, J. F. Eastman and M. J. Sepaniak, Anal. Chem., 56 (1984) 2246.
10 S. D. Schwab and R. L. McCreery, Anal. Chem., 56 (1984) 2199.
11 B. J. Tromberg, J. F. Eastham and M. J. Sepaniak, Appl. Spectrosc., 38 (1984) 38.
12 W. B. Whitten and H. H. Ross, Anal. Chem., 51 (1979) 417.
13 J. M. Ramsey, G. M. Hieftje and G. R. Haugen, Appl. Optics, 18 (1979) 1913.
14 R. E. Russo and G. M. Hieftje, Appl. Spectrosc., 36 (1982) 92.
15 G. M. Hieftje, G. R. Haugen and T. Hirschfeld, unpublished results.
16 I. H. Malitson, J. Opt. Soc. Am., 55 (1965) 1205.

Analytica Chimica Acta, 192 (1987) 155—163
Elsevier Science Publishers B.V., Amsterdam — Printed in The Netherlands

COMPUTER-ASSISTED OPTIMIZATION OF AN IMMOBILIZED-ENZYME FLOW-INJECTION SYSTEM FOR THE DETERMINATION OF GLUCOSE

C. L. M. STULTS, A. P. WADE[a], and S. R. CROUCH*

The Chemistry Department, Michigan State University, East Lansing, Michigan, 48824 (U.S.A.)

(Received 14th July 1986)

SUMMARY

A flow-injection system utilizing the Trinder reaction for the determination of glucose is designed and optimized. Glucose is converted to gluconic acid by passing it through a single-bead-string reactor (SBSR) onto which glucose oxidase enzyme has been immobilized. As it flows through a second SBSR, the gluconic acid reacts with a reagent stream of horseradish peroxidase, 4-aminoantipyrine and 3,5-dichloro-2-hydroxyphenyl sulfonate. The absorbance of the quinoneimine dye produced is then monitored at 510 nm in a flow-through cell. Optimum operating conditions were sought by using both univariate and Composite Modified Simplex procedures. Seven variables were considered. The performance of the system was improved by a factor of 22.5 relative to the starting conditions. A calibration curve obtained at the optimum conditions was linear for 0—3.3 mM glucose and usable for 0—5.5 mM glucose. The optimization procedures revealed some interesting aspects of the Trinder reaction. Scatter diagrams generated from the simplex data showed definite trends for each of the seven variables. These are discussed.

This paper reports the use of an automated flow-injection system for the development and optimization of a method for quantifying glucose. A novel feature of this system is the immobilization of the enzyme (glucose oxidase) on nonporous glass beads of a single-bead string reactor.

The Trinder reaction [1] is one of the most commonly used methods for the spectrophotometric quantitation of glucose. The reaction scheme originally proposed involves the reaction of glucose and molecular oxygen in the presence of glucose oxidase to produce hydrogen peroxide:

$$H_2O + O_2 + \beta\text{-D-glucose} \xrightarrow{\text{glucose oxidase}} \text{gluconic acid} + H_2O_2 \qquad (1)$$

Hydrogen peroxide then reacts with 4-aminoantipyrine (AAP; also known as 4-aminophenazone) and phenol in the presence of peroxidase to produce a colored dye with an absorption maximum at 505 nm. Trinder later found that when the phenol was replaced by 3,5-dichloro-2-hydroxyphenyl sul-

[a]Permanent address: British Petroleum Research Centre, Chertsey Road, Sunbury-on-Thames, Middlesex, TW16 7LN, Great Britain.

0003-2670/87/$03.50

fonic acid (DCPS), the reaction was four times more sensitive and the absorbance maximum shifted to 510 nm [2]:

$$H_2O_2 + AAP + DCPS \xrightarrow{\text{peroxidase}} \text{red dye} + H_2SO_4 \quad (2)$$

It is well known that there are significant advantages to immobilizing enzymes onto an inert support [3—6]. Advantages include better economy and simplification of the flow system. Care must be taken in choosing operating conditions (pH, temperature, etc.) to ensure the enzymes are not degraded. Many workers have immobilized glucose oxidase for use in flowing systems [7—16]. Some have used it in flow-injection systems in conjunction with the Trinder reaction [17—19]. However, to date no mention has been made concerning attempts to optimize such a system, nor has there been any report of a successful simplex optimization for seven variables of a conventional flow-injection system.

In this work, glucose oxidase was first immobilized on nonporous glass beads which were then used to make a single-bead-string reactor (SBSR) [20]. It has been shown that such reactors with the enzyme immobilized on the beads provide an excellent configuration for use in flow-injection systems [10]. An SBSR limits the longitudinal dispersion more than an open tube, and thus longer residence times can be utilized without loss of peak height. This is particularly advantageous for enzyme reactions where reaction rates are often slower than would normally be used in an open-tube flow-injection system.

Some preliminary experiments were also done with immobilized peroxidase. However, peroxidase is relatively inexpensive and efficient immobilization is difficult, and so insufficient advantage would be gained from immobilizing the peroxidase. Co-immobilization of both enzymes on one SBSR would have produced a simpler flow system, but was ruled out because of the different pH optima for the two enzyme-catalyzed reactions.

A flow-injection system incorporating the immobilized glucose oxidase reactor was assembled. An optimum set of operating conditions was sought for seven experimental variables; these were the flow rate, temperature, pH of the carrier and reagent, and concentrations of peroxidase, AAP and DCPS. The aims were to improve the performance of the system and to learn more about interactions of the system variables. The commonest method of optimizing analytical systems is that of varying one parameter at a time, keeping all others fixed. In thorough studies, each variable may be considered several times. If such an approach were used to evaluate the optimum to within 20% in each of the seven dimensions for the system chosen, a total of 175 experiments would be required. Under the same conditions a pattern search would require 78 125 experiments. A better alternative than these methods has been shown to be a simplex optimization [21], which allows simultaneous variation of all parameters. The simplex method is widely applied and accepted in analytical chemistry [22], and therefore will not be discussed in detail here. Since the pioneering work of Deming and Morgan [23], many modifi-

cations have been suggested which attempt to improve the speed and reliability of the method. These have been reviewed elsewhere [24]. For this work the method chosen was the Composite Modified Simplex [25]. It has been shown [26] that a judicious choice of the response function can expedite the optimization process. Such a response function allows a number of parameters to be optimized simultaneously, and takes the form of a mathematical equation that combines two or more system parameters (peak height, cost, throughput, etc.) in an appropriately weighted fashion.

Simplex optimization was previously attempted on the original Trinder reaction in a static system [27], but no optimum was found. The focus of this work is the simplex optimization of a modified Trinder reaction in a flow-injection system.

EXPERIMENTAL

Apparatus

A diagram of the apparatus used is shown in Fig. 1. The temperature of the solutions and the immobilized-enzyme SBSR was controlled by a thermostated circulating water bath. The sample was injected via a pneumatically actuated 6-port injection valve with a 30-μl sample loop (Rheodyne) into the carrier stream which was pumped by a 12-channel peristaltic pump (Ismatec). Flow-rated pump tubing was used (Technicon). The sample passed first through an SBSR composed of chemically-modified 0.6-mm-diameter nonporous glass beads (Proper Mfg., NY) in 0.86-mm i.d. teflon tubing (Benton-Dickinson). It was then joined by the peroxidase reagent solution at a tee-joint. The flow rate of the carrier was made ten times that of the reagent by appropriate choice of pump tubing. After reaction while passing through a plain SBSR, the sample/reagent mixture entered a miniaturized flow-through detection system which was designed by Patton and Crouch [28] and assembled in this laboratory. An in-house designed [29] Intel 8088-based microcomputer controlled the pump speed, injection, and data acquisition. The software was written in FORTH (Forth, Hermosa Beach,

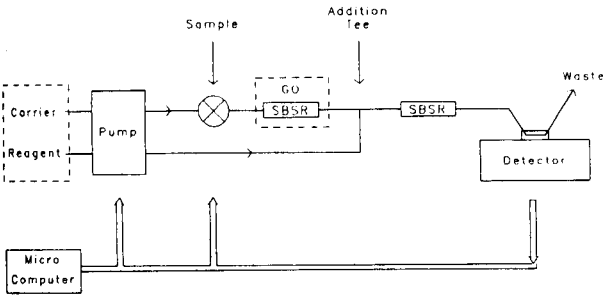

Fig. 1. Flow-injection manifold for glucose determinations with glucose oxidase (GO). Components boxed with dashed lines were temperature-controlled.

CA). Data were passed to a DEC LSI 11/23 for post-experiment processing. The composite modified simplex program, provided by Betteridge and Wade [30], was run on a separate IBM PC compatible microcomputer (PC Designs).

The 10:1 ratio of pump tubing was selected in order to minimize both the consumption of peroxidase and dilution of the sample. The lengths of the SBSR's were empirically chosen so that a minimal amount of glucose oxidase was required and a measurable absorbance value could be obtained at the maximum flow rate. The lengths of the immobilized-enzyme SBSR and the second SBSR were 10 cm and 40 cm, respectively.

Reagents

All solutions were prepared with distilled water and filtered as necessary. All chemicals (reagent grade) were used without further purification.

A peroxidase solution was prepared by dissolving 20.0 mg of horseradish peroxidase (E.C.1.11.1.7, Sigma Type II, specific activity ca. 200 units mg^{-1} at 20°C) in 2.000 ml of water immediately before use to avoid decomposition. The reagent solution consisted of the desired volumes of peroxidase solution, 10 mM 4-aminoantipyrine (Sigma), and 10 mM 3,5-dichloro-2-hydroxyphenyl sulfonic acid (Sigma) mixed together and then diluted with a previously prepared universal buffer solution [31] of the desired pH to 10 ml in a volumetric flask. The reagent solution was prepared immediately before use.

Glucose (Sigma) standards were made from a 2 g l^{-1} stock solution that contained 0.5 g l^{-1} benzoic acid as preservative.

Procedures

Glucose oxidase immobilization. Glucose oxidase (E.C.1.1.3.4, Sigma Type II from *Aspergillus niger*, specific activity ca. 17 800 units g^{-1} at 35°C) was immobilized on nonporous glass beads by the following procedure. The beads were first cleaned with ethanolic 5% (w/v) potassium hydroxide. The surface was then roughened by treatment with a saturated solution of ammonium hydrogenfluoride in methanol. The solution was decanted and the beads were placed in a sealed glass tube at 450°C for 3 h. Then silanization was accomplished by putting the beads in a 1% (v/v) solution of 3-aminopropyltriethoxysilane in acetone first for 30 min at 22°C, and then for 15 h at 70°C. These silanized beads were washed thoroughly with acetone and water and then were allowed to react for 3 h in a 2% (v/v) solution of glutaraldehyde in 0.05 M phosphate buffer at room temperature (22°C). After the beads had been rinsed with the same phosphate buffer the enzyme was attached to the glutaraldehyde group by placing the reacted beads in a solution of glucose oxidase (5 mg ml^{-1} in 0.05 M phosphate buffer, pH 6.86) for 24 h at 4°C. The beads were finally rinsed with, and stored in, the 0.05 M phosphate buffer at 4°C.

Data collection. Each experiment involved an injection of glucose stan-

dard and monitoring of the detector signal with the digital data-acquisition system; the signal was converted to absorbance. Five replicates were done for each experiment. The response function for each experiment used the average values for the peak height and the time of the peak maximum. A baseline absorbance value was established for each set of experimental conditions by running an experiment under the initial (start) conditions (settings for the seven parameters) shown in the first line of Table 1.

Choice of the response function. The response function chosen was based on three considerations. First, the activity of the enzymes involved changes over long periods of time; secondly, the achievement of a sampling rate of at least 60 h^{-1} was desired; finally, the sampling-rate factor should contribute no more than 30% to the overall response. The function chosen was:

$$\text{Time-corrected absorbance ratio} = [80\ s/(60\ s + t_p)]\ (A_{exp}/A_{base})$$

where A_{exp} is the absorbance at peak maximum for a set of experimental conditions, A_{base} is the absorbance at peak maximum for the baseline set of conditions, and t_p is the time (s) after injection at which the peak maximum occurred.

Simplex optimization. The initial simplex was obtained by entering the information listed in Table 2 into the composite modified simplex program. Because there were seven variables, eight experiments were needed to form the initial simplex. The first point of the simplex was the response obtained from the baseline experiment done at the initial (start) conditions (see

TABLE 1

Initial and optimal experimental conditions

	Exp. No.	Flow rate[a] (ml min^{-1})	Temp.[b] (°C)	POD[c] (mg ml^{-1})	AAP (mM)	DCPS (mM)	pH carrier	pH reagent	Ratio[d]
Start	1	1.13	22.2	0.20	0.50	0.50	9.00	9.00	1.11
Top 6	59	0.52	32.8	0.94	0.27	1.34	7.18	8.10	25.0
	63	0.57	31.8	0.78	0.51	1.14	6.78	8.42	19.7
	65	0.64	28.5	0.60	0.58	1.20	7.24	8.52	19.1
	66	0.52	35.6	0.88	0.27	1.48	7.49	8.36	23.2
	68	0.54	29.5	0.74	0.49	1.22	6.62	8.32	19.9
	70	0.57	31.7	0.80	0.34	1.26	6.46	9.02	20.1
Average optimum[e]		0.57	31.6	0.79	0.41	1.27	6.96	8.46	21.2
SD[e]		0.05	2.5	0.12	0.13	0.12	0.40	0.31	2.4

[a]Relationship of flow rate (FR) to pump setting (PS): $FR = 0.0141\ PS + 0.00167$. [b]Relationship of SBSR temperature (T) to water bath temperature (BT): $T = 0.5051\ BT + 11.07$. [c]Peroxidase. [d]Time-corrected absorbance ratio. [e]For the top 6.

TABLE 2

Range and precision of variables for simplex optimization

Variable	Reverse boundary	Forward boundary	Experimental precision
Pump setting	99	20	1
Bath temperature (°C)	21.0	51.4	0.2
[Peroxidase] (mg ml^{-1})	0.05	1.0	0.02
[AAP] (mM)	0.1	2.5	0.01
[DCPS] (mM)	0.1	2.5	0.01
pH carrier, sample	10.00	5.00	0.02
pH reagent	10.00	5.00	0.02

Table 1). Thereafter, each time the simplex program specified a set of experimental conditions, that experiment was done and the time-corrected absorbance ratio was calculated and entered. This process was terminated when an optimum set of conditions was deemed to have been reached (see below).

RESULTS AND DISCUSSION

Choice of variable parameter ranges and baseline conditions

Some univariate experiments were done prior to the optimization in order to ascertain an acceptable range for each of the parameters. The settings listed under Reverse in Table 2 are those which gave low absorbance values and those under Forward gave high absorbance values. Some other considerations also played a role in this decision-making process. The minimum pump setting (flow rate) indicates that a minimum sampling rate of 24 h^{-1} was required. The bath temperature was limited at the low end by room temperature and at the high end by 37°C, the maximum temperature considered advisable for use with this enzyme. The high end of the peroxidase concentration was set at 0.8 mg ml^{-1} because it was desirable to limit the cost of the experiments and there appeared to be no substantial gain in absorbance above that concentration. The upper limits for the AAP and DCPS concentrations were such that if both were used at their highest concentrations, the reagent solution composition would be no more than 25% (v/v) in each. The pH of the carrier and sample were made independent of the pH of the reagent because it was unknown whether the two reactions would have different optimal pH values. The range for each was selected partially on the basis that the working range of the universal buffer is between pH 5.00 and 10.00.

The initial conditions were known to be suboptimal, but exhibited acceptable reproducibility (1% RSD). It was found that a 400 mg l^{-1} glucose standard, when used with a new glucose-oxidase SBSR, gave a maximum absorbance value that was in the middle of the detectable range and was therefore suitable for use in the optimization.

Obtaining optimum conditions

The simplex rapidly improved the response at first. This was followed by a more gradual increase and eventually no improvement. This same pattern has been seen and explained elsewhere [21]. After 27 experiments, the data suggested that a "false maximum" had been found. To check this, that particular experiment was repeated and found to be in error. After 43 experiments, it was intuitively felt that the rate of improvement might be enhanced by use of a simplex that was larger in the dimensions of temperature and peroxidase concentration. Further optimization was done with the current simplex points, but two of those experiments were replaced by two experiments at higher temperatures and/or peroxidase concentrations. The scatter diagrams in Fig. 2 show the results.

Because the composite modified simplex method is a search procedure in which contraction around a maximum will take place, it is likely that there will exist several sets of conditions in the final data set that are near a true surface maximum. By taking the average of the values for each of the parameters for the experimental conditions that gave the six largest time-corrected absorbance ratios (i.e., those yielding a response that was 75% or more of the largest value found), a rough measure of the width of the optimum in each dimension was possible. These results are shown in Table 1.

The performance of the system was improved by a factor of 22.5. A calibration curve obtained at the optimum conditions was linear for 0—3.3 mM glucose and usable for 0—5.5 mM glucose with the reagent concentrations specified.

Interpretation of the data set

From the conditions giving best responses and the scatter diagrams, several observations can be made. The response was found to increase as the flow rate was decreased in a univariate manner. In the simplex study, a maximum was evident indicating that there was some interaction between flow rate and the other parameters. This would be expected from kinetic arguments. The behavior of the response as a function of temperature did not differ markedly from what was expected; there was a steady rise followed by a plateau region. A rise in temperature would be expected to increase the rate of the reaction. Modelling studies have suggested that it may also decrease the dispersion [32]. There was no evidence of major interaction between temperature and other variables in the system. The peroxidase concentration was also found to enhance the response, and exhibited a curve typical of that which might be expected for enzymes. The effect of changing the concentrations of the AAP and DCPS was significant. The reaction scheme would suggest that the AAP to DCPS concentration ratio should be 1:1, but the results showed that the optimum ratio of the two was closer to 1:3. The pH of the carrier and sample showed a maximum near pH 7. This was somewhat higher than that considered optimum for glucose oxidase [33]. This behavior may have been due to the

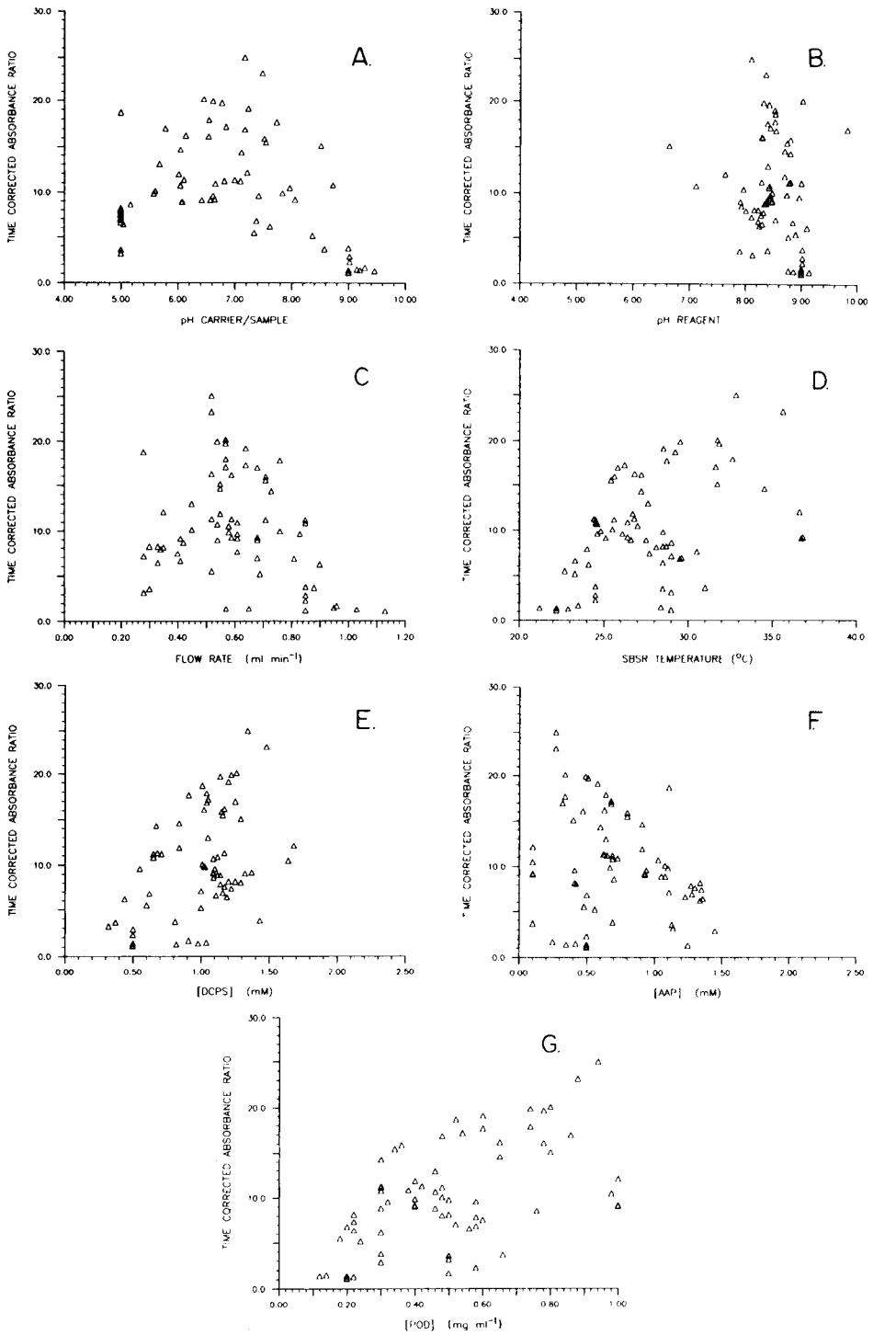

Fig. 2. Effect of experimental variables on response function: (A) pH of carrier and sample; (B) pH of reagent; (C) flow rate, ml min^{-1}; (D) SBSR temperature, °C; (E) DCPS concentration, mM; (F) AAP concentration, mM; (G) POD concentration, mg ml^{-1}.

difference between the pH of the bulk solution and that seen by the enzyme. The optimum pH of the reagent solution was also found to be higher than that considered optimum for peroxidase in solution [34], however it is known that the optimum is dependent upon the particular substrate and type of buffer used [35].

This work was partially supported by National Science Foundation grant No. CHE 83-20620. A. P. W. thanks The British Petroleum Company for facilitating his secondment to Michigan State University.

REFERENCES

1 P. Trinder, Ann. Clin. Biochem., 6 (1969) 24.
2 D. Barham and P. Trinder, Analyst, 97 (1972) 142.
3 H. H. Weetall, Anal. Chem., 46 (1974) 602A.
4 L. D. Bowers and P. W. Carr, Anal. Chem., 48 (1976) 544A.
5 D. N. Gray, M. H. Keyes and B. Watson, Anal. Chem., 49 (1977) 1067A.
6 L. D. Bowers, Anal. Chem., 58 (1986) 513A.
7 P. Cremonesi and R. Bovara, Biotechnol. Bioeng., 18 (1976) 1487.
8 B. Olsson, L. Ogren and G. Johansson, Anal. Chim. Acta, 145 (1983) 101.
9 M. K. Weibel, W. Dritschilo, H. L. Bright and A. E. Humphrey, Anal. Biochem., 52 (1973) 402.
10 H. Mottola, Anal. Chim. Acta, 145 (1983) 27.
11 B. Watson, D. N. Stifel and F. E. Semersky, Anal. Chim. Acta, 106 (1979) 233.
12 M. Masoom and A. Townshend, Anal. Chim. Acta, 166 (1984) 111.
13 T. Yao, M. Sato, Y. Kobayashi and T. Wasa, Anal. Chim. Acta, 165 (1984) 291.
14 T. Hara, M. Toriyama and M. Imaki, Bull. Chem. Soc. Jpn., 55 (1982) 1854.
15 M. Tabata, C. Fukunaga, M. Ohyabu and T. Murachi, J. Appl. Biochem., 6 (1984) 251.
16 J. N. Miller, B. F. Rocks and D. T. Burns, Anal. Chim. Acta, 93 (1977) 353.
17 R. Q. Thompson, Ph.D. Dissertation, Michigan State University, 1982.
18 P. J. Worsfold, Anal. Chim. Acta, 145 (1983) 117.
19 L. Gorton and L. Ogren, Anal. Chim. Acta, 130 (1981) 45.
20 J. M. Reijn, W. E. van der Linden and H. Poppe, Anal. Chim. Acta, 123 (1981) 229.
21 D. Betteridge, T. J. Sly, A. P. Wade and J. E. W. Tillman, Anal. Chem., 55 (1983) 1292.
22 S. N. Deming and S. L. Morgan, Anal. Chim. Acta, 150 (1983) 183.
23 S. N. Deming and S. L. Morgan, Anal. Chem., 46 (1974) 1170.
24 D. Betteridge, A. P. Wade and A. G. Howard, Talanta, 32 (1985) 723.
25 D. Betteridge, A. P. Wade and A. G. Howard, Talanta, 32 (1985) 709.
26 D. Betteridge, A. F. Taylor and A. P. Wade, Anal. Proc., 21 (1984) 373.
27 J. A. Lott and K. Turner, Clin. Chem., 21 (1975) 1754.
28 C. J. Patton and S. R. Crouch, Anal. Chim. Acta, 179 (1986) 189.
29 B. H. Newcome and C. G. Enke, Rev. Sci. Instrum., 55 (1984) 2017.
30 D. Betteridge and A. P. Wade, British Petroleum Research Centre, Sunbury-on-Thames, UK, Personal communication, February 1986.
31 H. T. S. Britton and R. A. Robinson, J. Chem. Soc., (1931) 1456.
32 D. Betteridge, C. Z. Marczewski and A. P. Wade, Anal. Chim. Acta, 65 (1984) 227.
33 D. Keilin and E. F. Hartree, Biochem. J., 42 (1948) 221.
34 H. U. Bergmeyer (Ed.), Methods of Enzymatic Analysis, Verlag Chemie, Weinheim, 1965, p. 990.
35 K. Zeile, in E. Bamann and K. Myrback (Eds.), Die Methoden der Fermentforschung, reproduced by Academic Press, New York, 1941, p. 2601.

Analytica Chimica Acta, 192 (1987) 165—173
Elsevier Science Publishers B.V., Amsterdam — Printed in The Netherlands

ANALYSIS OF COMPLEX MIXTURES BY PHOTOIONIZATION MASS SPECTROMETRY WITH A VACUUM-ULTRAVIOLET HYDROGEN-LASER SOURCE

THOMAS C. HUTH and M. BONNER DENTON*
Department of Chemistry, University of Arizona, Tucson, Arizona 85721 (U.S.A.)
(Received 28th February 1986)

SUMMARY

Trace organic analysis of a complex matrix presents one of the most challenging problems in analytical mass spectrometry. Inselective electron-impact ionization often requires extensive sample clean-up to isolate the analyte from the matrix. Sample preparation can be greatly reduced when a hydrogen laser is used for selective photoionization of only a small fraction of the compounds introduced into the ion source. This device produces parent ions only for all compounds with ionization potentials that lie below a threshold value limited by the photon energy of 7.8 eV. The only observed interference arises from electron-impact ionization when scattered laser radiation interacts with metal surfaces, producing electrons which are then accelerated by potential fields inside the source. These can be suppressed to levels acceptable for practical analysis through proper instrumental design. Results are presented which indicate the ability of this ion source to discriminate against interfering matrix components in simple extracts from real samples such as brewed coffee, beer, and urine.

The need for selective techniques in mass spectrometric analysis for components in complex mixtures has been well documented [1]. Mass spectrometry is one of the most sensitive techniques available for trace analysis, but for typical samples, the lack of ionization selectivity afforded by common ion sources usually necessitates complex and tedious preseparation steps in order to produce interpretable results. The problem is compounded by the extensive fragmentation produced by these sources, resulting in a large number of ion masses for each component present. One approach to achieving selectivity in the ionization process is laser-induced photoionization, which can be accomplished in various ways that involve resonant and non-resonant single- and multi-photon processes [2]. Selective single-photon ionization of compounds from simple mixtures has been demonstrated, using the Lyman band output from a molecular hydrogen laser [3]. Ions produced by this process consist of parent molecular ions only. Species with ionization potentials that lie above the radiation energy of 7.8 eV are completely rejected. Among the types of compounds ionized below this threshold are many amines and nitrogen heterocycles, a class which encompasses a large number of pharmacologically-active molecules.

The aim of this study is to demonstrate the capabilities of vacuum-

0003-2670/87/$03.50

ultraviolet hydrogen-laser photoionization mass spectrometry for selective analysis of real matrices. Of particular interest is its applicability in the area of rapid screening of drugs and drug metabolites in biological samples. Reduction of non-selective ionization by electron impact is discussed. This was established in previous work as the most important source of interference for simple mixtures [3]. It results from acceleration of stray electrons produced in the ion source, primarily by interaction of scattered laser radiation with metal surfaces. Spectra obtained from extracts of spiked beer, coffee, soy sauce, urine, and blood serum are shown. The food matrices were chosen as models for this work because they are well-characterized, readily available, and are known to contain nitrogen compounds of the type suitable for ionization by the hydrogen laser.

EXPERIMENTAL

Instrumentation

The hydrogen-laser photoionization mass spectrometer (H_2-LPMS) system used in this study has been described previously [3, 4]. The mass spectrometer is a time-of-flight device designed after that of Wiley and McLaren [5]. For these experiments, the laser was operated at a pulse repetition rate of 10 Hz.

For this work, the electrostatic multiplier was replaced with a Galileo Electro-Optics M-306 magnetic electron multiplier (Galileo Electro-Optics Corp., Galileo Park, Sturbridge, MA 01518), operated at a dynode voltage between −1500 and −1950 V. The spectra in Figs. 1 and 2 were acquired using a specially developed wide-bandwidth high-gain electrometer preamplifier. This device amplifies the multiplier output current pulses with a voltage/current characteristic of 5×10^6 V A^{-1} at a bandwidth greater than 50 MHz. At the signal levels of the present experiment, its output is of the order of 1 V.

To introduce solid extraction residues, a direct probe inlet was constructed using a 22.9-cm length of 6.4-mm o.d. stainless steel tubing. This probe rod was inserted into the ion source through a ball valve vacuum lock, to which the rod was attached using a Cajon Ultra-Torr vacuum fitting (Cajon Co., 9760 Shepard Rd., Macedonia, OH 44056). A sample vial at the end of the probe rod was heated with 1.0 A d.c. through a 10-cm length of 30-gauge Nichrome wire wound around the vial. Leads for heating the filament were threaded through the center of the rod, and sealed at the top with a drop of high-vacuum epoxy. The side of the ball valve exposed to the atmosphere was also fitted with a side-arm for roughing after attachment of the rod. The ion source was held at 80°C during the acquisition of all spectra reported here.

For the electron-impact experiments, liquids and solutions were injected through the heated inlet system described previously [3], also operated at 80°C.

Several modifications were made with the aim of reducing photoelectron production from metal surfaces in the ion source. A 6.4-mm diameter circular aperture was installed at the point of entry of laser radiation into the source housing to restrict the divergent beam. The aperture was placed on the laser side of the CaF_2 lens which seals the ion-source vacuum. A metal sleeve attached to the aperture of the direct probe inlet prevents acceleration of thermionic electrons from the hot filament. The bottom of the sleeve is covered with a layer of fine tungsten mesh grid material. Finally, an angled exit-window assembly directs reflected laser radiation downward so that the formation of electrons occurs at a location remote from the accelerating fields. Because the laser beam is not polarized, the exact angle of the window is not critical, so long as it is less than Brewster's angle [6]. The window assembly used in these experiments had an angle of 45°. A collector electrode was installed inside the window mount, but was observed to have no effect on the magnitude of electron-impact signals at applied voltages from zero up to the accelerating voltage of +500 V, and was therefore not used in these experiments.

Spectra were acquired by photographing the oscilloscope trace with Polaroid Type 47 film (ASA 3000). Each spectrum represents an average of approximately 1000 traces. Thus, the intensity of an ion peak for a particular compound is determined by both its concentration in the sample, and its volatilization profile in the ion source.

Materials

For the extraction of complex matrix samples, ACS reagent-grade dichloromethane and spectrophotometric-grade n-heptane were used as received. Reagent-grade isoamyl alcohol was purified by redistillation.

Coffee, soy sauce, and an American lager beer were purchased directly from a grocery as complex matrix models. The coffee was drip-brewed fresh for each run according to manufacturer's instructions, and extracted immediately thereafter as described below. The soy sauce and beer were used directly from their containers. Soy sauce was stored at room temperature, while beer was stored at 2°C, a fresh sample being used for each run.

The urine was a pooled sample collected from seven volunteers, and stored in a polyethylene bottle at 2°C. Total storage time over the course of these experiments was approximately 2 wks.

Lyophilized human control serum (Ortho Diagnostics, Raritan, NJ) was reconstituted fresh for each run. The dry sample was stored at 2°C.

Reagent-grade 4-methoxyaniline was recrystallized from hot water, and thereafter stored at 2°C in the dark. Stock solutions (1 mg ml^{-1}) were prepared fresh every 2 days in 0.1 M HCl, and were also stored between runs at 2°C in the dark.

Samples of the phenothiazine tranquilizers, chlorpromazine hydrochloride and trimeprazine tartrate (Smith, Kline and French Laboratories, Philadelphia, PA) and promethazine hydrochloride (Wyeth Laboratories, Malvern,

PA), were supplied by the manufacturers. Stock solutions (5 μg ml^{-1}) were prepared fresh every 7 days, and were stored at 2°C in amber glass bottles.

Polycarbonate centrifuge tubes (Nalge Co., Rochester, NY) were used.

Sample preparation

For the food matrices, a basic extraction was done with 10 ml of sample, spiked with 50 μg l^{-1} 4-methoxyaniline. This was placed in a glass centrifuge tube and made alkaline to pH 11 with 1 M NaOH. The solution was then extracted with 10 ml of dichloromethane, by mechanical shaking for 20 min. The mixture was centrifuged, and the organic layer transferred by suction to a clean tube. This was back-extracted with 10 ml of 0.1 M HCl in the same manner. The acid phase was again separated and transferred to a clean tube, adjusted to pH 11, and re-extracted with another 10 ml of dichloromethane. The final organic extract containing the basic fraction of the sample was removed into a tapered glass tube and evaporated to approximately 150 μl in a 60°C water bath under a stream of nitrogen. The solution was then transferred to a direct-probe sample vial, and evaporated to dryness in the water bath. The photoionization mass spectrum of the residue was measured immediately.

Because it has been reported that free base phenothiazines are adsorbed strongly on glass surfaces [7], polycarbonate centrifuge tubes were used for the extraction of these drugs from urine and serum. For these samples, a single extraction was done on a 10-ml aliquot, spiked with the drugs to 100 μg l^{-1}. The sample, made alkaline to pH 11 with 1 M NaOH, was extracted once with n-heptane/1.5% isoamyl alcohol by mechanical shaking for 20 min. Because the phenothiazines are light-sensitive [7], especially in their free-base forms, the extraction tubes were covered with aluminum foil during the shaking period to exclude room light. The mixture was centrifuged, and the organic layer separated by suction. This was evaporated on a 60°C water bath, under a stream of nitrogen, to 150 μl. After transfer to a sample vial, the solution was evaporated to dryness under vacuum at room temperature, and the spectrum was measured immediately.

Diphenylamine was used as a mass marker in these experiments, and was added to sample vials just prior to running of the spectra.

RESULTS AND DISCUSSION

Electron-impact interference

In initial experiments with this system [3], it quickly became clear that a major source of interference in the analysis of mixtures was electron-impact ionization caused by stray electrons in the ion source. For low concentrations, it is crucial that interaction of the vacuum ultraviolet laser beam with metal surfaces inside the ion source be minimized. Following the instrumental modifications outlined above, this interference was reduced to the level shown in Fig. 1. The intensity of the $CHCl_2^+$ signal produced by

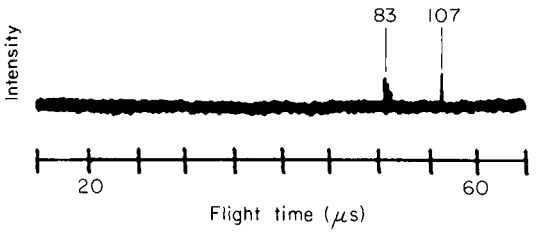

Fig. 1. Spectrum (H_2-LPMS) of 50 ng of 4-aminotoluene (107 amu) injected in 1 μl of chloroform.

electron impact for a 1-μl injection of chloroform, is at approximately the level of photoion signal for 50 ng of 4-aminotoluene.

The fragmentation observed for electron-impact signals in these spectra indicates that much of this ionization is produced by low-energy electrons. The fragment ion cluster at 50—52 amu observed in the 70-eV electron-impact spectrum of benzene is also present here, but at greatly reduced intensity relative to the molecular ion (Fig. 2A). This is consistent with the proposition that the electrons effective in producing detectable ions are actually low-energy secondary electrons sputtered from the source electrodes [8].

When ion signals produced by electron impact are relatively strong, they can often be distinguished from photoions by simple inspection, because the former tend to occur in clusters rather than isolated single-mass ions. However, as the level of electron-impact interference is reduced, the fragment-ion signals which give rise to these clusters disappear below the detection limit, and only the intense molecular ions remain (Fig. 2B). Under these conditions, it becomes more difficult to distinguish between electron impact and photoionization (Fig. 3). This can, however, be accomplished through adjustment of ion-source parameters [8].

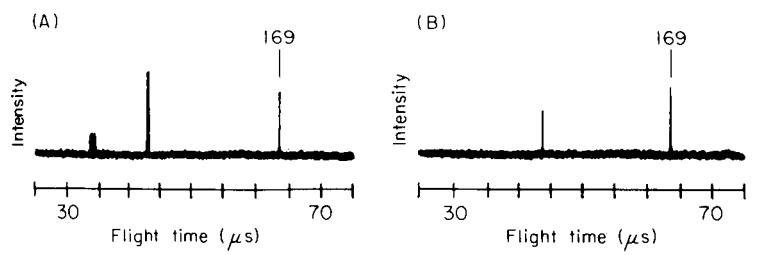

Fig. 2. Electron-impact signals for benzene (0.5-μl injections): (A) before modifications, (B) after modifications. Signal at 43.5 μs is the benzene molecular ion; in (A), this signal is off scale. The actual intensity exceeds that shown by a factor of about 5. Signal at 34 μs is the fragment ion near 50 amu. The diphenylamine mass marker appears at 169 amu.

Complex mixtures

The photoion mass spectra of alkaline extracts of spiked beer, coffee, and soy sauce are shown in Fig. 3; the ion masses are listed in Table 1.

Many compounds ionized below the H_2-laser photon energy of 7.8 eV are amines and *N*-heterocycles [3], which will be concentrated into the alkaline fraction if they are present. Alkaline fractions of food extracts consist mainly of heterocyclic nitrogen compounds such as pyrazines and pyridines [9]. For coffee, a number of pyrroles, indoles, and quinolines are also present [10]. In all, over 100 compounds have been identified in this fraction for coffee [10—12], and about 35 each for beer [13] and soy sauce [14]. Selective photoionization greatly simplifies the mass spectra of these mixtures to a few signals. Although it is clear in each case that several matrix compounds are ionized, the lack of fragmentation prevents this fact from greatly confusing the spectra. It should be noted that fragmentation can also be suppressed by using low-energy electron impact, but this is accompanied by a reduction in ionization efficiency, resulting in a substantial loss of sensitivity.

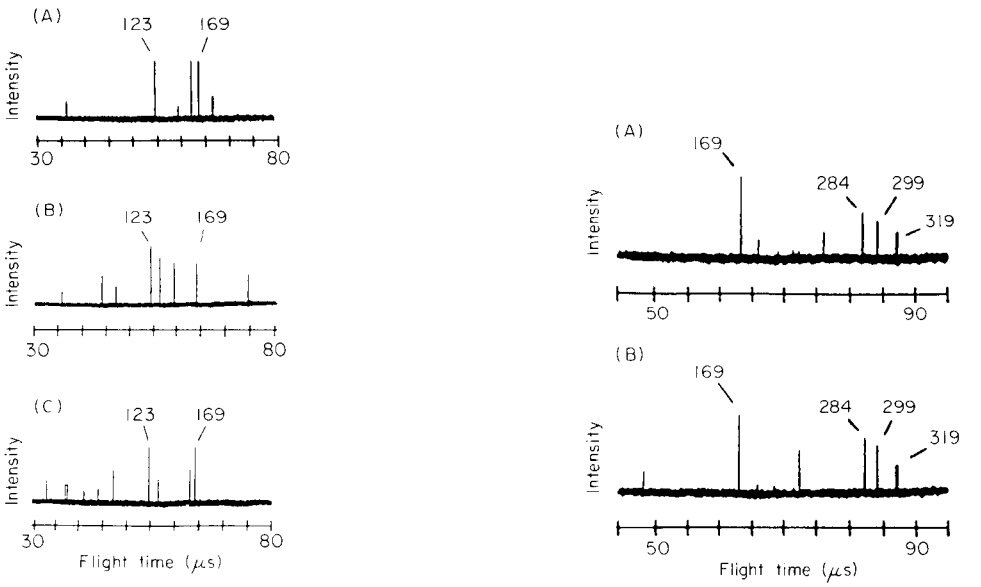

Fig. 3. Spectrum of alkaline extracts: (A) beer; (B) coffee; (C) soy sauce. 10-ml samples spiked with 50 $\mu g\ l^{-1}$ 4-methoxyaniline (123 amu) prior to extraction. The diphenylamine mass marker appears at 169 amu.

Fig. 4. Spectrum of extracts: (A) urine; (B) serum. 10-ml samples spiked with 100 $\mu g\ l^{-1}$ each of promethazine hydrochloride (284 amu), trimeprazine tartrate (299 amu), and chlorpromazine hydrochloride (319 amu) prior to extraction. The diphenylamine mass marker appears at 169 amu.

TABLE 1

Ion masses for mass spectra of alkaline extracts of foods

Matrix	Ion flight time (μs)	Mass[a] (amu)	Origin
Beer	37.1	55	matrix
	54.7	123	4-methoxyaniline spike
	59.0	144	matrix
	62.3	160	matrix
	63.9	169	diphenylamine marker
	66.9	186	matrix
Coffee	36.8	55	matrix
	44.4	82	matrix
	47.1	92	matrix
	54.3	123	4-methoxyaniline spike
	56.2	132	matrix
	59.0	145	matrix
	63.6	169	diphenylamine marker
	73.7	228	matrix
Soy sauce	32.9	43	matrix
	36.9	55	matrix
	37.4	56	matrix
	41.2	69	matrix
	44.5	81	matrix
	47.3	92	matrix
	54.6	123	4-methoxyaniline spike
	56.4	131	matrix
	62.8	165	matrix
	63.6	169	diphenylamine marker

[a]Unknown ion masses were calculated with respect to the diphenylamine mass marker using flight times measured directly from the low-resolution spectra shown. The standard deviation of 17 replicate mass determinations made in this manner for the promethazine molecular ion (284.4 amu) was 1.4 amu.

Spectra of all pure compounds and synthetic mixtures obtained thus far by H_2-LPMS consist of parent molecular ions only. The spectra in Fig. 3, however, contain several low-mass ions, which are not likely to represent intact molecules. They may be fragments that result from pyrolysis on the hot filament used to heat the tip of the direct probe. This phenomenon has been reported previously in electron-impact experiments [15, 16]. The possibility that they arise from a two-photon process cannot be discounted, although the probability of such an event is smaller than that for single-photon ionization by at least five orders of magnitude under the conditions of this experiment. This would imply a very large excess of the precursor. The laser radiation at 7.8 eV represents a rather small excess of energy (1 eV or less) over the ionization potentials of even the most easily ionized

of molecules. Under these conditions, dissociative ionization proceeding through autoionizing states of the neutral molecule, when energetically possible, would not be expected to produce fragments much smaller than the molecular ion [15]. These signals do not appear to arise from stray electron impact, because their intensities are not affected by the hardware changes described above.

Electron-impact signals that do remain in these spectra appear as a weak, diffuse background. They are, in general, barely detectable on the photographs.

The spectra of simple extracts of urine and blood serum spiked with 100 $\mu g\ l^{-1}$ each of three phenothiazine tranquilizers are shown in Fig. 4, Although the relationship between blood level of these drugs and therapeutic effect has not as yet been clearly defined [18], the level of 100 $\mu g\ l^{-1}$ is well within the estimated "therapeutic window" for chlorpromazine [19]. Excretion of phenothiazines in urine concentrates them into the $mg\ l^{-1}$ range [20].

The photoion mass spectra of these extracts are remarkably clear, with only a few significant matrix signals observed. In extracts of unspiked urine, a single ion is observed at 245 amu. This ion appears at 76.6 μs in Fig. 4A. The peak at 66.9 μs in this spectrum is a contaminant. For unspiked serum extract, two ion signals are observed, at 96 and 221 amu; these occur at 48.5 and 72.7 μs, respectively, in Fig. 4B.

A detailed evaluation of the quantitative aspects of H_2-LPMS was impractical under the conditions of this study because of the photographic method of data acquisition. However, further work is in progress which will address this issue using a computer-controlled transient waveform recorder for digital integration of spectra. It is clear now that the sensitivity is fully adequate for the determination of at least one class of easily ionized drugs at physiologically meaningful levels. It should also be noted that a signal was observed on the oscilloscope trace for as little as 10 ng of 4-aminotoluene.

The instrumentation required for the H_2-LPMS experiment is simple and inexpensive to build and operate. Speed is enhanced by the ability to introduce samples directly by solution injection. Based on these results, and the fact that many pharmaceuticals and drugs of abuse contain easily ionizable functionalities, H_2-LPMS appears to be well suited to screening applications for trace levels of drugs. The technique is much more sensitive than thin-layer chromatography, and is not subject to cross-reactivity interferences which occur in methods based on immunoassay. When easily ionized metabolites are also present, it should be possible to obtain a "fingerprint" spectrum which would allow a clear identification to be made. Further studies that bear on the applicability of H_2-LPMS in this area are currently in progress, including the quantitative studies mentioned above and evaluation of the ionizability of a wider range of drugs.

We thank Smith, Kline and French Laboratories and Wyeth Laboratory for providing the samples of phenothiazines. This study was partially supported by the Office of Naval Research.

REFERENCES

1 K. Beyermann, in S. Facchetti (Ed.), Applications of Mass Spectrometry to Trace Analysis, Elsevier, Amsterdam, 1982, pp. 1—67, and references therein.
2 R. J. Cotter, Anal. Chem., 56 (1984) 485A.
3 T. C. Huth and M. B. Denton, Int. J. Mass Spectrom. Ion Phys., 67 (1985) 199.
4 J. S. Babis, T. C. Huth and M. B. Denton, Rev. Sci. Instrum., 56 (1985) 1969.
5 W. C. Wiley and I. H. McLaren, Rev. Sci. Instrum., 26 (1955) 1150.
6 F. A. Jenkins and H. E. White, Fundamentals of Optics, 4th edn., McGraw-Hill, New York, 1976.
7 S. H. Curry, Anal. Chem., 40 (1968) 1251.
8 T. C. Huth, Ph.D. dissertation, University of Arizona, 1986.
9 J. A. Maga and C. E. Sizer, Crit. Rev. Food Technol., 4 (1973) p. 57.
10 O. G. Vitzthum and P. Werkhoff, Z. Lebensm. Unters. Forsch., 156 (1974) 300.
11 O. G. Vitzthum and P. Werkhoff, J. Food Sci., 39 (1974) 1210.
12 O. G. Vitzthum and P. Werkhoff, J. Agric. Food Chem., 23 (1975) 516.
13 R. J. Harding, H. E. Nursten and J. J. Wren, J. Sci. Food Agric., 28 (1977) 225.
14 N. Nunomura, M. Sasaki, Y. Asao and T. Yokotsuka, Agric. Biol. Chem., 42 (1978) 2123.
15 A. G. Harrison, in F. W. McLafferty (Ed.), Mass Spectrometry of Organic Ions, Academic Press, New York, 1963, p. 21.
16 A. J. B. Robertson, Proc. Roy. Soc. Ser. A, 199 (1949) 394.
17 J. Berkowitz, Photoabsorption, Photoionization, and Photoelectron Spectroscopy, Academic Press, New York, 1979.
18 J. G. B. M. Noten and D. R. A. Uges, in F. W. H. M. Merkus (Ed.), The Serum Concentration of Drugs, Excerpta Medica, Amsterdam, 1980, p. 126.
19 S. H. Curry, Psychopharmacol. Commun., 2 (1976) 1.
20 J. A. F. deSilva, in K. Tsuji (Ed.), GLC and HPLC Determination of Therapeutic Agents, M. Dekker, New York, 1978, p. 592.

Analytica Chimica Acta, 192 (1987) 175—182
Elsevier Science Publishers B.V., Amsterdam — Printed in The Netherlands

DETERMINATION OF PHOSPHORUS IN ORGANIC COMPOUNDS AND METAL COMPLEXES BY INDUCTIVELY-COUPLED PLASMA ATOMIC EMISSION SPECTROMETRY

M. ŠIROKI*, G. VUJIČIĆ, V. MILUN, Z. HUDOVSKY and Lj. MARIĆ

Laboratory of Analytical Chemistry, Faculty of Science, University of Zagreb, Strossmayerov trg 14, 41000 Zagreb (Yugoslavia)

(Received 2nd July 1986)

SUMMARY

Phosphorus is determined by inductively-coupled plasma atomic emission spectrometry at 213.618 nm. Different types of organic and inorganic phosphorus compounds and metal complexes were examined after direct dissolution in water, aqueous ethanol or acid, or after decomposition by oxygen flask combustion or Kjeldahl digestion; results were within the usual limit of precision and accuracy for such determinations. The effect of small (<20%) ethanol concentrations in the aqueous solution on the signals obtained from a low-power (1200 W) argon plasma is examined and discussed.

Recently, there has been increased interest in the application of inductively-coupled plasma/atomic emission spectrometry (i.c.p./a.e.s.) not only for multi-element determinations but also for single elements. The results reported here demonstrate the usefulness of this technique for the determination of phosphorus in organic compounds and complexes. For soluble samples, no drastic procedures are needed for destroying the substance and breaking the carbon—phosphorus bond because the chemical form of phosphorus in solution is of no consequence. This is an advantage over all chemical methods for phosphorus determination, for which complete conversion of phosphorus to orthophosphate or phosphoric acid is a prerequisite.

EXPERIMENTAL

Instrumentation and chemicals

Details of the instrumentation and operating conditions are given in Table 1.

The principal phosphorus resonance line at 178.29 nm, which is the most sensitive phosphorus line and the least subject to spectral interferences, is not available with the instrument used, but is preferred with i.c.p. systems having vacuum spectrometers [1]. The 213.618- and 214.914-nm lines are the most sensitive phosphorus lines observed above 200 nm and so are the most commonly used [2—4]. The 214.914-nm line exhibits a poorer line-to-

0003-2670/87/$03.50

TABLE 1

Plasma equipment and operating conditions

Plasma equipment	Applied Research Laboratories, ARL 35000 C-ICP
Spectrometer	1-m Czerny-Turner mounting, grating 1200 lines mm^{-1}
R.f. generator	Henry quartz controlled, max. power 2000 W, operating power 900—1600 W, reflected power <5 W
Operating frequency	27.12 MHz
Plasma torch	Three concentric quartz tubes, Fassel type
Nebulizer	Glass concentric, Meinhard type
Spray chamber	Conical glass
Argon flow	Coolant 10.2 l min^{-1}, plasma 0.8 l min^{-1}, carrier 1.0 l min^{-1}
Observation height	15 mm above the work coil
Integration time	1 s
Instrument control and data manipulation	PDP 11/03 (Digital Equipment Corp.)

background intensity ratio and is more subject to spectral interferences so the 213.618-nm line was selected for use.

Deionized-distilled water was always used. A stock standard solution of phosphorus (1000 μg ml^{-1} P) was prepared by appropriate dilution of orthophosphoric acid (Merck Titrisol) with water. Metal salts and most of the phosphorus-containing organic compounds were laboratory-reagent grade. The tetraphenylphosphonium ion-pairs of various metal-organic complexes were prepared in the laboratory; their purity was checked by CHN determinations. Thus, the anionic complex ions of 4-(2′-pyridylazo)resorcinol (PAR) with cobalt, indium, copper, niobium, palladium and vanadium(V) were prepared, as well as the tantalum complexes with malic, glycolic and tartaric acids. (The tantalum complexes were prepared by N. Brničević, Ruder Bošković Institute, Zagreb.) The phosphorus content of these compounds was checked by titration [5].

Preparation of sample solutions

Soluble compounds were simply dissolved in water, ethanol or acids. Compounds which were not soluble in these solvents were decomposed by Schöniger oxygen-flask combustion or Kjeldahl digestion.

Oxygen flask combustion. Burn 2—10 mg of organic substance in the usual way in a 300—500 ml flask containing 10 ml of 10% (v/v) nitric acid as absorbing solution. After shaking for 20 min, transfer the solution to a 25-ml volumetric flask. If some carbon is formed, remove it by pouring through a coarse filter paper. Add 2.0 ml of ethanol and make up to volume with water.

Kjeldahl digestion. Digest 5—10 mg of substance in a Kjeldahl flask with 1 ml of concentrated sulphuric acid to which 2—3 drops of concentrated nitric acid have been added. Repeat the nitric acid addition three times. Transfer the solution to a 25-ml volumetric flask, add 2.0 ml of ethanol and dilute to the mark with water.

RESULTS AND DISCUSSION

Many organic compounds and complexes in which phosphorus has to be determined are much more soluble in ethanol than in water. Therefore ethanolic solutions were used first. Preliminary experiments with pure ethanol showed that, even at an increased power level of 1600 W, the plasma operated satisfactorily only for a short period. Plasma instability with alcohols has been observed by other investigators [6—8]. Attention was therefore paid to water/ethanol mixtures. By introducing a series of solutions of different ethanol content into the i.c.p. under the conditions which are optimum for an aqueous solution (r.f. power 1200 W, nebulization gas flow 1.0 l min^{-1}, free aspiration rate 2 ml min^{-1}), stable plasma operation was obtained with up to 12% ethanol. The plasma resistance, as indicated by the reflected power, strongly increased with the ethanol content. Under the experimental conditions used, the reflected power could be decreased (by manual adjustment) to less than 5 W for solutions containing up to 12% of ethanol. The plasma was extinguished at ca. 20% ethanol.

A solution in 8% ethanol was found to be best for the phosphorus determination. Some improvements were noticed compared to pure aqueous solution. These are listed in Table 2. The detection limit (DL) was practically the same, but the concentration equivalent to background (BEC) was lower as a result of increased phosphorus intensity, which is also evident from the total line-to-background intensity ratio (I/I_b).

The results obtained by varying the applied r.f. power at a fixed observation height (15 mm) and nebulizer gas flow (1.0 l min^{-1}) are illustrated in Fig. 1A. The variation of background intensity, net line emission intensity and the I/I_b ratio are shown for aqueous solution and 8% (v/v) ethanol in water. The intensity of the P 213.618-nm line rises steadily with increasing power, the relative increase in the presence of ethanol being greater. The ratio is practically constant over the power range 1150—1250 W, so 1200 W was used in further work. Figure 1B shows the effect of carrier gas flow rate. Maximum I/I_b values were achieved at 1.0 l min^{-1} for the entirely aqueous solution and 0.9 l min^{-1} for the 8% ethanol. The relative decrease in intensity as the carrier gas flow increases above the maximum signal was greater for the ethanolic solution.

The increased phosphorus intensity in the presence of ethanol compared to aqueous solution can be interpreted as the effect of ethanol on nebulization efficiency and on the excitation conditions in plasma. The latter may be a result of change in the excitation temperature [9] and in the configuration and structure of the plasma. The longitudinal distribution of spectral intensity changed with ethanol concentration, as was shown by Ito et al. [10]. The radial distribution of the argon line intensity was observed 15 mm above the coil. The results in Fig. 2 indicate that in the presence of the ethanol, the axial tunnel in the plasma becomes wider, which may diminish resistance

TABLE 2

Comparison of some characteristics of aqueous and aqueous 8% (v/v) ethanol systems (P 213.618-nm line; 50 μg ml^{-1} P as orthophosphoric acid

Figure of merit[a]	Aqueous solution	Aqueous 8% ethanol[b]	
		1.0	0.9
DL (μg ml^{-1})[c]	0.04	0.05	0.04
BEC (μg ml^{-1})	4.70	3.20	2.70
I/I_b	11.67	16.30	19.62
I_{eth}/I_w[d]	—	1.62	2.25

[a]For definition, see text. [b]At carrier flow rates of 1.0 and 0.9 l min^{-1}. [c]Concentration of phosphorus equivalent to twice the standard deviation of the background signal as measured on a set of 11 matrix blanks. [d]$I_{eth} = I - I_{beth}$; $I_w = I - I_{bw}$, where I_{beth} and I_{bw} are the ethanol and water blank intensities respectively.

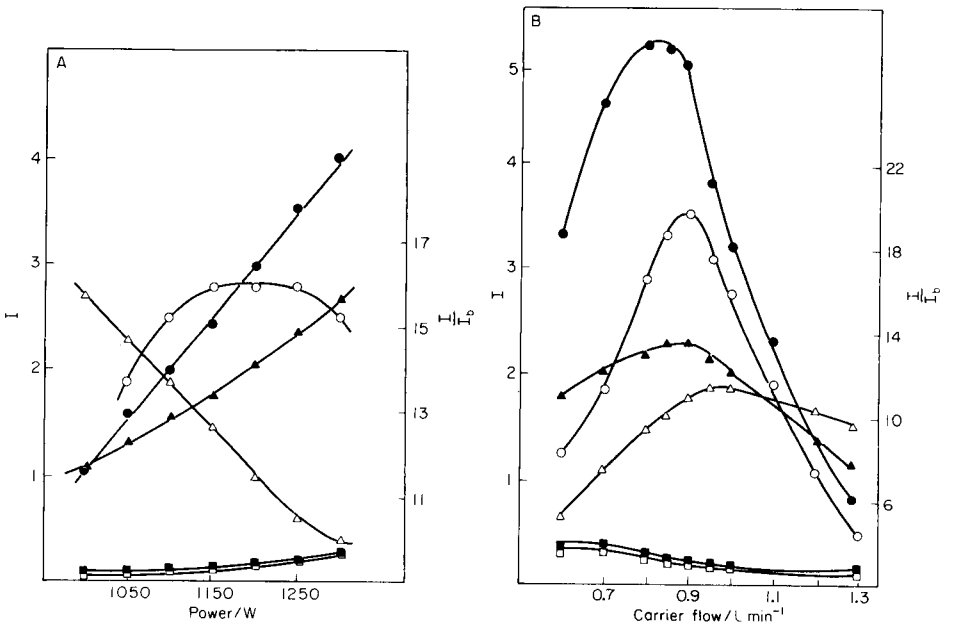

Fig. 1. (A) Effect of r.f. power and (B) effect of carrier gas flow rate on the intensity of the P 213.618-nm line. Intensity for 50 μg ml^{-1} P as orthophosphoric acid: (●) in 8% ethanol; (▲) in water. Intensity of blank: (■) in 8% ethanol, (□) in water. Sample-to-blank intensity ratio: (○) in 8% ethanol; (△) in water. Intensity is given in arbitrary units.

to the introduction of aerosols. More detailed studies of the effect of ethanol on the determination of several elements are in progress.

Studies on phosphorus determination in organic compounds and complexes

The wavelength scans around the P 213.618-nm line for aqueous and 8% (v/v) ethanolic solutions containing 10 μg ml^{-1} P added as orthophosphoric

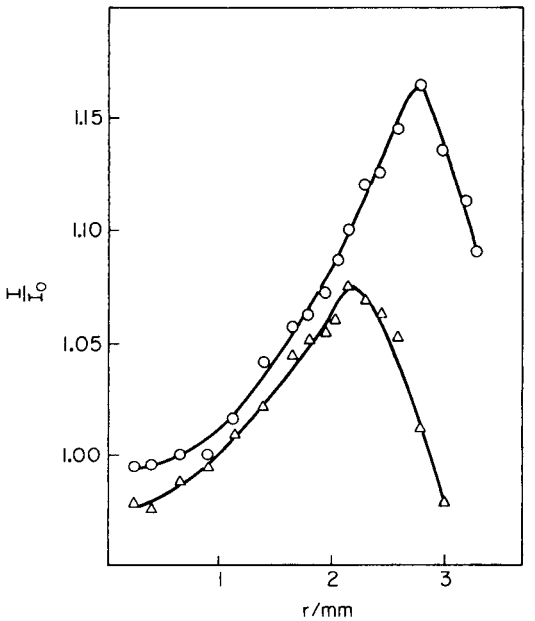

Fig. 2. Radial distribution (r = distance from plasma centre) of intensity of the Ar 355.471-nm line measured at an observation height of 15 mm: (○) 8% (v/v) ethanol; (△) water. I_0 is the intensity at the centre of the plasma (r = 0).

acid and tetraphenylphosphonium chloride were recorded. The differences in line intensities between the inorganic and organic compounds were negligible in both media, but the phosphorus signal from the 8% ethanol solution was significantly increased. The background levels were measured with different blanks: water, 8% (v/v) ethanol, 8% ethanol with tetraphenylarsonium chloride (200 μg ml^{-1}) and PAR, monosodium salt (100 μg ml^{-1}). The background spectra and intensities for the different blanks were very similar. Moreover, no significant effect on the intensity of phosphorus or the blanks was observed when different acids (sulphuric or nitric acid) were used in the same concentration range (2—5%).

To examine potential spectral interferences by metals present in the complexes, wavelength scans for phosphorus in solutions containing 10 μg ml^{-1} P (as phosphoric acid) and a particular metal ion (40 μg ml^{-1}) were recorded. Of the metals studied (Cu, Nb, V, Fe, Zn, Co), only copper seriously interfered at the P 213.618-nm and P 214.914-nm lines. For the determination of phosphorus in copper complexes, copper must be removed previously from solution by ion exchange. The spectral interference of copper on phosphorus could probably also be overcome by using a spectrometer with better resolving power.

Some evidence of the short- and long-term stability at the 213.618-nm and 214.914-nm lines is presented in Table 3. The short-term variability of phosphorus emission over the range 10—50 μg ml^{-1} expressed as relative standard

TABLE 3

Short- and long-term stability

No.	Phosphorus (μg ml^{-1})			Phosphorus (μg ml^{-1})		
	Added	Found[a]	Rel. error	Added	Found	Rel. error
	213.618-nm line			*214.914-nm line*		
1	10.22	10.25 (0.7)	+0.30	10.22	9.83 (0.8)	−3.80
2	25.00	24.84 (0.6)	−0.60	25.00	25.01 (0.8)	+0.04
3	51.20	51.00 (0.8)	−0.30	51.20	51.27 (0.7)	+0.13
4	10.22	10.43 (3.4)	+2.05	10.22	9.74 (4.4)	−4.70
5	25.00	25.19 (4.2)	+0.76	25.00	24.54 (5.4)	−1.80
6	51.20	51.82 (3.7)	+1.21	51.20	50.16 (4.8)	−0.08
7	10.22	10.31 (4.8)	+0.90	10.22	9.70 (5.4)	−5.10
8	25.00	25.08 (5.2)	+0.30	25.00	24.48 (6.3)	−2.10
9	51.20	51.10 (4.7)	+0.20	51.20	50.05 (5.2)	−0.30

[a]Mean result with r.s.d. in parentheses. (1—3) mean of 5 determinations over 3 min; (4—6) mean of 8 sets of 5 determinations over a 4-h period; (7—9) mean of all determinations over a 6-day period.

deviation (r.s.d.) was 0.6—0.8%. The r.s.d. for the blanks was about the same. Long-term stability (4-h measurements without adjustment of operating parameters) was 3—6%, calculated from 8 sets of 5 determinations on the same day; all measurements made over six days had an r.s.d. of 6%.

Preparation of sample solution and method of analysis

Sample solutions were prepared as described in the Experimental section. The simplest case was when the sample was appreciably soluble in water, ethanol or acid (sulphuric or nitric acid) and a clear solution was obtained after dilution. The precipitate of free ligand formed by dissociation of some of the complexes during dissolution did not affect the phosphorus results, if the precipitate was removed.

Compounds which were not soluble in the above solvents had to be decomposed by oxygen flask combustion or by Kjeldahl digestion. During the oxygen flask combustion, carbon was sometimes formed, indicating incomplete decomposition, so that the solution had to be filtered.

The calibration graphs used for the determination of phosphorus in organic compounds and metal complexes were prepared after blank signal subtraction. Ethanol and acid were added to the blank and calibration standards to match the major components of solutions. Phosphorus was added as aqueous orthophosphoric acid 0—50 μg ml^{-1} P).

The results obtained for several organophosphorus compounds and metal complexes are shown in Tables 4 and 5. The results obtained are reproducible and reasonably accurate. The three sample preparation methods gave comparable results. In a few cases, results were reproducible but not accurate enough. These compounds were impure, as was confirmed by determination of carbon and hydrogen by a standard microanalytical method.

TABLE 4

Results obtained for different phosphorus compounds
(Sample weight 1—10 mg; phosphorus concentration in measured solution 5—15 μg ml^{-1}.)

Compound[a]	Phosphorus			n	Sample solution prep.[c]
	Calc.	Found[b]	Diff. (%)		
$(C_6H_5)_3PO$	11.13	11.03 (2.34)	−0.10	15	D
		10.87 (3.75)	−0.26	7	C
$(C_6H_5)_4PCl$	8.26	8.15 (3.37)	−0.11	12	D
		8.09 (3.03)	−0.17	6	C
$C_4H_{11}O_3P$	22.46	21.28 (1.34)	−1.18	7	D
Na-MOABP	7.79	7.64 (2.33)	−0.15	6	C
KDETP	14.90	14.03 (0.94)	−0.87	5	D
Fosalon	8.43	8.23 (1.68)	−0.20	5	D
NaH_2PO_4	25.84	25.61 (0.74)	−0.23	5	D
$Na_4P_2O_7 \cdot 10H_2O$	13.90	13.53 (0.91)	−0.37	5	D

[a]MOABP, monooctyl-α-anilinobenzylphosphonate; KDETP, potassium diethylthiophosphate; Fosalon, 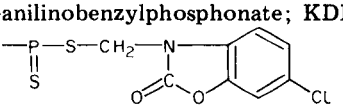 [b]Mean result with relative standard deviation (%) in parentheses. [c]D, dissolution; C, oxygen flask combustion.

TABLE 5

Determination of phosphorus in metal complexes
(Sample weight 4—10 mg, phosphorus concentration in measured solutions 4—10 μg ml^{-1}.)

Complex	Phosphorus (%)			Sample solution prep.[b]
	Calc.	Found[a]	Diff. (%)	
$[Ph_4P][Co(PAR)_2)] \cdot 2H_2O$	3.60	3.39	−0.21	D
		3.41	−0.19	C
		3.55	−0.05	K
$[Ph_4P][In(PAR)_2]$	3.59	3.59	0.00	D
		3.49	−0.10	C
$[Ph_4P][Cu(HPAR)PAR]$	3.73	4.04	+0.31	C
		3.59	−0.14	K, IE
$[Ph_4P][NbO(C_2O_4)PAR]$	4.13	3.97	−0.16	D
		3.95	−0.09	C
$[Ph_4P][Pd(Cl)PAR]$	4.46	4.20	−0.26	D
		4.34	−0.12	C
$[Ph_4P][VO_2PAR \cdot H_2O]$	4.68	4.45	−0.23	D
		4.65	−0.03	C
		4.06	−0.62	K
$[Ph_4P]_2[Ta\text{-mal.}]$	3.07[c]	3.11	+0.04	D
$[Ph_4P][Ta\text{-glyc.}]$	2.66[c]	2.61	−0.05	D
$[Ph_4P][Ta\text{-tart.}]$	2.45[c]	2.46	+0.01	D

[a]Mean of 3 determinations. [b]D, dissolution, C, oxygen flask combustion; K, Kjeldahl digestion; IE, copper removed by cation-exchanger. [c]Determined by titration [5].

REFERENCES

1 J. M. Cook and D. L. Miles, Analyst, 110 (1985) 547.
2 T. Ishizuka, K. Nakajima and H. Sunahara, Anal. Chim. Acta, 121 (1980) 197.
3 G. F. Kirkbright, A. F. Ward and T. S. West, Anal. Chim. Acta, 62 (1972) 241.
4 R. K. Winge, V. J. Peterson and V. A. Fassel, Appl. Spectrosc., 33 (1979) 206.
5 Lj. Marić, M. Široki and Z. Štefanac, Microchem. J., 21 (1976) 129.
6 W. Nisamaneepong, D. L. Haas and J. A. Caruso, Spectrochim. Acta, Part B, 40 (1985) 3.
7 A. Miyazaki, A. Kimura, K. Bausho and Y. Umeraki, Anal. Chim. Acta, 144 (1982) 213.
8 A. W. Boorn and R. F. Browner, Anal. Chem., 54 (1982) 1402.
9 H. Benli, Spectrochim. Acta, Part B, 38 (1983) 81.
10 T. Ito, H. Kawaguchi and A. Mizuko, Bunseki Kagaku, 28 (1979) 648; Chem. Abs., 92 (1980) 120316d.

Analytica Chimica Acta, 192 (1987) 183—195
Elsevier Science Publishers B.V., Amsterdam — Printed in The Netherlands

OPTIMIZATION OF A DIRECT-CURRENT PLASMA EMISSION ECHELLE SPECTROMETER

MARTHA S. HENDRICK[a] and ROBERT G. MICHEL*
Department of Chemistry, University of Connecticut, Storrs, CT 06268 (U.S.A.)
(Received 1st January 1986)

SUMMARY

Simplex optimization and Box-Behnken partial factorial experimental design techniques were used to optimize the quantitative performance of a direct-current plasma system. Argon pressure and plasma position were selected as variables. The simplex optimization located the region of optimum sensitivity, and the partial factorial design generated quadratic equations describing the relationship between the variables in this area. Results compared well with the results of a univariate search done in the region of optimum sensitivity. Canonical analysis of the response-surface equations showed that there was no unique optimum, but rather a stationary ridge, with combinations of conditions which give similar sensitivities. Studies of response surfaces for imprecision and drift failed to identify one optimal region. Comparison of the imprecision and drift contours with the sensitivity results showed that a significant improvement in precision or drift cannot be made by changing the instrumental conditions.

Many of the quantitative characteristics of the three-electrode direct-current plasma (d.c.p.) have been reported [1, 2], including the observation that signal drift was significantly improved over the two-electrode d.c.p. The aim of this study was to establish if the drift could be minimized and the signal-to-noise ratio improved by careful optimization of the instrumental factors and by a rigorous study of the interactions among those factors.

The d.c.p. has several instrumental variables which must be adjusted by the operator; they include argon gas pressure to the nebulizer and the electrode sleeves, the position of the plasma image on the entrance slit, which is controlled by an x-y positioner, and the slit dimensions. Relatively few factors are involved, but the problem is complicated because there are obvious interactions among the factors. Typically, for a particular combination of flow rates, signal is maximized by manually adjusting the position of the plasma while aspirating a sample of interest. The background can be checked by aspirating a blank. Unfortunately, a subsequent change of the flow rate may require a repetition of the entire procedure. Accordingly, it was considered necessary to study the relationships among the variables.

[a]Present address: United States Coast Guard Central Oil Identification Laboratory, Avery Point, Groton, CT 06340, U.S.A.

0003-2670/87/$03.50

Both the sequential and simultaneous (factorial design) approaches were used in this study. The sequential simplex optimization was used to define the region of factor space of most interest [3]. Factorial design and a response-surface analysis were used to study the interactions among the factors. A discussion of these two approaches can be found in Massart et al. [4]. The sequential simplex optimization technique has had several applications in atomic spectrometry [5—9]. Morgan and Deming [3] stressed the need to verify the optimum by another experiment. Univariate mapping (changing the factor levels of one variable at a time in the region of the optimum) is useful for indicating approximately how critical a particular variable is, but it is not sufficient to prove the existence of an optimum because interaction effects cannot be observed. A second-order model to approximate the response surface is sufficient to verify the presence of an optimum and to estimate the sharpness of curvature and the importance of interaction effects [10]. A recent study by Parker et al. [9] combined response-surface mapping and simplex optimization to study the hydride generation of arsenic and selenium for i.c.p. spectrometry.

In the present study, the simplex method was used to narrow the limits for the factors by optimizing the sensitivity of response for a copper wavelength. Copper was selected because its wavelength is used to align the multielement detector on the spectrometer. For the subsequent partial factorial design experiment, four factors were studied, which required twenty-seven experiments. Three responses (precision, drift and sensitivity) were calculated. Responses for six elements were collected simultaneously by using the multielement capability of the d.c. plasma emission spectrometer, for comparison with the copper results. The response-surface analysis for copper was compared with the results of a univariate search.

EXPERIMENTAL

Instrumental

A Spectraspan III echelle spectrometer system (Beckman Instruments), with a three-electrode d.c. plasma, was modified by removing the plasma from its uncalibrated positioners and mounting it on a laboratory-constructed support with calibrated positioners (C. A. Norgren Co.). A cassette with multiple exit slits and corresponding photomultiplier tubes provided multielement capability. The elements, species, and emission wavelengths were Cu I 327.4 nm, Co I 345.4 nm, Fe II 259.9 nm, Pb I 405.8 nm, Ni I 314.4 nm, and V I 437.9 nm. The entrance and exit slits were 0.050 × 0.300 mm, except for copper, nickel and iron, for which the exit slits were 0.025 × 0.300 mm.

Software

The simplex optimization software was based on an algorithm by Nelder and Mead [11]. Modifications [3] included the variable-step-size option

and the $n + 1$ rule. The response-surface analyses were based on the experimental design of Box and Behnken [12]. Canonical analysis [13, 14] was used to transform the second-order polynomial equations by translation to the center of the system and rotation of the axes to eliminate interaction terms. Such manipulation allows for easier interpretation of the polynomial equations. Listings of the simplex and canonical-analysis programs (BASIC) are available elsewhere [14]. The Box-Behnken response-surface program is listed in Fortran in [15].

Contour diagrams were prepared by using SAS Graph software (SAS Institute, Cary, North Carolina) on an IBM 3081 computer based on the polynomial equations generated by the Box-Behnken experiments. The simplex optimization, the calculations for the factorial design, and the canonical analysis were implemented on a Tektronix 4052 computer. A Data General Nova computer was used for the Box-Behnken response-surface analysis.

Experimental conditions for simplex

Factor selection for the simplex was based on variables which affect the plasma formation and the position of the plasma on the entrance slit. Plasma current is constant and cannot be changed. Instrumental variables, such as slit width, integration time, and photomultiplier tube voltage, which have physical properties which are well understood, were not optimized. New electrodes were used for each run. The variable boundaries for the experimental region were +5 to −5 mm from the reference point for the horizontal and vertical plasma positions, argon pressures of 35—55 psi for the nebulizer and 10—30 psi for the sleeves, and a full 360° rotation for the orientation of the solution inlet on the nebulizer. Boundaries for the factors were determined by the range in which the plasma would operate without visible turbulence. Initial vertices and step sizes were calculated according to a procedure described by Yarboro and Deming [16].

Evaluation of simplex response. The signal-to-noise (S/N) ratio was the response selected for simplex optimization. A 2 μg ml^{-1} aqueous solution of copper, which was within the linear region of the calibration curve, was aspirated into the plasma alternately with deionized water. The square root of the background measurement was used to approximate the deviation of the background. This assumes that the dominant noise is shot noise, but the S/N of the d.c.p. is not shot-noise limited. Hence, this response was not a true indicator of the S/N. However, the shot-noise calculation was done rapidly, and used to locate the region of interest for the factorial design experiment.

Experimental conditions for the factorial design

Four factors (the two position variables and the two argon flow variables) were used. The variables and values used for each level are shown in Table 1. The values of each variable were coded: high (+1), low (−1), and a midpoint (0). The rationale for the selection of a subset of experiments of a full factorial design is discussed in Box et al. [13].

TABLE 1

Variables and levels in Box-Behnken factorial design

Variable name		Coded factor levels		
		−1 low	0 midpoint[a]	+1 high
x_1	Horizontal position (mm)	−0.25	0	+0.25
x_2	Vertical position (mm)	−0.635	0	+0.635
x_3	Nebulizer pressure (psi)	20	25	30
x_4	Electrode sleeve pressure (psi)	44	47	50

[a]For each block of experiments, the nebulizer and sleeve flows were set at their midpoint values, and the x-y positioner was adjusted to the position of maximum signal intensity, which was then assigned the midpoint level.

Procedure. For each experiment, the instrument sensitivity was maximized on the copper line. A mixed-element standard solution containing each element (at concentrations from 2 to 5 μg ml^{-1}) was measured six times with an integration time of 10 s, and with a 6-s pause between integrations. A deionized water blank, acidified to 0.2% nitric acid, was run in the same manner, followed by a repetition of the above signal measurements. A pause of 1 min was allowed between each set of measurements. The instrument was not restandardized during each run, so that drift could be observed within the time scale of the experiment. Any experimental drift would increase the experimental error, because the experiments were run in random order.

Three responses were calculated for each experiment for all elements. First, sensitivity was evaluated as the average net signal (standard − blank) for the standard measurements divided by the standard deviation of the blank solution; these values were normalized with respect to the sensitivity of the standard used to calibrate the instrument at the midpoint of the experiment. Second, precision was evaluated as the average net signal divided by the standard deviation of six replicate integrations; this is the inverse of the relative standard deviation. Third, drift was evaluated as the absolute difference between the two sets of background-corrected average signal measurements divided by the mean of the two sets. Formulas for these calculations have been listed [15]. The responses as calculated were used to generate the Box-Behnken response-surface equations. For the purpose of displaying the results, it was later decided to express the responses in terms of percentages, but the original units were used in computations.

RESULTS AND DISCUSSION

Simplex optimization and univariate search at optimum

The simplex made rapid progress toward achieving an optimum signal-to-background ratio. Thirty-seven points were evaluated as vertices. Responses

were accepted or rejected according to the predetermined simplex rules [3]. This was done automatically by the computer program. The experiments were discontinued when the plasma became unstable because of electrode erosion. The simplex had located an area of greatly improved signal-to-noise ratio.

The results of holding the variables at the midpoint of the final simplex and changing one variable at a time are shown in Fig. 1. The arrows on each graph are directed to the experimental conditions when the simplex was terminated. This univariate search verified the importance of the four variables shown. The horizontal plasma position (Fig. 1A) was critical because the analytical region is small. The signal distribution for the horizontal plasma position was symmetrical, consistent with the plasma geometry. The zero position refers to the reference position at which the signal was peaked at the start of the experiments. The vertical plasma position (Fig. 1B) was also critical, probably because of the small size of the excitation region. The background from a water blank (Fig. 1A and B) increased as the plasma was moved. This increase corresponded to the approach of the image of the plasma core toward the slit. The vertical plasma position had its maximum signal response at the reference position, 0.0. The solid lines in Fig. 1 repre-

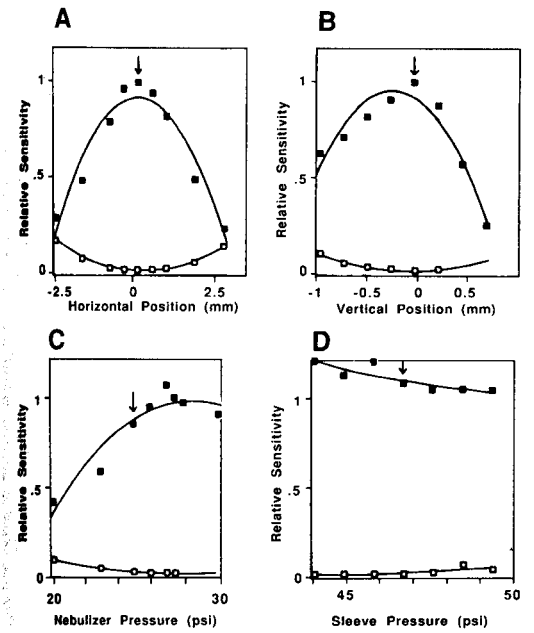

Fig. 1. Univariate search at mean of final simplex (horizontal and vertical positions adjusted to zero with nebulizer argon flow 17 psi, electrode sleeve flow at 47 psi). Variable parameter: (A) horizontal plasma position; (B) vertical plasma position; (C) nebulizer flow; (D) electrode sleeve flow. Background (□) and net signal (■) responses are shown.

sent the best quadratic fit for the experimental data shown. This second-order fit is shown in order to allow a comparison with the response surfaces discussed later, which are also based on quadratic equations. The use of second-order curve fits here is not meant to imply that the experimental points are best fitted to a second-order model.

Figure 1 (C and D) shows the effects of the nebulizer and electrode sleeve argon pressure. As the nebulizer flow was decreased, the background showed an increase which was similar to the variation of the vertical position. This was due to the plasma core image illuminating the slit. The plasma sleeve flow was the least critical of the four variables, and this search did not indicate an optimum at the mean value of the final simplex. The fifth variable, nebulizer position, did not have a reproducible effect on response, so it is not shown, and was fixed in one position for subsequent experiments.

Response surface

The Box-Behnken experiments resulted in a second-order regression equation with interaction terms, of the form

$$R = B_1 + B_2x_1^2 + B_3x_2^2 + B_4x_3^2 + B_5x_4^2 + B_6x_1 + B_7x_2 + B_8x_3 + B_9x_4 + B_{10}x_1x_2 + B_{11}x_1x_3 + B_{12}x_1x_4 + B_{13}x_2x_3 + B_{14}x_2x_4 + B_{15}x_3x_4 \quad (1)$$

where the B's are coefficients and the x's represent the coded levels for each factor shown in Table 1.

Before response-surface diagrams were examined, it was important to assess how well the regression equations fitted the experimental data. This was done by testing the goodness of fit of the data to the second-order model and by analysis of variance. The goodness of fit is defined as the square of the correlation coefficient, r. However, r^2 alone is not sufficient to evaluate the statistical significance of the results, because as r^2 decreases, it becomes more probable that there is so much variance in the experimental data that the theoretical model would fit equally well to randomly selected points. It is necessary for there to be more degrees of freedom than are required for the coefficients in the model. The goodness of fit, the number of experiments, and the degrees of freedom are all important in statistical interpretation of the results. The statistical significance of the results was assessed by means of analysis of variance. In this procedure, a critical value of F for the F-test is calculated from r^2, the number of coefficients, n, and the degrees of freedom, v_1, as

$$F = v_1 r^2/[n(1 - r^2)] \quad (2)$$

The Box-Behnken experiment resulted in 15 coefficients (Eqn. 1). The number of degrees of freedom, v_1, is calculated from the number of experiments, N, according to $N - (n + 1)$. In this experiment, $N = 27$, so that $v_1 = 27 - (15 + 1) = 11$. In these experiments, the critical value of F was 2.51, based on 11 and 15 degrees of freedom and a 95% confidence level.

The models were evaluated for statistical significance by the *F*-test, using the 95% confidence level as the criterion. The results for copper sensitivity passed the *F*-test; sensitivity results for the other elements did not. The precision responses for four elements (copper, cobalt, lead and vanadium) and the drift responses for five elements (copper, cobalt, lead, nickel and vanadium) passed the *F*-test. Box-Behnken coefficients, for statistically significant results, have been tabulated [15].

Contour diagrams

Sensitivity. Contour diagrams of copper sensitivity as a function of horizontal and vertical plasma position are shown for several different combinations of argon flow conditions in Fig. 2. It can be observed in Fig. 2A that an area of maximum sensitivity was found at the midpoint for the system. This area was located at the 0.0 position, which was where the sensitivity was maximized each day before the experiments were run. Sensitivity is expressed here as a percentage of the maximum sensitivity observed after peaking the plasma intensity. Changing the flow rates (Fig. 2B) to a high nebulizer and low sleeve flow moved the area of the maximum, but did not affect the sensitivity. Figure 2C shows low nebulizer and sleeve

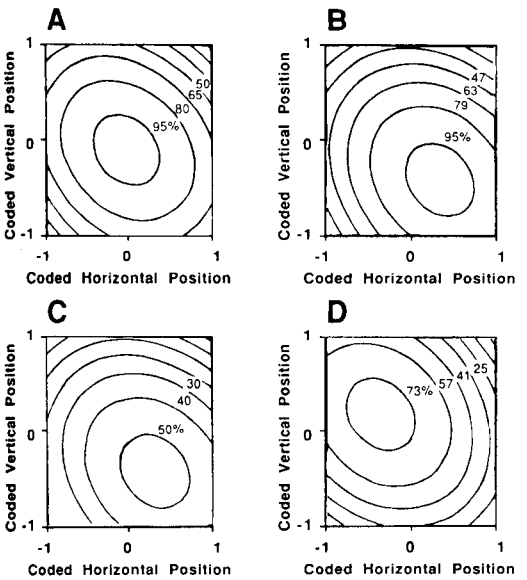

Fig. 2. Contour diagrams of Box-Behnken response-surface analysis for copper sensitivity, in units of percent of maximum sensitivity observed. Horizontal and vertical plasma positions are shown for different combinations of argon flows. Coded levels (see Table 3) are used in the axes. (A) Moderate nebulizer flow, moderate electrode sleeve flow; (B) high nebulizer flow, low sleeve flow; (C) low nebulizer flow, low sleeve flow; (D) low nebulizer flow, high sleeve flow.

flows; a contour similar to Fig. 2B was obtained, but with only half of the maximum sensitivity response. Figure 2D shows a shift in the location of the optimum plasma region with low nebulizer flow and high sleeve flow. This time, 75% of the maximum observed response was observed. The significance of the results shown in Fig. 2 is that changing plasma sleeve flow and nebulizer flow shifted the location of the area of maximum sensitivity, and that the maximum response was sometimes affected. More important, however, is the observation that sensitivity did not always deteriorate with changing plasma position.

Sensitivity results for cobalt, iron, lead, nickel and vanadium did not pass the *F*-test at the 95% confidence level. This is probably due to the fact that copper was the element that was used to maximize the response of the multielement cassette. It is possible that small shifts in the maximum signal for the other elements relative to copper from one day to another were great enough to prevent reproducibility in the sensitivity values. Because these were relative signals which were normalized for each set of experiments, the magnitudes of the shifts and their effects cannot be determined.

Precision and drift. Figure 3 shows the precision and drift of the copper data. These can be compared with the sensitivity contours in Fig. 2A. The contours in Fig. 3 were relatively flat compared to the sensitivity contours, which decreased much more steeply from the maximum. A small improvement in the precision (expressed here as the relative standard deviation) in Fig. 3A was observed upon moving the plasma horizontally and vertically relative to the reference position. A negative value in the vertical direction indicates lowering the plasma. As the plasma was moved toward more negative values, radiation from the plasma core increased the background. Moving the plasma horizontally had the same effect. Here negative values were defined as lateral movement of the plasma, so that the left side of the plasma image moved toward the slit. The plasma image was inverted by a lens, so that actual movement was in the opposite direction, although the direction of the movement in fact has no significance in the context of this paper. The exact relationship of the reference position to the plasma image was not quantitatively established, because of the very small plasma region considered. However, the image of the plasma at the reference position appeared to lie along the plane of symmetry of the plasma and offset from the plasma core in the vertical direction.

The drift (Fig. 3B) showed that the region of maximum sensitivity did not coincide with the region of minimum drift. The worst drift was apparently recorded for the best sensitivity. This is probably a result of the fact that flicker noise is proportional to signal size. Hence, at the boundaries of the experimental region, the signals were so small that drift, as defined here, was not detected, thus making it appear that noise had improved.

Results for other metals were similar to the drift results for copper illustrated by Fig. 3B. Compared to the sensitivity plots, precision and drift

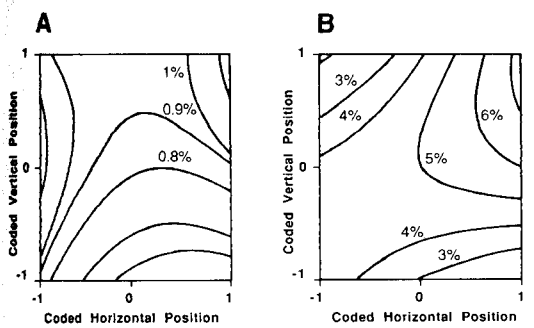

Fig. 3. Contour diagrams of Box-Behnken response-surface analysis for copper. Effects of variation of horizontal and vertical plasma positions are shown for argon flows at the midpoint. Coded levels (Table 1) are given. (A) Precision; (B) drift. Both are expressed as percent relative standard deviation.

were less sensitive to changes in instrumental conditions and showed less curvature. Precision varied between 0.85 and 1.25% (relative standard deviation, RSD) and drift varied between 2 and 6%. The lowest drift was observed at positions close to the plasma core.

Comparison with univariate search. Cross-sections of contour diagrams for comparison with the univariate search are shown in Fig. 4. These contours, generated by the same equations used for the response surfaces, were based on fewer points than the univariate search and show *S/N* ratios rather than net signals. However, the shapes of the curves are similar to the quadratic fit

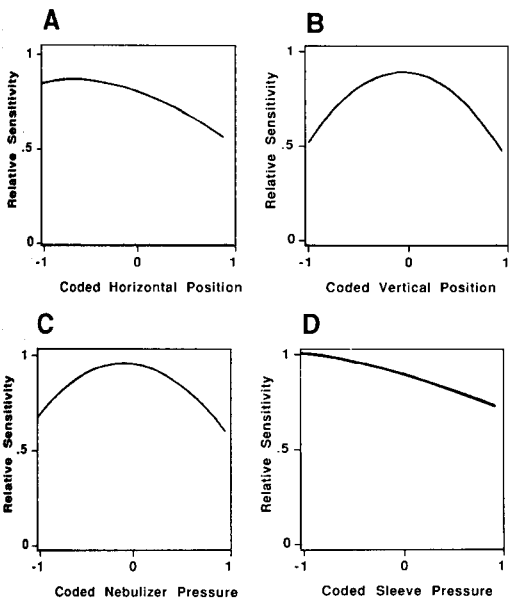

Fig. 4. Response-surface cross-sections for copper sensitivity for the conditions used in the univariate search (Fig. 1). Variable parameter: (A) horizontal plasma position; (B) vertical plasma position; (C) nebulizer flow; (D) electrode sleeve flow are shown. Sensitivity values are normalized. Coded levels (Table 1) are used on the axes.

shown in Fig. 1, so that the conclusions about the relative effect of the different factors are the same. Comparison of the curves of Fig. 4 with both the experimental points and the quadratically-fitted curves (Fig. 1) suggests that deviation from the line is caused by the lack of fit of the response-surface equations to a second-order model. This does not affect the location of the area of the optimum.

Canonical analysis

The mathematical technique of canonical analysis was used to transform the regression equations from the Box-Behnken response surface to forms which were more easily interpreted. This involved translating the origin to a new point, and rotating the axes with respect to the axes of the contours. This eliminated first-order terms as well as interaction terms, so that the form became

$$R = A_0 + A_1 X_1^2 + A_2 X_2^2 + A_3 X_3^2 + A_4 X_4^2 \quad (3)$$

The canonical equation is much simpler than Eqn. 1, although the information contained in the two equations is the same. According to Box et al. [13], inspection of the form of the canonical equation is sufficient to identify whether the system has a local maximum, a local minimum, a saddle point, or a ridge.

The canonical equations which resulted from this experiment had only one major canonical axis, which indicates a stationary ridge [13]. Although four coefficients were always evaluated, coefficients for three axes were so small (less than 10^{-6}) that they could be neglected. This resulted in one major axis for each system. The coefficients for the major axes are shown in Table 2. The determination of only one major axis, or stationary ridge, means that there is no one combination of variables which gives an optimum response. This is the most desirable situation for quantitative applications.

If a unique optimum had been found, it would have been located at the center of the system, the point to which the system was translated. The experimental conditions at the calculated center for the canonical analysis of each system are listed in Table 3. For ease of interpretation, the coded factor levels have been expressed in physical units for each variable, rather than coded factor levels. These systems had stationary ridges, so the location of the center of the system does not have a physical meaning. This is because the response-surface equation extended outside the experimental area, where it may not describe the true physical response.

The predicted optimum response for the system is listed in Table 3. This was calculated by substituting $X = 0$ into the canonical equation. When the center of the system lies significantly outside the experimental areas bounded by +1 to −1, the predicted response cannot be relied upon. In the case of vanadium, the results were physically impossible. This illustrates the problems of extrapolating an equation outside of the experimental area which was used to develop it. Measurements of drift and precision in areas of

TABLE 2

Canonical equations for Box-Behnken optimization

Feature	A_0 [a]	A_1 [b]
Sensitivity		
Cu	0.95	−0.30
Drift		
Cu	0.05	0.03
Co	0.03	−0.02
Fe	0.04	0.05
Ni	0.08	−0.02
V	0.04	−0.03
Precision		
Cu	108	−31
Co	86	−10
Pb	53	18
V	−5.6	−24

[a]Coefficient for intercept from Eqn. 3. [b]Coefficient for slope from Eqn. 3. A_2–A_4 are not listed (coefficients $<10^{-6}$).

TABLE 3

Coordinates and responses at the center of the system

Feature	Horizontal position (mm)	Vertical position (mm)	Nebulizer flow (psi)	Plasma sleeve flow (psi)	Optimum response
Sensitivity					
Cu	−0.091	0.13	23.6	50.1	95%[a]
Drift					RSD[b]
Cu	0.056	0.36	24.8	48.4	5.1
Co	−0.034	0.21	27.1	47.4	3.2
Fe	0.049	−0.10	27.2	47.1	4.2
Ni	0.018	0.04	25.7	47.4	7.8
V	−0.004	0.56	25.9	47.9	3.6
Precision					RSD[c]
Cu	−0.036	0.15	24.0	48.0	0.9
Co	−0.025	0.10	26.0	47.4	1.2
Pb	0.36	0.62	20.6	44.5	1.9
V	0.47	1.47	32.4	51.4	−18.0

[a]Sensitivity is expressed relative to the conditions set before each block of experiments. [b]Drift was originally expressed as a fraction of the signal, rather than a percentage, so that the calculated response was multiplied by 100 to obtain the values in this table. [c]Precision was expressed here as the relative standard deviation (RSD), the reciprocal of the response used in the response surface equation.

low signal may not reflect true improvement. For this reason the quantitative relationships for the best response for any metal for drift and precision cannot be relied upon.

Implications for the selection of analytical conditions

The instrument response was maximized before each block of Box-Behnken experiments in a routine manner by alternately aspirating standard solutions and blank, and seeking the highest standard response and the lowest blank as the x- and y-positioners were adjusted. For copper sensitivity, the results of the experiment verified that conditions which had previously been selected in the optimization procedure compared very favorably to those indicated by the Box-Behnken response-surface analysis. This is because the optimizing procedure is a univariate search. In the presence of a stationary ridge, such a search can be expected to locate an optimum.

Precision and drift both showed less than optimum conditions in the region of maximum sensitivity. However, the region of maximum sensitivity was surrounded by areas of relatively small change in both precision and drift. It is preferable to select this normal quantitative region and correct for drift by using either recalibration or mathematical techniques than to operate in a region of poor sensitivity. These experiments served to characterize drift as intrinsic to all operating conditions, revealing no particular instrumental conditions which both maximized sensitivity and minimized drift.

Acknowledgement is made to the United States Coast Guard Research and Development Center, Groton, CT, for the use of facilities and the d.c.p. instrument. R. G. M. was supported by a Research Career Development Award from the National Institutes of Environmental Health Sciences under grant number ES00130.

REFERENCES

1 G. W. Johnson, H. E. Taylor and R. K. Skogerboe, Spectrochim. Acta, Part B, 34 (1979) 197.
2 R. J. Decker, Spectrochim. Acta, Part B, 35 (1980) 19.
3 S. L. Morgan and S. N. Deming, Anal. Chem., 46 (1974) 1170.
4 D. L. Massart, A. Dijkstra and L. Kaufman, Evaluation and Optimization of Laboratory Methods and Analytical Procedures, Techniques and Instrumentation, Elsevier, Amsterdam, 1978, p. 215.
5 L. Ebdon, M. R. Cave and D. J. Mowthorpe, Anal. Chim. Acta, 115 (1980) 179.
6 S. P. Terblanche, K. Visser and P. B. Zeeman, Spectrochim. Acta, Part B, 36 (1981) 293.
7 J. J. Leary, A. E. Brookes, A. F. Dorrzapf and D. W. Golightly, Appl. Spectrosc., 36 (1982) 37.
8 R. G. Michel, J. Coleman and J. D. Winefordner, Spectrochim. Acta, Part B, 33 (1978) 195.
9 L. R. Parker, Jr., N. H. Tioh and R. M. Barnes, Appl. Spectrosc., 39 (1985) 45.
10 A. S. Olansky and S. N. Deming, Anal. Chim. Acta, 83 (1976) 241.
11 J. A. Nelder and R. Mead, Comput. J., 7 (1965) 308.
12 G. E. P. Box and D. W. Behnken, Technometrics, 2 (1960) 455.

13 G. E. P. Box, W. G. Hunter and J. S. Hunter, Statistics for Experimenters, Wiley, New York, 1978, p. 532.
14 S. L. Morgan, Ph.D. Dissertation, Emory University, 1975, Diss. Abst., 36 (1976) 3343.
15 M. S. Hendrick, Ph.D. Dissertation, Univ. of Connecticut, 1985, Diss. Abst., 46 (1986) 2281.
16 L. Yarboro and S. N. Deming, Anal. Chim. Acta, 73 (1974) 391.

Analytica Chimica Acta, 192 (1987) 197—203
Elsevier Science Publishers B.V., Amsterdam — Printed in The Netherlands

TRANSFER OF NEAR-INFRARED MONOCHROMATOR CALIBRATIONS FOR TOBACCO CONSTITUENTS TO TILTING-FILTER INSTRUMENTS

ROBERT A. HECKMAN*, JOHN T. DIFFEE and L. ARTHUR MILHOUS, Jr.

R. J. Reynolds Tobacco Company, Bowman Gray Technical Center, Reynolds Boulevard, Winston-Salem, NC 27102 (U.S.A.)

(Received 27th March 1986)

SUMMARY

Near-infrared calibrations for water, reducing sugar, glycerin, propylene glycol, nicotine, and menthol in tobacco blends were first obtained with a monochromator instrument. Transfer of calibrations to a tilting-filter instrument for factory trials is shown to be facilitated greatly by the computer-assisted scheme MTRAN. By means of this software, calibration equations were established for a Neotec 51A instrument that is sufficiently rugged for factory use. The predictive capabilities of the transferred calibrations are similar to those of the research monochromator.

The use of diffuse-reflectance measurements in the near-infrared (i.r.) region (1100—2500 nm) for routine determinations of major components in agricultural commodities dates from the late 1960s. More recently, this technique was extended to the analysis of ground tobacco by McClure and co-workers [1—3]. The chief advantages of this instrumental method are its speed and potential for real-time process monitoring.

Most near-i.r. instruments are committed to measurement of moisture, oil, protein and starch in grain and forage crops. There seems to be a paucity of published reports where near-i.r. spectrometry has been utilized for in-plant monitoring of other constituents and products. Even rarer are explicit, published protocols whereby an analytical method developed on a scanning instrument in a laboratory can be transferred to one or more slave instruments. The scheme described herein requires a normalization set of ca. 20 samples. In contrast, recalibration for several of the tobacco constituents would have required >100 samples, including replicate analyses of these samples by independent laboratory methods.

Research in this laboratory generally begins with calibration work using a grating monochromator equipped with capabilities for derivative mathematics, graphics and statistics. This requires the availability of analytical data from a primary or referee laboratory method that is accurate and precise. For the past five years, investigators in this laboratory [4] have developed near-i.r.

0003-2670/87/$03.50

calibrations for a variety of tobacco constituents and additives, including moisture, nicotine, sugar, glycerin, propylene glycol and menthol. Most of this work was originally done on a research instrument. Because this instrument is not rugged enough for factory operation, it is necessary to transfer the calibration equations derived for the research instrument to a more rugged, cheaper, tilting-filter instrument. This task is not trivial because of optical differences between the instruments and differences in the smoothing routines used in derivative transformations by the various instruments.

A multiple-term linear regression equation for near-i.r. use has the general form

$$\% Y = C0 + C1(X1) + C2(X2) + \ldots Cn(Xn)$$

where Y is a tobacco constituent or additive, $C0$ is the Y intercept, $C1$, $C2 \ldots Cn$ are coefficients (slope constants) for $X1$, $X2 \ldots Xn$, the mathematically treated optical data (usually derivatives).

Whereas equations can simply be keyed into a second or slave instrument, followed by appropriate slope and/or bias corrections indicated by subsequent performance, this is not an attractive method of transfer to tilting-filter instruments where center frequencies of filters are specified to ±5 nm. A computer-assisted protocol for such transfers has been provided by Pacific Scientific Co., the manufacturer of the instrumentation used in this investigation. The primary tool for making such transfers is a computer program called MTRAN. This program redefines the wavelengths and coefficients for each term in the new equation individually. This treatment is quite different from a simple bias and slope correction (which would uniformly adjust all coefficients). The primary goal of the research reported in this paper was to exercise and evaluate MTRAN by transfer of multiple calibration equations from the Neotec 6350 monochromator instrument to the 51A tilting-filter instrument.

EXPERIMENTAL

Instrumentation

A hard-wired communication link was required between the two computer-operated spectrophotometer systems. The first or "master" system was a Pacific Scientific 6350 near-i.r. instrument consisting of a model 6100 monochromator and NOVA-4 computer with various peripherals. The second or "slave" instrument was a Pacific Scientific six-filter 51A scanning near-i.r. instrument that was controlled by a NorthStar ACT-1 computer equipped with an Epson FX-80 printer. The 51A instrument is also capable of stand-alone operation by means of an inboard microprocessor. A communication link was established between the back plane of the NOVA-4 and the RS232 port on the NorthStar ACT-1 computer that is normally used to interface with the 51A instrument. All software for operation, data acquisition and storage, and file transfer was supplied by the Pacific

Scientific Company. The program used for general operation of the 51A instrument is referred to as NSAS.

Development of calibrations

All of the calibrations described herein were developed on the 6350 system. Following the regression and iterative work to derive tentative equations, these equations were applied to sets of prediction samples for assessment of predictive capability. Next, sample sets consisting of 20—25 samples were presented to both the 6350 and 51A instruments. The TRANSFER programs associated with both instruments were then used to transfer data file and calibration file data to the ACT-1 computer (after setting the ACT-1 baud rate to 2400 by UART) from the 6350 system. With both data files and the 6350 calibration file resident in the same disk sector of the ACT-1, MTRAN is then used to re-establish new wavelengths (in pulse points, an engineering term directly related to wavelength in nm for a specified configuration of filters) and coefficients suitable for 51A operation.

After the revised equation had been obtained, the new equation was applied to a set of 20—25 samples (the above normalization set can serve for this purpose) with the 51A spectrometer. From the prediction statistics obtained, a standard error of bias (SE_{bias}) was calculated [5] as $SE_{pred}/n^{1/2}$ where n is the number of samples in the prediction set and SE_{pred} is the standard error of prediction.

To require a bias adjustment, the bias (obtained automatically from each prediction result using the PERCENT program, and numerically equal to the intercept resulting from linear regression of reported vs. calculated $\%Y$) must fall outside $0 \pm 2SE_{bias}$. Likewise, the standard error of the slope was calculated for each revised equation according to the equation [5] $SE_{slope} = [(1-r^2)/(n-1)]^{1/2}$, where r is the multiple correlation coefficient (obtained from the regression results). To require a slope adjustment, the slope (also obtained from the regression results) must fall outside $1 \pm 2SE_{slope}$. The above criteria were applied to all calibration equations described herein, and the slopes and biases were corrected, if required.

Tobacco constituents

Data pertaining to the original and transferred equations for various tobacco constituents are summarized in Table 1. Brief background information regarding the calibration effort for individual constituents is given below.

Moisture. The original (6350) water (moisture) calibration was done using only mentholated cut filler tobacco. However, the normalization samples for the purpose of calibration transfer were numerous brands of packaged cigarette products (metholated and regular) as well as test products. Sample selection was based entirely on obtaining a good range (8—13%) of moisture values. As for all of the constituents described below, the prediction work was done with the normalization file data.

TABLE 1

Calibration transfer results

Model 6350			Model 51A		51A linear regression results			
Coefficient		λ (nm)	Coefficient	λ (nm)	Slope	Intercept	SE_{pred}	Multiple r
Moisture[a]								
$C0$	15.377	—	10.8691		1.00	0.00366	0.336	0.971
$C1$	105.888	1910	143.4946	1939				
$C2$	−89.945	2424	−126.2787	2446				
Glycerin[b]								
$C0$	−0.800	—	−4.6759		0.999	0.00639	0.339	0.843
$C1$	−355.712	2272	−578.8540	2267				
$C2$	−99.0832	2220	175.6598	2208				
$C3$	−39.445	2330	−27.2241	2292				
Propylene glycol[b]								
$C0$	−0.649	—	−0.8829		1.00	0.000406	0.193	0.507
$C1$	−202.035	2260	90.4198	2264				
$C2$	193.634	2460	−100.8188	2408				
$C3$	−128.773	2404	53.2020	2402				
Nicotine in 40-mesh tobacco[b]								
$C0$	1.9909	—	5.1248		1.00	0.00105	0.141	0.978
$C1$	−176.683	2248	542.9519	2243				
$C2$	−178.422	2448	430.1403	2227				
Nicotine in 10-mesh tobacco[b]								
$C0$	1.9909	—	4.3643		0.998	0.00623	0.148	0.976
$C1$	−176.683	2248	660.8517	2239				
$C2$	−178.422	2448	−425.9769	2280				
Nicotine in cut tobacco filter[b]								
$C0$	1.9909	—	3.1127		0.998	0.00525	0.176	0.965
$C1$	−176.683	2248	587.5582	2235				
$C2$	−178.422	2448	−254.7876	2339				
Reducing sugar in 40-mesh tobacco[c,d]								
$C0$	−6.519	—	−12.3589		1.10	−0.856	1.13	0.863
$C1$	9.088	2454/2282	11.7702	2449/2282				

[a] $\log 1/R$. [b] $D2$ ($\log 1/R$). [c] $D1$ ($\log 1/R$). [d] Similar results were obtained for 10-mesh tobacco and cut tobacco filler.

Glycerin and propylene glycol. The monochromator work for these constituents utilized duplicate samples of 52 cigarette brands (regular and mentholated) chosen to provide a reasonable range for both constituents. Optical data for the 51A instrument were averages of triplicate sample values.

Nicotine and reducing sugar. The calibration work regarding nicotine and sugar in dried, 40-mesh, flue-cured tobacco was done in 1981 [6]. The

sample set consisted of 200 samples from 1977 to 1978 crop years. Half of the samples were used for calibration, and the other half was used to test the accuracy and reliability of those calibrations. The normalization sample set (also used to predict the resulting 51A calibrations) consisted of specially prepared blends of typical commercial blend components that were designed to afford a nicotine range of 1.2—3.7%. Reducing sugar values, which were allowed to "float", fell in the range 5.9—13.8%. Two additional normalization sets were prepared from the original blends of cut filler. One was prepared by grinding in a Wiley mill at ambient humidity to 10 mesh; the other set was dried and ground to 40 mesh in preparation for the routine (Auto-Analyzer) laboratory method. Each set consisted of 26 samples; the near-i.r. data were acquired in triplicate for the cut filler samples.

Menthol in cut filler

The original monochromator research utilized 13 different blends of mentholated cut tobacco filler ranging from 0 to 1% in menthol abundance. Eight replicate samples were examined and the results averaged for each reference laboratory result. Near-i.r. data were recorded for triplicate samples, and each sample was scanned in triplicate. The best performing regression resulting from examination of 135 samples utilized a second-derivative transformation and displayed a standard error of calibration (SE_{cal}) of 0.091 (multiple r = 0.963) and a standard error of prediction (SE_{pred}) of 0.100 for a 63-sample set.

The calibration was transferred to the 51A instrument by use of different application software; this program (INTERFACE, a predecessor system of MTRAN) was operated on the 6350 NOVA-4 computer after a 20 sample normalization set had been read by both instruments. The original and newly-established equations are described in Table 2. Both instruments were used to predict % menthol in the 20 normalization samples. Prior to examination of a second independent set of 20 samples, the new calibration was manually keyed into the model 51A filter instrument for stand-alone operation. The standard errors of prediction for the normalization set (interfaced to the NOVA-4) were 0.177 (6350) and 0.183 (51A), and for the independent set (stand-alone mode) were 0.173 and 0.161, respectively.

The 51A instrument was next relocated in a cigarette factory where 12 samples per day (average of 3 sample cup readings per sample) were analyzed for three consecutive days. These data, together with corresponding laboratory wet-chemical data were used to correct for bias. Two equations were finally developed for routine use, one for products containing high percentages of expanded tobacco, and another for all other products. A total of 104 samples, representing five different brands, were than analyzed at this location over several weeks. The overall SE_{pred} was 0.093 with a bias of 0.03.

TABLE 2

Calibration transfer results for menthol

Model 6350 coefficient		λ (nm)	Model 51A coefficient		λ (nm)
*C*0	0.678		*C*0	−1.5206	
*C*1	−353.604	2302	*C*1	−664.663	2305
*C*2	365.967	2436	*C*2	831.885	2430
*C*3	−352.644	2266	*C*3	−701.429	2277

DISCUSSION

Calibration and operation of near-i.r. instruments can be done in either of two modes, depending on the overall purpose. These are an enumerative mode, involving calibration and prediction on a closed sample population, and an analytical mode, for calibration on a closed sample population to predict an open population. The latter mode requires demonstration of a cause and effect mechanism, such as exists in absorption band spectroscopy.

Near-i.r. spectra, including various derivative transformations, of numerous tobacco constituents and additives had been recorded previously [4]. However, these data and calibration research results have not previously been published. As can be seen from Table 3, quite good agreement exists between visually prominent maxima and minima present in the spectra of these materials and the primary wavelengths resulting from 6350 calibration work. Primary wavelengths resulting from the transfer of equations to the 51A instrument are also in good agreement with these values.

Observations on the use of MTRAN

MTRAN is menu-driven and was found to run smoothly. In all the preceding work, the resulting 51A wavelengths were selected by the system. With some calibrations (e.g., nicotine, propylene glycol), the system-selected secondary or supporting wavelengths for 51A calibration were very different from those for the original 6350 calibration. In all cases, the newly-defined wavelengths and equations were accepted for 51A use.

Shortly after this work was completed, it was learned from Pacific Scientific personnel that other users of MTRAN had experienced difficulty in effecting calibration transfers with this software when care was not exercised to ensure that the 51A was properly configured with filters so as to accommodate the wavelengths in the master or 6350 calibration equation. Consequently, a new protocol was developed whereby monochromator data files are compressed to simulate a tilting-filter instrument. The resulting data file is used to re-establish the calibration equation. CALTRAN, a program formerly used only for calibration transfer between filter instruments, is used to effect calibration transfer.

TABLE 3

Comparison of spectral maximum/minimum and primary calibration wavelengths

Constituent[a]	Wavelength (nm)		
	λ[b]	6350	51A
Water	1940	1910	1939
Glycerin	2277	2272	2267
Propylene glycol	2263	2260	2264
Nicotine	2250	2248	2243
Reducing sugar	2420—2460	2454	2449
Menthol	2301	2302	2298

[a]Calculation as in footnotes to Table 1. [b]Spectral maximum or minimum.

Results for particular constituents

Prediction work with equations transferred to the 51A yielded SE_{pred} and multiple correlation values comparable to those obtained by use of the 6350 monochromator. However, by maintaining control charts for extended use, it became obvious that some equations predicted much better than others; i.e., the nicotine and moisture equations performed much better than those for the humectants, glycerin and propylene glycol (as might be expected from the multiple r values). The humectant calibrations were selected for transfer prior to completion of the monochromator work; they were simply the only equations containing wavelengths that could be supported by the current filter configuration residing in the 51A instrument.

The authors gratefully acknowledge the assistance of Mrs. Rebakah J. Dunn and Ms. M. Katherine Craver for sample preparation and instrumental work, Mr. Ted A. Harper for blend preparation, and the R&D Analytical Services Division for analytical support.

REFERENCES

1 W. F. McClure, K. H. Norris and W. W. Weeks, Beitr. Tabakforsch., 9 (1977) 13.
2 A. Hamid, W. F. McClure and W. W. Weeks, Beitr. Tabakforsch., 9 (1978) 267.
3 W. F. McClure and R. E. Williamson, Beitr. Tabakforsch., 11 (1982) 219.
4 J. T. Diffee and P. J. Cooper, unpublished work.
5 J. L. Casciero, E. J. DiGiovanni, P. J. Cooper, T. G. Kelly, T. W. Nolan, L. D. Stokes and K. A. Taschner, Operator's Manual for the Mark II 6350 System Near-Infrared/Visible Research Composition Analyzer, Pacific Scientific Co., Silver Spring, MD, 1983, pp. 574—583.
6 P. J. Cooper, unpublished results.

Analytica Chimica Acta, 192 (1987) 205—213
Elsevier Science Publishers B.V., Amsterdam — Printed in The Netherlands

PULSED COULOMETRIC DETECTION OF CARBOHYDRATES AT A CONSTANT DETECTION POTENTIAL AT GOLD ELECTRODES IN ALKALINE MEDIA

GLEN G. NEUBURGER and DENNIS C. JOHNSON*
Department of Chemistry, Iowa State University, Ames, IA 50011 (U.S.A.)
(Received 21st August 1986)

SUMMARY

A significant increase in the signal-to-noise ratio for the pulsed amperometric detection (PAD) of carbohydrates at gold electrodes is obtained by increasing the length of the current integration period (t_i) from the traditional value of 16.7 ms (i.e., 1/60 Hz). For $t_i \gg 16.7$ ms, the integrated response (q, coulombs) is plotted as the signal. This pulsed coulometric detection (PCD) is applied in a flow-injection system. For t_i = 500 ms, the detection limit with the instrumentation used is 1 μM (S/N = 2) for glucose which is a significant improvement on the value 35 μM found with PAD. The absolute detection limits for glucose and sucrose are ca. 50 pmol and 125 pmol, respectively, in 50-μl samples. Calibration plots (q_p vs. C^b) for PCD are linear over significantly larger dynamic ranges than those observed for PAD because of the lower detection limits.

Pulsed amperometric detection (PAD) at platinum and gold electrodes has been applied successfully to flow-injection and liquid chromatographic systems for numerous aliphatic compounds including virtually all alcohols and carbohydrates [1—8], amines and amino acids [9], aminoglycosides [10] and sulfur compounds [11—13]. Most of these compounds are not detected under direct current (d.c.) conditions and photometric detection does not offer suitable sensitivity without prior chemical derivatization. Liquid chromatography with PAD has been commercialized successfully for determinations of carbohydrate mixtures [5—7]. A disadvantage of PAD at noble-metal electrodes in flowing systems is that the linear dynamic range (i_p vs. C^b) is observed in many cases to be rather limited [4]. Because of the surface-controlled nature of the detection mechanism, calibration plots of $1/i_p$ vs. $1/C^b$ have been suggested to linearize data over a larger dynamic range [4, 10, 11]. However, the use of such "reciprocal plots" is not now recommended [12]. Present efforts to improve the quantitative convenience of PAD are designed to increase the linear dynamic range by lowering substantially the limit of detection. Significant improvement has been achieved in the detectability of carbohydrates by PAD at gold electrodes by integration of the amperometric response over a period substantially longer than is applied conventionally for PAD.

0003-2670/87/$03.50

The success of PAD at noble-metal electrodes for aliphatic organic compounds is due to the multistep potential waveform which manages sequentially the process of detection followed by oxidative and reductive reactivation of the electrode surfaces [1, 2, 8, 9, 11]. The effectiveness of surface cleaning and reactivation resulting from formation and dissolution of surface oxides at noble metal electrodes has been well recognized (see, e.g., [14–17]). Cleaning of carbon electrode surfaces resulting from potential pulses also is known [18–23], although the mechanism probably does not involve formation followed by dissolution of some analog to surface oxide.

It is the customary practice in pulsed amperometric techniques, e.g., pulse polarography, to integrate the transient amperometric response for 16.7 ms (i.e., 1/60 Hz). The integral divided by the integration period (coulomb s^{-1}) is presented to a digital or analog recording device as an amperometric signal. The choice of the 16.7-ms period is intended to reject the high-frequency noise originating from the alternating-current (a.c.) power supply. Brumleve et al. [24] explained the benefit of this practice as the result of minimizing "high- and low-frequency noise received and amplified by the high impedance circuitry associated with the reference and working electrodes." This same procedure for discrimination against 60-Hz noise was applied in the development of the first generation of instruments for PAD [5–7]. However, with the use of microprocessor-controlled instrumentation, the integration period can easily be varied, adding another dimension to the optimization of the pulsed detection techniques.

THEORY

The total amperometric response observed at a noble-metal electrode for anodic detection following a positive potential step in PAD is described by

$$i_{tot}(t) = i_{ox}(t) + i_{dl}(t) + i_{ads}(t) + i_{mt}(t) \tag{1}$$

where $i_{ox}(t)$, $i_{dl}(t)$, $i_{ads}(t)$ and $i_{mt}(t)$ represent, respectively, the partial currents caused by oxide formation on the electrode surface, charging of the double layer, oxidation of adsorbed analyte, and oxidation of analyte reaching the electrode by convective-diffusional mass transport during the detection period. Including superposition of sinusoidal a.c. noise having amplitude A_j and time constants τ_j, the total amperometric response is given by

$$i_{tot}(t) = i_{ox}(t) + i_{dl}(t) + i_{ads}(t) + i_{mt}(t) + \sum_j A_j \sin(2\pi t/\tau_j) \tag{2}$$

Integration of Eqn. 2 over a time period $t_i = t'' - t'$ yields

$$q_{tot}(t_i) = \int_{t'}^{t''} i_{tot}(t)\,dt \tag{3}$$

$$= q_{ox}(t_i) + q_{dl}(t_i) + q_{ads}(t_i) + q_{mt}(t_i) + \sum_j \int_{t'}^{t''} A_j \sin(2\pi t/\tau_j) \tag{4}$$

The enhancement in signal-to-noise ratio (S/N) resulting from increasing values of t_i can be illustrated by the simple example of a constant amperometric response with a superimposed sinusoidal noise component of single frequency and low amplitude. Integration of $i_{tot}(t)$ produces a time-dependent response, $q_{tot}(t)$, with a noise component of amplitude and frequency equal to that of the noise in $i_{tot}(t)$ but which is 180° out of phase with the noise in $i_{tot}(t)$. The contribution of the a.c. noise in $i_{tot}(t)$ to noise in $q_{tot}(t)$ is at a minimum for t_i equal to integral multiples (k) of τ_j (i.e., $k = t_i/\tau_j$). Because the predominant source of a.c. noise in electroanalytical measurements is correlated with the 60-Hz line frequency, τ_j is equal to 16.7 ms. Hence, the coulometric response is characterized by a S/N which increases with increasing values of $t_i = 16.7 \times k$ ms (k = integer) and this increase in S/N is a result of increased signal strength and is not due to a decrease in the noise component.

The integration of the transient amperometric response for the minimal value of $t_i = 16.7$ ms in pulsed amperometric techniques is a necessity for minimizing noise; however, the goal remains that of approximating the amperometric signal at some time value following application of a potential pulse. The fact that the integrated amperometric response for $t_i \gg 16.7$ ms, when divided by t_i, does not give a meaningful approximation of the transient amperometric response made it necessary to plot the integrated signal (coulombs) as a function of real time (t). Hence, the technique can be named pulsed coulometric detection (PCD) when applied to flow-injection and liquid chromatographic systems. As with PAD, several variations of the applied-potential waveform are possible. Here, PCD with $t_i \gg 16.7$ ms is discussed for a detection at constant potential. The increase in S/N for PCD (i.e., $k \gg 1$) as compared to PAD (i.e., $k = 1$) can be estimated from a comparison of the integration times for the two experiments:

$$(S/N)_{PCD}/(S/N)_{PAD} = t_{i(PCD)}/t_{i(PAD)} = t_{i(PCD)}/16.7 = k \text{ (an integer)} \qquad (5)$$

where t_i values are expressed in milliseconds. In effect, a ten-fold increase in integration time for a constant signal current should yield a ten-fold increase in S/N. This approximation (Eqn. 5) becomes exact only for systems which yield a steady-state amperometric response. Smaller improvements are expected for more complicated detection mechanisms in which diffusional transport has not yet achieved a steady-state value following a potential step, i.e., short time, and where surface fouling and catalytic deactivation cause a significant attenuation of the signal below the steady-state value during the detection period. Hence, improvements in PCD over PAD should not be expected to be as large as predicted by Eqn. 5 for these complex systems.

The waveform for pulsed coulometric detection is summarized in Fig. 1. At the detection potential E_1 (period t_1), integration is done for a period t_i (digital control I in Fig. 1) by an analog integrator. The integral is sampled for 16.7 ms (digital control 0) during the last 18 ms of the integration

period, t_i, in t_1. A delay period, t_d, in t_1 (digital control D) is added prior to the start of the integration period for discrimination against the background currents, i_{ox} and i_{dl}; hence, $t_1 = t_d + t_i$. After the detection period, the potential is stepped to a more positive value, E_2 (period t_2), to ensure anodic removal of all adsorbed detection products, reactants or solution impurities. The surface is renewed further by the negative step of potential to E_3 which results in the cathodic dissolution of surface oxide with concomitant adsorption of analyte. At E_3 (period t_3), the integrator is reset (digital control S) prior to the start of the new cycle. This waveform differs from PAD only in the width of the integration period t_i at the end of t_1 for E_1.

EXPERIMENTAL

Instrumental

The computer-controlled pulsed-amperometric and pulsed-coulometric instrumentation was based on two Hewlett-Packard computers (models 86B and 6942A) in series coupled to a Model 174A potentiostat (EG&G Princeton Applied Research, Princeton, NJ) via a home-built interface. The basic computer system has been described [7] and differs only in the addition of the circuitry needed to accomplish digital control of analog integration. The power of the system lies in the coupling of two computers; the microcomputer is in control of all waveform variables, based on user-defined criteria, whereas the mainframe has the sole task to output the predefined waveform and acquire and store data at specified times. This allows the two computers to work relatively independently of each other and results in improved precision and rate of data acquisition.

The interface between the potentiostat and 6942A mainframe contained circuits for amplification, current integration, and sample-and-hold operations. Analog signal integration was accomplished after the current at the working electrode had been converted to a proportional voltage and amplified. The integration cycle was initiated by the closing of a signal switch concurrently with the opening of a shorting switch. At the close of the integration cycle, the opposite switching operation was performed after the output had been sampled by the sample-and-hold circuit for 16.7 ms. This latter signal was monitored by a recording device and/or sampled by an analog-to-digital converter (ADC). All operations were controlled via simple BASIC statements from the microcomputer which posed no speed limitations because of the independent nature of the coupled computer systems.

The flow-injection system was based on a low-pressure peristaltic pump with computer-controlled injection of samples and has been described [7]. The flow-through detector for flow-injection studies (Dionex Corporation, Sunnyvale, CA) was of the thin-layer design containing a gold indicating (0.02 cm^2), glassy-carbon counter electrode and a reference electrode. The normal Ag/AgCl reference electrode was replaced by a miniature SCE (Fisher Scientific, Fair Lawn, NJ) connected to the reference port of the

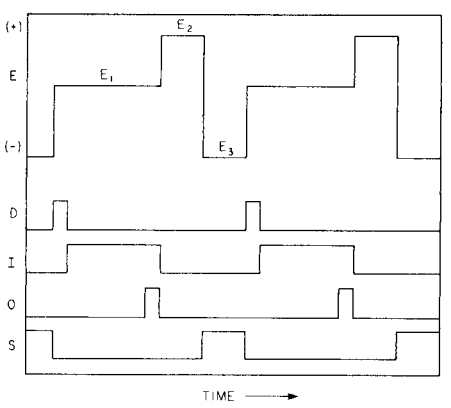

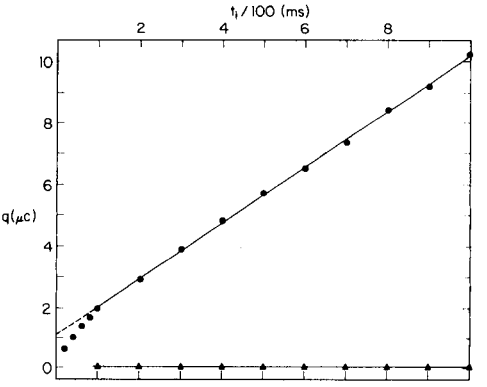

Fig. 1. Potential/time profile for the three-step waveform used in PCD. Timing parameters: (D) delay time before integration; (I) integration time; (O) sampling time for signal output; (S) shorting time of integrator.

Fig. 2. Charge response as a function of the integration time by PCD for 3 mM hexacyanoferrate(II) in 0.18 M H_2SO_4. Waveform: E_1 = 0.90 V (t_i varied; t_d = 1 μs); E_2 = 1.70 V (t_2 = 200 ms); E_3 = 0.40 V (t_3 = 200 ms). Conditions: 0.5 ml min^{-1} flow rate; 50-μl sample injected. Curves: (●) peak charge response; (▲) peak-to-peak background noise.

flow-through detector by a home-built interface constructed from Kel-F.

Charge/potential (q/E) plots were obtained by the application of a three-step waveform (Fig. 1) with variation of the detection potential E_1 at a gold rotated-disk electrode (RDE, 0.05 cm^2, Pine Instrument Co., Grove City, PA) mounted in a model MSR rotator (Pine Instrument Co.) under computer control.

Chemicals

All solutions were prepared from reagent-grade chemicals (Fisher Scientific, Fair Lawn, NJ) and deionized/triply distilled water. The supporting electrolyte was 0.20 M sodium hydroxide. Because of the slow decomposition of carbohydrates in alkaline media, solutions were prepared just prior to use. Where applicable, dissolved oxygen was removed by purging with reagent-grade nitrogen (99.99%).

RESULTS AND DISCUSSION

An understanding of the expected increase in S/N for PCD in comparison to PAD can be obtained with the application of these techniques to the detection of hexacyanoferrate(II) in sulfuric acid. The anodic response for this ion is characterized by mass-transport limited currents in a region of applied potential where no appreciable gold(III) oxide is formed. Furthermore, the reaction does not suffer from surface fouling caused by adsorption of reaction products. The plot of the peak value of charge (q_p) vs. t_i

obtained with the flow-injection system (Fig. 2) is linear for t_i = 100-1000 ms. The linearity of q_p vs. t_i is characteristic of a steady-state, mass-transport-limited response at the RDE for $t_i > 100$ ms. The background noise level does not change with a change in t_i. Both of these observations are consistent with the conclusion that *S/N* increases as a result of an increased signal strength and is not due to a decrease in the noise.

The primary motivation for the development of PCD was an increased linear dynamic response resulting from the lowering of detection limits. The non-linear response of the PAD in a flow-injection system for glucose and fructose at concentrations above 0.1 mM is shown by the normalized plots in Fig. 3, where N is the normalization constant which was chosen so that $N\ i_p/C^b = 1$ for the linear response obtained at a bulk concentration $C^b < 0.1$ mM. Nonlinear response at high C^b is the result of electrode fouling during the detection process by adsorbed detection product. The detection limits in this case (50-μl samples) were ca. 0.035 mM for glucose and 0.050 mM for sucrose. The linear dynamic response is very limited for these compounds by PAD, i.e., less than one decade.

The implementation of PCD, with particular emphasis upon background rejection, is simplified after examination of q/E plots for glucose at a RDE

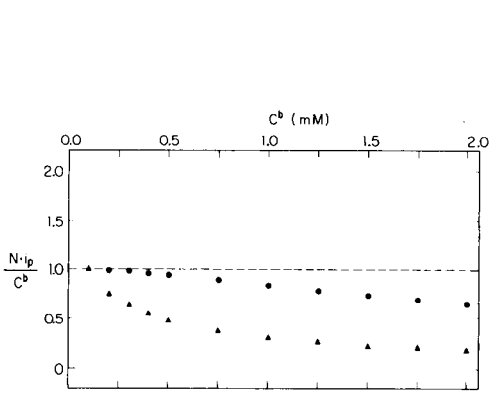

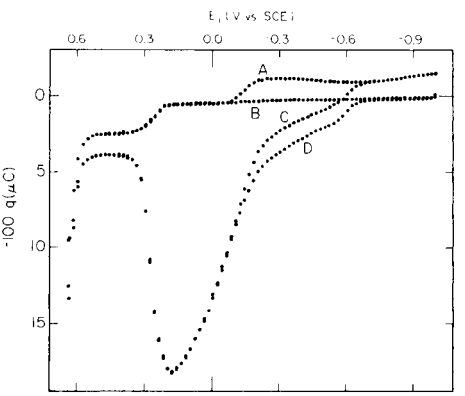

Fig. 3. Normalized calibration plots for glucose and sucrose by flow injection with PAD obtained with a three-step waveform in 0.20 M NaOH. Waveform: E_1 = 0.175 V (t_1 = 250 ms); E_2 = 0.75 V (t_2 = 100 ms); E_3 = —1.00 V (t_3 = 100 ms). Conditions as in Fig. 2. Curves: (●) normalized peak-current response of glucose ($N = 5.32 \times 10^{-2}$ mM μA^{-1}); (▲) normalized peak-current response of sucrose ($N = 5.00 \times 10^{-2}$ mM μA^{-1}).

Fig. 4. Charge/potential plots with PCD at a gold RDE for 1.0 mM glucose in 0.20 M NaOH. Waveform: E_1 = varied (t_1 = 500 ms; t_d = 1 μs, t_i = 500 ms); E_2 = 0.75 V (t_2 = 200 ms); E_3 = —1.00 V (t_3 = 200 ms). Curves: (A) air-saturated 0.20 M NaOH; (B) nitrogen-saturated 0.20 M NaOH; (C) air-saturated 1.0 mM glucose/0.20 M NaOH; (D) nitrogen-saturated 1.0 mM glucose/0.20 M NaOH.

in 0.20 M sodium hydroxide (Fig. 4). At the potential of maximum response, ca. 0.175 V vs. SCE, there is very little background charge; that observed is due only to charging of the double layer. Normalized calibration plots for glucose and sucrose are shown in Fig. 5 for PCD in the flow-injection system using a waveform of E_1 = 0.175 V (t_1 = 500 ms; t_d = 1 μs, t_i = 500 ms), E_2 = 0.75 V (t_2 = 200 ms), and E_3 = —1.0 V (t_3 = 200 ms). The plots are linear over the concentration range shown (5–50 μM) with intercepts of 1.0 which correspond to observed intercepts of 0.0 for the

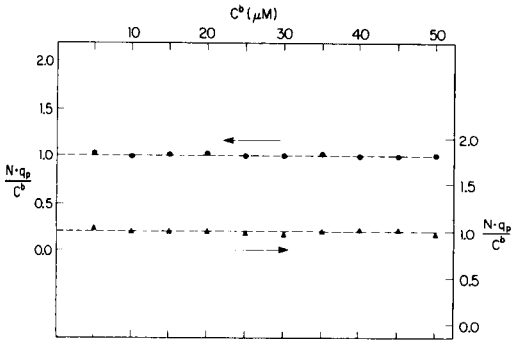

Fig. 5. Normalized calibration plots for glucose and sucrose with PCD in a flow-injection system. Waveform: E_1 = 0.175 V (t_i = 500 ms; t_d = 1 μs, t_i = 500 ms); E_2 = 0.75 V (t_2 = 200 ms); E_3 = —1.00 V (t_3 = 200 ms). Conditions as in Fig. 2. Curves: (●) normalized peak charge for glucose ($N = 6.19 \times 10^1$ μM μC^{-1}); (▲) normalized peak charge for sucrose ($N = 9.42 \times 10^1$ μM μC^{-1}).

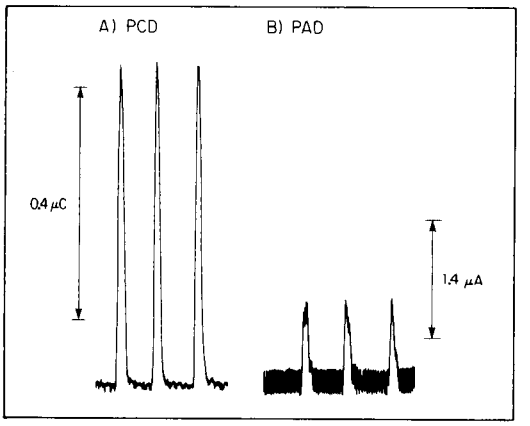

Fig. 6. Comparison of the peak response obtained by PAD and PCD for 35 μM glucose in a flow-injection system. Curves: (A) PAD; (B) PCD. PAD waveform: E_1 = 0.175 V (t_1 = 250 ms); E_2 = 0.75 V (t_2 = 100 ms); E_3 = —1.00 V (t_3 = 100 ms). PCD waveform: E_1 = 0.175 V (t_i = 500 ms; t_d = 1 μs); E_2 = 0.75 V (t_2 = 200 ms); E_3 = —1.00 V (t_3 = 200 ms). Conditions as in Fig. 2.

more common q_p/C^b plots. Based on studies of the effects of scan rate and rotation speed at a gold rotated-disk electrode, it is concluded that adsorption of the carbohydrate at E_3 contributes an insignificant amount to the signal measured at E_1. Furthermore, at these very low concentrations fouling of the surface by adsorption of reaction products is minimal.

It is apparent from the normalized calibration plots that the detection limits for PCD have been greatly lowered compared to those for PAD. For direct comparison of detection limits between PCD and PAD methods, a well-conditioned electrode was used, i.e., further surface reconstruction over the time period of the comparison was negligible. Detection limits ($S/N = 2$) obtained for glucose and sucrose by PAD with this instrument were 0.035 mM and 0.05 mM, respectively. Detection limits for glucose and sucrose by PCD were found to be 1.0 μM and 2.5 μM, respectively. The decrease in detection limits of 20—35 fold reported here was typical of those obtained for other monosaccharides, e.g., sorbitol and fructose. The upper values of C^b at which negative deviation from linear response occurred were virtually the same for PCD and PAD. Hence, the linear dynamic range for glucose by PCD was ca. 2.2 decades and, for sucrose, ca. 1.7 decades. A comparison of the S/N obtained for 35 μM glucose utilizing both methods of detection is shown in Fig. 6.

Conclusions

The improvement in detectability and linear dynamic range observed here for PCD, in comparison to PAD, was demonstrated for only one class of compounds, i.e., carbohydrates. Similar improvements are to be expected for all classes of compounds for which PAD has been found applicable.

The authors gratefully acknowledge Rob Synovec for his enlightening discussions of the concepts included here. This work was supported by the National Science Foundation through Contract CHE-8312032.

REFERENCES

1 S. Hughes, P. L. Meschi and D. C. Johnson, Anal. Chim. Acta, 132 (1981) 1.
2 S. Hughes and D. C. Johnson, Anal. Chim. Acta, 132 (1981) 11.
3 S. Hughes and D. C. Johnson, J. Agric. Food Chem., 30(4) (1982) 712.
4 S. Hughes and D. C. Johnson, Anal. Chim. Acta, 149 (1983) 1.
5 P. Edwards and K. Haak, Am. Lab., April (1983) 78.
6 R. D. Rocklin and C. A. Pohl, J. Liq. Chromatogr., 6(9) (1983) 1577.
7 W. T. Edwards, C. A. Pohl and R. D. Rubin, TAPPI J., in press.
8 G. G. Neuburger and D. C. Johnson, Anal. Chem., 59 (1987) 150, 203.
9 J. A. Polta and D. C. Johnson, J. Liq. Chromatogr., 6 (1983) 1727.
10 J. A. Polta, D. C. Johnson and K. E. Merkel, J. Chromatogr., 324 (1985) 407.
11 T. Z. Polta and D. C. Johnson, J. Electroanal. Chem., 209 (1986) 159.
12 T. Z. Polta, G. R. Luecke and D. C. Johnson, J. Electroanal. Chem., 209 (1986) 170.
13 M. B. Thomas and P. E. Sturrock, J. Chromatogr., 357 (1986) 318.
14 S. Gilman, in A. J. Bard (Ed.), Electroanalytical Chemistry, Vol. 2, M. Dekker, New York, 1967.

15 R. N. Adams, Electrochemistry at Solid Electrodes, M. Dekker, New York, 1969, Chap. 7.
16 D. Clark, M. Fleischman and D. Pletcher, J. Electroanal. Chem., 36 (1972) 137.
17 A. MacDonald and P. D. Duke, J. Chromatogr., 83 (1973) 331.
18 B. Fleet and C. J. Little, J. Chromatogr. Sci., 12 (1974) 747.
19 B. Fleet, U.S. Patent No. 4,059,406; Nov. 22, 1977.
20 T. A. Berger, U.S. Patent No. 4,496,454; Jan. 19, 1985.
21 H. W. van Rooijen and H. Poppe, Anal. Chim. Acta, 130 (1981) 9.
22 A. G. Ewing, M. A. Dayton and R. M. Wightman, Anal. Chem., 53 (1981) 1842.
23 J. Wang and P. Tuzhi, Anal. Chem., 58 (1986) 1787.
24 T. R. Brumleve, R. A. O'Dea, R. A. Osteryoung and J. Osteryoung, Anal. Chem., 53 (1981) 702.

Analytica Chimica Acta, 192 (1987) 215—223
Elsevier Science Publishers B.V., Amsterdam — Printed in The Netherlands

GLASSY CARBON ELECTRODES COATED WITH CELLULOSE ACETATE FOR ADSORPTIVE STRIPPING VOLTAMMETRY

JOSEPH WANG*, MOJTABA BONAKDAR and MARTY M. PACK

Department of Chemistry, New Mexico State University, Las Cruces, New Mexico 88003 (U.S.A.)

(Received 30th June 1986)

SUMMARY

The utility of glassy carbon electrodes coated with cellulose acetate for adsorptive stripping voltammetry of oxidizable organic compounds is evaluated. This surface modification alleviates the co-adsorption problem commonly encountered at conventional electrodes. Interferences from electro-inactive surfactants and, in certain situations, from adsorbable electroactive substances, are minimized. Quantitation of the drugs, chlorpromazine and trimipramine, is not affected by the presence of up to 120 mg l^{-1} albumin or gelatin. The chlorpromazine response is not affected by the bilirubin or perphenazine peaks which overlap at uncoated electrodes. The adsorptive stripping response at the coated electrode is evaluated with respect to hydrolysis time, preconcentration time, concentration dependence, reproducibility, and other variables. The detection limit for chlorpromazine is 1.3×10^{-8} M (5-min preconcentration). Applicability to assays of urine and serum samples is illustrated.

A recent advance in electroanalysis is the development of adsorptive stripping voltammetry for trace quantitation of adsorbable electroactive species [1, 2]. The method is based on a controlled interfacial accumulation of the analyte onto the working electrode, followed by voltammetric stripping of the surface-bound species. As a result, the scope of stripping voltammetry is substantially expanded towards numerous species (organic compounds and metal ions) that cannot be preconcentrated electrolytically, but adsorb strongly and reproducibly on the electrode.

While the adsorptive stripping method provides reproducible results at the submicromolar and nanomolar concentration levels, with detection limits as low as 2.5×10^{-11} M [3], it suffers from interferences caused by co-adsorbing electro-active and electro-inactive compounds. These species compete for adsorption sites, resulting in diminished sensitivity. Electro-inactive surfactants may be responsible also for a gradual decrease of electrode activity. In addition, co-adsorbing electroactive substances may yield overlapping responses if they have a redox potential similar to that of the analyte. Several approaches have been proposed to reduce interferences from electro-inactive surfactants in adsorptive stripping measurements. Among these are various sample pretreatment procedures [4, 5], careful

0003-2670/87/$03.50

adjustment of the preconcentration time or potentials [4, 6, 7], or appropriate use of calibration curves or standard-addition measurements [7, 8]. The sample pretreatment procedures required for severe surfactant interference are time-consuming and/or may introduce contamination. No solutions have been proposed to minimize interferences from co-adsorbed electro-active substances.

The aim of the present work was to develop and explore a new means of alleviating the co-adsorption problem in adsorptive stripping voltammetry. For this purpose, the working electrode is modified by coating it with an appropriate polymeric film, the discriminative properties of which can provide an in-situ separation at the electrode surface. In particular, base-hydrolyzed cellulose acetate films are shown to be advantageous for this purpose. It has been demonstrated recently that different permeabilities of cellulose acetate films can be achieved by hydrolysis in alkaline media for different times [9, 10]. These characteristics were found to be extremely useful for improving the selectivity and stability for amperometric detection of organic compounds [9] and for anodic-stripping measurements of trace metals [10]. Similarly, the ability of control access to the surface may be beneficial in adsorptive stripping voltammetry. Because most compounds quantified by this method are small molecules (m.w. < 1000), while common electro-inactive interferents are macromolecules, the size-exclusion characteristics of cellulosic coatings appear to be very useful in overcoming the surfactant problem. In addition, fine control of the film permeability can alleviate interferences from co-adsorbed electroactive substances. (Contributions from nonadsorbable electro-active species are commonly eliminated using the medium-exchange procedure [11].) These and other characteristics and advantages of adsorptive stripping voltammetry at cellulosic-coated carbon electrodes are discussed below. Chlorpromazine and trimipramine are used as model analytes.

EXPERIMENTAL

Apparatus and reagents

The cell was a Bioanalytical Systems Model VC-2 voltammetric cell. The working electrode (glassy carbon disk, Model MF 2012, Bioanalytical Systems), reference electrode (Ag/AgCl, Model RE-1, Bioanalytical Systems) and the platinum wire auxiliary electrode were introduced into the cell through holes in the teflon cover. The cell was placed on a magnetic stirrer, and a 1-cm long magnetic bar was used for stirring. Most current/voltage data were recorded with a Princeton Applied Research Model 364 polarographic analyzer and Houston Omniscribe strip-chart recorder. Cyclic voltammograms were obtained with the Princeton Applied Research Model 264 voltammetric analyzer.

Stock solutions (5×10^{-4} M) of chlorpromazine, bilirubin, perphenazine and trimipramine (Sigma) were prepared daily. Solutions (5000 mg l^{-1}) of

organic surfactants were prepared weekly. Cellulose acetate (39.8% acetyl content) was purchased from Aldrich Chemical Co. All solutions were prepared with double-distilled water. Normal Control Serum (Ortho Diagnostics, Lot 020A02) was dissolved in double-distilled water as recommended by the manufacturer. The urine samples were obtained from a healthy volunteer. Supporting electrolytes in the chlorpromazine and trimipramine experiments were 0.05 M phosphate buffers of pH 7.4 and 9.0, respectively.

Procedure

The glassy carbon disk was coated with 3 μl of the 5% (w/v) cellulose acetate solution; the resulting film was hydrolyzed in 0.07 M potassium hydroxide. Details of the coating and hydrolysis steps were described previously [9]. The preconcentration step was done by immersing the coated electrode in a stirred 10-ml sample solution for a given time with a 0.0-V potential applied to the electrode. Stirring was then stopped and the surface species was measured by applying a differential pulse ramp. In experiments involving medium-exchange, the preconcentration proceeded at open circuit; the electrode was then removed from the sample, rinsed slightly with water and immersed in an electrolytic blank solution where the differential pulse ramp was applied. After the potential scan, the electrode was cleaned by applying +1.0 V (chlorpromazine) or +1.4 V (trimipramine) for 1 min.

RESULTS AND DISCUSSION

Adsorptive stripping behavior of cellulose-acetate-coated electrodes

Figure 1 illustrates the electrode protection achieved by coating the glassy carbon disk with a cellulose acetate film. At the bare electrode (A), a substantial depression (ca. 45%) of the chlorpromazine voltammetric peak is observed after addition of 100 mg l^{-1} albumin (compare a and b). In contrast, essentially the same chlorpromazine response is observed at the coated electrode (B) in the absence (a) and presence (b) of 100 mg l^{-1} albumin. Apparently, the cellulosic coating prevents large macromolecules from reaching the glassy carbon surface, thus minimizing competition for adsorption sites.

The interfacial and redox behaviors at the coated and uncoated electrodes can be evaluated from repetitive cyclic voltammograms for 2.5×10^{-6} M chlorpromazine following 2-min preconcentration at 0.0 V (Fig. 2). At both electrodes, a large anodic peak, associated with the oxidation of the surface-bound species, is observed in the first scan (designated as 1); no peaks are observed on scanning in the negative direction. Subsequent scans yield a sharp decrease of the oxidation peak, indicating a rapid desorption from the surface. While similar peak potentials and peak widths are observed at both electrodes, the peak current of the uncoated electrode is approximately two-fold larger than that of the coated electrode. Such differences are

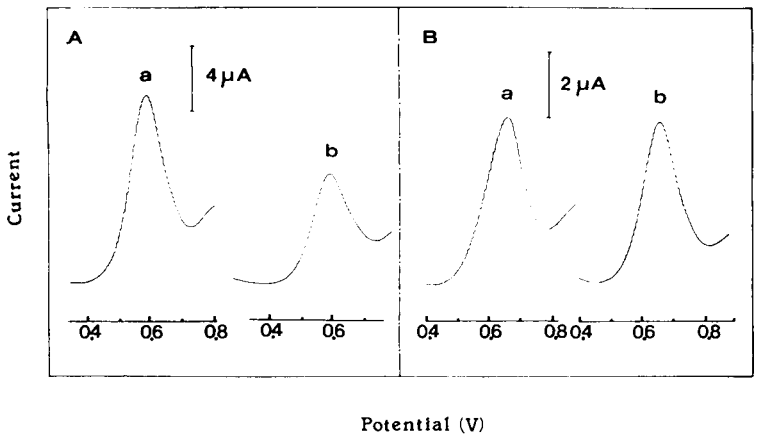

Fig. 1. Adsorptive stripping voltammograms for 1×10^{-6} M chlorpromazine at the uncoated (A) and coated (B) glassy carbon electrodes, before (a) and after (b) addition of 100 mg l^{-1} albumin. Conditions: preconcentration for 2 min, at 0.0 V, with 400 rpm stirring; differential pulse waveform with 5 mV s^{-1} scan rate and 50 mV amplitude; supporting electrolyte, 0.05 M phosphate buffer (pH 7.4); hydrolysis time (B), 40 min.

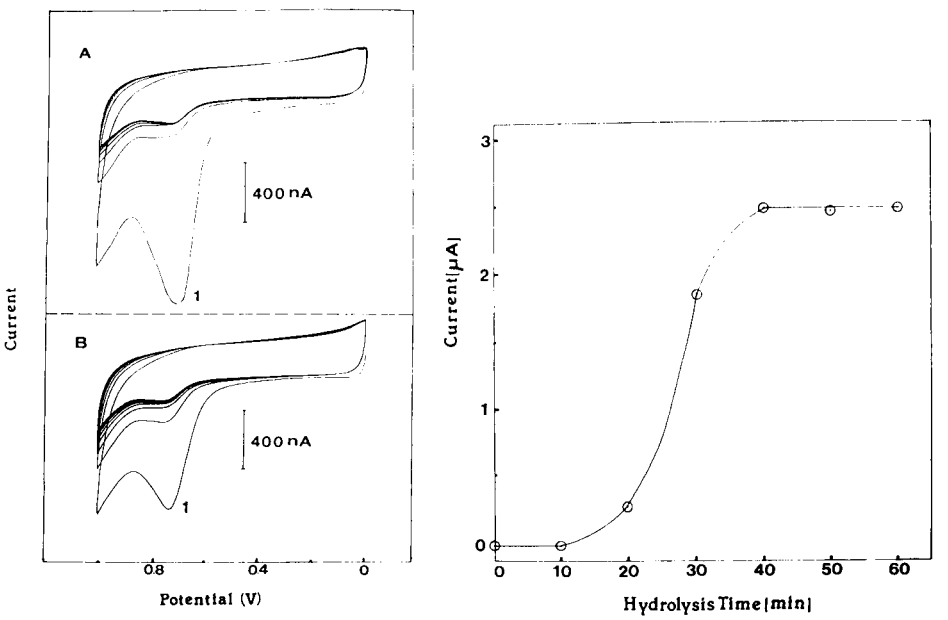

Fig. 2. Repetitive cyclic voltammograms for 2.5×10^{-6} M chlorpromazine following 2-min preconcentration at 0.0 V at uncoated (A) and coated (B) electrodes. Hydrolysis time (B), 40 min; scan rate, 50 mV s^{-1}.

Fig. 3. Dependence of the chlorpromazine adsorptive peak current on the hydrolysis time. Other conditions as in Fig. 1.

attributed to additional diffusional resistance, associated with the transport through the film, during the preconcentration period. As is shown below, such a decrease in peak height is not a matter of major concern, because nanomolar detectability is still maintained.

The adsorptive stripping response depends strongly on the time used to hydrolyze the cellulosic coating, i.e., the film permeability (Fig. 3). No response is observed with hydrolysis time shorter than 10 min, because the chlorpromazine molecules are excluded from the surface. The chlorpromazine peak rapidly increases upon extending the hydrolysis period from 20 to 40 min; no further change in the response is observed for hydrolysis times longer than 40 min, the time used for most experiments described in this paper. (Shorter periods were used in experiments intended to improve the selectivity between two adsorbable electroactive compounds.) Profiles of current vs. hydrolysis time similar to the one shown in Fig. 3 should be constructed when different adsorbable analytes (with different permeabilities through the coating) are involved. Approximately four out of five coated electrodes exhibited similar permeability profiles and response characteristics. The thickness of the cellulosic layer increased from 5 to 8 μm after hydrolysis for 40 min, indicating significant water swelling.

As observed with uncoated electrodes, the coated electrode exhibits nonlinear dependences of the adsorptive stripping response on the preconcentration time and analyte concentration (Fig. 4). For example, curvature in the response is observed when the preconcentration time is increased from 0 to 10 min. An eight-fold peak enhancement is obtained with 10-min preconcentration, compared to the response without accumulation. The calibration plot (Fig. 4) exhibits linearity at low concentrations (up to 5×10^{-7} M), the deviation from linearity observed at higher concentrations is expected for a preconcentration step of this nature. Means to extend the linear range have been discussed [2]; alternatively, reciprocal plots, e.g., $1/i$ vs. $1/c$, can be used. Competition on surface sites by co-adsorbing surfactants in "real" samples is minimized with the coated electrode (see below).

To evaluate the detection limits voltammograms were recorded for 4×10^{-7} M chlorpromazine after 5-min preconcentration (other conditions as in Fig. 1). A detection limit of about 1.3×10^{-8} M was calculated based on the signal-to-noise characteristics ($S/N = 3$) of the response. Thus, very low detection limits are maintained at the coated electrode, despite the additional diffusional resistance during the preconcentration step. (Results obtained throughout this study show that the response of an uncoated electrode is only 2—4-fold larger than that of the coated electrode.)

Discrimination against co-adsorbing substances

Figure 5 shows the effects of albumin and gelatin on the adsorptive stripping response of chlorpromazine and trimipramine. Successive additions of these surfactants, over the 0—120 mg l^{-1} range, caused significant peak-current depressions at the uncoated electrode (ca. 90% for trimipramine and

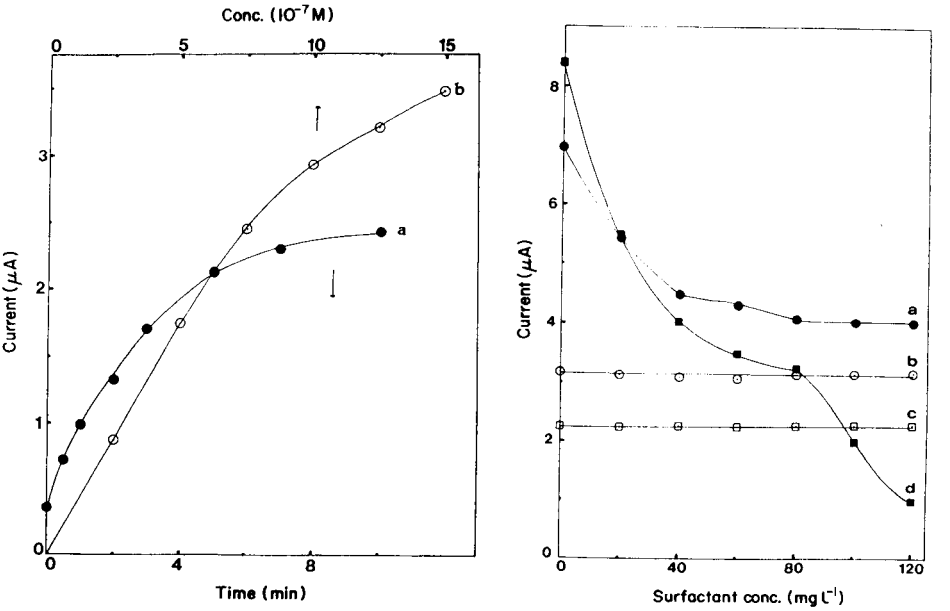

Fig. 4. Dependence of the chlorpromazine peak current: (a) on preconcentration time for 4×10^{-7} M chlorpromazine; (b) on concentration after preconcentration for 2 min. Other conditions as in Fig. 1.

Fig. 5. Effect of albumin (a, b) and gelatin (c, d) on the stripping peaks of 1×10^{-6} M chlorpromazine (a, b) and 2×10^{-6} M trimipramine (c, d) at the uncoated (a, d) and coated (b, c) electrodes. Conditions as in Fig. 1, except that a phosphate buffer solution (pH 9) was used for (c, d).

ca. 45% for chlorpromazine). In contrast, with the coated electrode, the response is stable for both drugs over the entire concentration range of the surfactants.

Repetitive adsorptive stripping measurements were used to evaluate the reproducibility of the data in the presence of surfactants (conditions as in Fig. 5). Measurements of 2×10^{-6} M trimipramine (with 20 mg l^{-1} gelatin present) resulted in a mean peak current of 2.82 μA, a range of 2.80—2.88 μA, and a relative standard deviation of 1.4% (n = 6). Similarly, successive measurements of 1×10^{-6} M chlorpromazine in the presence of 20 mg l^{-1} albumin yielded a mean peak current of 3.15 μA, a range of 3.08—3.18 μA, and a relative standard deviation of 1.3% (n = 6). Analogous measurements of chlorpromazine in the absence of albumin yielded a relative standard deviation of 1.5%. These data indicate that the minimization of surfactant adsorption is maintained over reasonable periods of time; in addition, the surfactants do not block the pores of the film. The good reproducibility also indicates effective removal of analyte from the film and the electrode during the cleaning period.

Interferences arising from co-adsorption of electroactive species were

also examined at the cellulose-coated glassy-carbon electrodes. Unlike interferences from large electro-inactive surfactants, electro-active interferents are commonly small molecules that can be transported through certain films. Thus, fine control of film permeability (i.e., careful choice of hydrolysis time) is required to deal with this type of interference. This can be achieved by constructing plots of response vs. hydrolysis time, similar to those of Fig. 3, for the compounds of interest. To minimize losses in sensitivity, the largest possible hydrolysis time that still excludes the interfering species should be used. Two examples related to situations that may be encountered in clinical analysis are given in Fig. 6. Measurements of chlorpromazine (m.w. 319) in the presence of bilirubin (m.w. 584) or the possible co-administered drug, perphenazine (m.w. 404), are illustrated. As a result of its adsorption and redox processes, bilirubin affects the chlorpromazine response at the uncoated electrode, giving a 35% depression of the peak and the appearance of new peaks at +0.28 V and +0.42 V, respectively (compare curves a and b in A). No such effects were observed at the coated electrode (curves c and d) when a 30-min hydrolysis period was used. A more severe interference was observed at the uncoated electrode in the presence of perphenazine (B). In this case, the two co-adsorbed compounds possess similar redox potentials. As a result, a substantial (42%) increase and broadening of the chlorpromazine peak is observed after addition of perphenazine (compare curves a and b in B). A judicious choice of the hydrolysis period

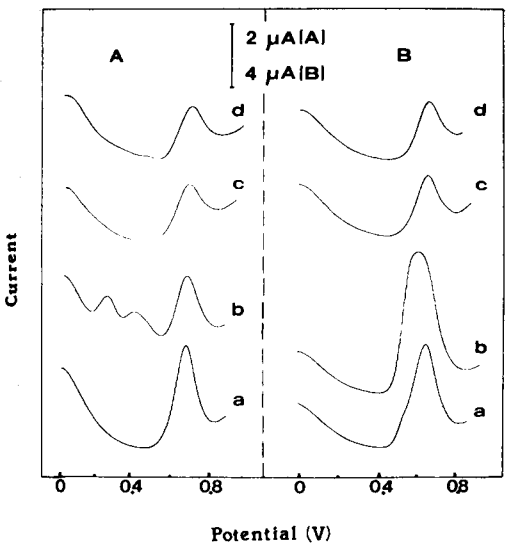

Fig. 6. Co-adsorption of two electroactive substances: (A): (a, c) 1×10^{-6} M chlorpromazine; (b, c) as (a, c) but with 1×10^{-6} M bilirubin added. (B): (a, c) 4×10^{-6} M chlorpromazine; (b, d) as (a, c) but with 4×10^{-6} M perphenazine added. Uncoated (a, b) and coated (c, d) electrodes, hydrolysis times (c, d), 30 (A) and 20 (B) min. Other conditions as in Fig. 1.

(20 min) permits exclusion of perphenazine molecules from the surface of the coated electrode; hence, chlorpromazine can be quantified without interference from a structurally-similar compound (compare curves c and d in B). It is not possible, however, to measure a given compound selectively in the presence of a smaller electro-active compound that also coadsorbs. Although molecular weight appears to be the major factor that affects the transport through the cellulosic layer, the permeability may be affected by other factors such as solute polarity [12]. In various situations it was possible to measure one adsorbable electro-active substance in the presence of another one using an uncoated electrode. For example, measurements of 1×10^{-6} M phenothiazine were not affected by the addition of 1×10^{-6} M chlorpromazine or trimipramine (conditions as in Fig. 1). Such behavior is attributed to preferential adsorption of the former.

Figure 7 illustrates the utility of adsorptive stripping voltammetry at uncoated and coated electrodes for assays of serum and urine samples. With an untreated, control serum sample, the uncoated electrode yields a broad peak at +0.55 V. With the coated electrode, two sharp peaks are observed (near +0.4 V and +0.7 V), possibly because of the oxidation of ascorbic acid and uric acid. It appears that the high protein content of the sample

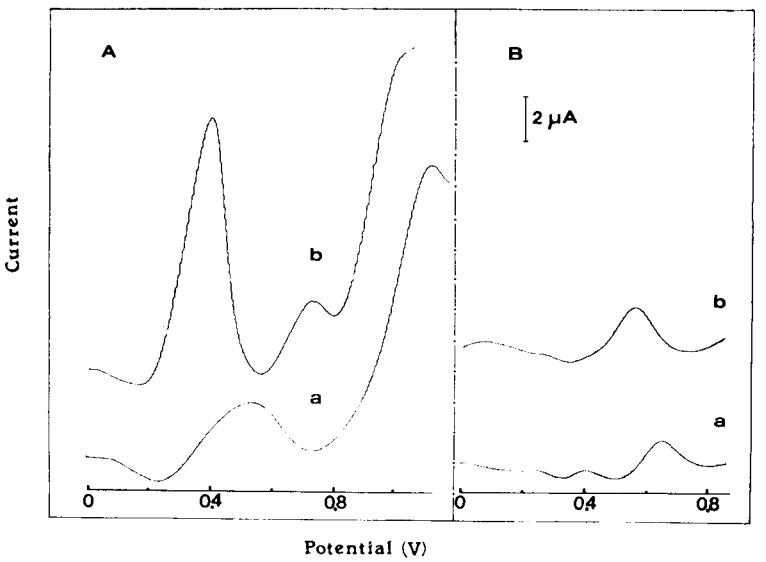

Fig. 7. Adsorptive stripping voltammograms for normal control serum (A) and urine (B) samples, diluted 1:1 at the uncoated (a) and coated (b) electrodes. The urine sample contained 1×10^{-6} M chlorpromazine and was assayed by using a medium-exchange procedure. Other conditions as in Fig. 1.

results in severe distortion and diminution of the response of the uncoated electrode. In particular, there is a substantial increase of the less positive peak at the coated electrode. Thus, the coated electrode may yield improved sensitivity relative to the uncoated electrode. Similar effects were observed in the determination of 1×10^{-6} M chlorpromazine in urine (Fig. 7B). The medium-exchange procedure [11, 13] was used in this assay to reduce interferences from nonadsorbable components (e.g., ascorbic acid), resulting in a defined chlorpromazine response. The peak is larger with the coated electrode because of reduced competition for surface sites by adsorbable sample components. No explanation is available for the shift in peak potential. Carefully controlled conditions, perhaps with a flow-injection system [13, 14], would be desirable for minimizing problems such as carry-over associated with the medium-exchange process.

The proposed method appears to be useful for assays of biological matrices with minimal sample preparation, and hence could have advantages over chromatography with respect to speed, simplicity and cost. Only oxidizable compounds which adsorb strongly and reproducibly onto the working electrode can be quantified. Chromatographic procedures, however, are much more general, are essential for resolving the parent drug and its major metabolites, and offer extended linearity. This concept is not applicable to adsorptive stripping quantitation of reducible species because of the difficulties in coating the hanging mercury drop electrode commonly used for this purpose. Analogous measurement schemes, based on other preconcentration procedures (e.g., ion-exchange or covalent reactions) may also benefit from the discriminative properties of cellulosic films [12]. The technique can be implemented in flow or discrete-sample clinical instruments.

This work was supported by a grant from the National Institutes of Health (Grant No. GM 30913-03).

REFERENCES

1 R. Kalvoda, Anal. Chim. Acta, 138 (1982) 11.
2 J. Wang, Am. Lab., 17(5) (1985) 41.
3 J. Wang, D. B. Luo, P. A. M. Farias and J. S. Mahmoud, Anal. Chem., 57 (1985) 158.
4 R. Kalvoda, Anal. Chim. Acta, 162 (1984) 197.
5 N. K. Lam and M. Kopanica, Anal. Chim. Acta, 161 (1984) 315.
6 V. Stara and M. Kopanica, Anal. Chim. Acta, 159 (1984) 104.
7 J. Wang, D. B. Lou and P. A. M. Farias, J. Electroanal. Chem., 185 (1985) 61.
8 E. N. Chaney and R. P. Baldwin, Anal. Chem., 54 (1982) 2556.
9 J. Wang and L. D. Hutchins, Anal. Chem., 57 (1985) 1536.
10 J. Wang and L. D. Hutchins-Kumar, Anal. Chem., 58 (1986) 402.
11 J. Wang and B. Freiha, Anal. Chim. Acta, 148 (1983) 79.
12 J. Wang and P. Tuzhi, Anal. Chem., 58 (1986) 3257.
13 J. Wang and B. Freiha, Anal. Chem., 55 (1983) 1285.
14 E. N. Chaney and R. P. Baldwin, Anal. Chim. Acta, 176 (1985) 105.

Analytica Chimica Acta, 192 (1987) 225—236
Elsevier Science Publishers B.V., Amsterdam — Printed in The Netherlands

ELECTRODEPOSITION AND ANODIC STRIPPING OF SILVER ON SINGLE CARBON FIBERS

JANUSZ GOŁAS[a] and JANET OSTERYOUNG*

Department of Chemistry, State University of New York at Buffalo, Buffalo, NY 14214 (U.S.A.)

(Received 13th June 1986)

SUMMARY

Silver is deposited electrolytically on carbon fibers from acetate buffer at pH 4.6 in the potential range from —0.3 to —0.8 V vs. SCE. Chronoamperometric and cyclic voltammetric measurements confirm that the mechanism of deposition is nucleation; the rate is higher than that at large circular glassy carbon electrodes. The silver deposits are more stable, especially with respect to oxidation by air, than are similar deposits of mercury. Preliminary results on codeposition of silver and mercury are reported.

Carbon fibers have been used to make microelectrodes for voltammetric or amperometric studies [1—6]. The two features important in applications of such electrodes are the complicated chemistry and electrochemistry of the electrode material itself [7] and the geometry and size of the electrode. Attempts to control the capacitative and catalytic properties of carbon microelectrodes for direct voltammetric studies generally involve time-consuming, inconvenient procedures which are not necessarily well-defined [8, 9]. At the present state of knowledge, it is not clear what approaches might ameliorate this situation [10]. Yet, it appears that quantitative results can be obtained for metal depositions without special pretreatment.

Aoki and coworkers have developed detailed theory for voltammetry at cylindrical electrodes [11—13]. The response depends in a complicated way on the radius of the cylinder and time scale of the experiment. The problem of deposition and stripping of a solid of variable activity at a cylindrical electrode has not been treated. O'Dea et al. [14] have investigated the voltammetric response for square-wave voltammetry at cylindrical carbon-fiber electrodes and suggested that peak shape and position depend only weakly on size and shape of the electrode. Aoki et al. [15] showed theoretically the ranges of parameters over which this observation applies and extended the treatment to restricted diffusion. Thus square-wave voltammetry appears from the fundamental point of view to be a good voltammetric technique for characterizing phenomena for which adequate theory is not available.

---

[a]Permanent address: Academy of Mining and Metallurgy, Institute of Material Sciences, 30-05g Krakow, Poland.

0003-2670/87/$03.50

The cylindrical geometry is attractive from the practical point of view because the quality of the seal between insulator and conductor is much less important in governing electrode performance than for a disk. In addition, the area is adjusted conveniently by choosing the length, independent of the radius, the latter of which alone governs the non-planar diffusional properties. Of course, the cylinder cannot be polished by the usual mechanical means, and thus an important component of most electrode pretreatment procedures is unavailable. On considering the art of polishing, one may conclude this is not a drawback.

In the analytical context, these electrodes can be used as substrates for anodic stripping voltammetry at mercury films [2, 3, 16—18]. Under easily accessible experimental conditions, the rate of accumulation of analyte by cylindrical diffusion during the plating process is equivalent to that at a rotating disk with a rotation rate of ca. 1000 rpm [11]. Although the chronoamperometric current at a cylinder does not reach a steady state, the time dependence of the current is slight enough that the amount accumulated during deposition is linear with deposition time over reasonable ranges of parameters within the overall accuracy of the experiment [30].

Several papers have dealt with deposition of mercury on carbon fibers [2, 3, 17]. Silver is also an attractive candidate for quantitative electrodepositions. Perone [19] has reported on the electrodeposition of silver at a large graphite disk electrode. The mechanism of deposition on glassy carbon substrates at high concentrations of Ag(I), which involves nucleation, has been studied in detail by Milchev et al. [20—22] and by Gunawardena et al. [23]. Deposition under more quantitatively pertinent conditions has been examined by Eisner and Mark [24] and by Brainina [25].

With these results as a starting point, the deposition of silver on cylindrical carbon-fiber electrodes was examined. It was expected that the process should be similar to that at glassy carbon electrodes, but not the same, as not only the size and shape but also the surfaces of the carbon fibers are different. Some preliminary observations are also reported on co-deposition of silver and mercury.

EXPERIMENTAL

A three-electrode system was used with a carbon-fiber indicator electrode, platinum-wire counter electrode and saturated calomel reference electrode. The reference electrode was placed in a salt bridge containing 1 M KNO_3. All potentials are reported versus this electrode. Voltammetric measurements were done with a computer-controlled potentiostat based on a Digital Equipment Corp. PDP-8/E minicomputer [26]. In the case of square-wave voltammetry, the current was sampled during the last third of each pulse. Coulometric results were obtained with an EG&G PAR Model 173 potentiostat and a Model 179 digital coulometer. Electron microscopy was done with a mini JSJ Model II electron microscope and optical microscopy with a Leitz Epivert metallograph.

For all measurements, the same microelectrode was used. It was prepared as described previously [16, 17]. A carbon fiber was sealed into tygon tubing and this was connected to a teflon holder by thermally shrinkable tubing, so that one end of the fiber contacted mercury inside the holder and the other end was exposed as the active electrode. The length of the exposed part was 9.1 mm, and the carbon fiber used (AESAR, Johnson Matthey) had a diameter of 8 μm. For one series of measurements an electrode of a different length was used as specified below. A micrograph of such an electrode is presented in Fig. 1.

After the electrode had been made, it was treated in an ultrasonic bath in sequence with Alconox solution, water, dilute (1:3) nitric acid, and finally water. The only other conditioning procedure was to polarize the electrode at +0.55 V for at least 1 min in the working solution before each voltammetric measurement. The working solution was chosen to be 1.25 M potassium acetate/1.7 M acetic acid buffer (pH 4.6), which was recommended by Eisner and Mark [24] for deposition of silver on glassy carbon. According to our experience it also is reasonably good for deposition of mercury [17]. The working solutions were prepared freshly before each experiment by proper dilution of 0.05 M stock solutions of silver nitrate and mercury(II) nitrate.

Solutions were purged with argon before measurement and blanketed with argon during measurement. For all anodic stripping experiments, square-

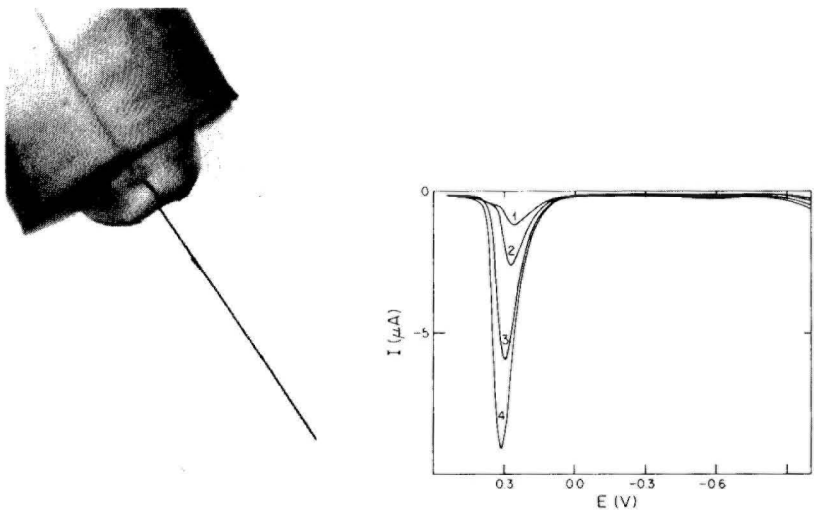

Fig. 1. Micrograph of a single carbon-fiber microelectrode made by sealing a carbon fiber (8-μm diameter) into tygon (inner tubing) and thermally shrinkable tubing (outer tubing).

Fig. 2. Anodic-stripping square-wave voltammograms of silver deposited on a carbon-fiber microelectrode. Silver concentration: (1) 10; (2) 20; (3) 40; (4) 80 μM. Conditions: 1.25 M potassium acetate/1.7 M acetic acid; square-wave voltammetry at E_{sw} = 24 mV, f = 100 Hz, ΔE_s = 4 mV, E_d = —1.0 V, t_d = 30 s.

wave voltammetry was used with the parameter values of E_{sw} = 24 mV, f = 100 Hz, ΔE_s = 4 mV. All depositions (and stripping voltammograms) were done in unstirred solution.

RESULTS AND DISCUSSION

The concentration of silver was varied in a series of depositions of silver. The deposition time was limited in most experiments to 2 min. Under this condition there is no stripping current for silver if the concentration of Ag(I) is lower than about 5 μM. The range of concentration investigated was 5—100 μM. Typical anodic stripping peaks are presented in Fig. 2.

Curves 1 and 2 in Fig. 2 display a small shoulder at more positive potentials. Calculated values of amounts deposited for these conditions combined with the bulk density of silver yield thicknesses of one and two monolayers, respectively, assuming a uniform deposit. Coulometric stripping in separate experiments gave amounts of charge equivalent to 1/3 and two monolayers, respectively. This phenomenon is familiar in stripping of solid deposits. Eisner and Mark [24] reported similar behavior on spectrographic pyrolytic graphite. But in their case, two well-separated peaks were observed, the more positive at ca. +0.02 V vs. SCE. This peak was attributed to stripping of the first monolayer. In the present case, the shoulder appears when less than a monolayer has been deposited, and it is more pronounced for a given concentration and deposition time when deposition is done at more negative potentials. Gunawardena et al. [23] showed that at short times the number density of nuclei increases exponentially with increasingly negative potential under conditions of high concentration ($\geqslant$0.01 M) and relatively low overpotential ($\geqslant$—350 mV). Under the present conditions of low concentration ($<$80 μM) even with large overpotential ($\leqslant$—1 V) nucleation may also be observed, as shown below. It therefore appears that the shoulder is due to stripping of silver bound to carbon, which may have penetrated beneath the carbon surface [23].

Under the experimental conditions of Fig. 2, the stripping peak current was found to be linear in silver concentrations (correlation coefficient 0.98, n = 3).

The nature of the electrodeposition process was investigated further by using chronoamperometry and chronocoulometry. Figure 3 shows the chronoamperometric response at various deposition potentials. The slowly increasing current transient at short times for $E_{dep} \geqslant 0$ V is characteristic of nucleation. At lower concentrations, the maximum of current (most clearly visible in curve 5) persists to more negative values of potential. For curves 6 and 7 of Fig. 3, the currents are two- to three-fold those predicted for diffusion-controlled currents [11]. Curve 6 corresponds to an overpotential of about —380 mV. At much higher silver concentration (0.05 M) for an overpotential of —340 mV, Gunawardena et al. [23] reported a current maximum at 270 ms at a large carbon disk. Thus the nucleation

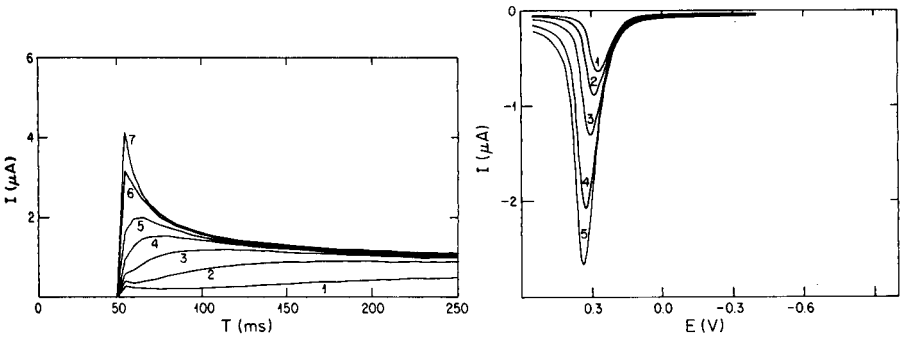

Fig. 3. Chronoamperometric curves for deposition of silver on a carbon fiber at different potentials. 160 μM Ag^+ in the acetate buffer pH = 4.6. Deposition potential: (1) +0.100; (2) +0.075; (3) +0.050; (4) +0.025; (5) 0.00; (6) −0.050; (7) −0.100 V. Electrode polarized at +0.055 V for the first 50 ms. Current sampled instantaneously every 5 ms.

Fig. 4. Anodic-stripping square-wave voltammograms of silver deposited on a carbon fiber at −0.4 V (20 μM Ag^+ in the acetate buffer pH 4.6). Deposition time: (1) 10; (2) 20; (3) 40; (4) 80; (5) 120 s.

process is much faster at the microcylindrical carbon fiber than at the large glassy carbon disk. More quantitative conclusions are beyond the scope of this initial survey.

Charge consumed during deposition and stripping peak current were measured for a range of deposition potentials ($-0.4\ V \leqslant E_{dep} \leqslant -1.0\ V$), concentrations of silver (10—40 μM), and deposition times (10—120 s). Typical stripping voltammograms are shown in Fig. 4. The peak width at half-height is constant at a value of 110 mV over the range of conditions used. Therefore peak height should be proportional to amount deposited. Parenthetically, this is a reasonable hypothesis, but theories for square-wave stripping of solid deposits have not yet been worked out.

First, the dependence of the amount of charge required during deposition on potential and concentration is considered. Representative values are given in Table 1. The values of charge are in the range predicted for accumulation under diffusion control. Results at −0.4 and −0.7 V are about the same, whereas the values obtained at −1.0 V are much larger. The charge appears to depend roughly linearly on concentration at higher concentrations. As predicted, the charge increases linearly with deposition time at −0.4 and −0.7 V, but at −1.0 V it increases with deposition time at a faster than linear rate. The increased charge at −1.0 V may be due to concomitant reduction of hydrogen ion which proceeds at a faster rate on the silver-covered surface than at the bare carbon substrate [27].

The efficiency of stripping, expressed by the ratio of peak stripping current to charge deposited, decreases with increasing deposition time. For example, for $E_{dep} = -0.4$ V and $C = 20\ \mu M$, the efficiency decreases from 1.4 A C^{-1} to 0.5 A C^{-1} on increasing t_{dep} from 10 s to 120 s. It is possible that at very negative potentials, large dendrites form and fall off

TABLE 1

Charge used for deposition of silver on a carbon-fiber microelectrode[a]

[Ag(I)] (μM)	Charge (μC) at E_{dep}(V) =		
	−0.4	−0.7	−1.0
0	0.1	0.1	0.2
10[b]	0.6	0.9	0.8
20[b]	2.5	2.6	4.1
40[b]	4.6	4.5	9.5

[a]1.25 M potassium acetate/1.7 M acetic acid, pH 4.6; t_{dep} = 60 s. [b]Total charge less charge for [Ag(I)] = 0.

during deposition, thus increasing the charge (and decreasing the stripping current). Over the potential range −0.4 to −0.7 V where the deposition process is well-behaved, the efficiency of stripping still is not constant with deposition time. The expected linear dependence on concentration and deposition time is only observed for the narrow range of conditions producing the equivalent of up to a few monolayers of silver.

The deposition of silver on carbon fibers is much better behaved and more reversible than deposition of mercury [17]. These processes are compared directly in Figs. 5 and 6. The voltammograms presented there are for Ag(I) in acetate buffer and for Hg(II) in thiocyanate solution which are the recommended conditions for each. The concentrations of mercury and silver were both 160 μM. The series of normal pulse voltammograms (Fig. 5) for Ag(I) shows well-defined waves for which the plateau improves with increase in pulse width. For a pulse width of 200 ms the parameters of the wave are $E_{1/2}$ = +0.095 V; i_L = 1.02 μA. (Under these conditions the anodic stripping square-wave peak of silver appears at E_p = +0.305 V.) To obtain a visible wave for reduction of Hg(II) with normal pulse, it was necessary to extend the pulse duration to 800 ms. Even then, the limiting current (i_L = 0.09 μA) was approximately ten-fold less than that for silver; and the difference between half-wave potential ($E_{1/2}$ = −0.425 V) and anodic stripping square-wave peak (E_p = −0.015 V for t_d = 40 s) was twice as large as for silver.

The current-potential curves at various times in Fig. 5 are explicable in terms of the current-time curves at various potentials in Fig. 3. For silver, nucleation is apparent as displayed by an increasing current transient only in a narrow potential range. In the limiting current region for the conditions of Fig. 5, the response does not depend significantly on the nucleation process and consequently the shapes of the normal pulse voltammograms are quite reasonable. It should be noted that the currents are about twice as large as predicted [11]. For mercury, it was necessary to extend the pulse width to 800 ms to obtain a reasonable, though very small, wave. For shorter pulse widths, the current was sampled from the increasing part of the current-time curve. These results suggest that nucleation of silver is much faster and more widespread than that of mercury.

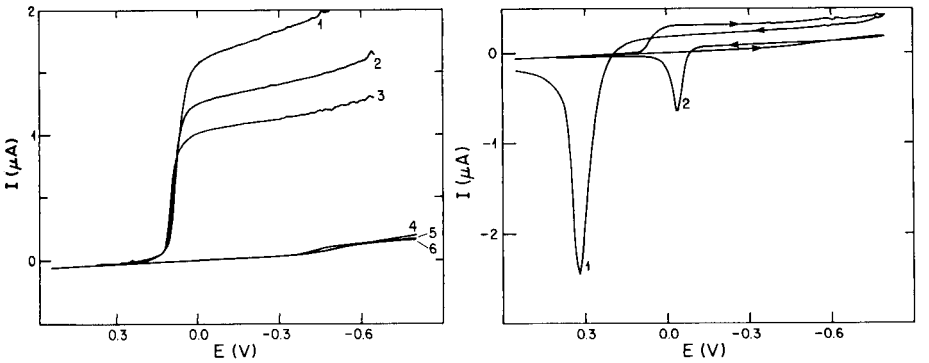

Fig. 5. Normal-pulse voltammograms of Ag(I) (160 μM in the acetate buffer pH 4.6) (curves 1—3) and Hg(II) (160 μM in 0.1 M KSCN) (curve 4—6) on a carbon-fiber microelectrode. Delay before pulse: 2 s. Pulse width, t_p: (1) 50; (2) 100; (3, 4) 200; (5) 400; (6) 800 ms.

Fig. 6. Cyclic staircase voltammograms of Ag(I) (160 μM in the acetate buffer pH 4.6) (curve 1) and Hg(II) (160 μM in 0.1 M KSCN) (curve 2) on a carbon-fiber microelectrode. Sweep rate 0.2 V s^{-1}, step height 4 mV, frequency 50 Hz.

This generalization is also supported by cyclic voltammetry (Fig. 6). For both elements, the crossover of the cathodic branch is caused by formation of a solid deposit. The cathodic wave of silver is flatter than that observed on a large disk electrode, but has the shape expected for very small cylindrical electrodes. The cathodic branch for mercury is poorly defined and shifted toward much more negative potential values. Comparison of the anodic peaks of silver and mercury shows clearly that deposition of silver is much more reversible.

The next question addressed is that of stability of silver deposits. Our previous experience with mercury films indicates that a short time (tens of seconds) of exposure to the air is sufficient to destroy the deposit almost completely. Stability was determined by comparing anodic stripping voltammograms recorded right after deposition and after periods of time during which the electrode was either disconnected but kept in the solution or disconnected and exposed to the air. This type of experiment was done for silver deposits on carbon-fiber microelectrodes. For this particular set of experiments, a carbon-fiber electrode of different length was used (l = 8.1 mm). Typical results are presented in Table 2.

The least stable deposit is that formed at —1.0 V, whereas the most stable are those deposited at —0.4 and —0.7 V. In all cases, the oxidation potential shifts towards more positive values with increasing time. A similar effect was observed with increasing deposition time (see Fig. 4), i.e., the longer the deposition time, the more positive the anodic stripping peak potential. This might be due to penetration of silver into the bulk of carbon [23].

The data in Table 2 also confirm the previous observation concerning the efficiency of deposition for different potentials. For E_{dep} = —0.4,

TABLE 2

Peak currents and potentials for anodic stripping square-wave voltammetry of silver deposited on a carbon-fiber microelectrode at different potentials (V)[a]

Stripping time[b–d]	E_{dep} = –0.1		E_{dep} = –0.4		E_{dep} = –0.7		E_{dep} = –1.0	
	i_p (μA)	E_p (V)	i_p (μA)	E_p (V)	i_p (μA)	E_p (V)	i_p (μA)	E_p (V)
b	8.76	0.365	11.40	0.360	11.39	0.350	11.72	0.350
c	7.06	0.405	9.60	0.395	10.15	0.400	8.82	0.395
d	7.39	0.410	8.40	0.395	8.30	0.390	7.10	0.380

[a] t_{dep} = 60 s, [Ag(I)] = 40 μM. [b] Immediately after deposition. [c] After 5 min at open circuit in solution. [d] After 5 min in air.

–0.7, –1.0 V, the anodic peak heights are approximately equal, whereas for E_{dep} = –0.1 V, the peak height is about 20–25% smaller. Also, for this electrode the charge consumed for deposition at –1.0 V was about twice that used at –0.4 or –0.7 V.

The stability of the silver deposit makes it possible to take electronmicrographs of carbon fibers with quantitatively deposited silver. Figure 7 shows carbon fibers on which have been deposited coulometrically the equivalent of about 10 and 100 monolayers of silver. The bare carbon surface is clearly visible in Fig. 7A, confirming that nucleation and growth occur at active sites rather than uniformly across the surface. In Fig. 7B, the surface appears to be covered with silver, but the deposit is rough and irregular, reflecting different rates of deposition at different sites.

Next, codeposition of silver and mercury is considered. The literature on this subject has been reviewed recently by Wrona and Galus [28] and discussed in more detail by Vydra et al. [29]. The solubility of silver in mercury is ca. 0.0007 mol Ag/mol Hg, but supersaturation and two-phase systems are commonly observed. For all of the results presented below, the ratio of the molar concentration of silver(I) to that of mercury(II) in solution far exceeds the solubility of silver in mercury. The separate experiments for Ag(I) and Hg(II) [17] in acetate buffer yielded stripping peaks at about the same potential (ca. +0.30 V for silver and ca. +0.25 V for mercury), the deposition and stripping of silver is much more reversible than that of mercury, and the stripping peaks for silver are about ten-fold larger than those for mercury under similar conditions. The following observations are intended to illustrate the influence of each metal on the other in the deposition and stripping steps.

In Fig. 8, stripping voltammograms for silver are shifted to more positive potential and diminished in height when the deposition is done at –0.1 V, where mercury(II) is not deposited on a bare carbon substrate. Changing the deposition potential to –1.0 V, where Hg(II) is deposited, increases the stripping peak for silver as expected in the absence of mercury (cf.

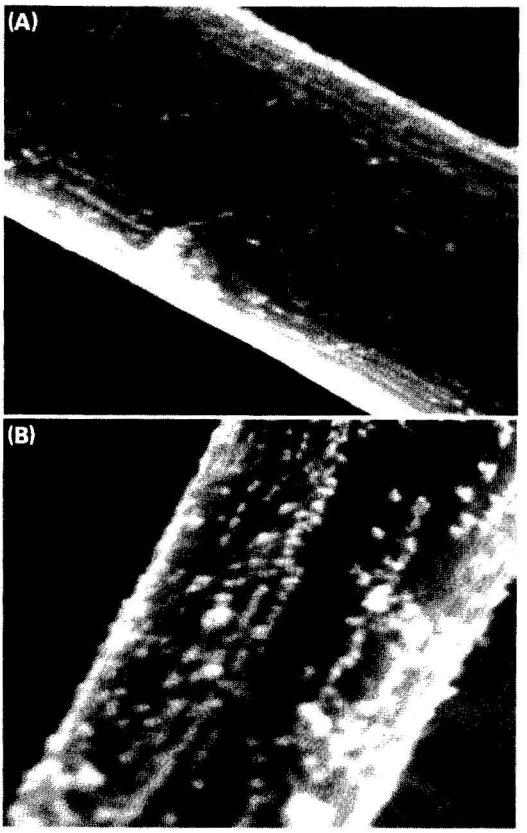

Fig. 7. Electron micrograph of an 8-μm diameter carbon fiber with silver deposited at −0.4 V in acetate buffer. Equivalent thickness of the deposit: (A) ca. 10 layers, (B) ca. 100 layers.

Table 2) but also results in a second peak at more negative potential. The silver stripping peak is shifted about 35 mV to less positive values and the second peak is about 70 mV less positive than would have been observed were silver absent. These investigations are not detailed enough to identify specific phases, but for brevity the more positive peak is referred to as the silver peak and the other as the mercury peak.

Both concentration and concentration ratio are important determinants of stripping behavior, as shown in Fig. 9. As the ratio of concentration [Hg(II)]/[Ag(I)] is increased, the mercury peak finally appears. Under these conditions, the mercury peak height doubles when the solution concentration is doubled at constant ratio, whereas the silver peak increases by only ca. 20%. It should be noted that the conditions of curve 5 correspond to the saturation region for deposition of mercury alone, in which peak height becomes independent of concentration.

The narrow range of conditions giving rise to two stripping peaks was investigated more closely with the results displayed in Figs. 10 and 11. It is

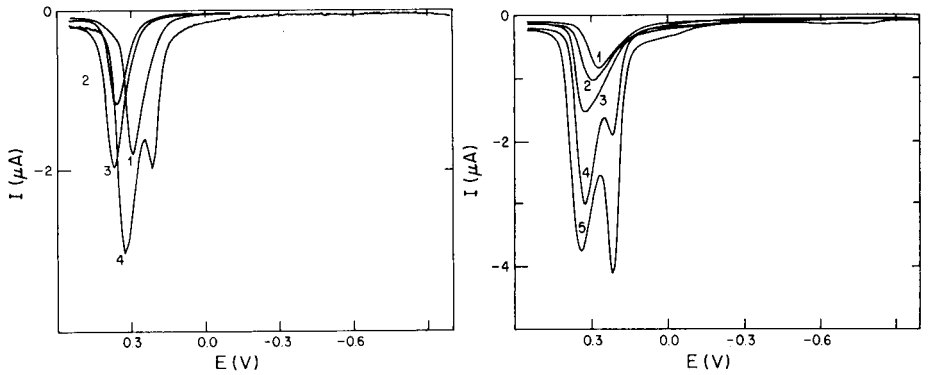

Fig. 8. Anodic-stripping square-wave voltammetry of silver in the presence of mercury at a carbon-fiber microelectrode (t_d = 30 s, acetate buffer pH 4.6). Deposition potential (V), Ag(I) concentration (μM) and Hg(II) concentration (μM): (1) —0.1, 10, 0; (2) —0.1, 10, 80; (3) —0.1, 20, 80; (4) —1.0, 20, 80.

Fig. 9. Anodic-stripping square-wave voltammetry of silver in the presence of mercury at a carbon fiber microelectrode (acetate buffer pH 4.6, E_{dep} = —1.0 V, t_{dep} = 30 s). Concentrations of Ag(I) and Hg(II) (μM): (1) 10, 0; (2) 10, 20; (3) 10, 40; (4) 10, 80; (5) 20, 160.

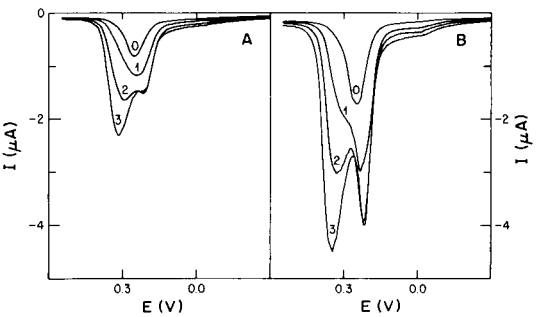

Fig. 10. Anodic-stripping square-wave voltammograms of silver and mercury (80 μM Hg(II) in the acetate buffer pH 4.6; E_{dep} = —10 V). Deposition time: (A) 30 s; (B) 90 s. Silver concentration: (0) 0; (1) 3; (2) 6; (3) 10 μM.

seen that the potential of mercury oxidation remains constant, whereas the peak for silver, while forming, approaches the values of anodic peak potential for silver deposited in the absence of mercury (see also Fig. 2). Also important in this experiment is the fact that longer deposition time improves deposition of mercury significantly in both cases. This is probably due to formation of amalgam and silver, both of which form a better substrate for further deposition of mercury.

Conclusions

Silver can be deposited on carbon-fiber surfaces. The relation between concentration and square-wave stripping peak current is linear at constant

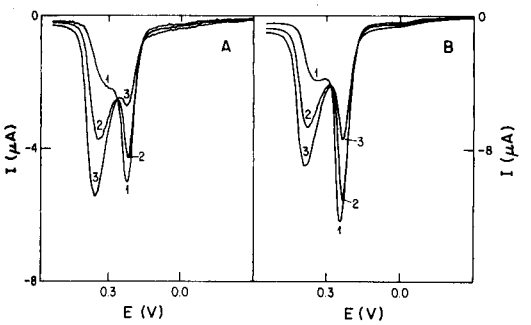

Fig. 11. Anodic-stripping square-wave voltammograms of silver and mercury. As for Fig. 10 but with 160 μM mercury(II). Silver concentration: (1) 10; (2) 20; (3) 30 μM.

deposition time, provided the total amount deposited is not more than a few equivalent monolayers. The suitable range of deposition potential is −0.3 to −0.8 V. At the lowest coverages, there is evidence for stripping of a first layer, and the current-time and current-potential behavior are those characteristic of the deposition mechanism of nucleation and growth. This process is much faster than reported at large glassy-carbon disk electrodes. It is not clear to what extent this is attributable to the high current densities which can be achieved at small cylindrical electrodes. Silver films are stable even when exposed to air, the worst case exhibiting a 30% decrease in stripping peak current after 5-min exposure. This permits simple experiments in which the fiber is plated in one solution, and then transferred to another for voltammetric studies. In all respects, the deposition of silver is better behaved than that of mercury. The codeposition of silver and mercury is quite complex, but deserves further study, for it presents the possibility of achieving substrates with favorable surface properties for analytical voltammetry.

This work was supported in part by the Office of Naval Research. J. O. gratefully acknowledges support from the Guggenheim Foundation. The authors thank Libardo Perez and George Nancollas for assistance with electron microscopy.

REFERENCES

1 J.-L. Ponchon, R. Cespuglio, F. Gonon, M. Jouvet and J.-F. Pujol, Anal. Chem., 51 (1979) 1483.
2 M. R. Cushman, B. G. Bennett and C. W. Anderson, Anal. Chim. Acta, 130 (1981) 323.
3 G. Schulze and W. Frenzel, Anal. Chim. Acta, 159 (1984) 95.
4 M. Ciszkowska and Z. Stojek, J. Electroanal. Chem., 191 (1985) 101.
5 M. A. Dayton, J. C. Brown, K. J. Stutts and R. M. Wightman, Anal. Chem., 52 (1980) 946.
6 R. S. Robinson and R. L. McCreery, Anal. Chem., 53 (1981) 997.
7 R. E. Panzer and P. J. Elving, Electrochim. Acta, 20 (1975) 635.
8 R. M. Wightman, M. R. Deakin, P. M. Kovach, G. W. Kuhr and K. J. Stutts, J. Electrochem. Soc., 131 (1984) 1581.

9 Hu Ing-Feng, D. H. Karweik and T. Kuwana, J. Electroanal. Chem., 188 (1985) 59.
10 L. Bjelica, R. Parsons and R. M. Reeves, Proc. 3rd Symp. on Electrode Processes, Proceedings Vol. 80-3, 1979, p. 190; Croat. Chem. Acta, 53 (1980) 211.
11 K. Aoki, K. Honda, K. Tokuda and H. Matsuda, J. Electroanal. Chem., 182 (1985) 267; 186 (1985) 79; 195 (1985) 51.
12 S. Sujaritvanichpong, K. Aoki, K. Tokuda and H. Matsuda, J. Electroanal. Chem., 199 (1986) 271.
13 K. Aoki, K. Tokuda and H. Matsuda, J. Electroanal. Chem., 206 (1986) 47.
14 J. J. O'Dea, M. Wojciechowski, J. Osteryoung and K. Aoki, Anal. Chem., 57 (1985) 954.
15 K. Aoki, K. Tokuda, H. Matsuda and J. Osteryoung, J. Electroanal. Chem., 207 (1986) 25.
16 J. Golas and J. Osteryoung, Anal. Chim. Acta, 181 (1986) 211.
17 J. Golas and J. Osteryoung, Anal. Chim. Acta, 186 (1986) 1.
18 V. J. Jennings and J. E. Morgan, Analyst, 110 (1985) 121.
19 S. P. Perone, Anal. Chem., 35 (1963) 2091.
20 A. Milchev, E. Vassileva and V. Kertov, J. Electroanal. Chem., 107 (1980) 323.
21 A. Milchev and E. Vassileva, J. Electroanal. Chem., 107 (1980) 324.
22 A. Milchev, B. Scharifker and G. Hills, J. Electroanal. Chem., 132 (1982) 277.
23 G. Gunawardena, G. Hills and J. Montenegro, J. Electroanal. Chem., 138 (1982) 241.
24 U. Eisner and H. B. Mark, Jr., J. Electroanal. Chem., 24 (1970) 345.
25 Kh. A. Brainina, Talanta, 18 (1971) 513.
26 T. R. Brumleve, J. J. O'Dea, R. A. Osteryoung and J. Osteryoung, Anal. Chem., 53 (1981) 702.
27 N. A. Shumilova and G. V. Zhutaeva, in A. J. Bard (Ed.), Encyclopedia of Electrochemistry of the Elements, Marcel Dekker, New York, 1978, Vol. VIII.
28 P. Wrona and Z. Galus, in A. J. Bard (Ed.), Encyclopedia of Electrochemistry of the Elements, Marcel Dekker, New York, 1982, Vol. IX, part A.
29 Electrochemical Stripping Analysis, F. Vydra, K. Stulik and E. Julakova, Ellis Horwood, Chichester, 1976.
30 J. Osteryoung and J. J. O'Dea, unpublished work.

Analytica Chimica Acta, 192 (1987) 237—242
Elsevier Science Publishers B.V., Amsterdam — Printed in The Netherlands

BIPOLAR PULSE CONDUCTIVITY MEASUREMENTS APPLIED TO ION-SELECTIVE ELECTRODES

JAMES R. SANDIFER*

Corporate Research Laboratories, Eastman Kodak Company, Rochester, New York 14650 (U.S.A.)

STANLEY GROSS

Analytical Technology Division, Eastman Kodak Company, Rochester, New York 14650 (U.S.A.)

(Received 16th May 1986)

SUMMARY

Bipolar pulse conductivity (BICON) measurements were evaluated as a means of using calcium ion-selective electrodes with an unpoised reference electrode. The study shows a change in total cell conductivity with Ca^{2+} concentration at low concentrations in the absence of other electrolytes but no change in conductivity with Ca^{2+} concentration in the presence of 0.1 M KCl. The computed voltage at zero current varied with Ca^{2+} concentration but electroactive species interfered with the measurements. For the conditions used, it is concluded that there is no change in conductivity of the ion-selective membrane with Ca^{2+} concentration and that reliable quantitation of Ca^{2+} is not feasible.

Bipolar pulse conductivity (BICON) measurements were introduced by Johnson and Enke [1] as a means of measuring the conductances of solutions (1 μS to 10 mS) rapidly (<40 μs) and accurately (0.01%) with minimum interference from capacitive charging effects. This approach was later extended by Daum and Nelson [2] to include the analogous approach with current pulses and voltage measurements. Further advances included computer control for chemical rate determinations [3].

The idea of using BICON measurements with ion-selective electrodes was introduced by Powley et al. [4] on the basis of their study of a commercially available calcium electrode. They observed apparent changes in the conductivity of the membrane with changes in calcium concentration in the solution. This observation is consistent with those made by Brand and Rechnitz [5], except that the latter study [5] indicated that resistance changes are observable only at low frequencies (ca. 10 Hz) while the BICON measurements were made with higher frequencies (10 kHz). A possible explanation for this discrepancy is that impedance measurements are typically done with an applied voltage of <10 mV while the BICON technique involves applied voltages up to 5 V. Higher applied voltages may lead to concentration-dependent effects.

0003-2670/87/$03.50

Additional BICON measurements were made with the Orion Model 94-09 fluoride ion-selective electrode [6]. Again, variations of conductivity with changing analyte concentration were noted, consistent with similar observations made by Cammann and Rechnitz [7], who used a current-transient technique and attributed their results to slow, concentration-dependent interfacial kinetics. As with the calcium-electrode study, the BICON measurements [6] and the current-transient measurements [7] were in different time domains and substantially different voltages were applied.

Further experiments with a calcium ion-selective coated-wire electrode [8] revealed no concentration-dependent conductance. It was shown, however, that a series of pulses with different voltage amplitudes could be used to generate a series of current responses, which could then be extrapolated to "zero-pulse current" to obtain "zero-current" voltages that varied with Ca^{2+} concentration.

Ion-selective electrodes have two generic limitations when used in the conventional manner. They require reference electrodes which usually have liquid junctions and so liquid-junction potentials, and they respond to activities rather than concentrations. Because the BICON technique promises a means for avoiding both of these problems, this study was initiated to evaluate its capabilities.

EXPERIMENTAL

Instrumentation

A PAR 273 potentiostat was programmed through a Hewlett-Packard 9816 desktop computer to act as a BICON instrument. (Programs are available from the authors upon request.) A typical experiment consisted of a series of ten bipolar voltage pulses, with amplitudes descending from 2 to 0 V. These were applied to the cell at 1-ms intervals. Each composite bipolar pulse consisted of a 100-μs voltage segment, followed immediately by a second segment of equal duration but opposite polarity. The polarity sequence was reversible under computer control. A relay in the PAR 273 potentiostat connected the cell only while the experiments were in progress. Each experiment was repeated 100—500 times, and the results were averaged to improve the signal/noise ratio (S/N). Best performance was obtained with a current range of 100 μA, and an IGAIN value of 5 (4% of full scale corresponds to 200 counts).

Results in Fig. 1 demonstrate the use of the instrument with a 100-kΩ resistor. Voltage rise and fall times are less than 10 μs and current responses show the expected overshoots caused by capacitive charging [1] when viewed on an oscilloscope.

Linear plots are produced when currents at the end of the BICON pulse are plotted against applied voltages. A linear least-squares routine was used to calculate the slope, intercept on the current axis, and correlation coefficient. The 100-kΩ resistor yielded a slope of 9.86 μS, an intercept at

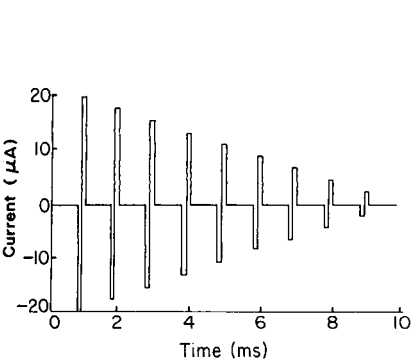

Fig. 1. BICON response of 100 kΩ resistor.

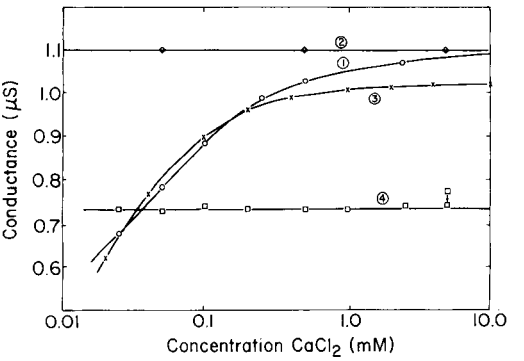

Fig. 2. BICON-measured conductivities (from regression slopes) of two calcium ion-selective electrodes in solutions with different calcium chloride and potassium chloride compositions. Curves: (1) Orion electrode with no potassium chloride added; (2) Orion electrode with 0.1 M potassium chloride added as supporting electrolyte; (3) theoretical response of Orion electrode (curve 1), assuming that all observed conductance changes occur in the solution and that the membrane resistance is constant; (4) Corning electrode with 0.1 M potassium chloride added as supporting electrolyte.

0.0778 μA, and a correlation coefficient of 1.000. These values translate into a "zero-current voltage" (intercept on the voltage axis) of −8 mV, which is the voltage offset of the instrument under these conditions. The standard deviation of the slope was 0.00115 μS. Results of similar quality were obtained with a 1-MΩ precision resistor. It is concluded that the resistances of the ion-selective electrodes used in this study, which vary between 0.1 and 1.0 MΩ, can be measured with an imprecision of 1%.

Linear current/voltage curves were also obtained with the ion-selective electrodes with correlation coefficients of marginally less than 1. This was probably due to minor interferences from parallel cell capacitance. Results which yielded correlation coefficients less than 0.985 were discarded.

Electrodes and solutions

Two commercially-available calcium ion-selective electrodes were used, the Orion Model 93-20 electrode, studied by Powley et al. [4], and the Corning 476041 electrode. The Orion electrode has two sensing modules, one of which was found to be too resistive to be used with the BICON instrument. The electrodes were calibrated potentiometrically both before and after each series of BICON experiments, and were found to retain their potentiometric function. A 6-mm diameter platinum counter electrode (Corning 476060) was used for the BICON measurements while potentiometric measurements were referred to an Orion double-junction reference electrode. Electrodes were contained in a standard holder and were spaced about 22 mm apart. Electrodes were inserted into 50-ml glass beakers containing the solutions of interest and were not disturbed during the experiment.

Solutions were prepared with distilled water from reagent-grade potassium chloride and calcium chloride. In a typical run, 0.1 M calcium chloride was added stepwise to 40 ml of either distilled water or 0.1 M potassium chloride, to vary the calcium concentration between 0 and 10 mM.

RESULTS AND DISCUSSION

Results obtained with both calcium ion-selective electrodes are shown in Fig. 2. Curve 1 was obtained with the Orion electrode in calcium chloride solutions without supporting electrolyte. Conductance increases almost linearly with log concentration up to about 0.1 mM, with decreasing slope above 1.1 μS. This value translates to a resistance (0.91 MΩ), which is close to the high-frequency limit (0.8 MΩ) reported by Brand and Rechnitz [5]. When 0.1 M KCl is included (curve 2), the conductance is constant at the high concentration limit observed without KCl. It is concluded that the measured cell resistance is the sum of the solution resistance and the high-frequency limiting resistance of the ion-selective membrane. As a test of this conclusion, the response expected assuming linear variation of solution conductance and fixed membrane resistance was computed (curve 3 in Fig. 2). The "best fit" results of these calculations agree adequately with experimental results (curve 1).

Similar results were obtained with the Corning electrode for the situation in which 0.1 M KCl was included (curve 4, Fig. 2). The higher point at 5 mM Ca^{2+} was found to be due to a depth effect that was eliminated when the solution level was lowered or the electrode was raised to a fixed depth of immersion. This effect is attributed to capacitive coupling through the walls of the ion-selective electrode itself. Raising the liquid level has the effect of increasing the number of conductive pathways, thus increasing the measured conductance. This effect was observed early in the course of this study, and was avoided by careful positioning of the electrodes.

"Zero-pulse currents" measured in the course of these experiments were examined to see if they could be used for quantitation. "Zero-current voltages" were calculated from these currents and the slopes of the current/voltage curves. These voltages vary with calcium chloride activity; however, because the voltages contain random variations in the potential of the unpoised reference electrode (platinum), the calibration plots are not linear. This is shown in Fig. 3, where "zero-current voltages" are compared to potentiometric responses referenced to an Orion double-junction electrode. Attempts to poise the potential of the platinum electrode by adding potassium hexacyanoferrate(II)/hexacyanoferrate(III) to the sample solutions were only partially successful, and caused the interference mentioned earlier [9]. It would appear that it is better to use a conventional reference electrode, in which case the conventional potentiometric measurement is probably also preferable.

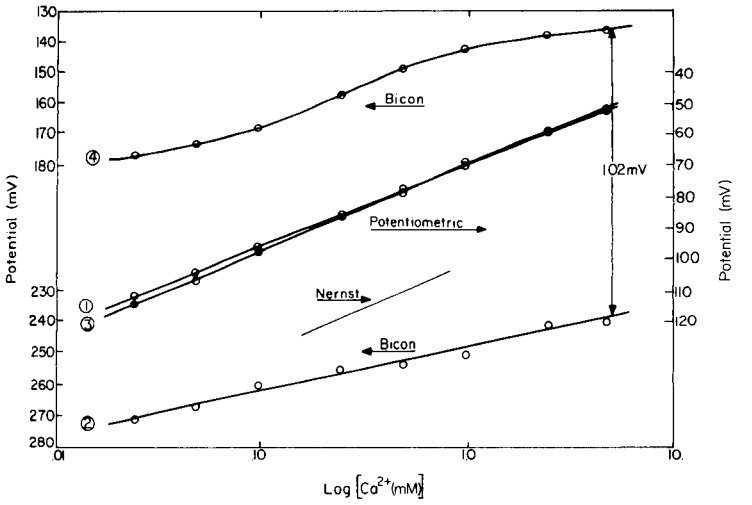

Fig. 3. Comparison of potentiometric and BICON "zero-current voltages". Ratio of potassium hexacyanoferrate(III) to hexacyanoferrate(II) is 10 for curves 1 and 2 and 0.1 for curves 3 and 4. The highest concentration in these ratios is 1 mM. Experiments were done in the order indicated to the left of each curve.

Conclusions

Although these studies were unsuccessful in applying the BICON technique as a viable way to use ion-selective electrodes, the idea of measuring the resistance or impedance of ion-selective electrodes is an interesting and intriguing one that is worth further investigation. The results of Kvastek and Horvat [10] suggest that silver ion concentrations can be determined from Warburg diffusional impedances measured at the surfaces of silver/silver halide electrodes of the second kind. Marecek and Samec [11] used a hanging electrolyte electrode to quantify acetylcholine concentration by differential-pulse polarography. Rubinstein [12], who demonstrated a voltammetric pH measurement with a surface-modified electrode and voltammetric internal-reference electrode, addresses the same issue. Although the present study did not achieve the desired goals, it is worthwhile to continue to seek processes by which a measurement traditionally made in a "passive" way can be made in an "active" way which renders a precisely poised reference potential unnecessary, without loss of the selectivity inherent in the composition of the electrode used.

REFERENCES

1 D. E. Johnson and C. G. Enke, Anal. Chem., 42 (1970) 329.
2 P. H. Daum and D. F. Nelson, Anal. Chem., 45 (1973) 463.
3 K. J. Caserta, F. J. Holler, S. R. Crouch and C. G. Enke, Anal. Chem., 50 (1978) 1534.
4 C. R. Powley, R. F. Geiger, Jr. and T. A. Nieman, Anal. Chem., 52 (1980) 705.
5 M. J. D. Brand and G. A. Rechnitz, Anal. Chem., 41 (1969) 1185.

6 C. R. Powley and T. A. Nieman, Anal. Chim. Acta, 139 (1982) 83.
7 K. Cammann and G. A. Rechnitz, Anal. Chem., 48 (1976) 856.
8 C. R. Powley and T. A. Nieman, Anal. Chim. Acta, 139 (1982) 61.
9 C. R. Powley and T. A. Nieman, Anal. Chim. Acta, 155 (1983) 1.
10 K. Kvastek and V. Horvat, J. Electroanal. Chem., 130 (1981) 67.
11 V. Marecek and Z. Samec, Anal. Lett., 14(B15) (1981) 1241.
12 I. Rubinstein, Anal. Chem., 56 (1984) 1135.

Analytica Chimica Acta, 192 (1987) 243—253
Elsevier Science Publishers B.V., Amsterdam — Printed in The Netherlands

DIRECT IDENTIFICATION OF PENTOSES AND HEXOSES BY PYROLYSIS/CAPILLARY GAS CHROMATOGRAPHY

D. R. BUDGELL[a], E. R. HAYES* and R. J. HELLEUR[b]
Department of Chemistry, Acadia University, Wolfville, Nova Scotia B0P 1X0 (Canada)
(Received 7th August 1986)

SUMMARY

The combination of rapid pyrolysis and capillary-column gas chromatography (pyrolysis/capillary g.c.) was used to identify the stereoisomers of pentoses and hexoses. Analytical pyrolysis is shown to be a viable alternative to the formation of volatile derivatives of carbohydrates for chromatographic separation. The individual stereoisomers (glucose, galactose, arabinose, xylose etc.) were positively identified by the retention times of their distinctive anhydrosugar products. The aldohexoses formed both 1,6-anhydrohexopyranose and 1,6-anhydrohexofuranose products; the aldopentoses formed 1,4-anhydropentopyranose products; and the ketohexoses, to a lesser extent, formed 2,6-anhydrohexofuranose products. The anhydrosugars were identified by mass spectrometry and many were authenticated with standard samples. Pyrolysis/capillary g.c. is rapid and direct and is useful for solids and solutions and for microscale samples. Sample preparation or prior derivatization is not required. Experimental parameters that are important for structural characterization and reproducibility include sample size, pyrolysis temperature, transfer zones and the type and film thickness of the capillary column.

The carbohydrates comprise several homologous series characterized by a plurality of asymmetric carbons having a hydroxyl group and at least one carbonyl functional group, an aldehyde or ketone, usually in the hemiacetal (hemiketal) form. Polysaccharides are polymers of these products having acetal linkages joining the component residues. Carbohydrates are non-volatile, thus requiring derivatization before gas chromatographic separation and identification of any of a large number of individual isomeric structures. Traditional identification of polysaccharides usually consists of isolation, hydrolysis, methylation or other derivatization steps, re-isolation and finally identification by an instrumental technique such as gas chromatography (g.c.) or mass spectrometry (m.s.). Satisfactory characterization of the sample requires substantial amounts of sample and good yields at each procedural step. Ideally, a more direct method for the identification of carbohydrates is needed.

Analytical pyrolytic techniques in combination with gas chromatography

[a]Present address: Chemistry Department, McGill University, Montreal, Canada.
[b]Present address: Chemistry Department, Memorial University, St. John's, Newfoundland, Canada.

0003-2670/87/$03.50

(py./g.c.), or mass spectrometry (py./m.s.) have been used extensively to identify small quantities of complex biological materials [1, 2]. Analytical pyrolysis has been used in many studies to characterize carbohydrates, but most involved the use of py./m.s. techniques [3, 4]. These studies have shown that individual monomers give rise to characteristic peak patterns providing a basis for distinguishing hexoses, pentoses, hexouronic acids and deoxysugars. The technique can also provide evidence for the presence of carbohydrate substituents, e.g., 6, *O*- or *N*-acetyl groups, amino groups or pyruvate substituents [2]. Although there are distinct advantages of py./m.s., disadvantages are the high cost and sophistication of equipment, difficulty in obtaining quantitative results and more importantly, its inability to distinguish between structural isomers. Because a great number of isomeric products are formed from the pyrolysis of carbohydrates, gas chromatography must be integrated in order to separate and identify them.

The py./g.c. technique has been used infrequently for the characterization of carbohydrates. Morgan and Jacques [5] reported the use of py./g.c. for the identification of simple carbohydrates. When glucose and galactose were sampled from water, their pyrograms were indistinguishable. However, sampling from aqueous boric acid solutions permitted characterization based on the comparison of product peak ratios because of the selective complex reactions of sugars with boric acid. Recently, py./g.c. has been used successfully in this laboratory as a rapid technique for characterizing the structural features of algal galactans by identifying the presence of simple anhydro, *O*-methyl and sulphated saccharide units [6, 7]. An important feature occurring during pyrolysis of galactans is that initial glycoside bond cleavage occurs, resulting in the formation of unique high-molecular-weight pyrolysis products, e.g., anhydrosugars, characteristic of individual polymeric units. It is remarkable that these very polar (and structurally significant) products are being eluted from the g.c. column.

This paper describes the results of further efforts to develop py./g.c. for the characterization of carbohydrates. This study is part of a systematic investigation to improve the use of analytical pyrolysis for the identification of biopolymers. The results of these studies of monosaccharides have greatly assisted in a subsequent study which uses py./g.c. to characterize the saccharide composition of oligosaccharides and polysaccharides [8].

Consideration was given to the overall design of the py./g.c. method so that pyrolysis, separation, detection and identification were undertaken in an integrated and efficient way to ensure simplicity, sensitivity and reproducibility. Some important operating parameters included pyrolysis temperature, sample size, product transfer and the type and thickness of the liquid phase of the capillary column. Mass spectrometry was used to identify the pyrolysis products.

EXPERIMENTAL

Apparatus

Analytical pyrolysis was done with a Chemical Data System (CDS) Pyroprobe 120 equipped with a platinum coil-heated probe. Commercially available quartz sample tubes were used. A CDS gas chromatographic interface, consisting of a heated box containing a metal tube into which the pyrolysis probe was inserted, was mounted horizontally and connected to the injection port of a Hewlett-Packard 5880A level-2 gas chromatograph (g.c.). The g.c. was equipped with a flame-ionization detector and a capillary column inlet. The front end of the installed capillary column was threaded up through the injection port and placed level with the bottom of the probe interface. The g.c. system was upgraded for peak integration by interfacing the detector to an Apple computer with the Adalab 'chromatochart' software program. Helium was used as the carrier gas. The capillary-column head pressure was adjusted to 10 psi.

The pyrolysis products were examined by pyrolysis/gas chromatography/mass spectrometry. The conditions of pyrolysis and chromatographic separation were as described below; the chromatograph used was a Finnigan Model 9610. The capillary-column outlet was lead directly into the ion source region of a Finnigan MAT 4500 quadrupole mass spectrometer. Mass spectrometric detection was done with 70-eV electron-impact ionization, an interface temperature of 250°C and an ion source temperature of 120°C. Chemical ionization work was done with isobutane (0.6 Torr instrument reading) as the reagent gas.

Samples

The hexose and pentose samples, all in the D-enantiomeric series (Sigma, St. Louis, MO) were used as received. Samples of 1,6-anhydroallopyranose, 1,6-anhydrogalactopyranose, 1,6-anhydrogalactofuranose, 1,6-anhydroglucopyranose, 1,6-anhydromannopyranose and 1,6-anhydrotalopyranose were provided by Dr. N. K. Richtmyer. Samples of 1,4-anhydroarabinopyranose, 1,4-anhydrolyxopyranose, 1,4-anhydroribopyranose and 1,4-anhydroxylopyranose were given by Dr. P. Köll, University of Oldenburg, West Germany.

Pyrolysis conditions

Galactose was pyrolyzed at different temperatures between 350 and 800°C. At low pyrolysis temperatures, substantial amounts of unwanted tar remained in the sample tube. At higher temperatures, the result was a larger production of structurally-insignificant low-molecular-weight products. A pyrolysis temperature of 650°C was selected, thus yielding reproducible pyrograms and high-molecular-weight products characteristic of the initial carbohydrate structure. With the pyrolysis heat ramp turned off, the final pyrolysis temperature of 650°C was reached in about 0.4 s. Samples were ground to a powder to insure efficient heat transfer throughout the sample

and to minimize secondary pyrolysis reactions. Samples were weighed to approximately 100 μg. A quartz sample tube was used because it could readily accommodate solid or small liquid samples, thus simplifying sample handling. The sample was placed on top of a quartz wool plug which was already inserted two thirds of the way along the tube. This space in the tube allowed for condensation of any unwanted tar or carbonized product.

The probe, containing a loaded sample tube, was inserted into the pre-heated interface (220°C, to insure minimum loss of product by condensation) and the chamber was purged with carrier gas at a flow rate of 50 ml min^{-1} for 20 s. The sample was then pyrolyzed at 650°C for 10 s. The pyrolysis products were quickly swept out from the interface onto the g.c. column at a total flow rate of 26 ml min^{-1}. The column flow rate was measured at 1.5 ml min^{-1} (10 psi through a 30-m capillary column). The calculated split ratio of 18:1, although high, was found to be necessary for rapid transfer of the gaseous pyrolysis products and resulted in better reproducibility.

Selection of capillary column and chromatographic conditions

The pyrolysis products were chromatographed on bonded-phase, fused-silica capillary columns (30 m × 0.329 mm). The initial temperature of 100°C was held for 2 min, then increased at 5° min^{-1} to 245°C and held for 5 min. The inlet and detector temperatures were 260°C; the column flow rate was 1.5 ml min^{-1} (column pressure at 10 psi) and the chart speed was 0.5 cm min^{-1}.

A 30-m column was required for satisfactory separation of the anhydrosugar products. Use of a bonded-phase column led to excellent stability even after repeated high temperature programming and hundreds of sample loadings. Three capillary columns examined were DB-5 (1 μm thick), a DB-1701 (0.25 μm thick) and a DB-1701 (1 μm thick). The more polar and thicker bonded-phase DB-1701 column showed the best performance. To evaluate the reproducibility, two triple sets of 80 μg and 120 μg samples of galactose were pyrolyzed. The retention times of the pyrolysis products varied only slightly, but, more importantly, the peak ratios of selected products varied by less than 10%.

RESULTS AND DISCUSSION

Pyrolysis mechanisms of monosaccharides

Shafizadeh [9] has identified many of the important pyrolysis products and provided a better understanding of carbohydrate pyrolysis. There are basically two classes of compounds formed from rapid pyrolysis of carbohydrates; they are anhydrosugars and furan derivatives. Typical pyrograms of aldohexoses obtained from the Pyroprobe py./g.c. system are given in Figs. 1 and 2. There are four major pyrolysis products in Fig. 1 (for glucose); they are 1,6-anhydroglucofuranose, 1,6-anhydroglucopyranose, 5-hydroxy-

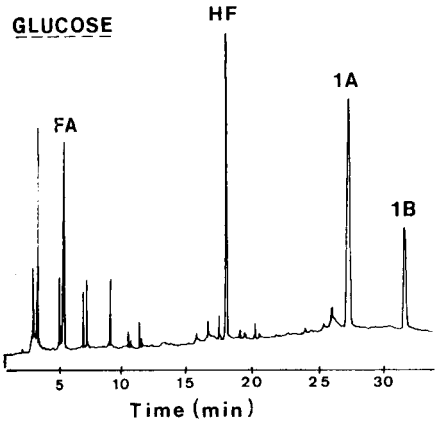

Fig. 1. Pyrogram of glucose. See Table 1 for identities of labelled peaks.

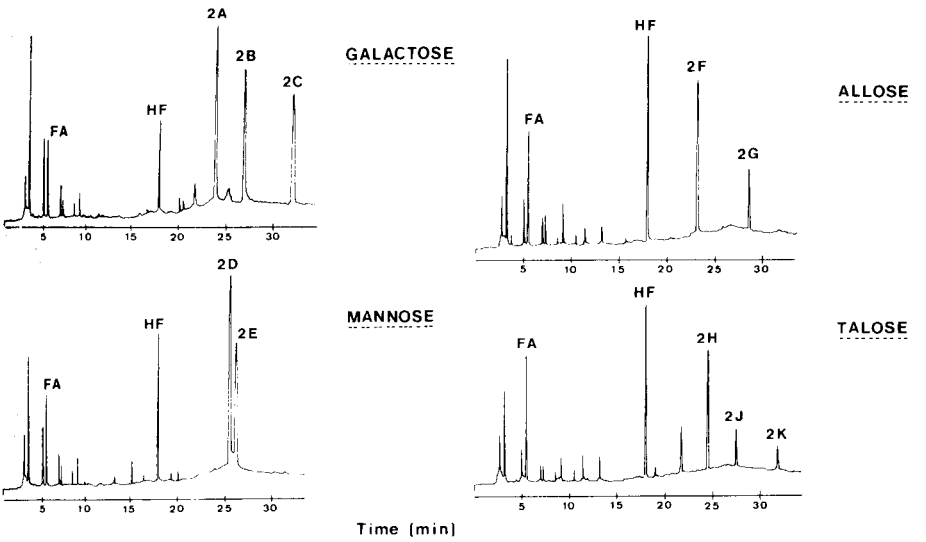

Fig. 2. Pyrograms of galactose, mannose, allose and talose. See Table 1 for identities of labelled peaks.

methylfuraldehyde and furaldehyde. An important result of this study is the detection of the anhydroaldohexoses (without derivatization). To date, only van der Kaaden et al. [10] have reported the detection of anhydroglucose in the py./g.c. of glucans; however, the resolution and peak shape of their observed anhydrosugar was not as good as that obtained in the present study.

The anhydrosugars are the most important pyrolysis products for successful application of py./g.c. in the characterization of carbohydrates. In most

reactions, anhydrosugars are formed by transglycosidation involving the glycoside bonds of polysaccharides. Polycondensation of monosaccharides has been found to occur at elevated temperatures, forming random polymers having linkages involving the C—1 glycosidic carbon [11]. In the pyrolysis conditions of this study, the preliminary purge step, which involves insertion of the sample probe into the heated interface (at 220°C), is responsible for initiating the required condensation reaction. The condensed product is then subjected to pyrolysis at 650°C and the polymer bonds are broken through intraglycosidation to form the stable 1,6-anhydrohexoses from aldohexoses (1,4-anhydropentoses from aldopentoses or 2,6-anhydroketoses from ketohexoses). The formation and structures of some of the characteristic anhydrosugars are illustrated in Fig. 3. It is thought that the uncondensed portion of the monosaccharide contributes to the formation of the dehydration products, 5-hydroxymethylfuraldehyde and/or furaldehyde.

The 1,6-anhydrohexoses are commonly found in large quantities in the pyrolysis products of aldohexoses as well as from polysaccharides [12] but only small amounts of anhydrosugars (i.e., 1% yield) have been detected from the pyrolysis of ketohexoses [13]. The pyrogram of fructose (see Fig. 4) reveals the presence of small amounts of 2,6-anhydrofructofuranose. Large quantities of 5-hydroxymethylfuraldehyde are formed from ketoses. Aldopentoses pyrolyze in the same manner as their hexose counterparts to form their characteristic anhydrosugars. For example, arabinose forms 1,4-anhydroarabinopyranose and this is seen in its pyrogram (Fig. 5). No other py./g.c. study has detected the presence of anhydropentoses, although one study confirmed the presence of anhydropentoses in the pyrolysis mixture [14]. Furaldehyde and an uncharacterized product, a structural isomer of anhydropentose, are also present in pyrograms of pentoses.

Py./g.c. distinction among the monosaccharides

Many of the pyrolysis products identified from sugars are common to all saccharides. In general, the presence of a substantial quantity of 5-hydroxymethylfuraldehyde in the pyrogram indicates that a hexose is present. Substantial amounts of furaldehyde and the absence of 5-hydroxymethylfuraldehyde in the pyrolysis products indicates the presence of a pentose.

The only pyrolysis product which retains the specific stereo-configuration of the parent sugar molecule which is also observed in the pyrogram is the anhydrosugar. Positive identification of the various anhydrosugars and sufficient g.c. resolution of each isomer afforded the means of identifying and discriminating among the hexoses and pentoses. In this study, the identity of glucose, galactose, mannose, talose and allose was confirmed by g.c./m.s. of authentic samples of their respective 1,6-anhydrohexopyranose (Table 1). In addition to 1,6-anhydrohexopyranose structures, aldohexoses can also form their 1,6-anhydrohexofuranose products [12]. Hence, the identity of galactose was also confirmed by an authentic sample of 1,6-anhydrogalactofuranose. From m.s. studies, it was noted that all anhydro-

ALDOHEXOSES

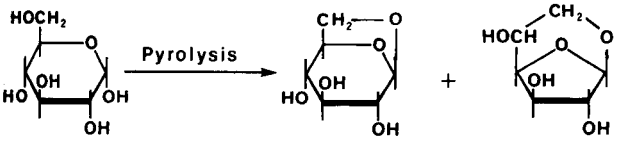

Glucose — 1,6-Anhydroglucopyranose — 1,6-Anhydroglucofuranose

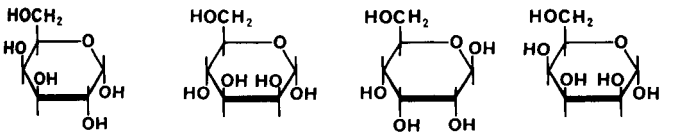

Galactose — Mannose — Allose — Talose

KETOHEXOSES

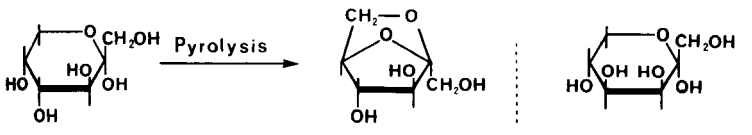

Fructose — 2,6-Anhydrofructofuranose — Tagatose

ALDOPENTOSES

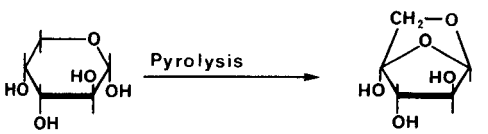

Arabinose — 1,4-Anhydroarabinopyranose

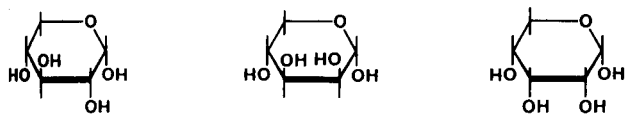

Xylose — Lyxose — Ribose

Fig. 3. Structures of monosaccharides and selected anhydrosugar products. Monosaccharides are in their D-enantiomeric form and drawn in their pyranose structure for simplicity and comparison.

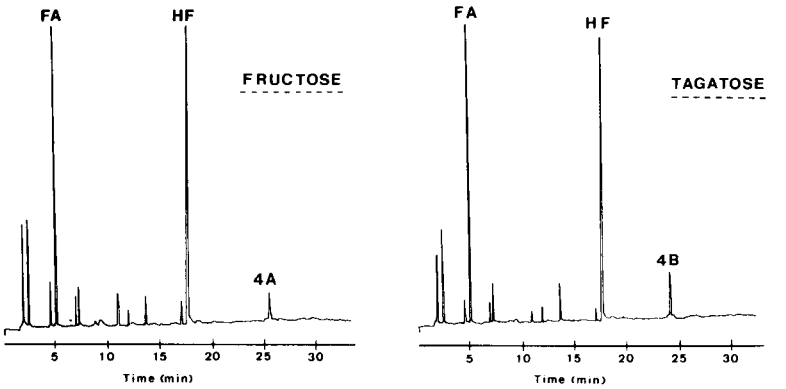

Fig. 4. Pyrograms of the ketohexoses fructose and tagatose. See Table 1 for identities o labelled peaks.

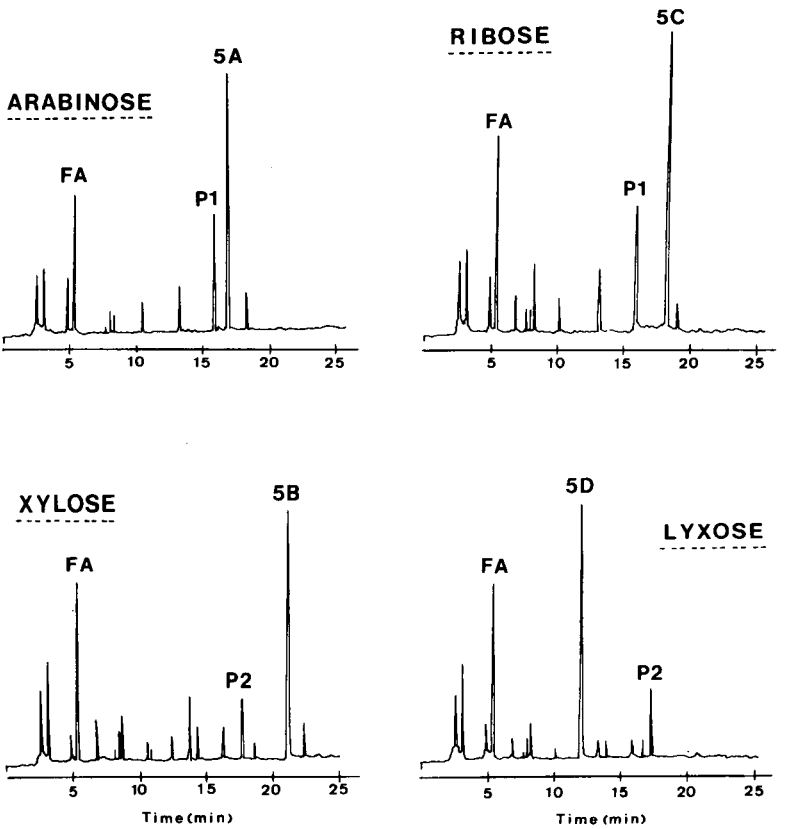

Fig. 5. Pyrograms of arabinose, xylose, lyxose and ribose. See Table 1 for identities o labelled peaks.

TABLE 1

Important pyrolysis products observed in pyrograms of monosaccharides

	Peak[a]	Retention time (min)	Compound (identification[b])
Common products			
	FA	5.45	2-Furaldehyde (r)
	HF	18.10	5-Hydroxymethyl-2-furaldehyde (r)
Aldohexoses (Figs. 1 and 2)			
Glucose	1A	27.40	1,6-Anhydroglucopyranose (m, r)
	1B	31.65	1,6-Anhydroglucofuranose (m, t)
Galactose	2A	24.10	1,6-Anhydrogalactopyranose (m, r)
	2B	27.10	1,4-Anhydrogalactopyranose (m, t)
	2C	32.30	1,6-Anhydrogalactofuranose (m, r)
Mannose	2D	25.60	1,6-Anhydromannopyranose (m, r)
	2E	26.40	1,6-Anhydromannofuranose (m, t)
Allose	2F	23.40	1,6-Anhydroallopyranose (m, r)
	2G	28.75	1,6-Anhydroallofuranose (m, t)
Talose	2H	24.65	1,6-Anhydrotalopyranose (m, r)
	2J	27.80	1,4-Anhydrotalopyranose (m, t)
	2K	32.15	1,6-Anhydrotalofuranose (m, t)
Ketohexoses (Fig. 4)			
Fructose	4A	25.75	2,6-Anhydrofructofuranose (m, t)
Tagatose	4B	24.10	2,6-Anhydrotagatofuranose (m, t)
Aldopentoses (Fig. 5)			
Arabinose	5A	17.05	1,4-Anhydroarabinopyranose (m, r)
Xylose	5B	21.30	1,4-Anhydroxylopyranose (m, r)
Ribose	5C	18.55	1,4-Anhydroribopyranose (m, r)
Lyxose	5D	12.10	1,4-Anhydrolyxopyranose (m, r)
(from arabinose, ribose)	P1	16.00	a pyranone ?
(from xylose, lyxose)	P2	17.35	a pyranone ?

[a]As indicated in the figures cited. [b]Identification by m, mass spectra; r, confirmed by retention time of authentic sample; t, tentative identification.

sugar isomers produce very similar electron-impact mass spectra. On this basis, 1,6-anhydrohexofuranose forms of the remaining four aldohexoses were tentatively confirmed by m.s. The pyrograms obtained from galactose and talose indicated the presence of a third type of anhydrosugar. It has been speculated that these are 1,4-anhydrohexopyranoses [15].

The presence of 2,6-anhydrofructofuranose and 2,6-anhydrotagatofuranose, products of fructose and tagatose respectively, were tentatively confirmed by matching their chemical-ionization mass spectra with those of authentic samples [16]. On pyrolysis, the pentoses arabinose, ribose, xylose and lyxose form their respective 1,4-anhydropentopyranoses, and again, their identities were confirmed with authenticated samples.

By using the appropriate capillary column (i.e., DB-1701, 1 μm thick 30 m long), the glucose (Fig. 1), galactose, mannose, talose and allose (Fig. 2) anhydrosugars are clearly resolved in the pyrograms. Their retention times are listed in Table 1. Pentose anhydrosugars are also chromatographically separated (see Fig. 5); their retention times are very different from one another. Unfortunately, 1,4-anhydroribopyranose cannot be resolved from 5-hydroxymethylfuraldehyde peak (Table 1). If product identity is in question, mass spectrometry could be used. The appearance of 2,6-anhydro fructofuranose in the pyrogram of fructose is well resolved from that of 2,6 anhydrotagatofuranose (Fig. 4) but the retention times of these anhydro ketohexoses are noticeably close to one or more of those of the anhydro hexoses as is seen in Table 1.

Mixtures and aqueous solutions of monosaccharides

A mixture of five monosaccharides was prepared with equal amounts of the aldopentoses, arabinose and xylose, and of the aldohexoses, glucose galactose and mannose. The resulting pyrogram of this complex mixture is shown in Fig. 6. All the anhydrosugars that would be expected to be formed are present and are chromatographically resolved. Interestingly, the peak areas (or the sum of peak areas for the aldohexoses) of the individual anhydrosugars products are almost equal. This result may prove promising in future pyrolysis studies involving quantitative measurements, i.e., composition of oligosaccharides and polysaccharides.

Analyses of aqueous solutions of carbohydrates by py./g.c. should prove useful in many studies. For example, experiments involving the identification of polysaccharides usually require hydrolysis of the polymeric sample to give the individual monosaccharides. Instead of lengthy isolation and derivatization steps, an aliquot of the hydroxylate could be analyzed by py./g.c to establish the monosaccharide composition. The pyrolysis of an aqueous

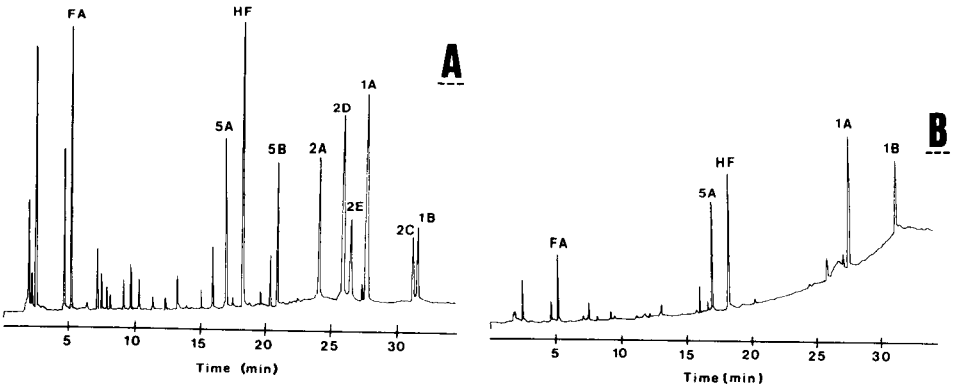

Fig. 6. Pyrograms: (A) monosaccharide mixture consisting of equal amounts of glucose galactose, mannose, arabinose and xylose; (B) an aqueous solution containing equal concentrations of glucose and arabinose.

mixture of equal amounts of arabinose and glucose (5 mg of each per ml of water) was studied. A 2-μl aliquot, representing 10 μg of each sugar, was placed on top of a quartz wool plug. The water was evaporated during the 20-s purge step and the residue was pyrolyzed. The resulting pyrogram is shown in Fig. 6. The pyrogram shows the individual anhydrosugars of the carbohydrates that were present in the solution.

The results of this investigation were used in a succeeding study of the characterization of oligosaccharides and polysaccharides by py./g.c. [8].

The authors thank the Atlantic Research Laboratory, NRC, Halifax for the use of the mass spectrometer and for financial assistance. Anhydrosugar standards from Drs. P. Köll and N. K. Richtmyer are greatly appreciated.

REFERENCES

1 W. J. Irwin, Analytical Pyrolysis: A Comprehensive Guide, M. Dekker, New York, 1982.
2 H. L. C. Meuzelaar, J. Haverkamp and F. D. Hileman, Pyrolysis Mass Spectrometry of Recent and Fossil Biomaterial, Elsevier, Amsterdam, 1982.
3 H.-R. Schulten, U. Bahr, H. Wagner and H. Herman, Biomed. Mass Spectrom., 9 (1982) 115.
4 H.-R. Schulten, U. Bahr and W. Gortz, J. Anal. Appl. Pyrol., 3 (1981/1982) 229.
5 S. L. Morgan and C. A. Jacques, Anal. Chem., 54 (1982) 741.
6 R. J. Helleur, E. R. Hayes, W. D. Jamieson and J. S. Craigie, J. Anal. Appl. Pyrol., 8 (1985) 333.
7 R. J. Helleur, E. R. Hayes, J. S. Craigie and J. L. McLachlan, J. Anal. Appl. Pyrol., 8 (1985) 349.
8 R. J. Helleur, D. R. Budgell and E. R. Hayes, Anal. Chim. Acta, 192 (1987) 367.
9 F. Shafizadeh, J. Anal. Appl. Pyrol., 3 (1982) 283.
10 A. van der Kaaden, J. J. Boon and J. Haverkamp, Biomed. Mass Spectrom., 11 (1984) 486.
11 J. W. Liskowitz and B. Carroll, Carbohydr. Res., 5 (1967) 245.
12 R. D. Guthrie, in W. Pigman and D. Horton (Eds.), The Carbohydrates: Chemistry and Biochemistry, Academic Press, New York, 1972, p. 423.
13 P. Köll, S. Deyhim and K. Heyns, Chem. Ber., 111 (1978) 2909.
14 P. Köll, S. Deyhim and K. Heyns, Chem. Ber., 106 (1973) 3565.
15 P. Köll, Chem. Ber., 106 (1973) 3559.
16 P. Köll, private communications.

Analytica Chimica Acta, 192 (1987) 255—265
Elsevier Science Publishers B.V., Amsterdam — Printed in The Netherlands

CORRELATION OF SOLUTE RETENTION IN GAS CHROMATOGRAPHY WITH PROPERTIES OF THE ANION FOR TETRA-n-BUTYLAMMONIUM SALTS

KENNETH G. FURTON[a], COLIN F. POOLE* and BRIAN R. KERSTEN
Department of Chemistry, Wayne State University, Detroit, MI 48202 (U.S.A.)
(Received 18th September 1986)

SUMMARY

Variations in the molar retention volume of organic solutes on thirteen tetra-n-butylammonium salts with a common liquid temperature range are correlated with the properties of the anion. The anions studied include the chloride, bromide, nitrate, nitrite, methanesulfonate, trifluoromethanesulfonate, ethanesulfonate, 4-toluenesulfonate, sulfamate, thiocyanate, picrate, pentacyanopropenide, and tetra-n-butylborate. The high melting points and poor thermal stabilities of camphorsulfonate, dihydrogenphosphate, hydrogensulfate, and perrhenate precluded their use. The properties of the anions have only small influences on the magnitudes of dispersive, orientative, and proton-donor interactions with the test solutes. Orientative interactions are strong for polar solutes but vary little with anion structure. There was no correlation between the dipole moment of the tetra-n-butylammonium salts and the retention of polar solutes. The structures of the anion do, however, have large influences on the retention of proton-donor solutes. For these solutes, a good correlation was found between molar retention volume and the basicity of the anions, represented by their pK_a values in aqueous solution.

Liquid organic salts offer new options as selective stationary phases for gas chromatography. Unlike inorganic molten salts, they show true partitioning of organic solutes, wide applicability to the separation of polar and non-polar solutes, and good support-wetting characteristics. Compared to the polymeric, nonionic liquids presently used as stationary phases in gas chromatography, they show unusually strong orientation and proton-donor/acceptor interactions and have well defined structures and physical properties. They are therefore suitable candidates for use as standard, polar, reference stationary phases. A review of their chromatographic properties and those of inorganic molten salts appeared recently [1].

Interest in the exploitation of liquid organic salt phases has increased recently with the discovery of several salts having stable liquid ranges exceeding 100—200°C from their melting points [1, 2]. Preliminary investigations have indicated that the tetra-n-butylammonium salts frequently have low melting points and reasonably wide liquid temperature ranges and are among

[a]Present address: Department of Chemistry, University College of Swansea, Swansea, Wales (Great Britain).

0003-2670/87/$03.50

the most generally useful chromatographically of the organic salts studied tc date [3, 4]. In this paper, a systematic attempt is made to correlate the retention of organic solutes on liquid tetra-n-butylammonium salts with the properties of the anion. In addition to salts studied previously, seven new tetra-n-butylammonium salts are included to enhance the range of anion properties available for correlation with the molar retention volume of test solutes selected to emphasize specific intermolecular interactions.

EXPERIMENTAL

Chemicals

Tetra-n-butylammonium bromide, chloride, hydrogensulfate, methane sulfonate, nitrate, nitrite, thiocyanate, 4-toluenesulfonate, trifluoromethane sulfonate, perrhenate, and dihydrogenphosphate were obtained from Fluka Tetra-n-butylammonium tetrabutylborate was obtained from Alfa Product: (Danvers, MA) and the picrate from RSA Corp. (Ardsley, NY). All salts obtained commercially were recrystallized to constant melting point prior to use. Sulfamic acid, R-10-camphorsulfonic acid, ethanesulfonic acid, tetra cyanomethylene, and tetra-n-butylammonium iodide and hydroxide were obtained from Aldrich. Test compounds were obtained as Theta kits (Anspec, Ann Arbor, MI) or were general laboratory chemicals from various sources.

Tetra-n-butylammonium sulfamate, camphorsulfonate and ethane sulfonate were prepared by adding a slight molar excess of an aqueous solution of tetra-n-butylammonium hydroxide (40% w/w) to an aqueous solution of the acid (20% w/v) accompanied by vigorous stirring. The water was removed on a rotary evaporator and the salt recrystallized to constant melting point from ethanol for the ethanesulfonate, from chloroform for the sulfamate, and from ethyl acetate for the camphorsulfonate. Tetra-n butylammonium ethanesulfonate was a white crystalline solid [m.p. 116.5–117.5°C, IR ν (S=O) 1184 and 1032 cm^{-1}; ^{1}H-NMR cation 1.0, 1.4, 1.7 3.2 ppm and anion 1.3 and 2.9 ppm ^{13}C-NMR cation 58.4, 23.5, 19.5, 13.8 ppm and anion 8.9 and 45.8 ppm]. Tetra-n-butylammonium sulfamate was a white crystalline solid [m.p. 99.5—100.5°C, IR ν (NH_2) 3316 cm^{-1}, ν (S=O) 1198 and 1045 cm^{-1}; ^{1}H-NMR cation 0.6, 1.1, 1.3, 2.9 ppm and anion 3.5 ppm; ^{13}C-NMR cation 57.4, 22.8, 18.5, 12.5 ppm]. Tetra-n butylammonium camphorsulfonate was a white crystalline solid [m.p 137.5—138.5°C; IR ν (CO) 1729 cm^{-1} ν (S=O) 1191 and 1038 cm^{-1} ^{1}H-NMR cation 2.8, 1.1, 0.9, 0.63 and anion 0.30, 0.47, 1.4, 1.7, 2.3 ppm ^{13}C-NMR cation 57.9, 23.4, 19.0, 13.0 ppm and anion 216.3, 77.1, 46.4 46.2, 42.9, 42.3, 26.4, 23.9, 19.7 ppm].

Tetra-n-butylammonium 1,1,2,3,3-pentacyanopropenide was prepared by a method analogous to that described by Middleton et al. [5]. A solution of pyridine in acetone/water (1:1) was added dropwise to an equivalent amount of tetracyanoethylene in acetone cooled to —50°C. The mixture was allowed

to warm slowly to room temperature and then mixed with a solution of tetra-n-butylammonium iodide in water (2% w/v) containing a molar equivalent of the iodide salt. The precipitate formed was collected by vacuum filtration, washed with water, and recrystallized to constant melting point from absolute ethanol. Tetra-n-butylammonium 1,1,2,3,3-pentacyanopropenide was obtained as a yellow crystalline solid [35% yield; m.p. 119.5–120.5°C, IR ν (CN) 2200 cm^{-1}; ^{1}H-NMR cation 0.6, 1.0, 1.2, 2.8 ppm, ^{13}C-NMR cation 58.3, 23.2, 19.1, 13.0 ppm and anion 135.0, 116.3, 113.2, 57.4 ppm].

Methods

Column packings containing from 3 to 15% (w/w) of the tetra-n-butylammonium salts on Chromosorb W-AW (100—120 mesh) were prepared by the rotary evaporator technique. After coating, the damp packing was dried in a fluidized-bed drier and then packed into glass columns, 1–3.5 m in length and 2-mm i.d., with the aid of vacuum suction and gentle vibration. Accurate phase loadings were determined by Soxhlet extraction of the packings according to the procedures detailed elsewhere [6, 7]. For column evaluation, a Varian 3700 gas chromatograph with heated on-column injectors, a temperature-programmable column oven, and flame-ionization detector was used. Separation conditions are given in the legends to tables and figures.

Solute retention volumes were measured as the molar retention volume, V_m, defined as the volume of carrier gas corrected to 0°C required to elute half the solute from an ideal column containing one mole of stationary liquid phase and across which there is no pressure drop. It was calculated from

$$V_m = (3M/2W_L)F_o\,(t_R - t_m)\,[1-(P_W/P_a)]\,[(P^2-1)/(P^3-1)]\,(273.2/T_a) \quad (1)$$

where V_m is the molar retention volume, M the molecular weight of the tetra-n-butylammonium salt, W_L the weight of liquid phase in the column, F_o the carrier-gas flow rate at the column outlet, t_R the retention time of the test solute, t_M the column dead time (assumed equal to the retention time of methane at the column operating temperature), P_W the vapor pressure of water at T_a, P_a the ambient pressure, $P = P_i/P_a$, P_i the column inlet pressure, and T_a the ambient temperature. Values for V_m were not corrected for non-ideality of the gas phase.

Dipole moments were measured in freshly purified dioxane with a model DM01 dipolemeter (Kahl Scientific Instrument Corp., El Cajon, CA). The dipolemeter cell was thermostated at 25°C by using a flow-through refrigerated circular cooler (Blue M, Blue Island, IL).

RESULTS AND DISCUSSION

The column operating characteristics for the seven new tetra-n-butylammonium salts are summarized in Table 1. The perrhenate salt showed

TABLE 1

Column operating characteristics for tetra-n-butylammonium salts

Anion	Melting point (°C)	Maximum operating temperature (°C)	Liquid temperature range (°C)	Average column efficiency (N/m)[a]
Ethanesulfonate	117	180	63	1900—2900
Sulfamate	100	150	50	2100—3100
R-10-Camphorsulfonate	138	180	42	1100—1600
Dihydrogenphosphate	154	190	36	100—500
Hydrogensulfate	171	190	19	1500—2500
Pentacyanopropenide	120	190	70[b]	1600—2400
Perrhenate	245	245[c]	—	500—1000

[a]Approximate values for a variety of test solutes on columns with a 10% salt loading. [b]Slow decomposition occurs in the region of the melting point. Columns are stable for several days at temperatures in the region of the melting point. Rapid decomposition with the formation of an unstable baseline occurs at >190°C. [c]Melting point and the onset of decomposition coincide.

poor column stability and efficiency. In this case, the melting point and the onset of column bleed coincided. The dihydrogenphosphate salt showed poor column efficiency and a limited liquid temperature range. The hydrogensulfate salt provided packings of reasonable efficiency but of limited liquid temperature range (171—190°C). Also, the relatively high melting point of this salt makes its use less attractive for general applications compared to other tetra-n-butylammonium salts. The camphorsulfonate salt provided packings of acceptable efficiency and moderate liquid temperature range. The most useful salts were ethanesulfonate, sulfamate and pentacyanopropenide. Unfortunately, the long-term thermal stability of the pentacyanopropenide above its melting point was poor. The pentacyanopropenide salt deteriorated rapidly when heated in the presence of air; otherwise, in an inert atmosphere, column packings were stable for several days. The salt was sufficiently stable to allow the accurate determination of solvent and thermodynamic properties but not sufficiently stable to use for chromatographic applications.

Because of a lack of a stable liquid temperature at 120°C, McReynolds' constants were determined for only three of the salts (Table 2). The tetra-n-butylammonium salts show weak interactions with the non-polar probes, *cis*-hydrindane, 2-octyne, and benzene. Orientation interactions are strong for all salts and fall in the order sulfamate > ethanesulfonate > pentacyanopropenide. The largest variation is seen for the proton-donor probe, butanol. Large interactions are seen for the sulfamate and ethanesulfonate salts with a much weaker interaction observed for the pentacyanopropenide salt. Only the sulfamate salt has available protons to donate to acceptor solutes.

TABLE 2

McReynolds' constants at 120°C for the tetra-n-butylammonium salts

Test probe	Anion		
	Sulfamate	Ethanesulfonate	Pentacyanopropenide
Benzene	417	320	294
Butanol	1023	911	476
2-Pentanone	517	429	456
Nitropropane	849	703	603
Pyridine	726	581	506
2-Methyl-2-pentanol	780	694	375
Iodobutane	124	182	271
2-Octyne	219	169	139
1,4-Dioxane	559	427	409
cis-Hydrindane	203	152	132

The proton-donor strength of the sulfamate is greater than that of the ethanesulfonate and pentacyanopropenide salts. However, the magnitude observed is not very great and one must conclude that proton-donor properties of the sulfamate salt are less important than orientation and proton-acceptor interactions. The most important contribution to the retention of 2-pentanone, pyridine, and dioxane (proton-acceptor probes) is most probably a dipole—dipole interaction rather than hydrogen-bond complexation.

The use of the McReynolds' system to characterize polar stationary phases such as the liquid organic salts may lead to erroneous information resulting from the anomalous retention of the n-alkanes used as retention index markers [7, 8]. This situation arises when adsorption at the gas/liquid interface makes a significant contribution to the retention of the n-alkanes while the polar probes are retained by partitioning with the bulk liquid phase. To avoid this inconsistency, the retentions of the McReynolds' test probes and a series of substituted benzenes are measured as their molar retention volumes, defined by Eqn. 1, and are summarized in Tables 3 and 4, respectively. For ease of interpretation, the molar retention volumes for five of the McReynolds' test probes as functions of the anion types are presented diagramatically in Fig. 1. Dispersive interactions (benzene) are substantially larger than average for the three salts with tetra-n-butylborate, pentacyanopropenide, and picrate. Conversely, dispersive interactions are less than average in the case of the sulfamate salt. Otherwise, for most anions (trifluoromethanesulfonate, thiocyanate, nitrate, 4-toluenesulfonate, methanesulfonate, ethanesulfonate, bromide, nitrite, and chloride) there is very little change in retention. In this case the choice of the anion does not significantly influence the selectivity of the interaction for benzene.

Orientation interactions are important for 1-nitropropane (D = 3.59) and pyridine (D = 2.37) (dipole moments from [9]). Pyridine is also capable of

TABLE 3

Molar retention volumes for McReynolds' test probes on tetra-n-butylammonium salts

Anion	Logarithm of molar retention volume[a]									
	1	2	3	4	5	6	7	8	9	10
Chloride	3.86	5.54	4.00	4.75	4.55	5.16	3.64	3.91	4.06	4.20
Nitrite	3.87	5.18	4.02	4.70	4.55	4.86	4.87	3.88	4.10	4.13
Bromide	3.84	5.14	4.04	4.73	4.59	4.83	3.91	3.90	4.12	4.19
Tetra-n-butylborate	4.14	—	4.60	4.74	4.65	4.34	3.98	4.32	4.40	4.65
Ethanesulfonate	3.85	5.01	4.03	4.69	4.53	4.76	3.93	4.09	4.26	4.06
Methanesulfonate	3.84	4.99	4.01	4.68	4.51	4.74	3.91	3.91	4.09	4.20
4-Toluenesulfonate	3.90	4.91	4.10	4.73	4.57	4.67	3.99	4.00	4.16	4.31
Sulfamate	3.74	4.83	3.89	4.61	4.46	4.55	3.48	3.72	4.03	4.02
Nitrate	3.88	4.82	4.06	4.70	4.57	4.60	4.37	3.88	4.15	4.15
Thiocyanate	3.87	4.73	4.05	4.62	4.55	4.49	4.43	3.81	4.11	4.12
Trifluoromethane-sulfonate	3.86	4.42	4.15	4.61	4.51	4.30	4.10	3.87	4.15	4.18
Picrate	4.04	4.36	4.30	4.73	4.66	4.30	4.36	4.07	4.36	4.46
Pentacyanopro-penide	4.04	4.32	4.36	4.76	4.64	4.31	4.37	4.11	4.31	4.49

1, Benzene; 2, butanol; 3, 2-pentanone; 4, 1-nitropropane; 5, pyridine; 6, methyl-2-pentanol; 7, iodobutane; 8, 2-octyne; 9, 1,4-dioxane; 10, *cis*-hydrindane.

TABLE 4

Molar retention volumes for substituted benzenes on tetra-n-butylammonium salts

Anion	Logarithms of the molar retention volume[a]												
	1	2	3	4	5	6	7	8	9	10	11	12	1
Tetra-n-butylborate	4.14	4.40	4.62	4.61	4.69	4.97	5.23	5.30	5.42	5.74	5.79	5.57	6
Chloride	3.86	4.04	4.22	4.21	4.60	4.89	5.26	5.40	5.53	5.84	5.98	6.21	6
Bromide	3.84	4.07	4.24	4.24	4.60	4.89	5.24	5.39	5.40	5.54	5.82	6.11	5
Nitrite	3.87	4.04	4.21	4.21	4.55	4.83	5.17	5.23	5.34	5.50	5.76	6.12	5
Ethanesulfonate	3.85	4.06	4.24	4.25	4.55	4.82	5.16	5.18	5.29	5.48	5.73	6.04	5
Methane-sulfonate	3.84	4.04	4.21	4.21	4.54	4.81	5.17	5.17	5.29	5.48	5.73	6.04	5
4-Toluene-sulfonate	3.90	4.10	4.29	4.28	4.59	4.86	5.23	5.21	5.53	5.52	5.77	5.95	5
Nitrate	3.88	4.08	4.25	4.25	4.58	4.85	5.19	5.21	5.36	5.55	5.78	5.98	5
Sulfamate	3.74	3.92	4.09	4.07	4.45	4.73	5.10	5.09	—	5.41	5.69	5.94	5
Thiocyanate	3.87	4.06	4.23	4.23	4.52	4.81	5.11	5.23	5.31	5.52	5.69	5.91	5
Trifluoro-methanesulfon-ate	3.86	4.07	4.25	4.24	4.46	4.72	5.01	5.02	5.20	5.46	5.58	5.66	4
Picrate	4.04	4.29	4.47	4.49	4.64	4.92	5.20	5.27	5.39	5.68	5.79	5.72	4
Pentacyano-propenide	4.04	4.29	4.49	4.51	4.62	4.90	5.17	5.23	5.36	5.58	5.67	5.61	4

[a]1, Benzene; 2, toluene; 3, xylene; 4, ethylbenzene; 5, chlorobenzene; 6, bromobenzene 1,2-dichlorobenzene; 8, iodobenzene; 9, benzaldehyde; 10, acetophenone; 11, nitrobenze 12, aniline; 13, hexanol.

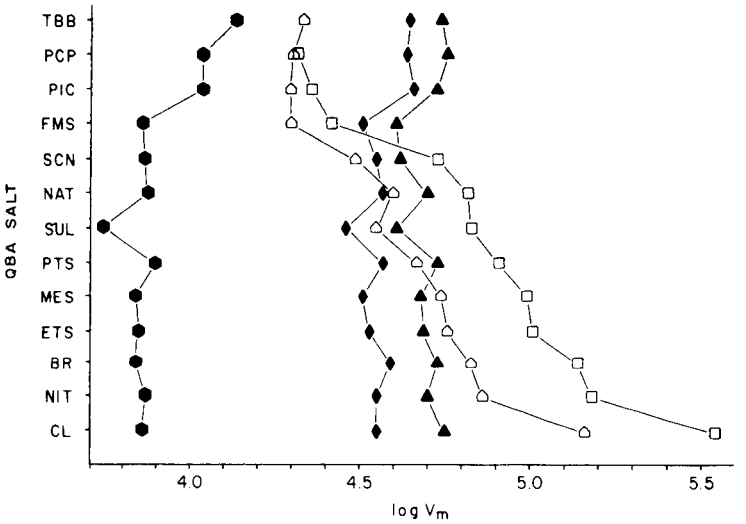

Fig. 1. The influence of the anion in a series of tetra-n-butylammonium salts on the molar retention volumes: (●) benzene; (□) butanol; (▲) 1-nitropropane; (♦) pyridine; (⌂) 2-methyl-2-pentanol. Anions: TBB, tetra-n-butylborate; PCP, pentacyanopropenide; PIC, picrate; FMS, trifluoromethanesulfonate; SCN, thiocyanate; NIT, nitrate; SUL, sulfamate; PTS, 4-toluenesulfonate; MES, methanesulfonate; ET, ethanesulfonate; BR, bromide; NIT, nitrite; CL, chloride.

proton-acceptor interactions but because neither the cation nor anions, except for the sulfamate, contain acidic protons, this interaction is not significant for the salts studied here. The orientation interactions are substantially stronger than the dispersive interactions but again are not a strong function of the anion type. The dipole moments for some tetra-n-butylammonium salts are given in Table 5. If the logarithms of the molar retention volume is plotted against the dipole moment of the tetra-n-butylammonium salts, there is no correlation between the retention of the polar probes (1-nitropropane, pyridine, and nitrobenzene) and the dipole moment of the salt, but rather a fortuitous correlation is observed for the retention of benzene, *cis*-hydrindane, bromobenzene, etc. In this instance, the increase in retention with increasing dipole moment is probably due to an increase in dispersive interactions. The dipole moments increase with the increase in interchange distance between ions, which in turn, can be taken as a measure of increasing anion size for this homologous series of salts. As was demonstrated in Fig. 1, the salts with the largest dispersive interactions (tetra-n-butylborate, picrate, and pentacyanopropenide) also have the largest dipole moments.

A possible inconsistency exists in the above approach. Dipole moments are determined by extrapolating the concentration of the salt to infinite dilution. It is most likely that under these conditions, the salts exist as simple ion-pairs surrounded by solvent molecules [10]. This may be a poor

TABLE 5

Dipole moments and dielectric constants for some tetra-n-butylammonium salts measured in dioxane

Anion	Dielectric constant	Dipole moment (D)
Bromide	55.89	6.15
Nitrate	66.66	6.75
Chloride	70.15	6.93
Nitrite	77.90	7.32
4-Toluenesulfonate	87.03	7.71
Trifluoromethanesulfonate	110.53	8.77
Methanesulfonate	112.50	8.84
Pentacyanopropenide	191.81	11.59
Picrate	322.71	15.07
Tetra-n-butylborate	342.46	15.54

model for the molten state for which most of the available evidence suggests that for the quaternary ammonium salts, the ions are kinetically free, each ion being surrounded by a sphere or envelope of oppositely charged ions [11]. Consequently, even in a qualitative sense, the dipole moments measured from dilute solution may be a poor representation of the capacity of a liquid salt to enter into orientation interactions.

The largest variation in retention for different anions is seen for the proton-donor solutes, n-butanol and 2-methyl-2-pentanol. The variation in retention here, exceeds an order of magnitude for the thirteen anions studied and might be expected to reflect the different basicities of the anions. Unfortunately, no independently derived scale of anion basicities for liquid organic salts is available for comparison. However, some useful correlations were found by using the pK_a of the anions measured in aqueous solution. The general trend of increasing retention with increasing pK_a values (i.e. increasing basicity of the anions) is shown for the halide and nitro anions in Fig. 2; pK_a values were taken from [12]. No similar trend is seen for the proton-acceptor/orientation probe, pyridine, thus supporting the general observation made above. A good correlation exists between the pK_a of the anions of a similar kind and the molar retention volume. When the pK_a values [13, 14] for the sulfonate anions, methanesulfonate, trifluoromethanesulfonate, ethanesulfonate, and 4-toluenesulfonate, were used, the correlation coefficient was $r = 0.9976$ for n-butanol and $r = 0.9990$ for 2-methyl-2-pentanol (Fig. 3). Added confidence in the legitimacy of the correlations is provided by the fact that a similar relationship was not found for the proton-acceptor/orientation probe, pyridine. Thus, the relative basicity of the anions measured with respect to water as solvent seems to be a fairly reliable predictor of the relative retention of proton-donor solutes.

The results obtained for the aromatic test probes are shown diagramati-

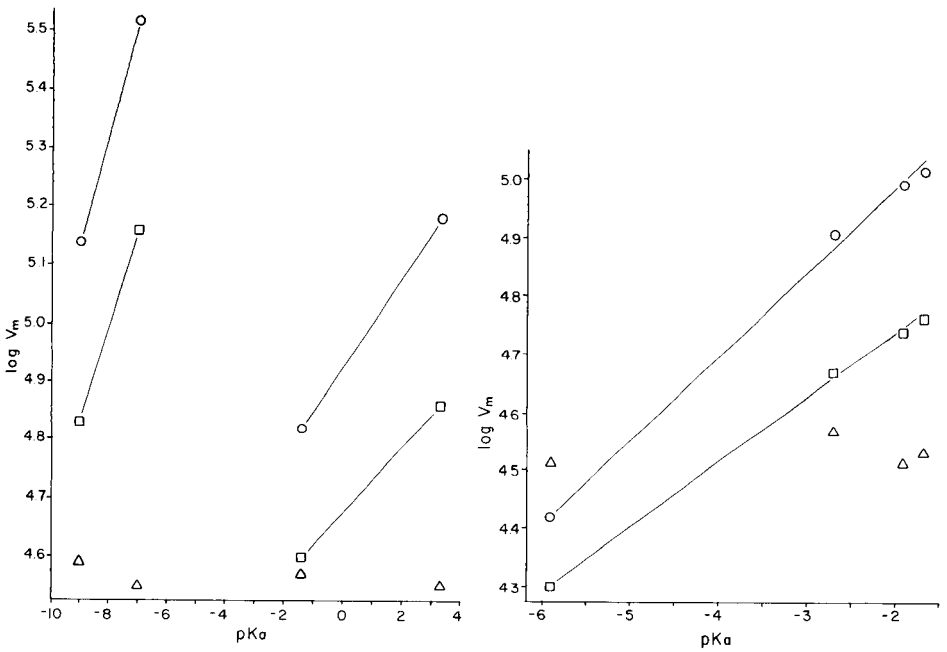

Fig. 2. Plot of the molar retention volume of benzene (○), 2-methyl-2-pentanol (□), and pyridine (△) as a function of the pK_a for halide, nitrate and nitrite anions with tetra-n-butylammonium cations. pK_a values: Br^-, −9; Cl^-, −7; NO_3^-, −1.4; NO_2^-, 3.3.

Fig. 3. Plot of the molar retention volumes of butanol (○), 2-methyl-2-pentanol (□), and pyridine (△) as a function of the pK_a of some sulfonate anions with tetra-n-butylammonium cations. pK_a values: $CF_3SO_3^-$, −5.9; 4-$CH_3C_6H_4SO_3^-$, −2.7; $CH_3SO_3^-$, −1.9; C_2H_5-SO_3^-, −1.7.

cally in Fig. 4. The data presented are entirely consistent with the interpretatin given previously and serve to summarize the results from this paper. For the tetra-n-butylammonium salts, changing the anion has only a small effect on the selectivity of dispersive and orientative interactions. For the anions tetra-n-butylborate, picrate, and pentacyanopropenide, a greater-than-average contribution to dispersion is observed and conversely a less-than-average contribution was observed for the sulfamate anion. The increase in dispersive interactions for the bulky anions correlates with their increasing molecular volume and is not unexpected [15]. These same trends are reflected in the retention of the orientation probes, bromobenzene, 1,2-dichlorobenzene, benzaldehyde, and nitrobenzene, suggesting that in this case the increase in dispersive interactions are responsible for the observed trends rather than an increase in orientation interactions. Some additional selectivity seems to exist for nitrobenzene on the picrate salt, which is probably specific in nature and related to the similarity in structure between the test solute and anion and the possibility of favorable charge-transfer interactions. Orientation interactions are important for explaining the

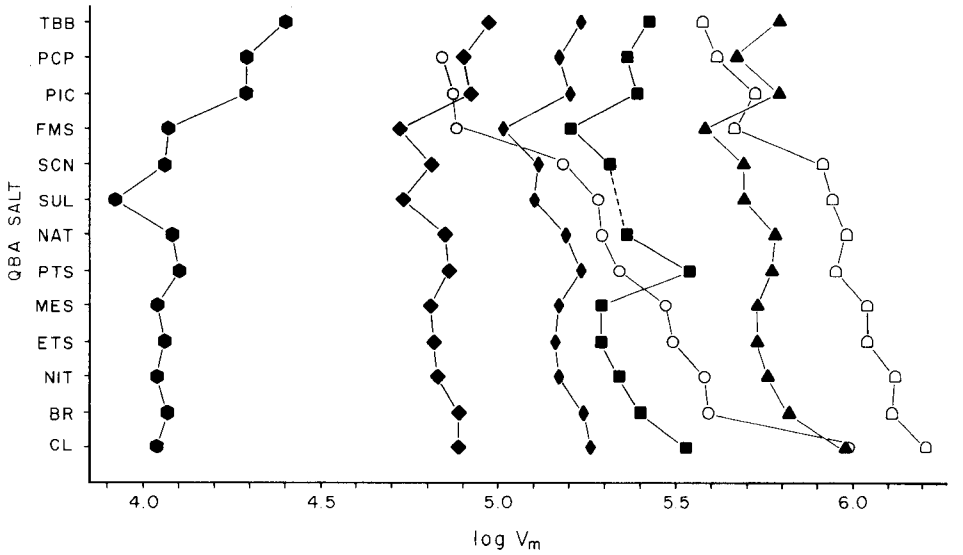

Fig. 4. The influence of the anion in a series of tetra-n-butylammonium salts on the molar retention volumes: (●) toluene; (○) hexanol; (◆) bromobenzene; (◆) 1,2-dichlorobenzene; (■) benzaldehyde; (□) aniline; (▲) nitrobenzene. The anions are identified in Fig. 1.

relative retention of polar solutes, but the strengths of these interactions are presumably governed by the magnitudes of coulombic forces within the salts, as they vary over a narrow range for ions having different structures. The largest variation in retention with anion structure is seen from the proton-donor solutes, hexanol and aniline. Here the structure of the anion and, in particular, its relative basicity, has a large and dominant influence on the retention of these solutes.

Conclusions

The role of the anion in controlling retention in gas chromatography of a wide range of organic solutes has been delineated for a series of tetra-n-butylammonium salts with thirteen different anions. Dispersive interactions do not change greatly for the anions investigated, except for the anions of large size (tetra-n-butylborate, picrate, and pentacyanopropenide), which show a greater-than-average dispersive interaction with all solutes. Orientation interactions are strong for all polar solutes but do not change greatly for different anions. Proton-acceptor interactions vary widely with changes in the anion. These changes for anions of a similar kind, for example the sulfonates, correlate well with the basicity of the anion as measured by its pK_a value in water.

REFERENCES

1 C. F. Poole, K. G. Furton and B. R. Kersten, J. Chromatogr. Sci., 24 (1986) 400.
2 K. G. Furton, S. K. Poole and C. F. Poole, Anal. Chim. Acta, 192 (1987) 49.
3 K. G. Furton and C. F. Poole, J. Chromatogr., 349 (1985) 235.
4 S. C. Dhanesar, M. E. Coddens and C. F. Poole, J. Chromatogr., 349 (1985) 249.
5 W. J. Middleton, E. L. Little, D. D. Coffman and V. A. Engelhardt, J. Am. Chem. Soc., 80 (1958) 2795.
6 E. F. Sanchez, J. A. G. Dominguez, J. G. Munoz and M. J. Molera, J. Chromatogr., 299 (1984) 151.
7 B. R. Kersten and C. F. Poole, J. Chromatogr., (1987) in press (Symp. Vol., Advances in Chromatography, Houston, TX, 1986).
8 W. A. Aue and V. Paramasigamani, J. Chromatogr., 166 (1978) 253.
9 A. L. McClellan, Tables of Experimental Dipole Moments, Vol. 2, Rahara Enterprises, El Cerrito, CA, 1974.
10 E. Grunwald, S. Highsmith and T.-P. I, in M. Szwarc (Ed.), Ions and Ion Pairs in Organic Reactions, Vol. 2, Wiley, New York, 1974, p. 448.
11 J. E. Lind, Adv. Molten Salt Chem., 2 (1973) 1.
12 N. L. Allinger, M. P. Cava, D. C. DeJongh, C. R. Johnson, N. A. Lebel and C. L. Stevens, Organic Chemistry, Worth Publishers, New York, 1976, p. 260.
13 R. Stewart, The Proton: Applications to Organic Chemistry, Academic Press, Orlando, FL, 1985, p. 17.
14 J. P. Gutherie, Can. J. Chem., 56 (1978) 2342.
15 K. G. Furton and C. F. Poole, J. Chromatogr., (1987) in press (Symp. Vol., Advances in Chromatography, Houston, TX, 1986).

Analytica Chimica Acta, 192 (1987) 267—275
Elsevier Science Publishers B.V., Amsterdam — Printed in The Netherlands

DESIGN AND EVALUATION OF A SANDWICH PHASE SEPARATOR FOR ON-LINE LIQUID/LIQUID EXTRACTION

C. DE RUITER, J. H. WOLF, U. A. Th. BRINKMAN and R. W. FREI*

Department of Analytical Chemistry, Free University, De Boelelaan 1083, 1081 HV Amsterdam (The Netherlands)

(Received 18th September 1986)

SUMMARY

Sandwich phase separators with various groove dimensions were constructed and tested as part of a post-column extraction detector for liquid chromatography and for a flow-injection system. The construction materials are stainless steel and PTFE; no membranes are used. The groove volumes vary between 8 and 43 μl; the dimensions of the groove are not critical. Several aqueous (acetonitrile/water and methanol/water mixtures) and organic (1,2-dichloroethane and n-heptane) phases were successfully separated by gravity as well as by wetting. Measurement of statistical second moments showed the total dispersion of the extraction system to be 2.5—4 s at the optimum separation efficiency (organic flow through detector/total organic flow) of 0.3—0.4.

Post-column extraction detectors are widely applied in liquid chromatography (l.c.) [1—5] and in flow-injection methods [6—8] for the enhancement of sensitivity and selectivity. A disadvantage of post-column extractors is the additional band broadening caused; the design of the phase separator is critical in this respect [9]. During the past few years, various new designs for phase separators have appeared in the literature [6—8, 10—15]. In general, many of these novel designs consist of a manifold, through which a segmented flow comes into contact with a hydrophobic (PTFE) membrane. A major drawback of membrane phase separators is the fact that the membranes are rapidly destroyed when samples of biological origin, especially serum and plasma, are involved. Up till now, only a few applications have been described. Burguera and Burguera [13] developed a method for the determination of cadmium in urine. The lifetime of their hydrophilic and hydrophobic phase-separating paper (Whatman cellulose and silica-treated Whatman paper, respectively) was 1.5 h. Apffel et al. [14] described a method for the determination of the anti-neoplastic agents VP-16 and VM-26 in urine, using a post-column extraction system, suitable for miniaturized l.c. The lifetime of their PTFE membrane was claimed to be several days, but routine analysis of urine samples was not reported. In preliminary experiments here, rapid destruction of membranes was observed on treatment with plasma samples.

In the present work, an evaluation of a sandwich phase separator is

0003-2670/87/$03.50

described, which has already been used in a post-column extraction detector for the determination of drugs in plasma and urine, without any problem of lifetime [16]. A single phase-separator design is used, because it was the aim of this study to establish the influence of the groove dimensions on the separation efficiency (defined as the ratio of the organic flow through the detector to the total organic flow) and the dispersion produced. Another goal was to decrease the groove dimensions to obtain separators suitable for miniaturized l.c.

EXPERIMENTAL

Apparatus

Figure 1 shows a diagram of the sandwich phase separator. The phase separator unit consists of two stainless steel blocks, one with (A) and one without (B) a groove, and a PTFE disc with a groove (C). These are held together by four screws. The inlets and outlets are machined into the blocks to accommodate 1/16-in. Valco male fittings. The aqueous outlet is connected to a MCV-50 micro needle valve (Scientific Glass Engineering, Melbourne, Australia) to allow the application of back-pressure to adjust the organic flow through the detector. The various groove dimensions investigated are summarized in Table 1. Figure 2 shows a diagram of the flow-injection system used. The aqueous and organic phase were delivered by using Kontron (Zürich, Switzerland) Model 414 l.c. pumps. In conjunction with these pumps, a Kontron pulse damper as well as a 100 × 4.6 mm i.d.

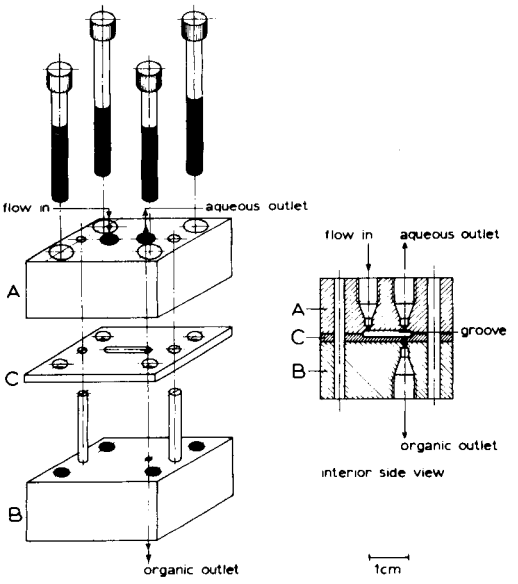

Fig. 1. Design of the sandwich phase separator. For explanation, see text.

TABLE 1

Groove dimensions of the phase separators investigated

Separator	Groove				I.d. of inlet and outlets (mm)	Distance between:	
	Length (mm)	Width (mm)	Depth (mm)	Volume (μl)		Centres of inlet and outlets (mm)	Centres of outlets and groove end (mm)
I	12.5	3.5	0.8	35	0.8	10.0	1.25
II	13.5	4.0	0.8	43	0.8	10.0	2.25
III	11.6	1.6	1.6	30	0.8	10.0	0.8
IV	13.1	2.0	1.6	42	0.8	9.8	2.4
V	8.3	1.4	0.7	8	0.6	7.0	0.8

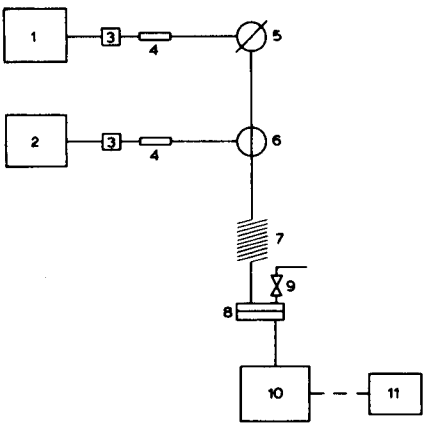

Fig. 2. Diagram of the flow-injection system: (1) aqueous phase pump; (2) organic phase pump; (3) pulse damper; (4) column; (5) micro injection valve; (6) T-piece; (7) extraction coil; (8) sandwich phase separator; (9) needle valve; (10) fluorescence detector; (11) recorder.

column, packed with 10-μm C_{18}-bonded material, were used to obtain optimal pulse damping. Samples were introduced via a Valco (Houston, TX) six-port valve, equipped with a 10-μl loop, or a home-made microvalve which can inject either 0.06 or 0.56 μl. The organic phase was added to the aqueous phase stream via a Valco T-piece with a 0.25-mm bore. The extraction took place in a 1.5 m × 0.8 mm i.d. stainless steel coil (helix diameter, 40 mm). After separation of the phases, the analyte was detected in the organic phase either with a Kratos (Ramsey, NJ) FS-970-LC fluorimeter (λ_{ex} = 386 nm, λ_{em} > 415 nm), equipped with a 5-μl flow cell, or a Perkin-Elmer LS-4 fluorimeter (λ_{ex} = 386 nm, λ_{em} = 465 nm), equipped with a 3-μl flow cell. The recorder used was a Kipp and Zonen (Delft, The Netherlands) multirange BD-8 instrument.

Chemicals

Acetonitrile and methanol were h.p.l.c. grade, and 1,2-dichloroethane and n-heptane were of analytical grade. All solvents were from J. T. Baker. The water used was demineralized water, treated in a Milli-Q (Millipore) ultrafiltration system. Analytical-grade disodium phosphate was also obtained from Baker. Perylene (99.99%) was purchased from Metron (Panther Valley Mall, Allamuchy, NJ, U.S.A.). All chemicals were used without further purification.

Procedures

Two band-broadening studies were done. In the first, the influence of different injection volumes on the total band broadening was investigated. The injectors used were the above-mentioned Valco six-port valve and the home-made microvalve. Injections of 5 ng of perylene were made. In the second study, separators I—V were tested. Injections of 50 ng of perylene in 0.56 μl of acetonitrile were made (ten times more perylene was used, to provide a more stable baseline for accurate peak measurements). Perylene was used as the test compound because it is strongly fluorescent and highly lipophilic.

Statistical second moments can be calculated by the method of Foley and Dorsey [17], which is based on the measurement of peak width and peak asymmetry at 10% peak height. However, because peak asymmetry repeatedly exceeded the value of 2.76, which is the upper limit for the utility of their equations, the modified Foley and Dorsey equation [18] was used, which covers a much wider range of peak asymmetry:

$$M_2 = (W_{0.1})^2/[7.35 + 22.6 \exp(-0.708 - (B/A)_{0.1})]$$

where M_2 is the statistical second moment (s^2), $W_{0.1}$ is the peak width (s) at 10% peak height, and $(B/A)_{0.1}$ is the peak asymmetry at 10% peak height.

RESULTS AND DISCUSSION

Efficiency of the phase separators

In preliminary experiments, the separators were tested with respect to their separation efficiency, by using various aqueous and organic phases. Although it is possible to isolate the aqueous phase for detection by connecting the micro needle valve to the organic outlet of the phase separator, in all these experiments the organic phase was passed through the detector, as occurs in most applications.

Heptane/aqueous systems. With acetonitrile/aqueous 50 mM sodium phosphate buffer pH 7 (20:80, v/v) as the aqueous phase and n-heptane (density 0.68 g ml^{-1}) as the organic phase, both at a flow rate of 1.0 ml min^{-1}, maximum separation efficiencies of 0.4—0.5 were obtained for the separators with groove volumes of 30—43 μl (separators I—IV). The maximum separation efficiency is the highest obtainable ratio of the organic

flow through the detector to the total organic flow, where no leakage of aqueous phase segments to the organic outlet is observed. Under these conditions, phase separation could not be achieved with the miniaturized separator V, which has a groove volume of only 8 μl. At lower flow rates, i.e., 0.2 or 0.5 ml min^{-1} for both aqueous and organic phase, maximum separation efficiencies for the miniaturized separator were 0.2 and 0.06, respectively. No influence of the orientation of the phase separator (organic phase flowing either below or above the aqueous phase) on the maximum separation efficiency was observed. Therefore, it can be concluded that in the n-heptane/aqueous system phase separation is primarily based on wetting.

Dichloroethane/aqueous systems. With acetonitrile/aqueous 50 mM sodium phosphate buffer pH 7 (20.80, v/v) and 1,2-dichloroethane (density 1.25 g ml^{-1}), both at a flow rate of 1.0 ml min^{-1}, maximum separation efficiencies were much higher than in the n-heptane/aqueous system. For separators I—III, values of 1.0—1.1 were obtained and a value of 0.9 was obtained for separator IV (V was not tested). Values above 1.0 are possible because part of the acetonitrile present in the aqueous phase will dissolve in the organic phase [19]. Changing the aqueous phase to acetonitrile/water (20:80, v/v), resulted in a decrease in maximum separation efficiency from 1.0—1.1 to 0.9 for separators I—III and from 0.9 to 0.6 for separator IV. For the miniaturized separator V, a value of 0.3 was measured. However, when the aqueous and organic phase flow rates were changed from 1.0 to 0.2 ml min^{-1} in separator V, a maximum separation efficiency of 1.0 was obtained, which indicates that the miniaturized separator has potential use in microbore l.c. In the two-phase system with 1,2-dichloroethane, it was found that the orientation of the phase separator was important. Phase separation could only be achieved when the organic phase was flowing below the aqueous phase. This suggests that in addition to wetting, gravity also plays an important role in the separation process.

With all five separators, and for all two-phase systems tested, problems tended to occur when the aqueous-phase flow rate was greater than that of the organic phase. Typically, at ratios of over 1.6, occasional leakage of aqueous phase segments to the organic outlet was observed. Conventionally, experiments were done at a phase ratio of 1.0. However, when the organic-phase flow rate exceeds the aqueous-phase flow rate, large ratios can be used without any problem.

Phase-separating tests with the widely applied l.c. mobile phase methanol/water as the aqueous phase in both two-phase systems, with either n-heptane or 1,2-dichloroethane as the organic phase, showed good phase separation up to methanol/water ratios of 80:20 (v/v) in the n-heptane system and up to ratios of 70:30 (v/v) in the 1,2-dichloroethane system. At higher methanol concentrations, the aqueous and organic phases become miscible.

Band broadening

It is not possible to evaluate the individual contribution to band broadening of all the different parts of the flow-injection system shown in Fig. 2, i.e.,

T-piece, coil and phase separator. Therefore, information about the contribution to band broadening of phase separators I—V was obtained by measuring the statistical second moments of the total system as a function of the separation efficiency.

In order to observe small differences in band broadening for the various separators, contributions from the other parts of the system must be small. A micro injection valve (0.56 μl) was used instead of the 10-μl valve, because the latter gave a major contribution to band broadening, as demonstrated in Fig. 3. From this figure, it is also clear that a further decrease in the injection volume from 0.56 to 0.06 μl did not result in a significant decrease in the total band broadening. In addition, a detector with a 3-μl cell was used. The results of the experiments are summarized in Fig. 4. Apart from the maximum separation efficiencies mentioned above, only minor differences in total band broadening are observed with the various phase separators. When the phase separators are used near their maximum separation efficiency, the lowest dispersion is observed, i.e., 1—2 s. However, working under that condition is not recommended, because small disturbances in the system can lead to leakage of aqueous phase segments to the organic outlet,

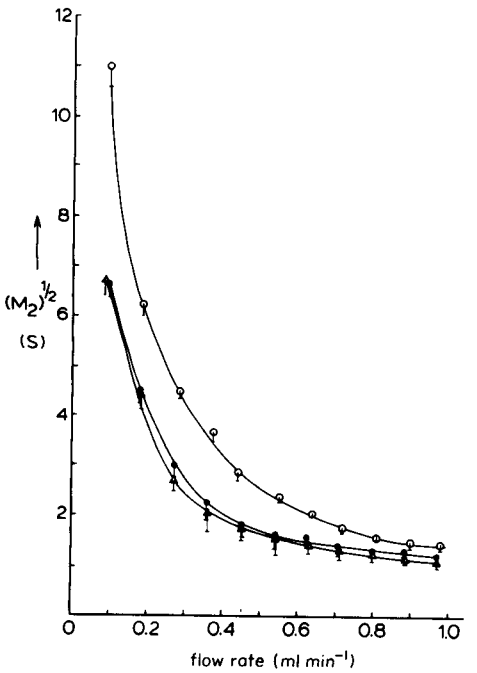

Fig. 3. Dependence of band broadening on the flow for the injector plus Kratos FS-970 fluorimeter with 5-μl flow cell: (○) macro injection valve with a 10-μl injection volume; (●) micro injection valve with a 0.56-μl injection volume; (△) micro injection valve with a 0.06-μl injection volume. Each point represents the mean and s.d. of 8 measurements.

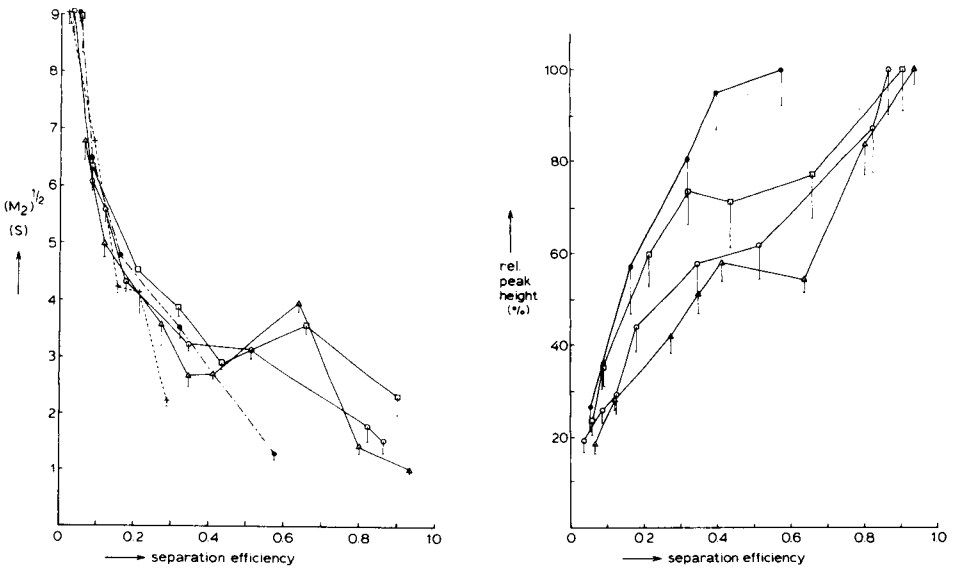

Fig. 4. Total band broadening in the flow-injection system including a phase separator as a function of the separation efficiency, with acetonitrile/water (20:80, v/v) as the aqueous phase and 1,2-dichloroethane as the organic phase, both at a flow rate of 1.0 ml min^{-1} . The detector was a PE LS-4 fluorimeter with a 3-μl flow cell. Separator used: (○) I; (□) II; (△) III; (●) IV; (+) V. Each point represents the mean and s.d. of five measurements.

Fig. 5. Dependence of relative peak height (peak height at certain separation efficiency/ peak height at maximum separation efficiency) on the separation efficiency in the two-phase system described in Fig. 4. Flow-injection system with phase separator: (○) I; (□) II; (△) III; (●) IV. Each point represents the mean and s.d. of 5 measurements. Standard deviations are relatively large as a result of the poor reproducibility of measurements at maximum separation efficiency.

which will cause major detection problems. Another important observation is that the curves for separators I—III, which can be operated at high separation efficiencies, show a region (separation efficiency 0.4—0.7), where no further decrease in band broadening is achieved with increasing separation efficiency. During the work in this range, it was observed that the aqueous outlet stream changed from a solvent-segmented type to an emulsion, probably as a result of eddies being formed in the separator groove under these conditions. The presence of eddies can cause mixing of the aqueous and organic phases and can contribute to band broadening. In addition, peak asymmetry increased markedly. Thus, it is not recommended to use separators I—III at phase separation efficiencies above 0.4. This is also true for separator IV, because values above 0.4 approach too closely the critical maximum separation efficiency of about 0.6. For the flow rates investigated, i.e., 1.0 ml min^{-1} for both aqueous and organic phases, the miniaturized separator V can only be used at a separation efficiency of 0.25 or less.

Peak heights

In order to evaluate in more detail the separation efficiency at which optimal results can be achieved, relative peak heights (defined as the ratio of the peak height obtained at a certain separation efficiency to the peak height at maximum separation efficiency) are plotted against separation efficiency for each of the separators I—IV (Fig. 5). It is interesting that even at separation efficiencies of 0.3—0.4, 55—80% of the maximum peak height is obtained. No further gain occurs until the separation efficiency reaches values of 0.6—0.7 with, self-evidently, a final increase to 100%. However, for the reasons outlined above, it is not recommended to operate at separation efficiencies above 0.4. Because the noise in the system used was almost constant over the entire separation efficiency range, it is clear that the phase separators I—IV with groove volumes of 30—43 μl, under normal l.c. conditions give optimal performance at separation efficiencies of 0.3—0.4. These findings are supported by earlier observations that in a post-column extraction detector, where the noise in the system was mainly due to co-extraction of a fluorescent ion-pairing agent, the best results in terms of band broadening, sensitivity and ease of operation, were obtained at separation efficiencies of 0.3—0.35 [16].

Conclusions

A series of sandwich phase separators has been constructed which are well suited to separate aqueous and organic phases at flow rates of typically 1.0 ml min^{-1}. The optimum phase separation efficiency is 0.3—0.4 and the contribution to band broadening (of the complete extraction system) is 2.5—4 s for the phase separators having groove volumes of 30—43 μl. Rather surprisingly, the groove dimensions are not critical. With separators having similar groove volumes (30—43 μl) and lengths (11.6—13.5 mm), the best results were obtained with separator III, which has a narrow (1.6 mm) and deep (1.6 mm) groove and a short distance between the centres of the outlets and the groove-end (0.8 mm). The results compare reasonably with data obtained by Apffel et al. [14], who developed a post-column extraction system, suitable for use with narrow-bore h.p.l.c., which consisted of a membrane phase separator with an internal volume less than 1 μl. There, a minimal total dispersion of between 1 and 2.5 s was found, without accounting for peak asymmetry. Under experimental conditions similar to those used here, conventional glass phase separators may well give a band-broadening contribution of some 6 s [20]. The sandwich phase separators are more rugged than membrane phase separators and they do not show lifetime problems when used in the analysis of real samples. In the past year, they have been used routinely for the determination of drugs in plasma and urine by means of h.p.l.c. [16].

The miniaturized sandwich phase separator with a groove volume of only 8 μl (separator V), though not very useful for conventional l.c. systems, shows excellent performance at aqueous and organic flow rates of ca. 0.2

ml min^{-1}, i.e., for narrow-bore l.c. A maximum separation efficiency of 1.0 was obtained. In addition, at aqueous and organic phase flow rates both of 1.0 ml min^{-1}, the total extraction system with the miniaturized phase separator gives a lesser contribution to band broadening than with separators I—IV, at a separation efficiency of about 0.3.

In the near future, such miniaturized separators will be used in a post-column extraction system to interface a micro-l.c. system with a mass spectrometer. Because, in contrast to the concentration-sensitive u.v. and fluorescence detectors, the mass spectrometer is a mass-sensitive detector, it may be interesting to use the miniaturized phase separator near its maximum separation efficiency in order to obtain optimal signal-to-noise ratios. The phase separators will also be used in further work on pre- and post-column clean-up and fluorescent and u.v.-labelling studies and their adaptation to real analytical problems.

The authors thank the Free University Workshop, and especially Mr. D. van Ieperen, for construction of the phase separators.

REFERENCES

1 J. F. Lawrence, U. A. Th. Brinkman and R. W. Frei, J. Chromatogr., 171 (1979) 73.
2 J. F. Lawrence, U. A. Th. Brinkman and R. W. Frei, J. Chromatogr., 185 (1979) 473.
3 R. J. Reddingius, G. J. de Jong, U. A. Th. Brinkman and R. W. Frei, J. Chromatogr., 205 (1981) 77.
4 C. E. Werkhoven-Goewie, C. de Ruiter, U. A. Th. Brinkman, R. W. Frei, G. J. de Jong, C. J. Little and O. Stahel, J. Chromatogr., 255 (1983) 79.
5 C. E. Werkhoven-Goewie, U. A. Th. Brinkman, R. W. Frei, C. de Ruiter and J. de Vries, J. Chromatogr. Biomed. Appl., 276 (1983) 349.
6 T. Imasaka, T. Harada and N. Ishibashi, Anal. Chim. Acta, 129 (1981) 195.
7 L. Fossey and F. F. Cantwell, Anal. Chem., 54 (1982) 1693.
8 L. Fossey and F. F. Cantwell, Anal. Chem., 55 (1983) 1882.
9 A. H. M. T. Scholten, U. A. Th. Brinkman and R. W. Frei, J. Chromatogr., 205 (1981) 229.
10 J. Kawase, Anal. Chem., 52 (1980) 2124.
11 L. Nord and B. Karlberg, Anal. Chim. Acta, 118 (1980) 285.
12 K. Ogata, K. Tagudi and T. Imanari, Anal. Chem., 54 (1982) 2127.
13 J. L. Burguera and M. Burguera, Anal. Chim. Acta, 153 (1983) 207.
14 J. A. Appfel, U. A. Th. Brinkman and R. W. Frei, Chromatographia, 18 (1984) 5.
15 K. Bäckström, L. G. Danielsson and L. Nord, Anal. Chim. Acta, 169 (1985) 43.
16 J. H. Wolf, C. de Ruiter, U. A. Th. Brinkman and R. W. Frei, J. Pharm. Biomed. Anal., 4 (1986) 523.
17 J. P. Foley and J. G. Dorsey, Anal. Chem., 55 (1983) 730.
18 D. J. Anderson and R. R. Walters, J. Chromatogr. Science, 22 (1984) 353.
19 H. J. van Nieuwkerk, H. A. Das, U. A. Th. Brinkman and R. W. Frei, Chromatographia, 19 (1984) 137.
20 C. E. Werkhoven-Goewie, U. A. Th. Brinkman and R. W. Frei, Anal. Chim. Acta, 114 (1980) 147.

Analytica Chimica Acta, 192 (1987) 277—287
Elsevier Science Publishers B.V., Amsterdam — Printed in The Netherlands

DEVELOPMENT OF A SELECTIVE POST-COLUMN DETECTOR FOR PHENOLS SEPARATED BY HIGH-PERFORMANCE LIQUID CHROMATOGRAPHY

S. K. RATANATHANAWONGS and S. R. CROUCH*
Department of Chemistry, Michigan State University, East Lansing, MI 48824 (U.S.A.)
(Received 13th September 1986)

SUMMARY

An on-line post-column reactor based on air-segmented continuous flow is described for the determination of phenols. The reaction used is the coupling of diazotized sulfanilic acid with phenols to form highly colored azo dyes. The effect of experimental parameters on the detector response was investigated by both univariate and simplex approaches in order to establish optimum reaction conditions. The aqueous reaction system is compatible with common reverse-phase solvents. The detection limit for phenol with the derivatization detector (71 $\mu g\ l^{-1}$) shows a 16-fold improvement over u.v. detection of the underivatized phenol. Imprecision, based on multiple injections of sample into the HPLC system and measurement of the peak heights, is ±0.64% (RSD). The technique is applied to the determination of phenols added to river water and present in residual fuel oil samples.

A limitation encountered in modern liquid chromatography is the lack of sensitive and specific detectors in applications involving complex samples. Conventional high-performance liquid chromatography (HPLC) detectors, such as ultraviolet (u.v.) absorption and refractive index detectors, often lack the selectivity and sensitivity required for such samples. Fluorescence and electrochemical detectors can be more selective and sensitive, but they are not as widely applicable. These techniques can be susceptible to such interferences as quenching and changes in mobile-phase composition. The problems mentioned above can be circumvented by reaction of the analytes to form derivatives with different and/or enhanced characteristics. The popularity of chemical-derivatization techniques in chromatography has increased considerably in the past decade, as reflected by the number of reviews assessing the current status of chemical reactor detectors in liquid chromatography [1—13] and publications reporting new applications. This rapid growth is partially due to the abundance of applicable selective reactions [14—19]. Among these are the reactions for phenols, most of which have not been investigated for potential use in post-column reactor (PCR) detectors. The majority of these reactions yield products that can be detected spectrophotometrically.

The reaction used in this work involves coupling between a phenol ($Ar'OH$) and a diazotized aromatic amine ($ArN_2^+Cl^-$) to form an azo dye [20—22].

0003-2670/87/$03.50

The general diazotization and coupling reactions are

$$ArNH_2 + NaNO_2 + 2HCl \rightleftharpoons ArN_2^+Cl^- + 2H_2O + NaCl \quad (1)$$

$$ArN_2^+Cl^- + Ar'OH \rightleftharpoons ArN{=}NAr'OH + HCl \quad (2)$$

The aromatic amine ($ArNH_2$) used in this case is sulfanilic acid. The performance of diazotized sulfanilic acid and several other coupling reagents has been evaluated for 126 different phenolic compounds by Koppe et al. [23]. Studies by Whitlock et al. [24] and Baiocchi et al. [25] to characterize the reaction and to establish the optimum reaction conditions for diazotized sulfanilic acid have not produced consistent results. It was therefore necessary to undertake an extensive study of the effects of experimental conditions on the response. Simplex optimization was used to confirm the optimum reaction conditions. The potential of the PCR for use with reverse-phase liquid chromatography was investigated by studying the effects of organic solvents on the diazo coupling reaction. To evaluate the usefulness of the system, the PCR was used to quantify phenols in fuel and spiked river-water samples.

EXPERIMENTAL

Apparatus

The instrumentation used is shown in Fig. 1. The main components of the HPLC unit were a Spectra-Physics SP8700 solvent-delivery system (Santa Clara, CA), a Rheodyne 7120 injection valve (Cotati, CA) with a 20-μl sample loop and a Chromatronix 220 u.v. detector (Berkeley, CA). Separations were done on a 5-μm Spherisorb ODS column (25 cm × 4.5 mm; Alltech Associates, Deerfield, IL). The PCR system is a miniaturized continuous flow system designed in this laboratory [26—28]. The peristaltic pump (Model IP-12, Brinkmann Instruments, Westbury, NY), used to add reagents to the column effluent, was modified from the original eight-roller assembly to one with 16 rollers for a smoother flow. A dual-channel colorimeter [27] with narrow-bandpass filters for wavelength discrimination was used to monitor the absorbance of the flow stream at 450 nm. Light was transmitted from the source to the colorimeter through a bifurcated fiber optic. The signal from the colorimeter was directed into a "bubble gate" circuit where the effect of the air segments was electronically removed [26].

As shown in Fig. 1, the sample is injected into the HPLC system where it undergoes separation followed by u.v. absorption detection. The column effluent is then directed to the PCR. The interface between the HPLC and PCR systems is a short piece of 0.01-in. i.d. stainless steel HPLC tubing, which is connected at one end to the output of the u.v. detector and at the other to a stainless steel reagent-addition block on the PCR manifold. The flow stream is immediately air-segmented by using the dual pump tube method described by Habig et al. [29]. Reagents are added to the column effluent via a 90° glass T-joint. Mixing and time delays are accomplished by means of glass

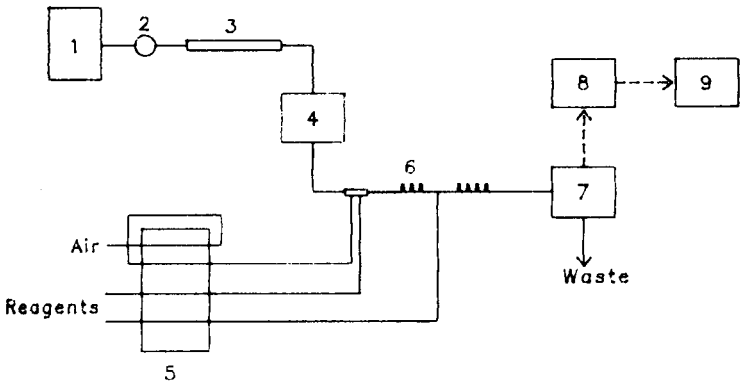

Fig. 1. Apparatus used for the post-column detection of phenols using an air-segmented continuous flow system. (1) Solvent reservoir; (2) injection valve; (3) analytical column; (4) u.v. detector; (5) peristaltic pump; (6) reaction coil; (7) colorimeter; (8) bubble gate; (9) readout device. (——) Flow-stream path; (— — —) electrical-signal path.

coils of various lengths. In the final stage, the stream containing derivatized products passes into a low-volume bubble-through flow cell (2 μl) mounted on a colorimeter and then out to waste.

Reagents

Commercially available chemicals were used without further purification. Diazotized sulfanilic acid was prepared by the procedure of Whitlock et al. [24] with some modifications. The sodium salt of sulfanilic acid (5 mmol) was dissolved in 50 ml of distilled water. A 10-ml aliquot of 50 mM sodium nitrite was transferred to this solution and then cooled to 0°C. After the addition of 2 ml of 2 M hydrochloric acid, the final volume was adjusted to 100 ml with chilled, distilled water. The diazotized sulfanilic reagent was tested for the presence of excess nitrous acid with starch-potassium iodide paper. If the test was positive, either sulfamic acid or urea was added to decompose the nitrous acid. The reagent was transferred to an amber bottle and stored at 5°C.

Standard solutions of phenol (Sigma Chemical Company) were prepared from a phenol stock solution (1 mg ml^{-1}). All other compounds used were purchased from Aldrich Chemical Company, Eastman Organic Chemicals, and K & K Laboratories. The pH of the 0.05 M sodium borate buffer was adjusted by the addition of HCl or NaOH. A surfactant, Brij-35 (Fisher Scientific Company), was added to all solutions in quantities of 0.5 ml^{-1}.

Spectral-grade HPLC solvents (Burdick and Jackson, Muskegon, MI) were filtered through a 0.45-μm filter and degassed with helium prior to use. Water samples collected from the Grand River (Lansing, MI) were filtered in the same manner prior to injection into the HPLC system. The residual fuel oil samples were obtained from the National Aeronautics and Space Administra-

tion. Sample preparation was done by sequential elution solvent chromatography [30, 31]. This method involves the use of nine solvent mixtures of varying polarities to elute compounds containing different functional groups; each fraction is collected and the solvent evaporated to yield a concentrated sample. A fraction containing phenols, fraction 7, was used in this work.

RESULTS AND DISCUSSION

Reaction characterization

The studies on characterization and optimization of the reaction were done on the miniaturized continuous-flow system without coupling to the HPLC unit. Phenol was used in all the characterization experiments. The effect of variables such as pH, reaction time, reagent-to-substrate ratio and temperature was investigated. The results shown are averaged values of duplicate absorbance measurements. Optimization was accomplished by both the univariate and simplex methods.

Univariate approach. The effect of pH on the detector response at varying reaction times is shown in Fig. 2. For all four curves, there are maxima at approximately pH 10. The general peak shapes can be explained by considering the following equilibria:

$$Ar'OH \rightleftharpoons Ar'O^- + H^+ \qquad pK_a = 9.99 \text{ (for phenol)} \qquad (3)$$

$$ArN_2^+ \rightleftharpoons ArN_2OH \rightleftharpoons ArN_2O^- \qquad pK_1 + pK_2 = 20.96 \qquad (4)$$

The color-forming reaction is an electrophilic aromatic substitution with the reactive species being the diazonium, ArN_2^+, and the phenolate ions. These two species predominate at conflicting pH conditions. Thus, the response increases to an optimum and then decreases as the ratios of the reactive species change with pH. The length of the plateau region observed in Fig. 2 at a reaction time of 55 s can be varied by changing the amount of diazotized sulfanilic acid added. Higher precision should be obtained in this region.

A distribution diagram for the diazonium and phenolate ions as a function of pH is shown in Fig. 3. Calculations involved the equilibrium constants given with Eqns. 3 and 4 [20, 32]. The hydrolysis characteristics of the diazonium ion are different from those of the "classic" dibasic acids in that $K_2 \gg K_1$. Thus, individual pK values are not available and the overall pK was used in these calculations. The distribution diagram shows that the amounts of diazonium and phenolate ions are maximized relative to each other at pH 10.2. In all the following experiments, solutions were buffered at the averaged pH value of 10.1.

The influence of the reagent-to-substrate concentration ratio was investigated by the addition of diazotized sulfanilic acid solutions of different concentrations to the buffered flow stream containing phenol. The absorbance values obtained at different reaction times and reagent-to-substrate ratios are shown in Fig. 4. A decrease in the time required for the reaction to go to

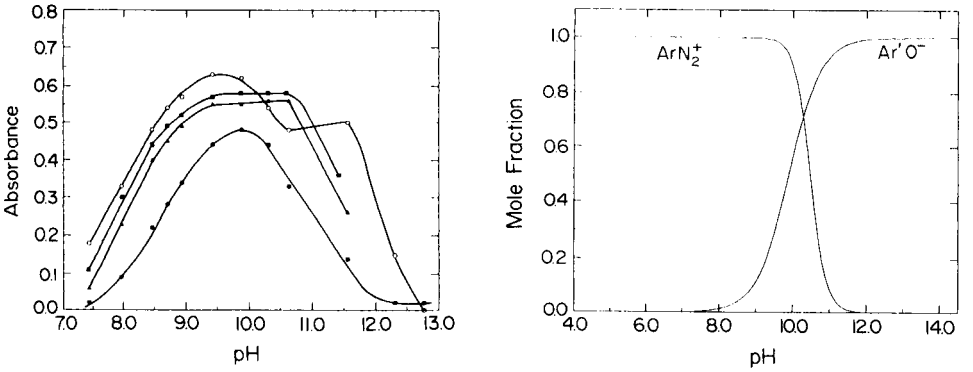

Fig. 2. Effect of pH on PCR response for different reaction times: (•) 15 s; (▲) 35 s; (■) 55 s; (□) 10 min. Conditions: 0.05 M sodium borate buffer adjusted to appropriate pH with NaOH or HCl; 30 μM phenol in borax buffer at 0.6 ml min^{-1}; diazotized sulfanilic acid at 0.03 ml min^{-1}.

Fig. 3. Distribution diagram for diazonium, ArN_2^+, and phenolate, $Ar'O^-$, ions at varying pH.

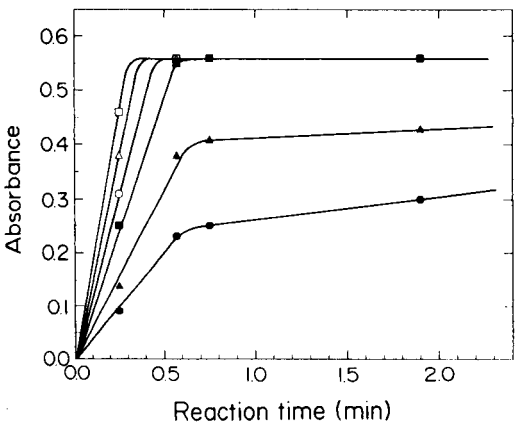

Fig. 4. Influence of diazotized sulfanilic acid/phenol ratios and reaction times on the PCR signal. Ratios: (•) 0.7; (▲) 1.2; (■) 2.8; (○) 6.7; (△) 12.4; (□) 27.8.

completion was observed as the amount of reagent added was increased. Results indicate that the mole ratio of the diazotized sulfanilic acid to phenol should be $\geqslant 3$ for the detector to attain maximum response in less than 60 s.

The effect of reaction time on detector response is demonstrated in Figs. 2 and 4. These studies were done by varying pump speeds and coil lengths as needed to produce the desired reaction times. Figure 2 demonstrates the responses obtained when pH and reaction time were varied. The reaction was 97% complete when a delay time of 35 s was used and 100% complete for a 55-s delay. Not shown is the curve obtained at 130 s, which gave the same

maximum absorbance as that for 55 s. When a reaction time of 10 min was used, secondary reactions may be taking place as evidenced by the increase in maximum absorbance and the appearance of a double maximum. Figure 4 shows that the time needed for the reaction to go to completion is less than 45 s when reagent/phenol ratios greater than 2.8 are used. Based on these results and considerations of throughput and sensitivity, the optimum reaction time selected was in the range 35—55 s.

Temperature studies were done with glass reaction coils built into plexiglas water jackets. A calibrated thermistor was used to measure the temperature of the thermostated flow stream as it left the flow cell. To prevent erroneous readings as air and liquid segments flowed past the thermistor, the flow stream was debubbled prior to measuring the temperature. The previously established optimum reaction conditions were used. No change in detector response was observed between 21.0 and 28.0°C. Therefore, normal fluctuations in room temperature should have little effect on the absorbance signal, and thermostating is not essential. A decreased signal observed at temperatures above 28.0°C can be attributed to the increased probability of secondary reactions.

Simplex optimization. An assumption inherent in the univariate approach described above is that all the variables are independent of each other. A false optimum may be found if this assumption is incorrect. Therefore, simplex optimization was used to verify the optimum conditions established by the univariate approach. The algorithm used was developed by Betteridge et al. [33]. Results indicated that pH was the major factor influencing the detector response. An optimum value at pH 10.1 was found in good agreement with that determined by the univariate method. The effect of reaction time and reagent concentrations also confirmed observations made previously.

Comparison with other reports. It should be noted that the optimum reaction conditions reported by other workers for this reaction are not entirely in agreement with those established here. Whitlock et al. [24] reported that, for phenol, the optimum pH was 8.5. A sodium hydrogencarbonate buffer was used, and the reaction required 2 min for completion. Preliminary experiments done in this laboratory to characterize the reaction also used hydrogen carbonate as the buffer. The optimum pH found with this buffer agreed with that reported by these workers. However, the buffer was changed to sodium borate because of the poor buffering capacity of hydrogencarbonate at pH 8.5. The two different optimum pH values obtained indicate that one or both buffers are not inert. Other observations made by Whitlock et al., such as the effect of excess of reagent and the stability period for the diazotized reagent are in agreement with present findings.

Baiocchi et al. [25] reported an optimum pH of 11.0 in their work on precolumn derivatization of phenols by sulfanilic acid. In this case, sodium hydroxide was added to obtain the desired pH. Their reported reaction time was 15 min, and the optimum reagent/phenol ratio was 40:1; both of these are much larger than values determined in this work. In addition, it was necessary to use the reagent within 10 min of its preparation. These observations may be due to improper preparation of the diazotized sulfanilic acid.

If the starting compound is sulfanilic acid, rather than its sodium salt, an indirect diazotization is needed [20]; prior to diazotization, sodium carbonate is added to the solution containing sulfanilic acid to convert it to the water-soluble form. This step was not reported by Baiocchi and co-workers.

System characterization

The optimized PCR for phenols was used in conjunction with an HPLC apparatus with u.v. detection for system characterization. The performance of the PCR was evaluated with respect to its compatibility with the chromatographic conditions, band-broadening contributions, detection limit, linear dynamic range and precision. For all experiments, the wavelengths of detection were 254 nm for the underivatized phenols and 450 nm for the azo derivatives.

Mobile phase effects. The effect of varying amounts of common reverse-phase solvents on the detector response was investigated. A 100-μM phenol solution prepared in pH 10.1 borax buffer was continuously added to, and mixed with, the column effluent. The manifold used was identical to that shown in Fig. 1. The u.v. and PCR responses were monitored while running a 2% min^{-1} gradient of water/acetonitrile or water/methanol. A drift of 1% in the detector signal was observed as the acetonitrile composition of the mobile phase spanned 0 to 80%. The upper limit was set by the solubility of sodium borate in acetronitrile. A decrease in the signal was observed when the percentage of methanol was increased beyond 60%. This effect may be attributed to a combination of different factors among which are solvent polarity and proton-donating ability. The blank signal shows no change for either solvent. From these results, it was concluded that acetonitrile is the more versatile solvent, especially for separations requiring gradient elution. Also, a slightly higher response was obtained for acetonitrile than for methanol.

Chromatographic figures of merit. The degree of band broadening and peak asymmetry introduced by the PCR were examined. For the most accurate results, pyrogallol was used. This trihydroxy phenol is weakly retained by the ODS column. From the ratio of the peak widths at half height of the u.v. and PCR responses, the amount of band broadening caused by the PCR was found to be 5—20%. The peak-asymmetry factor, calculated at 10% peak height, showed no additional contributions from the PCR. These observations demonstrate the effectiveness of air-segmentation and the miniaturized continuous-flow instrument in limiting dispersion.

Statistical figures of merit. The detection limit ($S/N = 2$) of this detector, based on the amount of phenol injected, is 71 $\mu g\ l^{-1}$. The molar absorptivity of the phenol derivative (2.25×10^4 l mol^{-1} cm^{-1} at 430 nm) (calculated) is 16 times that of phenol itself (1400 l mol^{-1} cm^{-1} at 270 nm) [34]. The linear dynamic range of the reaction spanned more than two orders of magnitude, from 0.071 to 14 mg l^{-1}. The upper limit was established by deviations from Beer's law which resulted from instrumental rather than chemical effects. The relative standard deviation, based on 15 injections of 100 μM phenol standards

into the chromatograph, was 0.64%.

Applications

The performance of the proposed detector for phenols was compared with that of the u.v. detector for real samples.

River water sample. Grand River (Lansing, MI) water, collected downstream from a coal-driven power plant, was examined for phenols but none were detected. The sample was then spiked with 1.9 mg l^{-1} phenol, 2.2 mg l^{-1} *o*-cresol, 2.4 mg l^{-1} 3,5-dimethylphenol and 2.2 mg l^{-1} resorcinol. The detector responses, before and after derivatization, are shown in Fig 5(a). The chromatographed peaks were barely discernible by u.v. detection. The figure clearly demonstrates the increased sensitivity obtained when post-column derivatization is used.

The class selectivity of the detector is demonstrated by the chromatogram shown in Fig 5(b) where the u.v. and PCR responses are compared. Here, the water sample was spiked with phenol, aniline, *o*-cresol and 3,5-dimethylphenol. Ultraviolet detection of the chromatographed sample showed the presence of all four compounds, with aniline as a major peak. The PCR detector showed only three peaks which corresponded to the phenols. This is a result of the different optimum reaction conditions needed for coupling of diazotized sulfanilic acid to phenol and to aromatic amines. In addition, the

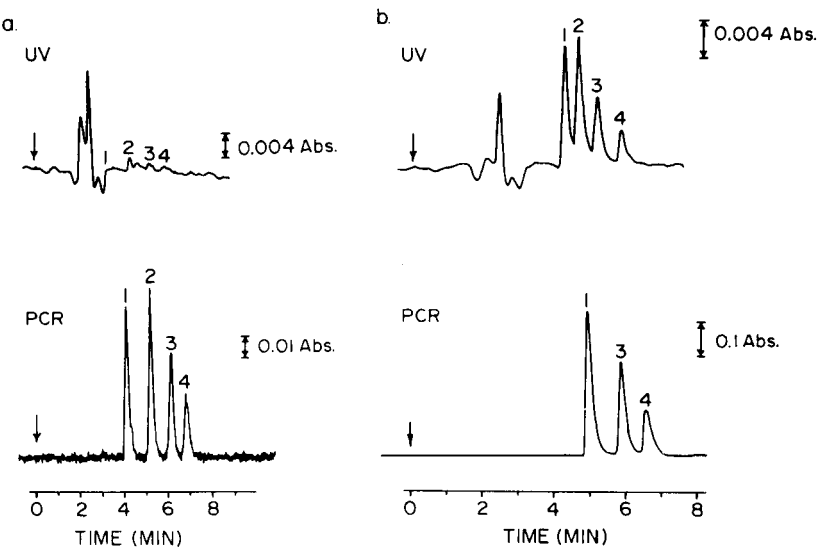

Fig. 5. Comparison of u.v. and PCR detection for the separation of phenols in a spiked river water sample (Grand River, East Lansing, MI). (a) Enhancement of sensitivity: (1) resorcinol, 2.2 mg l^{-1}; (2) phenol, 1.9 mg l^{-1}; (3) *o*-cresol, 2.2 mg l^{-1}; (4) 3,5-dimethylphenol, 2.4 mg l^{-1}. (b) Comparison of selectivity: (1) phenol, 18.8 mg l^{-1}; (2) aniline, 19.6 mg l^{-1}; (3) *o*-cresol, 21.6 mg l^{-1}; (4) 3,5-dimethylphenol, 24.4 mg l^{-1}. HPLC: Spherisorb ODS column; acetonitrile/water (50:50) mobile phase; flow rate of 1 ml min^{-1}; u.v. detection at 254 nm. PCR: flow rates as given in Fig. 2 caption; detection at 450 nm.

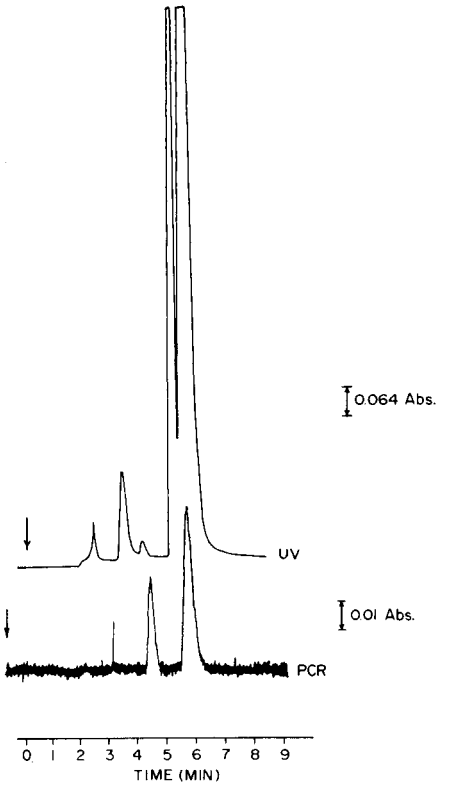

Fig. 6. Reverse-phase separation of residual fuel oil fraction 7. Separation conditions and flow rates as in Fig. 5.

column void-volume peak was not observed by the PCR detector.

Residual fuel oil fractions. A residual fuel oil sample was separated into fractions of different functional-group types by sequential elution-solvent chromatography. The fraction containing phenols was chromatographed under isocratic conditions with a 50:50 acetonitrile/water mobile phase. Several peaks were observed in the u.v. trace as shown in Fig. 6. Only two peaks were evident in the PCR response. These peaks were tentatively identified by retention times and spiking experiments to be phenol and a cresol. Standard-addition experiments showed that other compounds were coeluting with phenol and *o*-cresol and were not detected by the derivatization detector. A sample that had been spiked with 90 mg l^{-1} phenol showed no measurable change in relative peak height for the u.v. detector response and a 10-fold increase for the PCR response. Addition of 400 mg l^{-1} phenol yielded increases in relative peak heights by factors of 2 and 43 for the u.v. and PCR signals, respectively. This application shows that a potentially complicated separation may be greatly simplified by using a selective detector.

The authors thank Dr. A. P. Wade for his help in setting up the simplex optimization experiments. This work was supported in part by NASA, Grant No. NAG 3-93 and by NSF, Grant No. CHE 8320620.

REFERENCES

1 R. W. Frei, H. Jansen and U. A. Th. Brinkman, Anal. Chem., 57 (1985) 1529A and references therein.
2 L. R. Snyder, J. Chromatogr., 125 (1976) 287.
3 R. W. Frei and A. H. M. T. Scholten, J. Chromatogr. Sci., 17 (1979) 152.
4 R. W. Frei, L. Michel and W. Santi, J. Chromatogr., 142 (1977) 261.
5 R. W. Frei, Fresenius Z. Anal. Chem., 279 (1975) 303.
6 I. S. Krull, C. M. Selavka, C. Duda and W. Jacobs, J. Liq. Chromatogr., 8(15) (1985) 2845.
7 R. W. Frei, Chromatographia, 15 (1982) 161.
8 R. W. Frei and W. Santi, Fresenius Z. Anal. Chem., 277 (1975) 303.
9 I. S. Krull, in S. Ahuja (Ed.), Chromatography and Separation Chemistry, American Chemical Society, Washington, DC, 1986, Chap. 9.
10 R. W. Frei and J. F. Lawrence (Eds.), Chemical Derivatization in Analytical Chemistry, Vol. 2: Separation and Continuous Flow Techniques, Plenum Press, New York, 1982, Chaps. 1 and 3.
11 R. W. Frei and J. F. Lawrence (Eds.), Chemical Derivatization in Analytical Chemistry, Vol. 1: Chromatography, Plenum Press, New York, 1981, Chaps. 1 and 4.
12 J. F. Lawrence and R. W. Frei, Chemical Derivatization in Liquid Chromatography, Elsevier, Amsterdam, 1976.
13 I. S. Krull (Ed.), Reaction Detectors in Liquid Chromatography, M. Dekker, New York, 1986.
14 S. Siggia and J. G. Hanna, Quantitative Organic Analysis via Functional Groups, 4th edn., Wiley, New York, 1979.
15 K. A. Connors, Reaction Mechanisms in Organic Analytical Chemistry, Wiley, New York, 1973, Chaps. 7—13.
16 N. D. Cheronis, J. B. Entrikin and E. M. Hodnett, Semimicro Qualitative Organic Analysis, Krieger, Malabar, FL, 1983, Part 3.
17 D. R. Knapp, Handbook of Analytical Derivatization Reactions, Wiley, New York, 1979, Part 2.
18 K. Blau and G. King, Handbook of Derivatives for Chromatography, Heyden, London, 1977, Chaps, 2—13.
19 T. Hanai (Ed.), Phenols and Organic Acids, CRC Handbook of Chromatography, Vol. 1, CRC Press, Boca Raton, FL, 1982, pp. 211—221.
20 H. Zollinger, Azo and Diazo Chemistry, Interscience, New York, 1961, p. 17, p. 51 and pp. 210—217.
21 K. Schank, in F. Zymalkowski (Ed.), Methodicum Chimicum, Vol. 6, Academic Press, New York, 1975, Chap. 7.
22 I. M. Kolthoff and P. J. Elving, Treatise on Analytical Chemistry, Part II, Vol. 15, Wiley, New York, 1976, p. 270.
23 P. Koppe, F. Dietz, J. Traud and Ch. Rubelt, Fresenius Z. Anal. Chem., 285 (1977) 1.
24 L. R. Whitlock, S. Siggia and J. E. Smola, Anal. Chem., 44 (1972) 532.
25 C. Baiocchi, M. C. Gennaro, E. Campi, E. Mentasti and R. Aruga, Anal. Lett., 15 (A19) (1982) 1539.
26 C. J. Patton, M. Raab and S. R. Crouch, Anal. Chem., 54 (1982) 1113.
27 C. J. Patton and S. R. Crouch, Anal. Chim. Acta, 179 (1986) 189.
28 C. J. Patton, Ph.D. Thesis, Michigan State University, East Lansing, MI, 1982.
29 R. L. Habig, B. W. Schlein, L. Walters and R. E. Thiers, Clin. Chem., 15 (1969) 1045.

30 M. Farcasiu, Fuel, 56 (1977) 9.
31 M. R. Danna, Ph.D. Thesis, Michigan State University, East Lansing, MI, 1985.
32 R. C. Weast and M. J. Astle (Eds.), CRC Handbook of Chemistry and Physics, 60th edn., CRC Press, Boca Raton, FL, 1980, p. D-166.
33 D. Betteridge, A. P. Wade and A. G. Howard, Talanta, 32 (1985) 709, 723.
34 O. H. Wheeler and L. A. Kapfan (Eds.), Organic Electronic Spectral Data, Vol. III, Wiley, New York, 1966, p. 65.

Analytica Chimica Acta, 192 (1987) 289—292
Elsevier Science Publishers B.V., Amsterdam — Printed in The Netherlands

Short Communication

CHEMILUMINESCENCE METHOD FOR DETERMINATION OF BENZOYL PEROXIDE IN SOLUTION

J. R. BOWYER and S. R. SPURLIN*
Department of Chemistry, Clemson University, Clemson, SC 29634-1905 (U.S.A.)
(Received 15th April 1986)

Summary. The chemiluminescence reaction of benzoyl peroxide with triethylamine is used to quantify benzoyl peroxide. The method is rapid with a detection limit for benzoyl peroxide in chloroform of 0.07 μg ml^{-1} and a relative standard deviation of 4% at 1 μg ml^{-1}. The technique is applied to the determination of benzoyl peroxide in pharmaceutical preparations.

Chemiluminescence techniques have increased in popularity recently as evidenced by several recent reviews [1—4]. These techniques possess low detection limits, often below 1 μg ml^{-1}, usually coupled with a rapid procedure and good selectivity. Burguera and Townshend [5] reported a chemiluminescence technique for triethylamine and diethylamine based on their reactions with benzoyl peroxide to produce visible chemiluminescence; the detection limit is 0.1 μmol ml^{-1} for triethylamine quantified by a pulse technique [6]. The simplicity of this procedure and its low detection limit suggested its application for quantifying benzoyl peroxide by its chemiluminescent reaction with triethylamine.

The need in the fiber industry for rapid and sensitive determinations of benzoyl peroxide was recently emphasized [7]. The increased usage of benzoyl peroxide in over-the-counter acne treatments has also generated interest in rapid and sensitive procedures suitable for pharmaceutical applications. Current techniques include gas chromatography [8], thin-layer chromatography [9], and liquid chromatography [10]. Presented here is a new chemiluminescent procedure for quantifying benzoyl peroxide based on its reaction with triethylamine.

Experimental

Equipment. The reaction cell is a standard round, 1-cm fused silica fluorescene cuvette. This is housed in a chamber constructed locally which attaches directly to the face of a 14-stage Amperex XP-2233B photomultiplier tube. The chemiluminescence signal is quantified with an Ortec 9315 photon counter unit equipped with an Ortec amplifier-discriminator or with a Nicolet 3905 storage oscilloscope. The photon-counter output is

0003-2670/87/$03.50

recorded on a strip-chart recorder with a 0.1-s response time. The oscilloscope data are monitored with an x-y recorder.

Procedure. After the reagent has been pipetted into the cell, a digital pipette is loaded with sample and placed in position over the cell. The sample is injected into the cell in less than 0.4 s and the luminescence is recorded until the baseline signal (dark noise) is regained. The peak heights are easily measured from the chart paper and these are the intensity values used throughout. To obtain peak areas, the output of the photomultiplier is either monitored with a digital oscilloscope or the counting time of the photon counter is extended.

Reagents and samples. All reagents were reagent grade and all solvents were dried by distillation. Triethylamine, pyridine, and other amino compounds were distilled each day and the benzoyl peroxide solutions were prepared immediately before use.

The benzoyl peroxide was quantified in two commercial acne preparations, Oxy-5 (5% benzoyl peroxide) and Clearasil Maximum Strength (10% benzoyl peroxide). The weighed samples, about 0.1 g, were dissolved in 10 ml of freshly distilled tetrahydrofuran (THF) using an ultrasonic cleaner to aid dissolution. The samples were then filtered to remove insoluble material and diluted to 25 ml in a volumetric flask. Portions of this sample were injected directly into triethylamine as noted above. Both standard addition and calibration curves were used to quantify benzoyl peroxide.

Results and discussion

Figure 1 presents results for three benzoyl peroxide concentrations at several different triethylamine concentrations (in chloroform). In all cases, a maximum signal is obtained with 100% triethylamine as the reagent. The effect of pyridine on the signal was also investigated. With 100% triethylamine as the reagent, pyridine had no effect; however, at low concentrations of triethylamine, pyridine enhanced the signal intensity as noted earlier [5]. Figure 2 shows the effect of water (0.01—0.3%) on intensity. Above about 0.2% water, the signal decreases linearly with increasing moisture content. Water added to the chloroform before preparation of the benzoyl peroxide solutions had a very different effect. The signal decreased in direct proportion to the amount of water (0.01—0.10%) added and also to the time the solution was left standing after mixing. This is due to the slow decomposition of benzoyl peroxide by water.

Both hydrogen peroxide and t-butyl hydroperoxide were tested for chemiluminescence with triethylamine. Hydrogen peroxide yielded no luminescence while t-butyl hydroperoxide did produce light at concentrations above 500 $\mu g\ ml^{-1}$. Neither phenylhydrazine nor hydrazine produced any measurable luminescence. Because benzoic acid is one of the reaction products and can be present in mixtures of benzoyl peroxide, its effects were also investigated. Concentrations below 1 mg ml^{-1} did not interfere

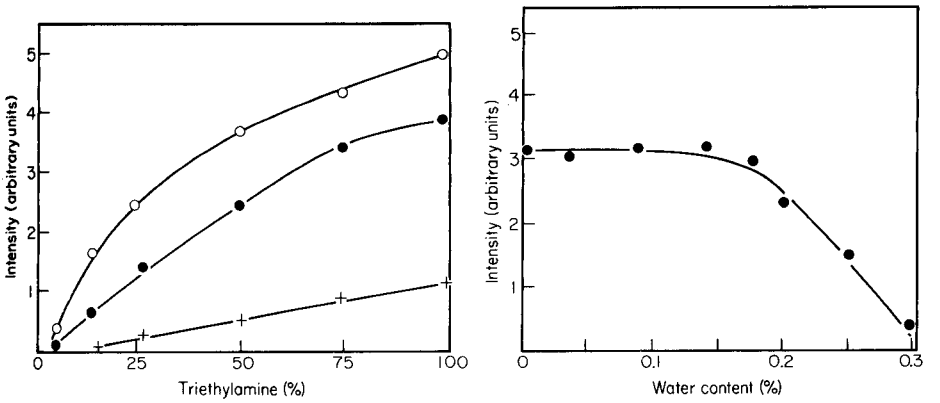

Fig. 1. Effects of triethylamine concentration on chemiluminescence intensity. All samples and reagent diluted with chloroform. Benzoyl peroxide concentrations (μg ml^{-1}): (○) 1000; (●) 500; (+) 10.

Fig. 2. Effect of water in the triethylamine on the intensity of the chemiluminescence signal from 50 μg ml^{-1} benzoyl peroxide.

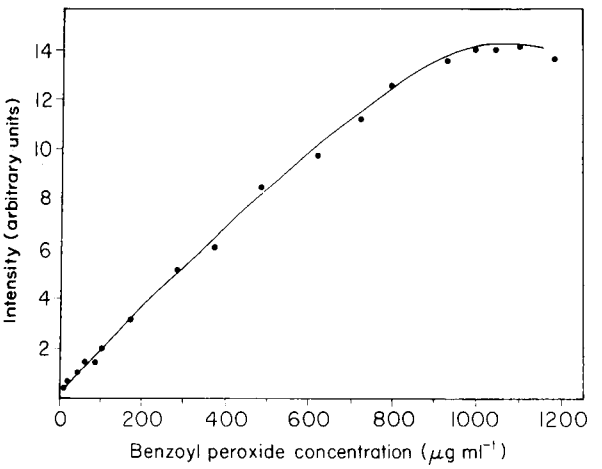

Fig. 3. Calibration plot for benzoyl peroxide in chloroform.

but above this level, the chemiluminescence signal from a 10 μg ml^{-1} benzoyl peroxide solution was depressed by 15—40%.

Figure 3 is the calibration curve for benzoyl peroxide in chloroform with triethylamine. The detection limit for benzoyl peroxide in chloroform was 0.07 μg ml^{-1} with a relative standard deviation of 4% at 1 μg ml^{-1}. The response was linear to 900 μg ml^{-1}; the curvature above this concentration probably is due to reagent depletion. The calibration curve in Fig. 3 has slight curvature at very low concentrations and appears to have a non-zero intercept. A set of low-concentration standards exhibited a slightly different slope for benzoyl peroxide concentrations below 10 μg ml^{-1} with a zero intercept.

Results obtained for commercial benzoyl peroxide preparations agreed with the stated values and with results obtained with a gas-chromatographic (g.c.) procedure [8]. The slope obtained for the standard additions curve was the same as that for the calibration curve in Fig. 3. This indicates that the THF extractions of benzoyl peroxide from the acne preparations are free from interferences and therefore a calibration curve can be used. When a calibration curve was used, the one-step extraction procedure yielded a value of 4.94 ± 0.05% for the 5% benzoyl peroxide cream and 9.53 ± 0.05% for the 10% benzoyl peroxide cream. The g.c. technique yielded values of 4.97 ± 0.03% and 9.59 ± 0.03% for the creams.

Up to 30 samples/hour can be processed with the method.

REFERENCES

1 A. Fontijn in E. L. Wehry (Ed.), Modern Fluorescence Spectroscopy, Vol. I, Heyden, London, 1976, p. 159.
2 B. A. Thrush, J. Photochem., 25 (1984) 9.
3 L. J. Kricka and G. H. G. Thorpe, Analyst, 108 (1983) 1274.
4 E. L. Wehry, Anal. Chem., 56 (1984) 156R.
5 J. L. Burguera and A. Townshend, Talanta, 26 (1979) 795.
6 U. Isacsson and G. Wettermark, Anal. Chim. Acta, 83 (1976) 227.
7 T. Perenich, Southeastern Assoc. of Analytical Chemists, Univ. of Georgia, Athens, GA, April, 1984.
8 R. M. Silverstein, Anal. Chem., 35 (1963) 154.
9 C. Chambley and T. Perenich, Text. Chem. Color., 16 (1984) 150.
10 C. K. Chou and D. C. Locke, J. Assoc. Off. Anal. Chem., 67 (1984) 913.

Analytica Chimica Acta, 192 (1987) 293—299
Elsevier Science Publishers B.V., Amsterdam — Printed in The Netherlands

Short Communication

FLUORIMETRIC DETERMINATION OF DANTHRON IN PHARMACEUTICAL TABLETS AND IN URINE

BLAIR E. MILLER and NEIL D. DANIELSON*
Department of Chemistry, Miami University, Oxford, Ohio 45056 (U.S.A.)
(Received 9th July 1986)

Summary. A simple, rapid determination is reported for danthron (1,8-dihydroxyanthraquinone) in pharmaceutical tablets. In a flow-injection system, danthron is reduced by sodium dithionite in 1/1 methanol/borate buffer to give a fluorescent complex. Linearity ranges from 30 $\mu g\ ml^{-1}$ to below 0.1 $\mu g\ ml^{-1}$. In urine samples, danthron is separated from other fluorescing species by reversed-phase high-performance liquid chromatography before its reduction by dithionite in a post-column reactor. Urine preparation requires no extraction. Spiked urine samples were studied in the working range of 0.02—2.0 $\mu g\ ml^{-1}$ danthron.

Danthron (1,8-dihydroxyanthraquinone, chrysazin) is commonly formulated in pharmaceutical cathartic laxatives. Of primary concern to pharmaceutical manufacturers is the rapid, accurate quantitation of the primary constituent in commercially produced drugs. The standard method for danthron uses u.v./visible spectrophotometry with benzene as the solvent [1]. Thin-layer chromatography (t.l.c.) [2] has also been used. Lane [3] studied the formation of a fluorescent complex by reduction of danthron with sodium dithionite in the presence of borate. Here, this reaction serves as the basis for a flow-injection system to determine danthron rapidly in pharmaceutical samples. This instrumentation, being an enclosed system, improved the reproducibility because reduced anthraquinone species are readily air-oxidized.

Danthron has been determined in complex matrices such as urine and feces. Several techniques have been investigated for quantifying danthron and sometimes other laxatives in complex samples. These include gas chromatography (g.c.) [4], g.c./mass spectrometry [5], t.l.c. [6, 7], and fluorescence [3]. Baars et al. [4] found Lane's fluorescent technique [3] unsuitable for real samples because of other fluorescing compounds in the matrices. In each of the previous cited studies, an extraction process requiring several steps was necessary before the measurement step. By combining high-performance liquid chromatography (h.p.l.c.) and the flow-injection system for post-column derivatization, it was possible to determine danthron in urine samples without prior clean-up.

0003-2670/87/$03.50

Experimental

The pharmaceutical samples used were Modane and Modane Plus tablets. Each Modane tablet contained 75 mg of danthron, and each Modane Plus tablet contained 50 mg of danthron and 100 mg of sodium docusate. Danthron and pharmaceutical tablets were stored in a desiccator at room temperature. Reagent-grade methanol was used to prepare solutions, and h.p.l.c.-grade methanol was used for h.p.l.c. work. Deionized and doubly distilled water was used in all cases. Sodium tetraborate decahydrate was used as the buffering agent for all studies. After several experiments, it was found that no adjustment of the pH 8.2 borate buffer was necessary for the optimum reaction conditions. The reagent solutions were kept stoppered when not in use and degassed before pumping.

The flow-injection system was composed of an FMI lab pump (Fluid Metering, Oyster Bay, NY), a Tecator FIAstar injector (Tecator, Herndon, VA) with a 30-μl loop, and a mixing coil. A pulse-dampener, which consisted of a 1-m tube (2 mm i.d.), was inserted between the pump and injector. All other tubing used was 0.3 mm i.d. teflon. The optimum mixing coil length was found to be 150 cm; this allowed satisfactory reaction time in both the flow-injection system and the post-column derivatization studies. An Aminco scanning spectrofluorimeter (SPF-125; SLM Instruments, Urbana, IL) fitted with a 3.5-μl flow cell (10 mm $\times$ 10 mm) was used as the detector. Both excitation and emission slit widths were 2 mm wide. The excitation and emission wavelengths were 388 and 510 nm, respectively. For comparison, a Hewlett-Packard 8450 u.v./visible spectrophotometer was used to quantify danthron in pharmaceutical preparations.

The h.p.l.c. post-column derivatization system consisted of an Altex model 110A pump (Beckman Instruments, Berkeley, CA), a Rheodyne 7010 injector with a 20-μl loop, and an IBM column (250 mm $\times$ 4.5 mm) packed with 5-μm methyl (C1) silica. A Valco low-dead volume tee joined the column outlet to the above-mentioned flow-injection system. The fluorimeter settings remained the same as given above. The fluorimeter sensitivity range was set according to the concentration range to be covered in a particular trial.

For the flow-injection method, standards were prepared by appropriate dilution of aliquots taken from a 100 μg ml^{-1} danthron stock solution in methanol. The laxative tablets were ground to a powder while being sonicated in methanol. Undissolved particles were filtered off. All sample solutions prepared from the stock solutions were diluted with methanol. All solutions were kept in the dark.

For post-column h.p.l.c., danthron standards were prepared using 80/20 methanol/water diluent. Three healthy volunteers (two males, one female) donated urine samples. Urine samples were treated as follows: a small amount of Modane or Modane Plus solution (3 ml or less) was added to a 25-ml volumetric flask and diluted to the line with urine. A 10-ml aliquot was pipetted into a 50-ml volumetric flask and diluted to the mark with

methanol. A urine blank was made by pipetting 10 ml of fresh urine into 40 ml of methanol. These solutions were shaken and filtered through a sintered glass crucible before use. If the sample was too concentrated to be in the working range of 2—0.1 $\mu g\ ml^{-1}$, a smaller amount of spiked urine was pipetted into the 50-ml flask, with water added to make the total addition to the flask 10 ml.

Results and discussion

Reaction characterization. A previous report [3] provided a basis for the study of the reduction of danthron in the flow-injection system. The formation of the fluorescent complex is due to both reduction by sodium dithionite and the presence of borate for complexation. This complex is probably a boron chelate of a substituted dianthranol. Initial results with injections of danthron into a buffered aqueous carrier phase indicated erratic fluorescent responses. Because of the limited solubility of danthron in water, it was believed that the danthron adhered to the inside of the teflon tubing when injected into a highly aqueous system. To improve solubility, methanolic buffer carrier phases were considered. Solutions of 2% sodium tetraborate with a dithionite concentration of 90 mM and varying from 0 to 50% in methanol content were used to study the effect of an organic solvent on the fluorescent intensity. Because sodium dithionite has limited solubility in methanol, 55% methanol was the highest percentage possible in the carrier phase. The results are shown in Fig. 1. A 20% increase in detector response was achieved with 1/1 methanol/2% borate buffer as compared with 100% aqueous buffer. The 1/1 methanol/borate buffer was used as the carrier phase in all subsequent flow-injection experiments.

Because of some discrepancies in previous work [3], the effect of dithionite concentration was investigated as a function of fluorescence signal. Dithionite concentrations of 30, 90, and 150 mM were dissolved in 1/1 methanol/2% sodium tetraborate. Results showed an increased fluorescent response with increasing dithionite concentration, but the difference between the 90 and 150 mM trials was only about 8%. Concentrations above 150 mM did not give significantly higher responses.

A study of dithionite reagent lifetime (Fig. 2) was done using these same reagent concentrations. The 30 mM sodium dithionite solution lost its strength rapidly. The 90 mM solution was quite stable for almost two weeks, while the 150 mM solution was similarly consistent for one week before precipitation problems occurred. Based on this study, a 90 mM dithionite solution was used for the remaining experiments because of its stability and greater reliability (Fig. 2).

Flow-injection system. A 90 mM sodium dithionite solution in 1/1 methanol/2% sodium tetraborate was pumped at 1.2 ml min^{-1} through the system. Linearity for danthron standards extended from 30 $\mu g\ ml^{-1}$ to below 0.1 $\mu g\ ml^{-1}$. The detection limit was 0.01 $\mu g\ ml^{-1}$. Table 1 gives the danthron content for a set of pharmaceutical samples. The calibration

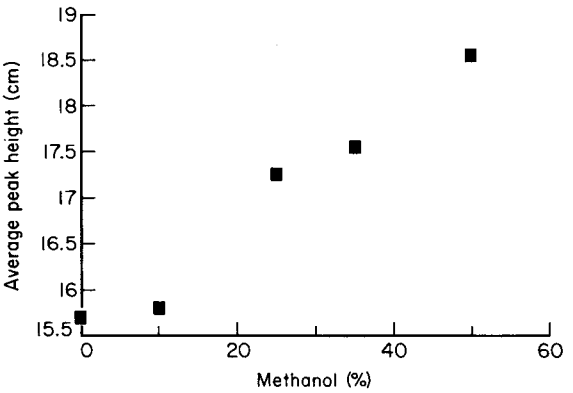

Fig. 1. Optimization of the reaction in f.i.a. with varying ratios of methanol to borate buffer in 90 mM sodium dithionite carrier phase. A 10 μg ml^{-1} danthron standard was injected.

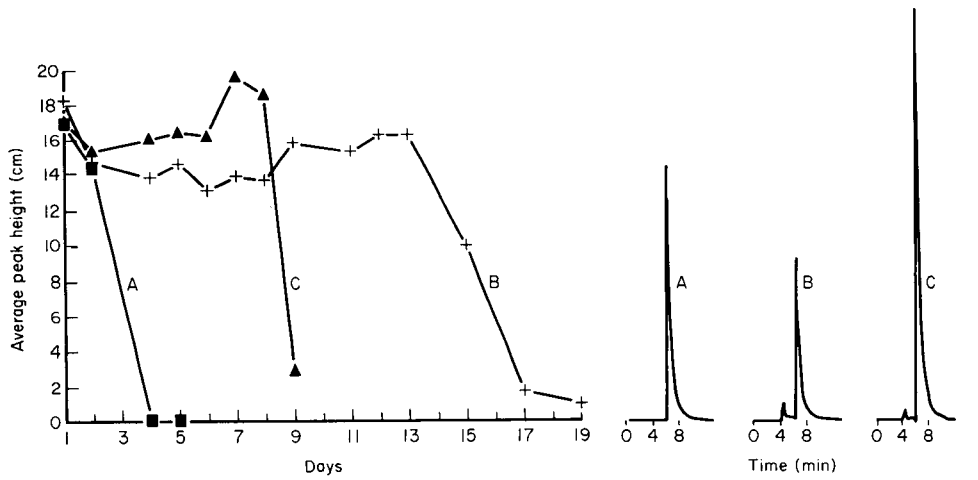

Fig. 2. Time study with varying concentrations of sodium dithionite as the carrier phase: (A) 30 mM; (B) 90 mM; (C) 150 mM. The dithionite solutions were made in 1/1 methanol/2% sodium tetraborate buffer. Standard solution injected was 10 μg ml^{-1} danthron.

Fig. 3. Separation of danthron in spiked urine samples on a C-1 column with post-column fluorescent derivatization. The mobile phase was 70/30 methanol/water pumped at 1.2 ml min^{-1}. A solution of 90 mM sodium dithionite in 2% borate buffer was pumped into the effluent at 0.4 ml min^{-1}. (A) Danthron standard (1 μg ml^{-1}); (B) urine spiked with 0.6 μg ml^{-1} Modane; (C) urine spiked with 1.6 μg ml^{-1} Modane Plus.

curve, consisting of seven points, covered 0—16 μg ml^{-1}. Five aliquots were injected for each sample or standard. A sample throughput of approximately 100 injections/h was possible. A blank reagent methanol gave a small response because of impurities. The correlation coefficient was 0.9997 with a slope of 0.816 ± 0.009 and a y intercept of 0.181 ± 0.070. As seen in Table 1, the experimental values for the flow-injection fluorimetric and the spectrophotometric techniques are dispersed around the stated concentrations of 75 mg per tablet for Modane and 50 mg per tablet for Modane Plus. The

TABLE 1

Results for danthron in pharmaceutical preparations by the flow-injection method

Sample	Danthron content		Spectrophotometry (mg/tablet)
	(μg ml^{-1})[a]	(mg/tablet)	
Modane 1	11.93 (0.11)	74.56	72.06
Modane 2	12.62 (0.05)	78.85	76.09
Modane 3	12.41 (0.07)	77.56	74.89
Modane 4	11.83 (0.21)	73.94	73.02
Modane+ 1	9.80 (0.03)	49.00	47.24
Modane+ 2	10.36 (0.05)	51.80	50.51
Modane+ 3	10.30 (0.03)	51.50	49.84
Modane+ 4	9.82 (0.03)	49.10	47.96

[a]Mean of 5 injections with standard deviation in parentheses.

average relative standard deviation of these data compared to stated literature values for these tablets was +1.16%. The danthron concentrations obtained by the flow fluorimetric method showed a small, consistent positive deviation compared to the spectrophotometric results.

Post-column derivatization. Because of the compatibility of the solvents used, the initial studies of the flow-injection system were easily applied to a post-column chemical derivatization system for h.p.l.c. The flow-injection procedure could not be used for urine samples because urine itself gave fluorescence at the set wavelengths probably because of bile pigments. A C-1 methyl silica column with a 70/30 methanol/water mobile phase pumped at 1.2 ml min^{-1} provided the separation of danthron from other fluorescing compounds in the urine matrix. The effluent was mixed with 90 mM sodium dithionite in 2% sodium tetraborate pumped at 0.4 ml min^{-1} for the fluorescent post-column reaction. Ultraviolet (254 nm) detection yielded two large blank peaks with a very small danthron peak on the side of the second peak, so that the detection limit was poor, and the certainty of the peak identification was questionable. This problem remained despite the use of a 4.6 × 250 mm C-18 column and a 60/40 methanol/water mobile phase.

As stated earlier, the limited solubility of danthron in aqueous solution posed a problem with real samples. Kok and Faber [5] listed the range of danthron concentration in urine as being 0.5—30 mg l^{-1}. If this were the case, much of the danthron would exist in precipitated form in the urine. Previous techniques have involved extraction procedures for real samples. Initial procedures in this study involved the use of 10—20% methanol to prepare solutions. Even with danthron concentrations as low as 2 μg ml^{-1} in 20% methanol, significant loss of detector response was found for the sample after only 0.5 h. Standard solutions prepared in 80% methanol, however, were stable for several hours for all concentrations of 2 μg ml^{-1} or below. Thus, an 80/20 methanol/water solution was used to ensure

TABLE 2

Results for urine samples spiked with Modane or Modane Plus by h.p.l.c. post-column derivatization

Concentration (μg ml^{-1}) in Modane			Concentration (μg ml^{-1}) in Modane+		
Original spike	Found[a]	Expected	Original spike[b]	Found[a]	Expected
0.9	0.18 (0.01)	0.18	1.0	0.24 (0.01)	0.20
0.9	0.20 (0.01)	0.18	2.0	0.40 (0.01)	0.40
3.0[c]	0.68 (0.01)	0.60	2.0	0.40 (0.01)	0.40
3.0[c]	0.57 (0.01)	0.60	6.0	1.23 (0.01)	1.20
3.0[c]	0.65 (0.01)	0.60	6.0	1.28 (0.04)	1.20
12.0	1.31 (0.01)	1.20	8.0	1.66 (0.02)	1.60
12.0	1.26 (0.03)	1.20			
18.0	1.96 (0.00)	1.80			
18.0	1.89 (0.01)	1.80			
24.0	1.23 (0.01)	1.20			
24.0	1.20 (0.01)	1.20			

[a]Mean of 4 or 5 injections with standard deviation in parentheses. [b]All urine samples from donor 2. [c]Urine samples from donor 1; other samples in this column from donor 3.

solubility of the danthron standards and urine samples in the post-column derivatization system. Some urine components were precipitated with this solvent system, but they were easily filtered without losing the danthron.

Representative peaks are shown in Fig. 3 for urine samples in the post-column system. The linear range of standards in the post-column derivatization system was 0.02—2 μg ml^{-1} danthron. A concentration of 0.006 μg ml^{-1} danthron was found to be the lowest detectable amount. Table 2 gives results for Modane-spiked urine samples. The correlation coefficient of the seven-point line was 0.9999 with a slope of 9.361 ± 0.0942 and a y intercept of —0.066 ± 0.043. Typically, the range of relative errors extended from —5.2% to +10.6% with the exception of two trials. The average recovery was 105%. Table 2 also has results for urine spiked with Modane Plus. A similar calibration curve as described for Modane was generated. At least four replicates were run for each sample and the relative errors compared to expected values were generally in the range from —1.0 to +6.8% with one exception. Again, the average recovery tended to be slightly high, about 103%.

The Modane and Modane Plus tablets were a generous gift from Adria Laboratories, Plain City, Ohio. Craig Duncan, an undergraduate student, did some of the initial work on f.i.a.

REFERENCES

1 The National Formulary, 13th edn., American Pharmaceutical Association, Washington, DC, 1970, p. 196.
2 G. S. Vasilikiotis and H. Alexaki-Tzivanidou, Microchem. J., 17 (1972) 655.

3 A. C. Lane, Anal. Chem., 45 (1973) 1911.
4 A. J. Baars, R. J. Vermeulen, and D. D. Breimer, J. Chromatogr., 120 (1976) 217.
5 R. M. Kok and D. B. Faber, J. Chromatogr., 222 (1981) 389.
6 F. A. de Wolff, E. J. M. de Haas, and M. Verweij, Clin. Chem., 27 (1981) 914.
7 D. W. Hill, T. R. Kelley, S. W. Matiuck, K. J. Langer, and D. E. Phillips, Anal. Lett., 15 (1982) 193.

Analytica Chimica Acta, 192 (1987) 301—308
Elsevier Science Publishers B.V., Amsterdam — Printed in The Netherlands

Short Communication

EXPERIMENTAL STUDIES ON THE EFFECT OF TEMPERATURE ON DISPERSION IN A FLOW-INJECTION SYSTEM

C. L. M. STULTS, A. P. WADE[a] and S. R. CROUCH*

The Chemistry Department, Michigan State University, East Lansing, Michigan, 48824 (U.S.A.)

(Received 7th August 1986)

Summary. The effect of temperature on dispersion in a flow-injection system is described. Systems both with and without chemical reaction were investigated. The reaction studied was that of *p*-nitrophenol with sodium hydroxide. The results indicate that temperature does indeed have a significant and predictable effect on the dispersion of a sample plug. Findings agree with the random walk model for flow-injection systems.

Considerable attention has been given to the study of dispersion in flow-injection systems [1—7]. Flow injection brought to analytical chemistry the concept of controlled dispersion [7]. Prior to this, complete mixing of sample and reagent solutions was considered a prerequisite for quantitative work. In most cases, it is desirable to control dispersion rather than minimize it, because some dispersion is usually required to facilitate a chemical reaction, dilute the sample, or produce a gradient. Sample throughput may be dispersion-limited for systems that merely transport a sample, and in these cases, minimum dispersion is advantageous.

Růžička and Hansen [1] quantified the dispersion, D, of a sample plug as $D = C^0/C^t$, where C^0 is the initial concentration of the sample and C^t is the maximum concentration at time, t. The C^0 term is related to H_{max}, the height of the peak obtained when the sample is undiluted, and likewise C^t to H, the height of the peak obtained following injection of a finite volume of sample after time, t. Attempts have been made to quantify dispersion by using numerical techniques to solve the diffusion-convection equation [8]. Reijn et al. [2] indicated the additive dispersive effects of the processes of injection, transport, and detection. Other workers have studied the various aspects of system design and experimental parameters which affect these. Růžička and Hansen [1] recognized the importance of dispersion when they included sample volume, tube length, flow rate, and the presence of a mixing chamber into seven rules for developing flow-injection systems. Vanderslice et al. [3] indicated that the diffusion coefficient and tube radius play a role

[a]Permanent address: British Petroleum Research Centre, Chertsey Road, Sunbury-on Thames, Middlesex, TW16 7LN, Great Britain.

0003-2670/87/$03.50

in dispersion. A further dispersive effect during the transport process has been attributed to chemical reaction [1, 4, 9, 10]. Painton and Mottola [11] also pointed out that the usefulness of the "practical dispersion number" can be invalidated or obscured when chemical reactions take place. The nature of the reaction manifold used (straight tubes, coiled tubes, single-bead-string reactors, etc.) has been shown to be a key factor [2]. Dispersion introduced during detection was recently partially attributed to the flow-cell configuration [12]. The complex interactions of all these factors in the ever-widening range of flow injection applications are still not well characterized. It is obvious that deeper theoretical and practical studies of the processes that cause a sample plug to become dispersed as it travels through a flow-injection system are necessary [7].

In all of the discussion concerning various sources of dispersion, there has been little mention of the effect of temperature. No experimental studies have been published, although the case for such is strong in light of the circumstantial evidence available. For example, in flow-injection viscometric studies, temperature control was necessary to obtain the required reproducibility of peak-height measurements [9]; simulation studies indicated that an increase in temperature (and the resultant decrease in viscosity) would promote radial mixing, decrease longitudinal dispersion and increase peak height [4, 13]; and peak shapes changed as the temperature of one flow-injection system was increased [14]. The reaction kinetics which take place in flow-injection systems will often be favored by higher temperatures. For slow reactions, this can be used to achieve greater sensitivity or decreased time per sample, because the "optimum" experimental conditions will change.

This communication reports an experimental investigation of the effect of temperature on dispersion, peak height, area and full width at half maximum height (FWHM) of the sample plug, for flow-injection systems with and without reaction, and over a range of flow rates.

Experimental

Apparatus. The flow-injection apparatus used (Fig. 1) consisted of the following: a 12-channel peristaltic pump (Ismatec) with flow-rated pump tubing (Technicon); a pneumatically actuated 6-port injection valve with a 30-μl sample loop (Rheodyne); 1 m of coiled, 0.8-mm i.d. tubing (2.0-cm coil diameter); a miniaturized flow-through filter colorimeter as designed and constructed in this laboratory [15]. The sample container, reagent container, and manifold coil were immersed in a thermostatically controlled water bath. An in-house designed Intel 8088-based microcomputer [16] controlled the pump speed, sample injection, and data acquisition; software was written in FORTH (Forth, Hermosa Beach, CA) [17].

Reagents. All solutions were prepared using distilled water and filtered as necessary. Alizarin red, potassium hydrogenphthalate, and *p*-nitrophenol were obtained from Matheson Coleman & Bell. A solution of alizarin red

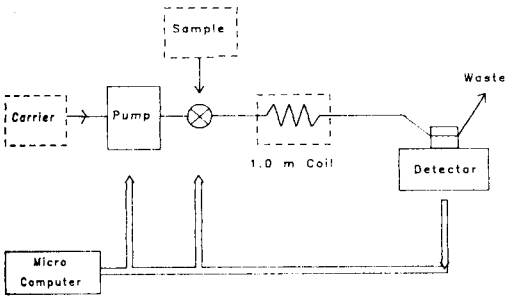

Fig. 1. Manifold for dispersion experiments. Hatched lines indicate the components immersed in the water bath.

(0.00048 M) was prepared on the day of use by adding 33.1 mg of the powder to a 200-ml volumetric flask and diluting to the mark with 0.05 M phosphate buffer. The solution was stirred until dissolution was complete. The *p*-nitrophenol stock solution (0.01 M) was prepared by adding 0.6958 g of *p*-nitrophenol to a 500-ml volumetric flask and diluting to the mark with water. The solution was stirred until dissolution was complete and then transferred to an amber bottle for storage at 4°C. On the day of use a 0.0002 M solution of *p*-nitrophenol was made by appropriate dilution. A sodium hydroxide stock solution (0.2 M) was prepared by diluting 12 ml of aqueous 50% (w/v) sodium hydroxide to 1 l with water; more dilute solutions were made from this stock solution. The sodium hydroxide solutions were standardized by titration against anhydrous potassium hydrogenphthalate with phenolphthalein as indicator.

Procedures. The dispersion behavior of a single-line manifold was investigated for a temperature range of 20—70°C at flow rates of 0.56, 1.20, and 1.88 ml min^{-1}, which were obtained with appropriate pump tubing and speed setting. Before injection, the sample solution, carrier solution, and reaction manifold were allowed to come to temperature equilibrium with the water bath.

For the experiments without reaction, a 30-μl sample of the alizarin red solution was injected into a carrier stream of phosphate buffer (0.05 M). The absorbance of the stream was monitored at 510 nm. The maximum response for the undiluted dye, H_{max} was measured by pumping a continuous stream of the dye.

For the experiments with reaction, a 30-μl sample of *p*-nitrophenol solution (0.0002 M) was injected into a carrier/reagent stream of sodium hydroxide (0.01 M) and the absorbance was monitored at 420 nm. Static experiments were also done, using three premixed solutions containing 0.0002 M *p*-nitrophenol and, respectively, 0.005 M, 0.01 M, and 0.05 M sodium hydroxide. These solutions were pumped sequentially through the manifold. The absorbance relative to water was monitored at 420 nm over the same temperature range as above, except that 15°C increments were used.

Following introduction of the sample, the output voltage of the detector was monitored and digitized with an analog-to-digital converter (ADC) and stored as ADC counts in a file on a floppy disk. The process was repeated for 5°C increments. Five replicate experiments were done for each set of experimental conditions. The files for each of the replicates were then transferred to a DEC LSI 11/23 minicomputer where the counts were converted to absorbance and plots of each peak were obtained with the aid of a two-pen plotter. A baseline correction for each plot was obtained by measuring the height of each peak by hand. For convenience, the FWHM was also measured by hand. The area of each peak was obtained by integration using Simpson's rule. In each case, the average of the five replicates was taken as the "true" value.

Accurate compensation for the slight heat loss that occurred as the solutions travelled from the thermostated vessels to the detector flow cell was attained by measuring the temperature of the stream as it entered the flow cell. For these temperature-calibration experiments only, a precision 30-kΩ thermistor (Fenwal Electronics, Framingham, MA), mounted inside a T-piece, was inserted immediately before the detector. Distilled water was then pumped through the system for the temperature range used. The resistance of the thermistor at each bath temperature and flow rate was recorded and later converted to a manifold temperature. Table 1 shows the slope, intercept and correlation coefficient for the linear relationships which related bath temperature (BT) to manifold temperature (MT) at each flow rate.

TABLE 1

Equations for temperature correction
Equation: $MT = A(BT) + B$

Flow rate (ml min^{-1})	A	B	Correlation coefficient
0.56	0.947	1.172	0.9999
1.20	0.952	1.024	0.9999
1.88	0.860	3.253	0.9997

Results and discussion

Effect of temperature on dispersion. The effect of temperature on dispersion for the system without reaction is shown in Fig. 2. The dispersion values were calculated by dividing H_{max} by H. For each of the flow rates studied, the same trend was seen; increased temperature resulted in decreased dispersion. Because no change in the total amount of dye present was expected, it was initially concluded that the change in dispersion was due to temperature. Over the temperature range 26—70°C, for the flow

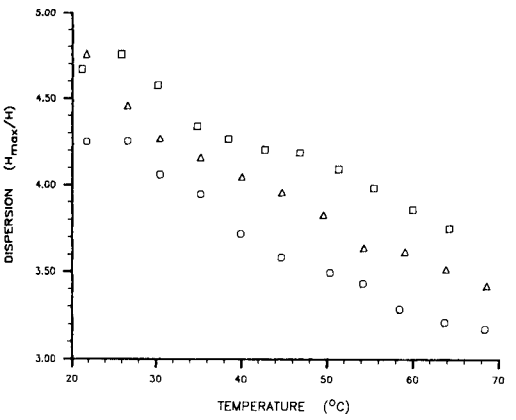

Fig. 2. Effect of temperature on dispersion without reaction. Flow rates: (○) 0.56 ml min^{-1}; (△) 1.20 ml min^{-1}; (□) 1.88 ml min^{-1}.

rates of 0.56, 1.2 and 1.88 ml min^{-1}, the dispersion, D, decreased by 24.5, 21.1 and 21.1% respectively.

Effect of temperature on peak area. To make totally sure that no change in total absorbance occurred as the dye travelled through the manifold, the effect of temperature on peak area was investigated. The horizontal lines obtained (Fig. 3A) indicated that, indeed, the peak areas did not change with temperature. The "areas" shown for the three different flow rates indicate that the integration of peak height was originally done over time, not volume. When these areas were multiplied by the appropriate flow rates they became equal within the limits of experimental error.

In the experiments with reaction, the slight positive slope below 50°C for the areas of the *p*-nitrophenol curves (Fig. 3B) indicated that the peak areas (and hence, total absorbance of product) were increased by temperature. It was thought that this effect might be due to a shift in the chemical equilibrium, rather than a reaction rate or mixing phenomenon. Therefore static experiments were done to see if product absorbance increased with temperature, irrespective of any sample dispersion effect. Because the sample would encounter a range of hydroxide concentrations in the flow injection system, a range of hydroxide concentrations was used in these confirmatory experiments. No change in absorbance with temperature was observed. Thus the change in peak area observed could not have been due to a shift in equilibrium, and was attributed to other causes. The reaction of *p*-nitrophenol with sodium hydroxide is very fast compared to the time the sample takes to traverse the manifold (ms compared to s). Thus, the most likely cause of the observed effect was one of temperature on the sample dispersion, i.e., in this flow injection system, at temperatures below 50°C, insufficient mixing occurred to facilitate complete reaction. This was corroborated by calculation of the number of tanks, N, for this system. Here N was approximately 5 for all three flow rates. This low value indicated

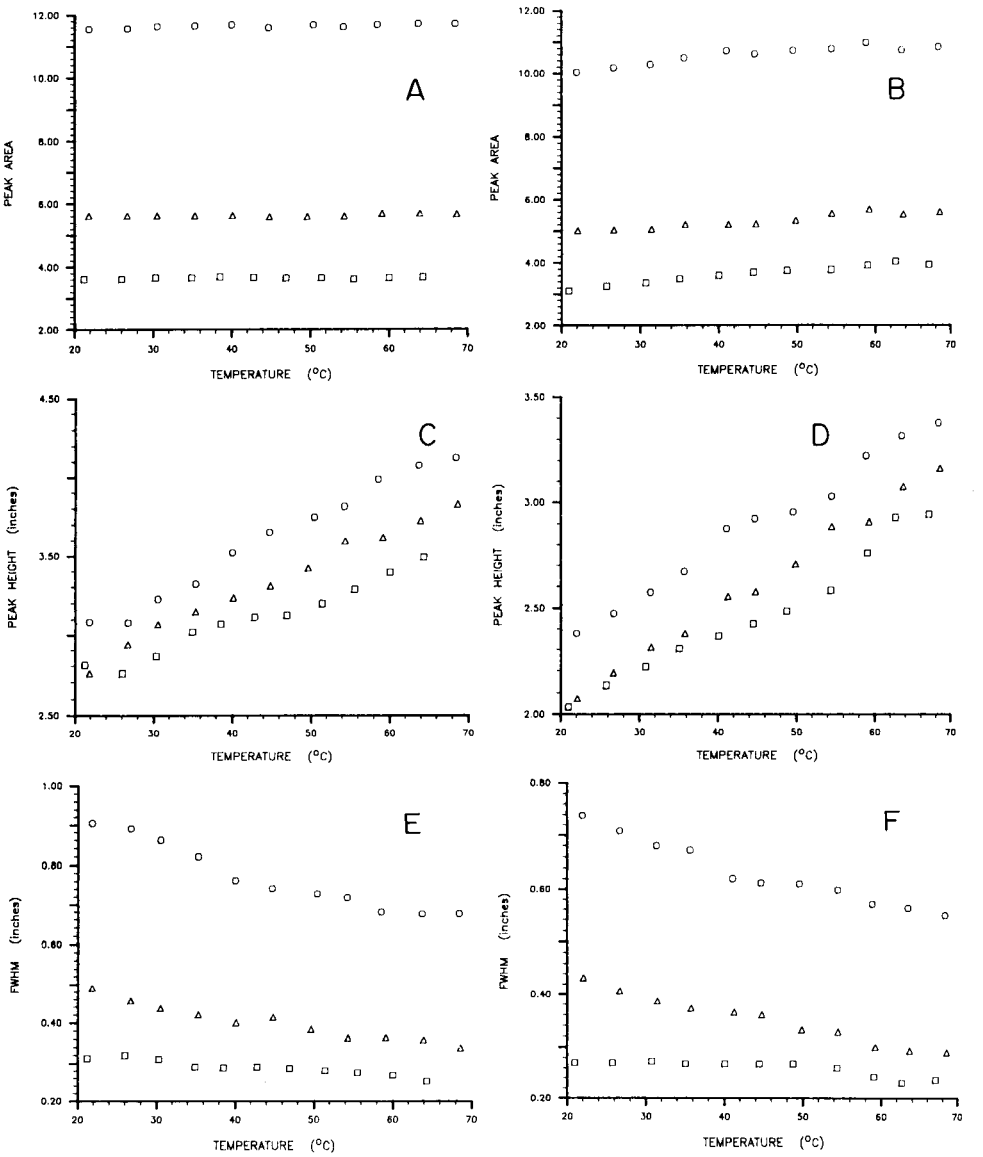

Fig. 3. Effect of temperature on: (A) peak area without reaction; (B) peak area with fast reaction; (C) peak height without reaction; (D) peak height with fast reaction; (E) FWHM without reaction; (F) FWHM with fast reaction. Flow rates: (○) 0.56 ml min^{-1}; (△) 1.20 ml min^{-1}; (□) 1.88 ml min^{-1}.

incomplete mixing. An additional set of experiments was also done using a 3.0-m coil in place of the 1.0-m coil. It was found that under these conditions the peak area did not increase with temperature. Thus incomplete mixing was confirmed as the cause of the artifact in the original data set.

The random walk theory for flow-injection systems shows that an increase in temperature increases radial diffusion and therefore enhances mixing. On

a short time scale, more complete reaction is predicted [4, 13]. The theory also predicts that a temperature-induced reaction rate enhancement will affect slower reactions more noticeably.

Effect of temperature on peak height. In the experiments with alizarin red, the peak heights increased with increased temperature and decreased flow rates (Fig. 3C). The experimental flow-rate dependence has been reported elsewhere [18] and is in accordance with trends predicted by theory [1, 4, 13]. In the experiments with reaction, the effect of temperature on peak height (Fig. 3D) was similar to that observed without reaction except that for the 1.20 ml min^{-1} flow rate, the peak height was lower than expected for temperatures below 40°C. This deviation could not be attributed to experimental error, and does not lend itself to an easy explanation.

Effect of temperature on FWHM. Figure 3E and 3F show that the peaks became narrower as the temperature increased. Also the steepness of the initial slope decreased as the flow rate increased. This was thought to be due to action of the flow rate and temperature upon the dispersion process. Theoretical predictions and interpretation given elsewhere [4, 13] indicate that decreased longitudinal dispersion may be directly attributed to an increase in radial mixing.

Conclusions

This experimental study shows that sample dispersion in flow-injection systems decreases with increasing temperature and substantiates the theoretical predictions of Betteridge et al. [4, 13]. This effect is especially important when high-precision results are required as, for example, in viscometry. Now that the magnitude of the effect is known (or, for other systems, can readily be quantified), the experimentalist is in a better position to decide whether rigorous temperature control is necessary for a particular flow-injection procedure.

For well-characterized reactions, it may be possible to "correct" a system for temperature changes, and so obtain improved repeatability without temperature control. Temperature-sensitive devices could be incorporated into manifolds routinely. Results which are independent of temperature could then be obtained by applying an appropriate multiplier to the peak height obtained, or by applying some transform to the peak shape. Such an approach could be of considerable utility for process control because a wider range of temperature conditions is more prevalent there than in the laboratory.

This work was partially supported by National Science Foundation grant No. CHE 83-20620. A. P. W. thanks The British Petroleum Company for facilitating his secondment to Michigan State University.

REFERENCES

1 J. Růžička and E. H. Hansen, Flow Injection Analysis, Wiley, New York, 1981, p. 15.
2 J. M. Reijn, W. E. van der Linden and H. Poppe, Anal. Chim. Acta, 126 (1981) 1.
3 J. T. Vanderslice, K. K. Stewart, A. G. Rosenfeld and D. J. Higgs, Talanta, 28 (1981) 11.
4 D. Betteridge, C. Z. Marczewski and A. P. Wade, Anal. Chim. Acta, 165 (1984) 227.
5 H. Wada, S. Hiroaka, A. Yuchi and G. Nakagawa, Anal. Chim. Acta, 179 (1986) 181.
6 J. F. Tyson, Anal. Chim. Acta, 179 (1986) 131.
7 J. Růžička and E. H. Hansen, Anal. Chim. Acta, 114 (1980) 19.
8 V. Ananthakrishnan, W. N. Gill and A. J. Barduhn, AIChEJ., 11 (1965) 1063.
9 D. Betteridge, W. C. Cheng, E. L. Dagless, P. David and T. B. Goad, Analyst, 108 (1983) 17.
10 C. C. Painton and H. A. Mottola, Anal. Chim. Acta, 158 (1984) 67.
11 C. C. Painton and H. A. Mottola, Anal. Chem., 53 (1981) 1713.
12 D. C. Stone and J. F. Tyson, Anal. Proc. (London), 23 (1986) 23.
13 C. D. Crowe, H. W. Levin, D. Betteridge and A. P. Wade, Anal. Chim. Acta, in press.
14 A. P. Wade, unpublished results, 1983.
15 C. J. Patton and S. R. Crouch, Anal. Chim. Acta, 179 (1986) 189.
16 B. H. Newcome and C. G. Enke, Rev. Sci. Instrum., 55 (1984) 2017.
17 E. H. Ratzlaff, Ph.D. Dissertation, Michigan State University, East Lansing, MI.
18 D. Betteridge, T. J. Sly, A. P. Wade and J. E. W. Tillman, Anal. Chem., 55 (1983) 1292.

Analytica Chimica Acta, 192 (1987) 309—313
Elsevier Science Publishers B.V., Amsterdam — Printed in The Netherlands

Short Communication

SENSITIVE DERIVATIZATION REAGENTS FOR HYDROXYL AND AMINO COMPOUNDS FOR THIN-LAYER OR HIGH-PERFORMANCE LIQUID CHROMATOGRAPHY WITH FLUORESCENCE DETECTION

YASUTO TSURUTA and KAZUYA KOHASHI*

Faculty of Pharmacy and Pharmaceutical Sciences, Fukuyama University, 985 Higashimura-cho, Fukuyama, Hiroshima, 729-02 (Japan)

(Received 29th April 1986)

Summary. Three fluorescent derivatization reagents for compounds having hydroxyl and/or amino groups are described. 4-(2-Phthalimidyl)benzoyl chloride, 3-(2-phthalimidyl)benzoyl chloride and 3-(2-phthalimidyl)-4-methoxybenzoyl chloride, prepared from the corresponding phthalimidylbenzoic acid, were stable at room temperature and condensed quantitatively with alcohols, amines and amino acids in the presence of alkali under mild conditions to give strongly fluorescent derivatives. The derivatives were separated by thin-layer and high-performance liquid chromatography.

Benzoyl chloride, 4-nitrobenzoyl chloride and 3,5-dinitrobenzoyl chloride have been widely used for derivatization of alcohols and amines, and applied in quantitative liquid chromatography with u.v. detection [1, 2]. However, these conventional reagents were considered to lack either stability or sensitivity in certain instances, and have been replaced by highly sensitive fluorescent derivatization reagents [3].

Some phthalimidylbenzoyl chlorides (phibyl-Cl: **I**, **II** and **III**) were found to be stable at room temperature and to be rapid and quantitative fluorescent derivatizing agents for alcohols, amines and amino acids. The present communication deals with the preparation of these three reagents, having both a fluorophore and a benzoyl chloride group, and their applicability to labelling of hydroxyl and amino compounds for thin-layer chromatography (t.l.c.) and high-performance liquid chromatography (h.p.l.c.) with fluorescence detection.

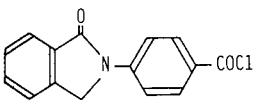

I

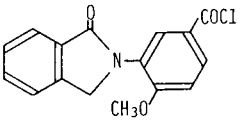

III

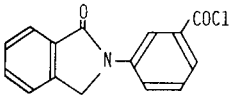

II

0003-2670/87/$03.50

Experimental

Synthesis of 4-(2-phthalimidyl)benzoyl chloride (I). *o*-Phthalaldehyde (1.34 g, 10 mmol) in diethyl ether (50 ml) and 4-aminobenzoic acid (1.37 g, 10 mmol) in diethyl ether (150 ml) were mixed. After overnight stirring at room temperature, the precipitate of 4-(2-phthalimidyl)benzoic acid was filtered off and dried. To the suspension of 4-(2-phthalimidyl)benzoic acid in chloroform (100 ml) was added thionyl chloride (6 ml), and the mixture was refluxed for 1 h. After evaporation of the solvent, the resulting residue was washed twice with chloroform (10 ml) and recrystallized twice from pure benzene to give **I** (0.8 g) as fine colorless needles. [M.p. > 230°C. Calc. for $C_{15}H_{10}NO_2Cl$: 66.4% C, 3.7% H, 5.2% N; found: 66.7% C, 3.8% H, 5.2% N. M.s. *m/z*, 271(M^+).]

Syntheses of 3-(2-phthalimidyl)benzoyl chloride (II) and 3-(2-phthalimidyl)-4-methoxybenzoyl chloride (III). The starting materials were 3-aminobenzoic acid for **II** and 3-amino-4-methoxybenzoic acid for **III**; the procedures were as for **I**. The crude products were recrystallized from benzene. Compound **II** (1.0 g) was obtained as fine colorless needles [m.p. 176—177.5°C. Calc. for $C_{15}H_{10}NO_2Cl$: 66.4% C, 3.7% H, 5.2% N; found: 66.5% C, 3.7% H, 5.2% N. M.s. *m/z*: 271(M^+)]. Compound **III** (1.2 g) was also obtained as fine colorless needles [m.p. 196.5—197.5°C sub. Calc. for $C_{16}H_{12}NO_3Cl$: 63.8% C, 4.0% H, 4.7% N, found: 63.9% C, 4.1% H, 4.7% N. M.s. *m/z*: 301(M^+)].

Chemicals and solutions. All chemicals were of analytical-reagent grade, unless otherwise stated. Solvents were purified by distillation prior to use. Compound **I, II** or **III** was dissolved in acetone to give a 5 mM reagent solution. For the test solutions, amino acids were dissolved in 0.01 M hydrochloric acid (except for tyrosine and cysteine in 0.05 M sodium hydroxide) and alcohols and steroids were dissolved in acetone.

Derivatization procedure. To a test solution (0.1—50 mM, 10 μl), sodium hydroxide (0.1 M, 20 μl) or dimethylformamide (DMF, 20 μl) and reagent solutions (100 μl) were added, and the mixture was allowed to stand at 25, 50 or 80°C for 30 min.

Thin-layer chromatography. An aliquot of the resulting mixture was applied to a silica gel plate (Merck) and developed at ca. 25°C with the appropriate solvent system: (A) benzene/acetone (9.5:0.5, v/v) for alcohols; (B) benzene/acetone (8.5.1.5, v/v) for amines; and (C) n-propanol/ammonia (8:2 v/v) or (D) n-butanol/acetic acid/ammonia (9.3:0.5:0.2 v/v) for amino acid. Visual detection of the fluorescent fractions on a silica gel plate was achieved with a Mineralight lamp (UVGL-15, Ultra-violet Prod., CA).

High-performance liquid chromatography. The apparatus used was a Bip-1 high-performance liquid chromatograph system (Jasco) equipped with a VL-614 injector (10-μl loop, Jasco) and a F-1000 fluorescence detector (Hitachi). The Finepak ODS C_{18} column (Jasco, 15 × 0.4 cm i.d.) was used under ambient conditions.

Results and discussion

o-Phthalaldehyde reacts with aromatic primary amines to give phthalimidines, which are highly fluorescent [4]. 4-(2-Phthalimidyl)benzoic acid, which is one of the most fluorescent phthalimidines, was obtained from the reaction of *o*-phthalaldehyde with 4-aminobenzoic acid, and was easily converted to I by treatment with thionyl chloride. The isomer II, and methoxy derivative III were prepared from 3-aminobenzoic acid and 3-amino-4-methoxybenzoic acid, respectively, in a similar manner. The three compounds were stable at room temperature for more than 6 months if kept dry. Condensation of hydroxyl or amino compounds with the reagents to form the benzoyl ester or benazmide was in the presence of alkali, and the resulting derivative was separated from the reagent on a t.l.c. plate. The fluorescence was detected visually under u.v. radiation.

The reactitivities of the phibyl-Cl reagents were examined for the following compounds; methanol, ethanol, n-propanol, iso-propanol, n-butanol, t-butanol, n-pentanol, n-hexanol, n-octanol, cyclohexanol, menthol, ethylene glycol and glycerine; cholesterol, androsterone, deoxycorticosterone and testosterone; n-propanolamine, iso-propylamine, n-butylamine, dimethylamine, piperidine and aniline; alanine, arginine, citrulline, cysteine, glutamic acid, glycine, histidine, homoserine, isoleucine, leucine, lysine, methionine, ornithine, phenylalanine, proline, serine, threonine, tryptophan, tyrosine and valine.

The phibyl-Cl compounds react quantitatively above 50°C with the primary, secondary, alicyclic and, importantly, tertiary alcohols to provide the corresponding esters in the presence of DMF. Condensation of polyalcohols such as ethylene glycol and glycerine with III showed one fluorescent spot, but with I and II two or three fluorescent products were separated on the t.l.c. plate with solvent system. The hydroxysteroids were esterified with I in the presence of sodium hydroxide at 50°C, and showed a weakly fluorescent spot.

Reactions of primary and secondary amines and amino acids with the phibyl-Cl reagents at 25°C in the presence of sodium hydroxide gave the corresponding benzamides. Condensation of the amines and the amino acids having both hydroxyl and amino groups with a phibyl-Cl reagent gave one fluorescent product with solvent system B and C, respectively.

The derivatives of ethanol, n-butylamine, piperidine and lysine were extracted with methanol from the fluorescent spots on the t.l.c. plate, and the fluorescent spectra were measured in methanol/water (2:1). The fluorescence maxima of the compounds are listed in Table 1. The fluorescence intensities in the methanol/water mixture were ca. 1.5 times higher than those in methanol.

The separation of fluorescent I-labelled amino acids was examined by two-dimensional t.l.c. A mixture of 19 amino acids (2 nmol each) was treated with I and 40 μl of the reaction mixture was spotted onto a silica gel plate (10 × 10 cm). The developing solvents C and D were used for the first and

TABLE 1

Fluorescence maxima of some compounds labelled with the phibyl-Cl reagents I—III

Compound	Fluorescence maxima (nm)					
	I		II		III	
	λ_{ex}	λ_{em}	λ_{ex}	λ_{em}	λ_{ex}	λ_{em}
Ethanol	342	412	312	424	292	454
n-Butylamine	320	425	308	432	297	454
Piperidine	298	436	291	430	280	440
Lysine	296	412	291	424	280	440

the second developments, respectively. The 19 amino acid derivatives could be separated successfully (Fig. 1). Reagents II and III gave similar results.

A mixture of four amino acids (glycine, proline, phenylalanine and lysine) treated with I was also separated by h.p.l.c., eluting with a gradient solvent system of methanol/0.0025 M phosphate buffer (pH 7.4) with a linear gradient from 25 to 70% methanol over 6 min, followed by 70% methanol for 7 min, at a flow rate of 1 ml min^{-1}. Retention times (min) were: blank (4.0, 11.2), glycine (4.5), proline (4.9), phenylalanine (6.7) and lysine (7.0). Highly sensitive detection was achieved and the peak heights were correlated to the concentrations of amino acids at least over the range 10 pmol to 1 nmol per injection. The detection limit (signal/noise = 2) for

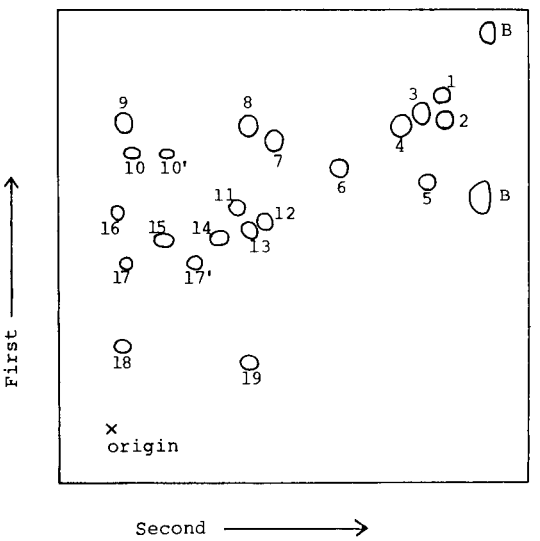

Fig. 1. Two-dimensional t.l.c. separation of amino acids derivatized with I. Spots: (1) Ile, (2) Leu, (3) Val, (4) Phe, (5) Tyr, (6) Ala, (7) Lys, (8) Orn, (9) Met, (10), (10') Trp, (11) Pro, (12) Gly, (13) Thr, (14) Ser, (15) Cit, (16) His, (17), (17') Cys, (18) Arg, (19) Glu, (B) Blank. Solvent systems: C for first direction; D for second direction.

lysine with I was 10 fmol per injection. The fluorescence intensity (peak height) of the lysine derivative with I, obtained by h.p.l.c., was compared with those of the lysine derivatives of *o*-phthalaldehyde (OPA) [5] fluorescamine (FLA) [6] and dansyl chloride (DNS) [7] under the same h.p.l.c. conditions as described above. Each reaction mixture (50 pmol lysine in 10 μl) was injected and detected at λ_{ex} = 340 nm and λ_{em} = 455 nm for OPA-lysine, 390 and 475 nm for FLA-lysine, and 350 and 530 nm for DNS-lysine. The ratio of the peak heights found was 100 (reagent I):21 (OPA):7(FLA):5(DNS).

The new reagents are also satisfactory with respect to stability. Acetone solutions were stable for at least 3 days if kept in a closed vial, and the derivatives were also stable for at least a week.

The application of the phibyl-Cl reagents to the determination of physiologically important substances in biological fluids is being studied.

REFERENCES

1 J. F. Lawrence and R. W. Frei, Chemical Derivatization in Liquid Chromatography, Elsevier, Amsterdam, 1976, p. 151.
2 J. Gasparič and J. Churáček, Paper and Thin-Layer Chromatography, Horwood, Chichester, 1978, p. 98.
3 K. Blau and G. S. King (Ed.), Handbook of Derivatives for Chromatography, Heyden, London, 1977, p. 346.
4 T. Amano, T. Sakano and S. Mizukami, Yakugaku Zasshi, 85 (1965) 1042.
5 J. R. Benson and P. E. Hare, Proc. Nat. Acad. Sci. U.S.A., 72 (1975) 619.
6 N. Nakai, C. Y. Lai and B. L. Horecker, Anal. Biochem., 58 (1974) 563.
7 C. Gros and B. Labouesse, Eur. J. Biochem., 7 (1969) 463.

Analytica Chimica Acta, 192 (1987) 315—319
Elsevier Science Publishers B.V., Amsterdam — Printed in The Netherlands

Short Communication

POTENTIOMETRIC DETERMINATION OF ENZYME ACTIVITIES WITH SLOPES COMPUTED WITH THE SAVITZKY-GOLAY DIGITAL FILTER

ORVILLE W. BUNKER III and MARK A. ARNOLD*
Department of Chemistry, University of Iowa, Iowa City, Iowa 52242 (U.S.A.)
(Received 24th June 1986)

Summary. The Savitzky-Golay least-squares differentiation digital filter is applied to the processing of potential/time response curves for quantifying enzyme activity with potentiometric membrane electrodes as detectors. The use of this filter avoids operator bias and provides a simple and rapid procedure for data processing.

Enzyme activity determinations are important in many areas of bioanalytical chemistry such as in the development of biosensors [1—3], tubular reactors [3], and enzyme-based homogeneous and heterogeneous immunoassays [4—6]. Potentiometric membrane electrodes are attractive detectors for enzymatic reactions because they are inexpensive, simple to operate, insensitive to moderate sample turbidity, and widely applicable. The rate of formation or consumption of a detectable species can be directly followed and the rate of potential change can be related to the enzyme activity or concentration [7—9].

The purpose of this communication is to report an evaluation of the well known Savitzky-Golay least-squares digital filter [10—12] for processing potential/time data for enzyme-catalyzed reactions. This filter has been successfully used with other detectors to process kinetic data for enzyme activity determinations [13] and it is preferred because of its rapid response and low distortion. Application of this filter to potentiometric data provides a rapid, simple, low-bias method for quantifying enzyme activities.

Experimental

Apparatus and materials. Potentials were measured with an Altex 71 pH/mV meter in conjunction with a Sargent-Welch XKR strip-chart recorder. The serial port of the meter was connected directly to an IBM System 9000 laboratory computer. An Orion model 95-12 ammonia gas-sensing probe was used for all ammonia measurements. A 0.02-μm microporous teflon membrane was used for the construction of these probes as described previously [14]. An internal electrolyte solution composed of 0.17 M sodium chloride and 0.03 M ammonium chloride was used to avoid osmotic effects [15]. All measurements were made in cells controlled at 25°C with a Fisher model 80 water bath.

0003-2670/87/$03.50

Distilled water was further treated with a Milli-Q water purification unit. Type I reagent-grade water was used to prepare all solutions. Urea, adenosine, urease (Lot 121F-7190), adenosine deaminase (Lot 81F-7190), and tris(hydroxymethyl)aminomethane (Tris) were from Sigma Chemical Co. All other reagents were reagent-grade quality.

Enzyme assays. Urease and adenosine deaminase were assayed by similar procedures. The sensing tip of the ammonia probe was immersed in 10 ml of a stirred 0.1 M Tris-HCl buffer, pH 7.5, and a fixed amount of the appropriate substrate was added. Final urea and adenosine concentrations were 50 and 4.8 mM for the urease and adenosine deaminase assays, respectively. After the addition of substrate, a steady-state baseline potential was attained and then a standard amount of the enzyme of interest was added. Ammonia produced by the enzymatic reaction was monitored continuously with either the strip-chart recorder or computer. Enzyme concentrations were calculated by using molecular weights of 480,000 and 120,000 daltons for urea and adenosine deaminase, respectively [16].

Data collection and processing. The serial printer output of the Altex 71 pH/mV meter was connected directly to a serial input port on the IBM System 9000 computer. This meter outputs data in the form of serial ASCII code at a baud rate of 300. The timed output feature of the meter was used to control the data acquisition rate with a maximum rate of 0.25 Hz. Software to acquire, manipulate, display, and store the potential-time data was written in Pascal and the IBM System 9000 Pascal version 1.2 compiler was used.

For the Savitzky-Golay filter, the size of the data window was variable from 5 to 999 and equations provided by Madden [12] were used to calculate the weighting coefficients and the normalization factors for the various sizes of data windows. Because of the smooth nature of potential/time response curves, a quadratic filter was used [10].

Results and discussion

Guilbault et al. [17] derived the following expression that relates the measured electrode potential rate (dE/dt) to the enzyme activity or concentration:

$$dE/dt = (S/[P])(d[P]/dt) = (S/[P])(k_3[E][s]/(K_m + [s])) \quad (1)$$

where S is the electrode response factor (ideally 0.059 at 25°C and $n = 1$) [P] is the concentration measurable product, k_3 is the forward rate constant for the dissociation of the enzyme/substrate complex, [s] is the concentration of substrate, and K_m is the Michaelis constant for the substrate. The substrate concentration is kept high with respect to K_m so that the expression is simplified to

$$[E] = ([P]/k_3 S)\,(dE/dt) \quad (2)$$

The initial slope of the potential/time curve is then directly proportional to the enzyme concentration.

The dynamic response of gas-sensing electrodes, especially at low analyte concentrations, is considerably slower than that of other classes of potentiometric membrane electrodes. The result is a sigmoidal potential/time curve in response to enzymatic reactions. Figure 1 shows a typical electrode response curve for the generation of ammonia from urea by the action of urease. The rate of potential change at the inflection point is commonly used to quantify reaction rate [7—9]. Use of the Savitzky-Golay digital filter to compute the slope should reduce the bias often associated with manual methods. Figure 2 shows the first derivative of the potential/time curve in Fig. 1. The maximum rate of change which corresponds to the inflection point is used to quantify enzyme activity. Figure 3 compares data obtained manually and with the digital filter. The discrepancy between the curves at higher rates probably results from lag in the response of strip-chart recorder and unavoidable bias in reading slopes from recorder tracings. The effect of the size of the data window on the quality of the first derivative curve was examined. Figure 2 shows the effect of using 7 and 31 points in the data window to obtain the first derivative of the potential/time curve in Fig. 1. A smoother first-derivative curve is obtained when the larger data window is used. Improvements in quality of the derivative curve are ultimately limited by the distortion that results when large data windows are used. The present studies indicate that acceptable first-derivative curves are obtained when approximately 25% of the available points are included in the data window.

It was observed (Fig. 4) that the position of the maximum rate of change of potential shifts toward lower potentials (higher product concentrations)

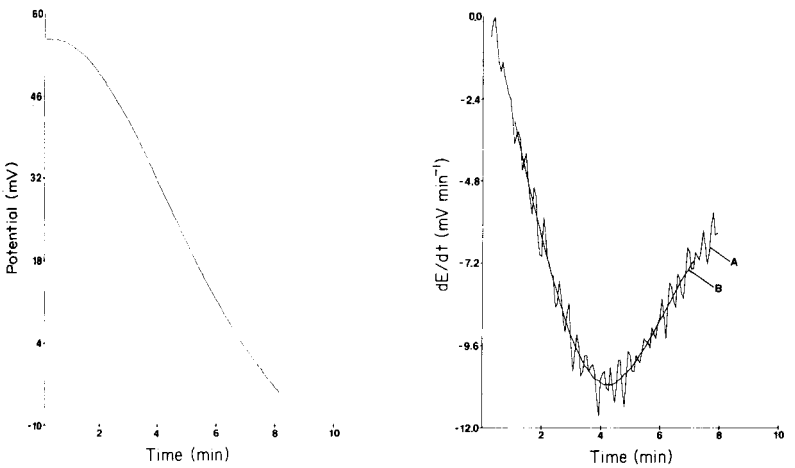

Fig. 1. Potential/time curve for deamination of urea by urease as measured by an ammonia gas-sensing probe.

Fig. 2. First-derivative curve of potential/time data shown in Fig. 1, with 7 (A) and 31 (B) points in the data window.

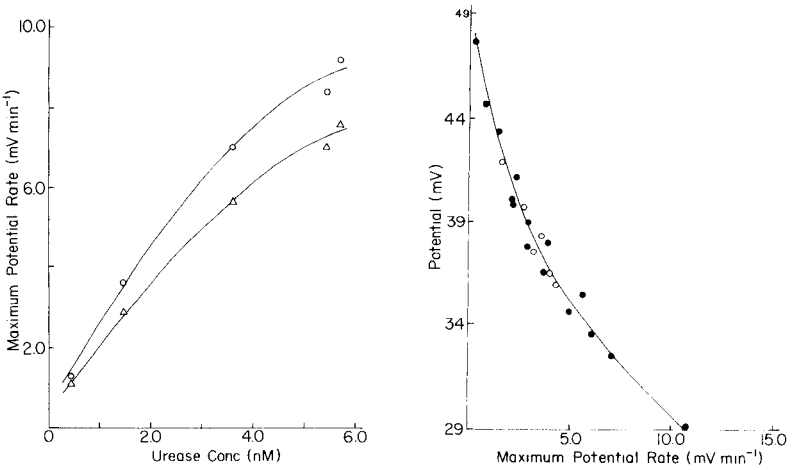

Fig. 3. Comparison of urease calibration curves with manual (△) and digital (○) methods for evaluating the maximum rate of potential change.

Fig. 4. Relationship between maximum rate of potential change and electrode potential for a series of adenosine deaminase (○) and urease (●) activities.

as the rate of the reaction increases. Based on Eqn. 2, it was expected that the changing product concentration at the measurement point would produce nonlinear calibration plots. The digital filter was used to compute rates at the same potential for different response curves, with the expectation that this might improve the linearity of response curves. As observed in Fig. 5, rate measurements at fixed potentials provide only a moderate improvement

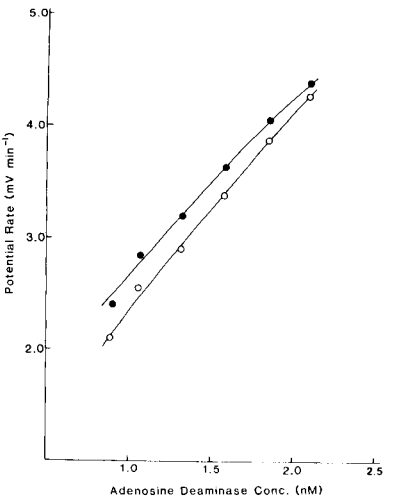

Fig. 5. Calibration curves for adenosine deaminase using the maximum rate (○) and the rate at 30 mV (●).

in linearity. Similar results were obtained for urease. Slow, non-Nernstian electrode response is the most probable cause of this nonlinear response.

We acknowledge the assistance of Gary W. Small with this project. Acknowledgement is also made to the donors of The Petroleum Research Fund, administered by the American Chemical Society, for support of this research.

REFERENCES

1 M. A. Arnold, Am. Lab., 15 (1983) 34.
2 M. A. Arnold and G. A. Rechnitz, Anal. Chem., 54 (1982) 777.
3 P. W. Carr and L. D. Bowers, Immobilized Enzymes in Analytical and Clinical Chemistry, John Wiley, New York, 1980.
4 M. E. Meyerhoff and G. A. Rechnitz, Methods Enzymol., 70 (1980) 439.
5 C. R. Gebauer and G. A. Rechnitz, Anal. Biochem., 124 (1982) 338.
6 S. B. Brontman and M. E. Meyerhoff, Anal. Chim. Acta, 162 (1984) 363.
7 P. D'Orazio, M. E. Meyerhoff and G. A. Rechnitz, Anal. Chem., 50 (1978) 1531.
8 M. A. Arnold and G. A. Rechnitz, Anal. Chem., 53 (1981) 515.
9 K. Cammann, Fresenius Z. Anal. Chem., 287 (1977) 1.
10 A. Savitzky and M. J. E. Golay, Anal. Chem., 36 (1964) 1627.
11 J. Steinier, Y. Termonia and J. Deltour, Anal. Chem., 44 (1972) 1906.
12 H. H. Madden, Anal. Chem., 50 (1978) 1383.
13 J. A. Fulton, T. D. Schlabach, J. E. Kerl, E. Clifford and A. R. Miller, J. Chromatogr., 175 (1979) 269.
14 M. A. Arnold, Anal. Chim. Acta, 154 (1983) 33.
15 M. A. Arnold and G. A. Rechnitz, Anal. Chim. Acta, 158 (1984) 209.
16 T. E. Barman, Enzyme Handbook, Springer-Verlag, New York, 1969.
17 G. G. Guilbault, R. K. Smith and J. G. Montalvo, Jr., Anal. Chem., 41 (1969) 600.

Analytica Chimica Acta, 192 (1987) 321—326
Elsevier Science Publishers B.V., Amsterdam — Printed in The Netherlands

Short Communication

ION-CURRENT SIGNAL OPTIMIZATION FOR LIPID MEMBRANE-BASED BIOSENSORS

U. J. KRULL

Chemical Sensors Group, Department of Chemistry, Erindale College, University of Toronto, Mississauga Road, Mississauga, Ontario L5L 1C6 (Canada)

(Received 30th June 1986)

Summary. The conductivities of bilayer lipid membranes are greatly affected by their lipid composition. Thus it is possible to prepare membranes having substantially different background or residual ion currents as observed when a direct voltage is applied across the membrane. Physical perturbation of the membrane by phloretin, valinomycin or receptor molecules provides current increases, which can be maximized by proper choice of residual current and membrane lipid chemistry. A compromise between provision of an efficient ion current pathway and minimization of residual current is necessary to optimize signal-to-noise ratio.

Bilayer lipid membranes (BLM's) have great potential for the development of sensitive and selective biochemical transducers [1]. Their operation is based on the transmembrane ion-current modulation caused by selective interaction of analyte with a membrane-embedded receptor. The perturbation of the physical-chemical properties of a membrane by these selective receptor interactions can detect biochemical stimulant concentrations at sub-picomolar levels, as derived from transmembrane ion current alterations. However, the magnitude of electroanalytical response of BLM's can vary greatly for any one selective interaction, and an investigation of the physical mechanisms responsible for signal optimization is necessary.

The simplest BLM experiment involves a small d.c. voltage across the membrane to act as a potential-energy driving force for ions. The ion current, i.e., the analytical signal, is actually measured as the relative change of transmembrane current with respect to a steady leakage or residual ion flux. This residual current provides the most significant contribution to the background noise of the measurement system and is governed by the same physical membrane parameters that are responsible for the analyte signal. This implies that any modification of the residual current should be reflected as a change in magnitude of analyte signal. Recent experimental results and calculations have shown that the dipolar potential and molecular packing/fluidity are the two predominant factors controlling ion current in neutral lipid membrane systems [2, 3]. It is possible to vary the lipid content to provide BLM configurations of differing physical character to ascertain how

0003-2670/87/$03.50

the latter parameters can influence the signal-to-noise relationship.

Most instruments attempt to suppress effects of background signals by either reducing the source of the interference (e.g., pulse polarography) or by differential comparison (e.g., double-beam spectrophotometer). Unfortunately, the latter approach is difficult to achieve with BLM's because well-matched membranes are almost impossible to manufacture at present [1], and reduction of residual ion current must be achieved by manipulation of membrane physical parameters which could also significantly reduce the analyte signal.

This work evaluates the electroanalytical response of BLM's of widely varying residual currents to ascertain the existence of an optimum signal-to-noise relationship. Membrane perturbations were achieved by use of the dipolar potential-modifying agent phloretin [4] and the hydrophobic ion-complexing agent valinomycin [5], so that the significantly increased complexity of receptor-induced BLM ion-current response could be avoided.

Experimental

The electrochemical cell consisted of two identical perspex blocks separated by a teflon sheet (0.1 mm thick) containing a circular aperture (1-mm diameter) used for BLM support. An external d.c. potential (+10 mV) was applied across the membrane between two Ag/AgCl reference electrodes (Orion Research, Cambridge, MA). The external circuitry consisted of a power supply and a digital electrometer (Model 616B, Keithley Instruments Cleveland, OH). The solution cell and sensitive electronic equipment were isolated in a grounded Faraday cage.

Each mixture used for BLM formation consisted of 20 mg of lyophilized egg phosphatidyl choline (Avanti Biochemicals, Birmingham, AL) and 20 mg of one of the following pure steroids; 5-cholesten-3β-ol, 5α-cholestan-3β,5α,6β-triol, 5α-cholestan-5α,6α-epoxy-3β-ol, and 5α-cholestan-3-one (Research Plus, Bayonne, NJ) in 1 ml of dry n-decane. These mixtures were used directly for BLM formation. Oxidized phosphatidyl choline/cholesterol mixtures were prepared by irradiation of the initial mixture in decane at 254 nm with a portable u.v. lamp (Mineralight UV-511, UV Products, San Gabriel, CA) at room temperature in air for times ranging from 1 to 30 min [3]. A capillary gas chromatographic assay was used to characterize the subsequent chemical composition [6].

All lipid mixtures were introduced by means of a fine sable hair brush into the teflon-sheet aperture between the two solution compartments containing 0.1 M potassium chloride. Membrane formation occurred spontaneously and was monitored by surface optical reflectivity and electrical properties. Each stirred solution compartment contained 5 ml of aqueous electrolyte adjusted to pH 5. The transmembrane ion current was measured after a 10-min stabilization period. This was followed by the addition of the electroactive probe molecule, phloretin or valinomycin (Sigma), as a methanolic solution from a variable-volume micropipette. The methanol concentra-

tions in the aqueous electrolyte never exceeded 1% by volume. All experiments were done at 21 ± 1°C.

Results and discussion

The variability of BLM residual ion current with lipid composition has been reported [2], and attempts have been made to design membranes with the desired characteristics [2, 3]. The ion current through BLM's can be described by two predominant physical parameters. The development of the membrane-surface dipolar potential depends on the magnitude of the molecular dipole, the density and the alignment of the lipid. The dipolar potential will be hundreds of millivolts in magnitude, and will pre-concentrate cations at the membrane/solution interface [7]. These ions must then traverse a large rate-determining energy barrier in the membrane interior. This barrier apparently originates from intermolecular interactions which provide transient physical interstitial spaces for ion residence within the hydrophobic acyl chain interior of BLM's. These two features combine to provide the final ion conductivity of the lipid matrix. The dipolar and energy-barrier characteristics for potassium ion permeation through various BLM's are summarized in Table 1; it is clearly possible to design membranes with substantially different residual currents by adjusting the chemistry of two-component lipid systems.

A theoretical treatment indicates that the relative residual current, i, can be approximated from the equation: $i = \exp[\phi] \exp[-E_a]$, where ϕ is the relative dipolar potential and E_a is the relative Arrhenius energy barrier (assuming that all other sources of energy barrier are controlled) [7, 8].

It is also possible to design BLM's of differing chemistry by starting with a prepared lipid mixture in bulk hydrocarbon solution, and oxidizing the phospholipid and steroid components to varying extents [2, 3]. The chemistry of such mixtures is significantly more complicated than that of the two-component mixtures listed in Table 1, but a large range of residual currents can be easily achieved [2]. Furthermore, the lipid content of these complicated mixtures can be quantified by chromatography [6], which is easily applied when information on speciation is required. The range of residual ion currents observed for BLM's prepared from oxidized lipid mixtures indicates that it is possible to produce non-conductive membranes, presumably with very large internal energy barriers, and very conductive membranes presumably of high dipolar potential and low internal energy barriers. The effect of this physical variability on analyte signals is shown in Figs. 1 and 2. In Fig. 1, maximum response occurs for a residual current of ca. 0.5×10^{-11} A, whereas in Fig. 2, maximum response with the highest concentration of phloretin used is at a residual current of 1×10^{-11} A.

The ability of valinomycin to shuttle ions across BLM's [5] is greatly influenced by intermolecular interactions in the hydrophobic region of the membrane. The observation of a maximum in Fig. 1, indicates the presence of competitive processes, which can be conceptualized as the result of two

TABLE 1

Control of residual ion current by chemical modification

Steroid	Arrhenius energy barrier[a] (eV)	Monolayer dipolar potential[b] (mV)	Residual ion current (10^{-10} A)
5-Cholestan-3β-ol	1.18 ± 0.03	490 ± 15	1.5 ± 0.3
5α-Cholestan-3β,5α,6β-triol	0.49 ± 0.16	200 ± 20	2.1 ± 0.2
5α-Cholestan-5α,6α-epoxy-3β-ol	0.35 ± 0.04	550 ± 25	3.3 ± 0.4
5α-Cholestan-3-one	0.19 ± 0.02	650 ± 20	4.1 ± 0.4

[a]Data from [4]. [b]Data from [6].

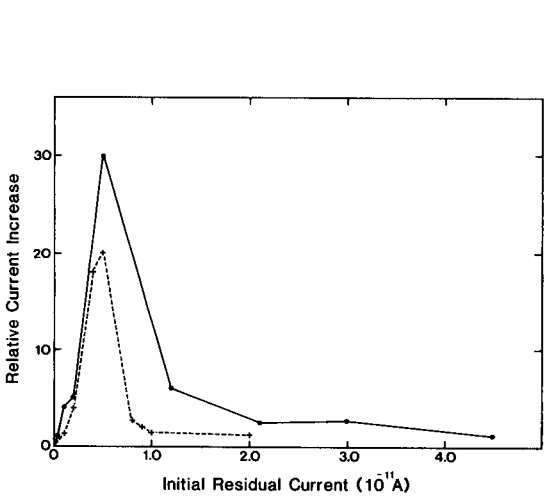

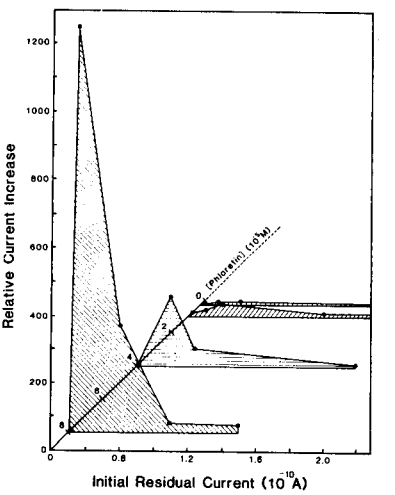

Fig. 1. Relative response to K^+ with valinomycin as a function of residual ion current. Valinomycin concentration in the aqueous electrolyte: (+) 1.6 X 10^{-7} M; (●) 2.5 X 10^{-7} M.

Fig. 2. Relative current changes induced in BLM by various concentrations of phloretin at varying residual ion currents.

distinct cases. First, at very low residual currents, there is little background noise, and it is expected that the signal-to-noise relationship will be optimized. However, the lack of significant residual current indicates that the conductive mechanism within the membrane is blocked so that membrane perturbation cannot produce an analyte signal. Second, at relatively high residual current values, the background interference is substantial. Membrane perturbation results in current changes which are insignificant in contrast to the large background ion flux previously established.

Therefore, a lipid membrane-based transducer should operate to provide an ion-conductive mechanism sufficient for unhindered ion permeability

during membrane perturbation, while maintaining a minimal residual ion current. Table 2 summarizes the essential components of the lipid membrane responsible for signal-to-noise optimization. The oxidation procedure provides alterations of the A and B rings of the steroids, and hydroperoxide formation in the acyl chain region of the phospholipid [6].

The results derived from the dipolar probe, phloretin, are shown in Fig. 2. Phloretin has been described as a dipolar probe which locates in the lipid membrane head-group zone to reduce the dipolar potential energy barrier to ion current [4]. The data in Fig. 2 again indicate that a maximum in total current change relative to residual current magnitude is present over a wide range of probe concentrations. Surprisingly, the residual current corresponding to the maximum response is almost identical to that for valinomycin at high phloretin concentration, even though the mechanism of phloretin operation has been accepted as totally different from that of valinomycin. This raises some doubt as to the validity of the previous descriptions of phloretin function.

It would appear likely that phloretin can cause significant acyl chain perturbation in the membrane, which is reflected by the position of the response maxima of Fig. 2 with respect to those shown for valinomycin, and furthermore by the non-linear enhancement of the response maxima with phloretin concentration. This view of phloretin action is consistent with previous work [4] which indicated that phloretin could affect dipolar potential as well as the BLM Arrhenius energy barrier. This is particularly significant in light of recent findings that the Arrhenius energy barrier for a BLM is almost independent of the relative magnitude of the dipolar potential [7]. This interpretation of phloretin action on BLM is consistent with that of valinomycin, and supports the proposed mechanism of signal-to-noise optimization.

TABLE 2

Major lipid constituents of oxidized BLM which provided signal-to-noise optimization

Lipid identification	Relative composition (%)	Lipid identification		Relative composition (%)
5-Cholesten-3β,7α-diol	0.5	Phospholipid	16:0	30.1
5α-Cholestan-5α,6α-epoxy-3β-ol	0.9	acyl chains	18:2	15.9
5-Cholesten-3β-ol	95.1		18:1	33.8
5α-Cholestan-3β,5α,6β-triol	0.8		18:0	2.2
			20:4	16.0
			22:6	0.5
Cumulative composition[a]	97.3[b]			98.5

[a]Minor constituents are not listed. [b]Steroids.

Conclusions

It is possible to modify bilayer membranes chemically to achieve differing levels of residual ion current. The physical interactions of the lipids are determined by their electrostatic, hydrogen and hydrophobic bonding. A survey of the chemical structures used in this work does not provide an obvious method for correlating the electrostatic and steric membrane effects with lipid chemistry. Future work will concentrate on developing techniques to predict complicated lipid interactions within membranes, and then tailor lipid molecules to provide predefined membrane properties. At present, this work serves as a basis for choosing lipid mixtures to produce lipid matrices which remain fluid to provide the transient interstitial spaces required for transmembrane ion migration, but adjust dipolar and packing/fluidity parameters to minimize the residual current.

The author is grateful to the Natural Sciences and Engineering Research Council of Canada for support of this work, and to M. Thompson for many useful discussions.

REFERENCES

1 U. J. Krull and M. Thompson, IEEE-Electron Devices, 32 (1985) 1180.
2 U. J. Krull, M. Thompson, E. T. Vandenberg and H. E. Wong, Anal. Chim. Acta, 174 (1985) 83.
3 U. J. Krull, M. Thompson, B. Winsborrow and H. E. Wong, Anal. Chim. Acta, 174 (1985) 95.
4 M. Thompson, U. J. Krull, L. I. Bendell-Young, I. Lundstrom and C. Nylander, Anal. Chim. Acta, 173 (1985) 129.
5 M. Thompson and U. J. Krull, Anal. Chim. Acta, 141 (1982) 33.
6 U. J. Krull, M. Thompson and A. Arya, Talanta, 31 (1984) 489.
7 U. J. Krull, M. Thompson and H. E. Wong, Bioelectrochem. Bioenerg., 15 (1986) 371.
8 U. J. Krull, Extended Abstracts, The Electrochemical Society, Boston, May 4—9, 1986, p. 860.

Analytica Chimica Acta, 192 (1987) 327—331
Elsevier Science Publishers B.V., Amsterdam — Printed in The Netherlands

Short Communication

SIMULTANEOUS DETERMINATION OF MULTIPLE COMPONENTS IN FLOW-INJECTION SYSTEMS BY SQUARE-WAVE AMPEROMETRY

T. P. TOUGAS* and C. Y. YUAN
Department of Chemistry, University of Lowell, Lowell, Massachusetts 01854 (U.S.A.)
(Received 14th July 1986)

Summary. Two or more components can be determined in a single sample by using a flow-injection system with an electrochemical detector, a microprocessor-based potentiostat, and a microcomputer. The computer generates a repeating staircase potential program with a superimposed square wave. Square-wave amperometric measurements at each potential step are used to construct the current/time response at the potential. By appropriate selection of step potentials, the reconstructed response from each step corresponds to the flow-injection response of a particular component. The approach is evaluated by applying it to the simultaneous determination of copper, lead, cadmium and zinc. Limits of detection range from 8 to 18 $\mu g\ l^{-1}$. Sample throughput is 80 h^{-1}.

Flow-injection systems [1] have many advantages for automating various steps associated with chemical determinations. These advantages can be extended with systems which allow the determination of two or more components simultaneously. One simple approach is to use multiple detectors either in series [1—4] or in parallel [4]. The obvious disadvantages are the added expense of multiple detectors, peak distortion caused by each subsequent detector cell (serial case), and reduction in sample size from splitting the sample among detectors (parallel case). Electrochemical approaches to multicomponent detection have included direct [5, 6] and stripping [7] voltammetry.

Buchanan and Bacon [8] described square-wave amperometric detection for use with ion-exchange chromatography. In the present communication, the simultaneous detection of up to four components in a single sample is demonstrated; the example used is the simultaneous determination of copper, lead, cadmium and zinc. The electrochemical detector is composed of a microprocessor-based potentiostat, a microcomputer, and a hanging mercury drop electrode. The applied potential is a repeating, large-amplitude staircase cycle on which a square wave is superimposed. The overall period of the cycle must be short relative to the width of the concentration profile. Currents are sampled at two points per square-wave cycle and the difference is stored in the computer. From these difference currents, multiple responses can be calculated. Data from a particular step on the overall cycle are used to generate the response at a potential corresponding to the step height. By

0003-2670/87/$03.50

appropriate selection of step potentials, it is possible to detect selectively several components in the same injected sample.

Experimental

Reagents and solutions. A 0.1 M acetate buffer was prepared with 0.1 M acetic acid and adjusted to pH 4.5 with 0.1 M sodium acetate. This was used as carrier stream for the flow-injection system and for dilution of the standards. Solutions of copper, cadmium, lead, zinc ions and mixtures of these ions were prepared by diluting certified standard solutions (1000 mg l^{-1}, Fisher Scientific) with the acetate buffer. Triply-distilled mercury (Bethlehem Apparatus Co.) was used in the static mercury drop electrode (SMDE; PAR model 310). All other reagents were reagent grade. Solutions were prepared with 17.7 MΩ cm distilled/deionized water (Barnstead Nanopure).

Equipment. The flow and sample-injection system (Fig. 1) consisted of a pressurized reservoir for the carrier stream, teflon tubing (0.5 mm i.d.) and a Rheodyne injection valve (model 50-20). A sample-loop volume of approximately 80 μl was used throughout. The distance between the injection valve and the inlet to the detector was 30 cm. Helium from a cylinder was used both to deoxygenate the carrier stream and to pressurize the carrier reservoir. Pressure was regulated with a pressure regulator (Wilkerson Corp.; model A2019-1, 0—15 psi). Flow rates up to about 8 ml min^{-1} were possible; the flow rate used was 0.4 ml min^{-1}.

An EG&G (PAR) Model 273 potentiostat was connected through an RS232-C interface to an IBM personal computer, which was connected to a printer-plotter. The electrode (static mercury drop) and flow cell used was the PAR model 310 polarographic detector. All potentials are reported with respect to an Ag/AgCl (saturated KCl) reference electrode. The entire electrochemical system was controlled through the microcomputer by a software program written in BASIC; details of this software are available from the authors.

Results and discussion

The applied voltage program. In principle, either a square-wave or a sinusoidal potential could be superimposed on the potential steps with similar results. The advantages of the square wave (s.w.) are the simplicity of generating the waveform, and the lower storage requirements for waveform

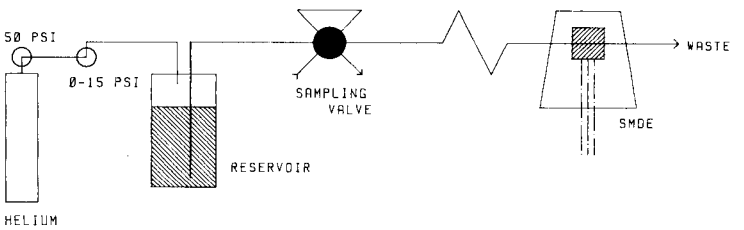

Fig. 1. Block diagram of flow-injection system.

and current data. A program was designed with which a square wave was superimposed on a series of potential steps. The entire cycle was repeated in a time frame consistent with the characteristics of the flow-injection system (10—500 ms). Currents sampled from each potential step were used to generate responses for the different components of interest.

Step potentials corresponded to peak potentials for the components of interest, which were established in prior s.w. voltammetric tests. Also it was necessary to select values of several other instrumental parameters. In particular, the frequency and amplitude of the square wave, the size of the mercury drop, the current-sampling time relative to the square wave, and the sampling aperture were considered. Theory developed for s.w. voltammetry of a reversible species [9] predicts that the difference current is proportional to the square root of the frequency. Figure 2A illustrates that is also the case for the amperometric experiment. In the case of Cu(II), there is a drop in current at higher frequencies, presumably because of kinetic complications. Based on these results, frequencies in the range of 200—400 Hz were selected for this mixture of components.

The maximum response in the flow-injection system was studied as a function of the amplitude of the square wave for all four metal ions; the results (Fig. 2B) showed that the amperometric response increases with amplitude up to a limiting value, as expected. The other factor to be considered in selecting the amplitude is the concomitant loss of selectivity [9]. Based on the results in Fig. 2B and voltammograms, 40 mV was selected as a compromise between maximum response and desired selectivity.

The minimum time for acquisition of a current sample is 100 μs, which is fixed by the data-acquisition system in the potentiostat. For this work, a sampling period of 250 μs was selected. This choice divides each square-wave half cycle into ten possible sampling points. Sampling can start at any of these points and any number of sequential points can be averaged. From

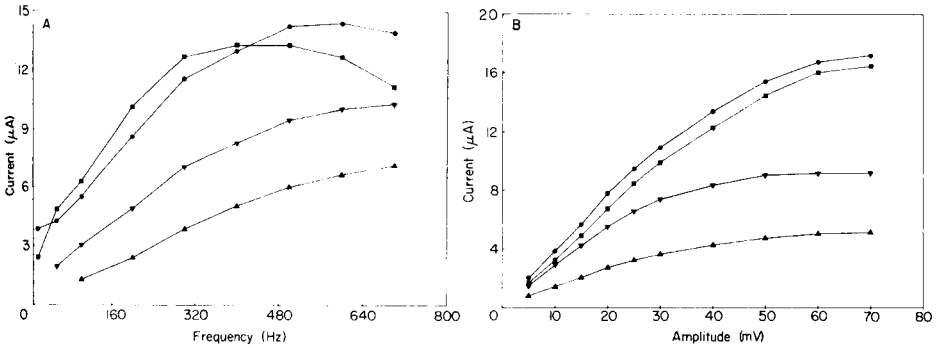

Fig. 2. A, Variation in response as a function of square-wave frequency for a mixture of Cu, Pb, Cd, and Zn. B, Variation in response as a function of the peak-to-peak amplitude of a 200-Hz square wave. (■) Cu detected at +10 mV; (▲) Pb detected at −390 mV; (▼) Cd detected at −570 mV; (●) Zn detected at −990 mV. General conditions: 40-mV amplitude; 0.4 ml min^{-1} flow rate; each metal at 10 mg l^{-1}.

the peak response and peak-to-peak background noise, signal-to-noise ratios (*S/N*) were examined as functions of sampling time and the number of points averaged. At a frequency of 200 Hz, the optimum sampling time lies somewhere in the last third of the half cycle (Fig. 3) and three points spanning a time period of 750 μs was shown to be the optimum (1—5 points were considered).

The SMDE allows a choice of three drop sizes: small, medium, and large, with relative areas of 1:1.6:2.5. The best drop size (best *S/N*) appears to be the medium drop (Fig. 4). There does, however, seem to be substantial variation between different metal ions and so this choice is a compromise.

Response with selected parameters. The response of each metal ion in mixtures was independent of the concentrations of the other metal ions over the range examined (up to 10 mg l^{-1}). Four separate responses were generated for each sample. Typical calibration data (Table 1) demonstrate

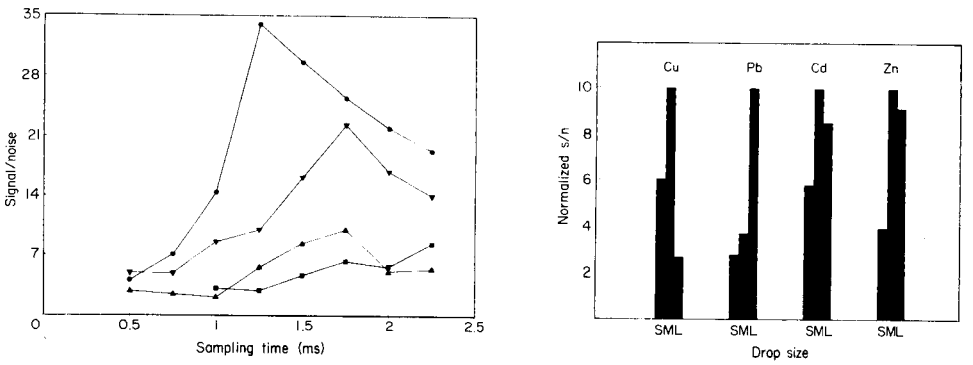

Fig. 3. Effect of timing on *S/N* ratio. Each current value obtained from average of three samples taken at 250-μs intervals (total period 750 μs). Frequency 200 Hz; amplitude 40 mV; flow rate 0.4 ml min^{-1}. Symbols and potentials as in Fig. 2. Sampling time corresponds to the midpoint of the sampling cycle.

Fig. 4. Effect of drop size (small, medium, large) on *S/N* ratio. Frequency 200 Hz; flow rate 0.4 ml min^{-1} ; amplitude 40 mV; potentials are the same as in Fig. 2.

TABLE 1

Calibration data[a] for four heavy metal ions

Metal ion	Slope (μA/mg l^{-1})	Intercept (μA)	Std. error of estimate (μA)	Correlation coefficient
Cu(II)	1.85 (0.032)	0.42 (0.17)	0.31	0.9992
Pb(II)	0.59 (0.021)	—0.055 (0.11)[b]	0.21	0.996
Cd(II)	0.976 (0.007)	0.021 (0.03)[b]	0.068	0.9998
Zn(II)	1.533 (0.0055)	0.51 (0.028)	0.052	0.99997

[a]Based on three samples at each of 7 concentrations (0.05—10 mg l^{-1}). Standard deviations are given in parentheses. [b]Intercepts do not differ from zero at the 95% confidence level (*t*-test).

the linearity of response. Detection limits measured for *S/N* 2 were 11, 13, 18, and 8 $\mu g\ l^{-1}$ for Cu, Cd, Pb and Zn, respectively. Sample throughput, based on a 4 σ criterion, was approximately 80 h^{-1}.

This research was aided by a Seed Money Grant from the University of Lowell. The authors acknowledge the Princeton Applied Research Corporation for the donation of the flow cell used. This paper was presented in part at the 37th Pittsburgh Conference, Paper No. 927, March 1986.

REFERENCES

1 J. Růžička and E. H. Hansen, Flow Injection Analysis, Wiley, New York, 1980.
2 J. H. Dahl, D. Espersen and A. Jensen, Anal. Chim. Acta, 105 (1979) 327.
3 H. Kagenow and A. Jensen, Anal. Chim. Acta, 114 (1980) 227; 145 (1983) 125.
4 A. Fernandez, M. D. Luque de Castro and M. Valcarcel, Anal. Chem., 56 (1984) 1146.
5 N. Thogersen, J. Janata and J. Ružička, Anal. Chem., 55 (1983) 1986.
6 P. A. Reardon, G. E. O'Brien and P. E. Sturrock, Anal. Chim. Acta, 162 (1984) 175.
7 J. A. Wise, W. R. Heineman and P. T. Kissinger, Anal. Chim. Acta, 172 (1985) 1.
8 E. B. Buchanan, Jr. and J. R. Bacon, Anal. Chem., 39 (1967) 615.
9 J. H. Christie, J. A. Turner and R. A. Osteryoung, Anal. Chem., 49 (1977) 1899.

Analytica Chimica Acta, 192 (1987) 333—338
Elsevier Science Publishers B.V., Amsterdam — Printed in The Netherlands

Short Communication

KINETIC DETERMINATION OF SOME INORGANIC AND ORGANIC COMPOUNDS BY OXIDATION WITH IODATE

I. I. KOUKLI and A. C. CALOKERINOS*

University of Athens, Laboratory of Analytical Chemistry, Solonos 104, 106 80 Athens (Greece)

(Received 9th June 1986)

Summary. Sulphite (5.0×10^{-5}—5.0×10^{-3} M), ascorbic acid and other compounds are oxidized by potassium iodate in dilute sulphuric acid; the production of iodide is monitored by an iodide-selective electrode. The time needed for a 40-mV potential change is inversely proportional to concentration. For sulphite (1.0×10^{-5}—1.0×10^{-4} M), selectivity is improved by sweeping the sulphur dioxide formed in acidic EDTA-containing solution into the iodate solution.

Potassium iodate is a powerful oxidant which is used in the titrimetric determination of a wide variety of inorganic and organic compounds [1—4]. The course of these titrations can be monitored potentiometrically [3]. The reaction products may be iodide, iodine or the iodonium ion I^+, depending on the conditions [5—7]. In this communication, a method is proposed for the kinetic determination of various inorganic and organic compounds in dilute sulphuric acid based on their oxidation by iodate, which is monitored with an iodide-selective electrode. The method can also be used to determine sulphite after evolution of sulphur dioxide, which is collected in the measuring cell.

Experimental

Apparatus. An Orion Model 94-53A iodide-selective electrode was used in conjunction with a Corning silver/silver chloride reference electrode, filled with saturated potassium chloride. The recording system was as previously reported [3]. All measurements were made at ambient temperature in a 50-ml beaker; stirring was done magnetically with a teflon-coated follower. The sulphur dioxide generation system used consisted of a three-necked 250-ml pear-shaped flask with ground joints, arranged as shown in Fig. 1. Nitrogen gas (160 ml min^{-1}) was continuously supplied to the system. Heating coil 1 maintained the solution at 40°C and heating coil 2 maintained the outlet at just above 100°C to prevent condensation of water vapour.

Reagents. All solutions were prepared with deionized-distilled water from reagent-grade materials, except where stated. A 0.01000 M potassium

0003-2670/87/$03.50

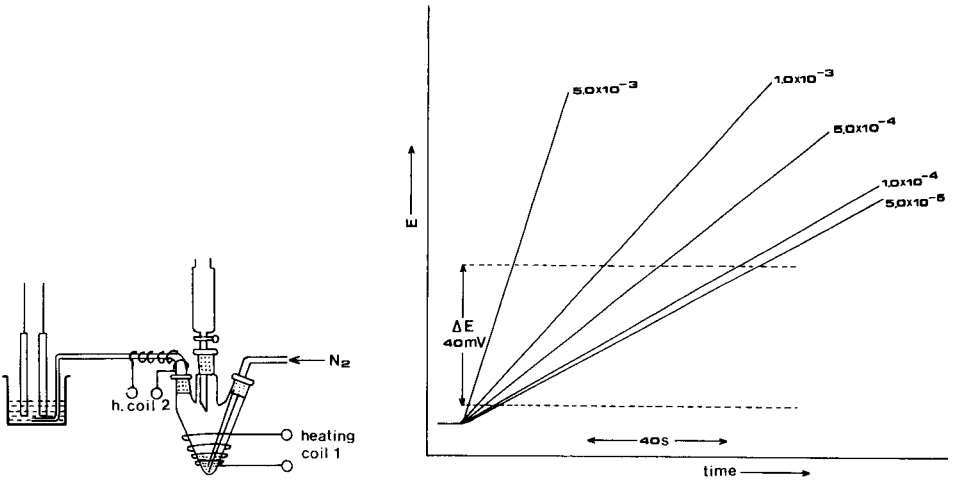

Fig. 1. Schematic diagram of the vapour-generation system used for evolution and measurement of sulphur dioxide (not to scale).

Fig. 2. Potential/time plots obtained for the initial sulphite concentrations (M) shown.

iodate stock solution was prepared by dissolving 2.1400 g of potassium iodate (Merck, p.a.), dried at 120°C for 1 h, in water and diluting with water to exactly 1 l. A 2.0×10^{-4} M iodate working solution was prepared from this stock solution by dilution with water.

Direct determination of inorganic and organic compounds. Transfer 10.00 ml of the potassium iodate working solution and 10.00 ml of the appropriate sulphuric acid solution (Table 2) into the measuring cell and start stirring and recording the potential. Inject 0.100 ml of sample solution, and record the change in potential with time. Empty the cell and repeat the procedure for each sample solution. Measure the time required for the recorded cell potential to increase from 5 mV to 45 mV.

Determination of sulphite by vapour generation. Transfer 10.00 ml of potassium iodate working solution and 10.00 ml of 0.50 M sulphuric acid to the measuring cell and start stirring and recording the potential. Transfer 5.00 ml of sulphite solution to the reaction cell of the generation system and add 2 ml of 0.50 M orthophosphoric acid through the funnel. This liberates sulphur dioxide which is continuously purged into the measuring cell. Record the change in potential with time, and measure the time required for the cell potential to increase from 5 mV to 45 mV. Empty both cells before repeating the procedure.

Calibration. Introduce aliquots of the appropriate standard solutions and measure the change in potential as above. Construct calibration graphs by plotting the reciprocal time ($1000/t$, s^{-1}) vs. concentration.

Results and discussion

In any kinetic method, the choice of initial reactant concentrations is governed by the reaction rate, the experimental technique and the sensitivity

of the measurement system. The rate of iodide generation during reduction of iodate depends on the initial concentrations of oxidant and sulphuric acid. Therefore, the effects of these parameters were investigated. The effect of two initial iodate concentrations at various initial sulphuric acid concentrations is shown in Table 1. The results indicate that the more concentrated iodate solution gives the greater reciprocal time differences between different sulphite concentrations, and that the most sensitive acid concentration is 0.10 M; this was used for all further measurements. At the optimum sulphuric acid concentration, sulphite calibration graphs were constructed for various initial iodate concentrations. The equation of the graph at 5×10^{-5} M iodate was $1/\Delta t = 10.3$ [sulphite] + 0.008 ($r = 0.9993$, $n = 7$) and at 1.0×10^{-4} M was $1/\Delta t = 15.3$ [sulphite] + 0.012 ($r = 0.995$, $n = 7$). Initial iodate concentrations of $>1.0 \times 10^{-4}$ M decreased the linear range of the calibration graph and increased the blank signal; therefore 1.0×10^{-4} M iodate was used for all further measurements. Figure 2 shows typical responses for the determination of sulphite (5.0×10^{-5}—5.0×10^{-3} M). After

TABLE 1

Effect of initial iodate and sulphuric acid (0.025—0.50 M) concentrations on the reciprocal time in the determination of sulphite

KIO_3 (M)	Reciprocal time[a] ($\times 10^{-3}$ s^{-1}) at different acidities				
	0.025 M	0.05 M	0.10 M	0.30 M	0.50 M
5.0×10^{-5}	26.0	33.5	46.3	39.5	30.8
1.0×10^{-4}	29.8	68.0	68.8	56.4	—[b]

[a]Difference in reciprocal times for 5.0×10^{-3} M and 5.0×10^{-4} M sulphite. [b]Reaction too fast for accurate measurement.

TABLE 2

Characteristics of the methods for the determination of inorganic and organic species

Compound	H_2SO_4[a] (M)	Calibration graph			Correlation coefficient ($n = 7$)
		Linear range (M)	Slope ($l\ mol^{-1}\ s^{-1}$)	Intercept (s^{-1})	
Sulphite	0.10	5.0×10^{-5}—5.0×10^{-3}	15.3	0.012	0.995
Sulphide	0.10	3.0×10^{-5}—1.0×10^{-4}	2880	—0.040	0.9993
Thiosulphate	0.10	3.0×10^{-5}—1.0×10^{-4}	2220	—0.022	0.9998
Arsenic(III)	0.25	1.0×10^{-3}—1.0×10^{-2}	2.52	0.010	0.93
Ascorbic acid	0.001	5.0×10^{-5}—5.0×10^{-4}	382	0.010	0.997
Isoniazid	0.25	1.0×10^{-4}—1.0×10^{-3}	10.8	—0.014	0.998
Hydrazine	0.50	2.0×10^{-4}—2.0×10^{-3}	67.3	—0.026	0.998

[a]Final concentration.

initiation of the reaction, a pre-measurement time corresponding to a 5-mV change was chosen to ensure thorough mixing of the reagents. The relative standard deviations for determinations of 2.5×10^{-4} and 2.5×10^{-5} M sulphite were 1.5% and 1.7% respectively ($n = 7$). Similarly, sulphide, thiosulphate and arsenic(III) were determined by the proposed procedure (Table 2). Thiocyanate reacts very slowly and cannot be measured by the proposed procedure.

Figure 3 shows the responses obtained during optimization of initial sulphuric acid concentration for the determination of ascorbic acid. At >0.001 M sulphuric acid, increased rates are observed but the linear range of the calibration is decreased. At >0.025 M sulphuric acid, the recorded responses change sign. Because this effect did not occur with only ascorbic and sulphuric acids present in the cell, the effect was attributed to formation of the monoiodonium ion I^+. Such responses, however, were not reproducible and could not be used analytically. No other compound examined caused the potential change to change sign.

Sulphite can also be determined by various methods after acidification and measurement of the evolved sulphur dioxide [8, 9]. Recently, a continuous-flow molecular-emission-cavity analyzer [10] was developed, based on

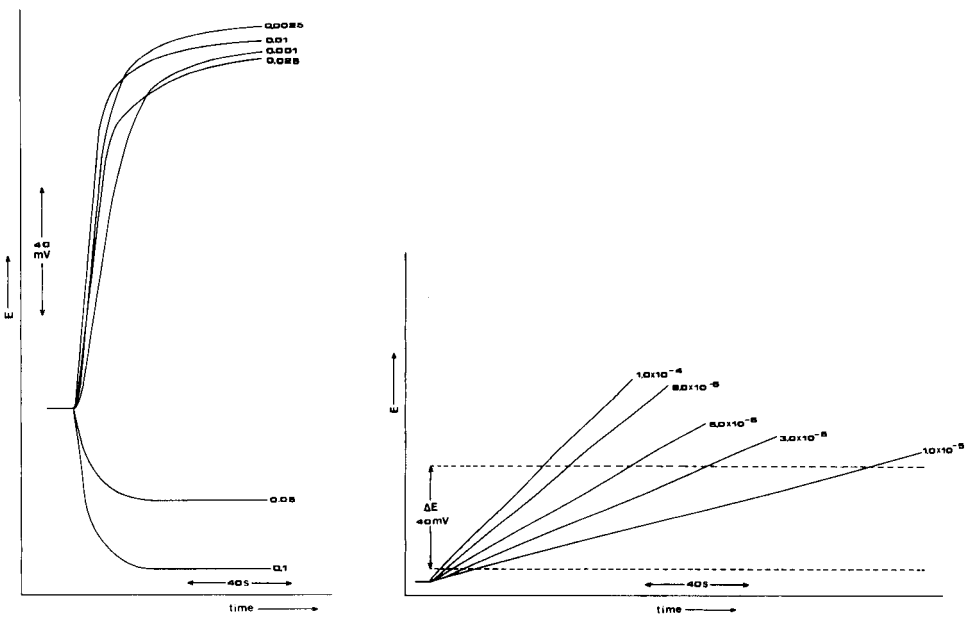

Fig. 3. Potential/time curves obtained for 3.0×10^{-4} M ascorbic acid at the initial sulphuric acid concentrations (M) shown.

Fig. 4. Potential/time plots obtained for the sulphite concentrations (M) shown after evolution of sulphur dioxide.

sulphur dioxide evolution, for the determination of sulphite. The procedure suffered severe interferences from various cations, EDTA eliminated only some of the interferences. Thus, the possibility of using the above potentiometric system to determine sulphur dioxide evolved from a conventional vapour-generation system was examined. The initial iodate concentration was that used for measurement of sulphite. When 0.10 M sulphuric acid was used with 2.0, 1.0 and 0.50 M orthophosphoric acid, the reciprocal times from 1.0×10^{-4} M sulphite were 4.2×10^{-3}, 4.4×10^{-3} and 8.1×10^{-3} s^{-1}, respectively. At <0.50 M orthophosphoric acid, evolution of sulphur dioxide was slow and incomplete. With 0.25 M sulphuric acid in the measurement cell and 0.50 M orthophosphoric acid added to the generator, the reciprocal time for 1.0×10^{-4} M sulphite was 30.0×10^{-3} s^{-1} at 25°C and 40.0×10^{-3} s^{-1} at 40°C in the generating flask. At >40°C, the reciprocal time did not increase significantly and water vapour was carried over to the measuring cell. The effect of nitrogen flow rate is shown in Table 3. Therefore, 0.25 M sulphuric acid and 0.50 M orthophosphoric acid were used for all further tests, sulphur dioxide was evolved at 40°C and purging was done with 160 ml min^{-1} nitrogen. Figure 4 shows typical responses for sulphite produced by evolution of sulphur dioxide. The calibration graph was linear in the range 1.0×10^{-5}—1.0×10^{-4} M sulphite ($1/\Delta t$ = 207 [sulphite] + 0.004, r = 0.9990, n = 7) and the relative standard deviation was 3.1% for a 1.0×10^{-4} M sulphite sample (n = 7).

The effects of Cd^{2+}, Cu^{2+}, Mn^{2+}, Co^{2+}, Fe^{3+}, Pb^{2+} and tetrachloromercurate(II) on the evolution of sulphur dioxide from 1.0×10^{-4} M sulphite were investigated. Tetrachloromercurate(II) and cadmium (both 1.0×10^{-7}—1.0×10^{-3} M) did not interfere but all the other cations studied interfered severely (Table 4) owing to the formation of stable complexes or insoluble compounds. All the interferences listed were eliminated by addition of 0.01 M EDTA in the generator except that of manganese(II), which was unaffected.

TABLE 3

Effect of nitrogen flow rate on the determination of 1.0×10^{-4} M sulphite by evolution of sulphur dioxide

Flow rate (ml min^{-1})	40	80	120	160	220	280
$1/\Delta t$ ($\times 10^{-3}$ s^{-1})	15.8	20.0	38.5	40.0	23.8	18.2

TABLE 4

Effect of foreign ions in aqueous solutions on evolution of sulphur dioxide from 1.0×10^{-4} M sulphite

Ion	Conc. (M)	$1/\Delta t$ (%)	Ion	Conc. (M)	$1/\Delta t$ (%)
Cu^{2+}	1.0×10^{-7}	−57.8	Fe^{3+}	4.0×10^{-5}	−34.6
	2.0×10^{-7}	−100		5.0×10^{-5}	−100
Mn^{2+}	1.0×10^{-5}	0	Pb^{2+}	1.0×10^{-7}	0
	$\geqslant 2.0 \times 10^{-5}$	−100[a]		1.0×10^{-6}	−7.8
Co^{2+}	$\geqslant 1.0 \times 10^{-10}$	−100		1.0×10^{-5}	−16.5
Fe^{3+}	1.0×10^{-5}	0		1.0×10^{-4}	−30.6[b]
	2.0×10^{-5}	−7.7		1.0×10^{-3}	−100[b]
	3.0×10^{-5}	−15.4			

[a]Brown precipitate formed. [b]Turbid solution.

REFERENCES

1 S. N. Nema and R. M. Verma, Analyst, 104 (1979) 691.
2 B. C. Verma, S. M. Ralhan and N. K. Ralhan, Mikrochim. Acta, (1976) 201.
3 A. C. Calokerinos and T. P. Hadjiioannou, Microchem. J., 28 (1983) 464.
4 J. K. Grime and B. Tan, Anal. Chim. Acta, 105 (1979) 361, 369.
5 R. A. Hasty, Mikrochim. Acta, (1973) 925.
6 M. I. Karayannis, S. M. Tzouwara-Karayanni and T. P. Hadjiioannou, Anal. Chim. Acta, 70 (1974) 351.
7 D. N. Samios, M. I. Karayannis and T. P. Hadjiioannou, Z. Phys. Chem., 104 (1977) 189.
8 A. Syty, Anal. Chem., 45 (1973) 1744.
9 A. C. Calokerinos and A. Townshend, Fresenius' Z. Anal. Chem., 311 (1982) 214.
10 N. Grekas and A. C. Calokerinos, Analyst, 110 (1985) 335.

Analytica Chimica Acta, 192 (1987) 339—343
Elsevier Science Publishers B.V., Amsterdam — Printed in The Netherlands

Short Communication

STUDIES OF AMPEROMETRIC GLUCOSE DEHYDROGENASE ELECTRODES FOR GLUCOSE

G. PALLESCHI[b] and G. G. GUILBAULT*

Department of Chemistry, University of New Orleans, New Orleans, Louisiana 70148 (U.S.A.)

G. J. LUBRANO and M. A. NABI RAHNI[a]

Universal Sensors Inc., 5258 Veterans Memorial Blvd., Metairie, Lousiana 70006 (U.S.A.)

(Received 26th June 1986)

Summary. Glucose sensors are constructed by immobilizing glucose dehydrogenase physically or chemically on a carbon or platinum electrode. Soluble coenzyme was used. The usefulness of the electrode is limited by interference from any molecule that can be oxidized at +450 mV. Because the cofactor must be in solution, and diffuse to the electrode, a low-molecular-weight cut-off filter cannot be used to block the interferences.

In recent years, several papers have been published on the use of NAD(P) and NAD(P)H as cofactors in enzymatic reactions involving glucose dehydrogenase [1—4]. The electrocatalytic oxidation of the reduced NAD(P)H, at platinum, carbon or chemically-modified carbon electrodes, has been studied [5—9] and proposed for the determination of glucose [4]. A glucose sensor based on a carbon (or platinum) electrode with glucose dehydrogenase (GDH) and NAD(P) does not require oxygen. It can thus be a useful substitute for sensors based on glucose oxidase when the oxygen concentration is low or variable.

In this communication, a glucose dehydrogenase sensor with NAD/NADH is studied. Because of the well known reaction:

$$\beta\text{-D(+)-glucose} + \text{NAD(P)}^+ \xrightarrow{\text{GDH}} \text{D-gluconic acid} + \text{NAD(P)H} \qquad (1)$$

the NAD(P)H reoxidation on Pt and carbon electrodes was studied in some detail. Linear-sweep voltammetric studies were done with NADH in phosphate buffer at pH 7.4. The electrode that gave the best signal/noise ratio was chosen, and evaluated for the quantitation of glucose and NAD with the

[a]Present address: Department of Chemistry, Pace University, Pleasantville, NY 10570, U.S.A.

[b]Present address: Department of Science and Chemical Technology, University of Rome Tor Vergata, 00173, Rome, Italy.

0003-2670/87/$03.50

enzyme in solution, as well as physically or chemically immobilized on the electrode surface. An unsuccessful attempt was made to immobilize both NADH and GDH on the electrode surface.

Experimental

Apparatus. A platinum electrode of approximately 20-mm^2 area and two carbon electrodes of approximately 8-mm^2 and 32-mm^2 areas were constructed. The reference electrode for all probes was Ag/AgCl. Carbon graphite rods were a gift from Ultra Carbon Corporation (Bay City, Michigan; purity designation Yu-40, 1/8 in. and 1/4 in. diameter). A Tacussel PRGE-DEC polarographic unit was used for linear-sweep voltammetric and constant-potential studies.

Signals were monitored with a Houston Instrument Omniscribe strip-chart recorder. The dialysis membranes had 1000, 3500, 25 000 and 50 000 molecular-weight-cutoff (MWCO) filters (Spectra Por 3; Spectrum Medical Industries, Los Angeles, CA).

Chemicals. The buffer used was a physiological phosphate buffer, pH 7.4, consisting of 137 mM NaCl, 2.7 mM KCl, 8.0 mM Na_2HPO_4 and 1.5 mM KH_2PO_4. β-D-Glucose, $NAD(P)^+$ 1-oxidoreductase (EC.1.1.1.47), NAD^+ and NADH and all other reagents were from Sigma Chemical Co.

Procedure. Carbon electrodes were cleaned with sandpaper (600 grit), and washed with deionized water. The platinum electrode was pretreated by washing with chromic acid solution for a few seconds, and then polarized at −200 mV for 2 min.

Glucose dehydrogenase was immobilized directly on the carbon and platinum electrodes by the BSA/glutaraldehyde method [10] in which 0.5 μl of 10% glutaraldehyde, 5.0 μl of bovine serum albumin (BSA) in 0.1 M phosphate buffer (pH 7.0), and 1—2 mg of glucose dehydrogenase were mixed on the surface of the electrode and allowed to dry. The layer was washed first with 0.1 M glycine in the above buffer, then with the buffer alone.

Solutions of NAD(P)H and NAD(P) were prepared in the pH 7.4 buffer and stored in the refrigerator when not in use. The electrode was stored at room temperature in buffer. Before every assay, the enzyme electrode was equilibrated in 4.0 ml of stirred buffer solution, which contained the appropriate concentration of cofactor. Glucose was injected and the change in current was monitored amperometrically.

Results and discussion

Linear-sweep voltammetric studies. Voltammograms from 0 to 900 mV were run both in buffer only and in buffer plus NADH at a scan rate of 10 mV s^{-1}, with the platinum and carbon electrodes, without stirring (Figs. 1 and 2). The platinum electrode (Fig. 1) gave the highest background current and the lowest reproducibility, but it showed good response to NADH.

The carbon electrode with the 8-mm^2 surface area gave better results and was chosen for further experiments. Figure 2 shows the voltammograms

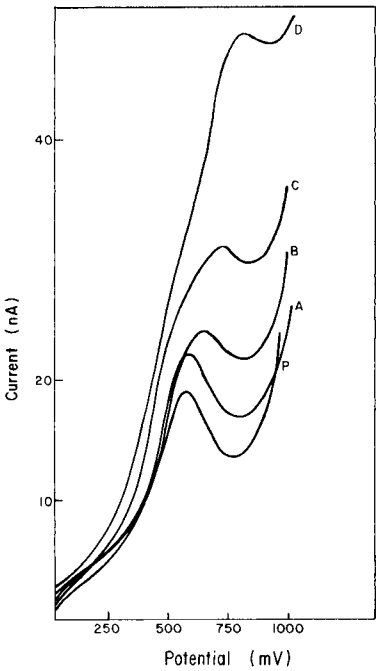

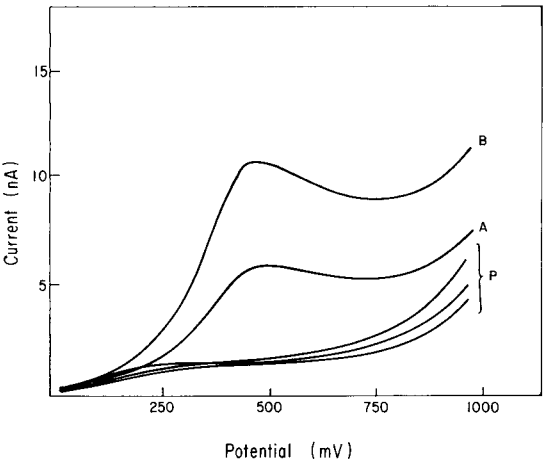

Fig. 1. Voltammograms of phosphate buffer and NADH in buffer at a platinum electrode. (P) Buffer alone. NADH (mg ml^{-1}): (A) 0.2; (B) 0.5; (C) 1.0; (D) 2.0. Scan rate, 10 mV s^{-1}.

Fig. 2. Voltammograms of phosphate buffer and NADH in buffer at the 8-mm^2 carbon electrode: (P) buffer alone; (A) 0.5 mg ml^{-1} NADH; (b) 1 mg ml^{-1} NADH.

obtained with this electrode, in both buffer and buffer plus NADH. The peak current for NADH was observed at +450 mV, with a half-wave potential at 335—340 mV. The peak current varied linearly with NADH concentration.

Constant potential studies. An applied potential of 450 mV was selected for constant-potential studies with the 8-mm^2 carbon electrode. With 0.024 and 0.048 mg dl^{-1} NADH, the current change was 200 and 400 nA, respectively, and the initial background current was 300 ± 10 nA.

Studies with glucose dehydrogenase. Preliminary studies were done with the enzyme in solution. Although the steady-state current did not vary linearly with glucose concentration, the initial rate varied linearly for glucose concentrations from 0.1 to 2×10^{-4} M. The glucose dehydrogenase (1—2 mg) was then trapped on the electrode surface with a 3500 MWCO membrane which allowed NADH and glucose to diffuse to the electrode surface. The steady-state current varied linearly with glucose concentration over the range 0.1—2×10^{-4} M; the correlation coefficient was 0.998 and the limit of detection was 5×10^{-6} M.

In further experiments, the enzyme was immobilized chemically on the carbon electrode. With or without stirring, there was no loss of enzyme

during several hours of use. The steady-state current varied linearly with glucose concentration from 1×10^{-6} to 1×10^{-4} M, with a correlation coefficient of 0.998. In this case, the response time was less than 1 min and the detection limit was 1×10^{-6} M.

Further experiments were done by covering the immobilized enzyme electrode with a dialysis (3500 MWCO) membrane to protect it from proteins, peptides, and other large molecules which may be present in biological solutions. Glucose measurements with this electrode, and the same NADH concentration as used with the uncovered enzyme electrode, exhibited a ten-fold increase in response time and a 2—3-fold decrease in sensitivity. The sensitivity was increased by more than 2-fold by increasing the NADH concentration to 3.75×10^{-3} M. Under these conditions, a linear calibration plot was observed for 2×10^{-6}—1×10^{-4} M glucose, with a correlation coefficient of 0.998, a detection limit of 2×10^{-6} M and a response time to steady state of 10 min. In an attempt to decrease the response time, dialysis membranes with MWCO of 50 000, 25 000, and 1000 were tested. With the 50 000 and 25 000 MWCO membrane, the steady-state current change was almost the same but the response time was only 10—15 s; no significant response improvement was observed with the 1000 MWCO membrane. Because membranes that block small molecules could not be used, without also blocking the cofactor, the electrode suffers interference from any small molecule that can be oxidized at potentials more positive than +450 mV.

When solid NAD was trapped between the electrode and a 1000 MWCO membrane, there was no response to glucose. An attempt to immobilize both enzyme and cofactor by the same BSA/glutaraldehyde technique yielded only a continuous current drift.

Effects of pH were evaluated with the electrode with no dialysis membrane. The maximum response was at pH 7.3 with a rapid decrease from 7.3 to 9 and also from pH 5 to 4. The optimum range was pH 6—8. The sensitivity almost doubled with increasing temperature between 25 and 30° C and then remained practically constant up to 40° C. The probe could be used for about 2 weeks with good sensitivity and with constant slope.

The selectivity of the system depends on both the enzyme [3, 4] and the carbon electrode. Some components that can be present in blood were examined using a bare carbon electrode at 450-mV applied potential. Acetaminophen, uric acid and ascorbic acid gave significant responses when injected at 10 mg dl^{-1} levels. Aspirin and cysteine increased the background noise but did not cause significant interference. Hydrogen peroxide gave a small response. Attempts to avoid such interferences by use of zero applied potential were unsuccessful because the NADH re-oxidation signal was 100 times lower than that at +450 mV.

The electrode is expected to be useful only in situations in which interferents are absent or can be removed previously.

REFERENCES

1 D. Banauch, W. Brummer and W. Ebeling, Z. Klin. Chem. Klin. Biochem., 13 (1975) 101.
2 R. Lutz and J. Fluckiger, Clin. Chem., 21 (1975) 1372.
3 J.-C. W. Kuan, S. S. Kuan and G. G. Guilbault, Clin. Chem., 23 (1977) 1058.
4 R. Appelqvist, G. Marko-Varga, L. Gorton, A. Torstensson and G. Johansson, Anal. Chim. Acta, 169 (1985) 237.
5 W. J. Blaedel and R. A. Jenkins, Anal. Chem., 47 (1975) 8.
6 L. C. Thomas and G. D. Christian, Anal. Chim. Acta, 78 (1975) 271.
7 N. K. Cenas, J. Rozgaite, A. Pocius and J. Kulys, J. Electroanal. Chem., 154 (1983) 121.
8 Z. Samec and P. J. Elving, J. Electroanal. Chem., 144 (1983) 217.
9 N. K. Cenas, J. J. Kanapieniene and J. J. Kulys, J. Electroanal. Chem., 189 (1985) 163.
10 G. J. Lubrano and G. G. Guilbault, Anal. Chim. Acta, 97 (1978) 229.

Analytica Chimica Acta, 192 (1987) 345—348
Elsevier Science Publishers B.V., Amsterdam — Printed in The Netherlands

Short Communication

APPLICATION OF REVERSED-PHASE HIGH-PERFORMANCE LIQUID CHROMATOGRAPHY FOR THE SEPARATION OF DEUTERIUM AND HYDROGEN ANALOGS OF AROMATIC HYDROCARBONS

R. BAWEJA[a]

Chemistry Division, Argonne National Laboratory, Argonne, Illinois 60439 (U.S.A.)

(Received 26th August 1986)

Summary. Substitution of hydrogen by deuterium in aromatic hydrocarbons can alter various properties significantly. Benzene, toluene, naphthalene, anthracene, phenanthrene, biphenyl and durene are separated from their deuterium analogs by reversed-phase (C_{18}) liquid chromatography with acetonitrile/water mobile phases and ultraviolet detection. Deuterium compounds always elute before the hydrogen analog; possible explanations are given. The elution pattern and retention times of anthracene and phenanthrene were unchanged when D_2O replaced H_2O as the mobile phase component.

Small- and medium-size aliphatic hydrocarbons are either gaseous or volatile liquid compounds and the method of choice for their determination is gas chromatography. Liquid chromatography has been applied successfully to the separation of larger hydrocarbons, especially the polynuclear aromatic hydrocarbons (PAHs) [1]. The determination of PAHs is important because of their carcinogenic properties and environmental pollution [2]. Silica gel as well as octadecylsilane (reversed-phase) columns have both been used extensively in high-performance liquid chromatographic (HPLC) studies involving separation of aromatic hydrocarbons [3]. Improved separation was observed when silica gel was modified by chemically bonded dinitroanilinopropyl (DNAP) groups [4]. Although many types of columns have been used none has attained the popularity of reversed-phase systems. Examples in which reversed-phase chromatography has been utilized include separating hydrocarbons present in tissues of marine organisms [5], in atmospheric particulate matter [6], and cigarette smoke condensate [7]. The first isotopic separation by HPLC was achieved on a reversed-phase column [8].

This study shows the facile separation of deuterium forms of aromatic hydrocarbons from their hydrogen analogs by reversed-phase HPLC with ultraviolet (u.v.) detection. The investigation is extended to evaluate the effect of replacing H_2O by D_2O for isotopic separations of anthracene and phenanthrene.

[a]Present address: School of Pharmacy, University of Wyoming, Laramie, Wyoming 82071, U.S.A.

0003-2670/87/$03.50

Experimental

Chemicals. The ordinary aromatic hydrocarbons used were benzene, toluene (both from Burdick and Jackson Laboratories, Muskegon, MI), naphthalene and nitrobenzene (both from J. T. Baker, Phillipsburg, NJ), anthracene (Matheson Co., East Rutherford, NJ), phenanthrene (Fluka, Buchs, Switzerland), durene (1,2,4,5-tetramethylbenzene; Eastman Kodak Co., Rochester, NY), and biphenyl (Mallinckrodt, St. Louis, MO). Deuterated aromatic hydrocarbons were kindly provided by Dr. Clyde A. Hutchinson, Jr., Department of Chemistry, University of Chicago. Acetonitrile and methanol were of HPLC grade (Burdick and Jackson Laboratories). Water was prepared with a Millipore deionization system. All samples and solvents were used as received.

Equipment. All of the separations were done with a Beckman Model 332 liquid chromatographic system equipped with two Model 110A metering pumps under the control of a 421 microprocessor. A Hitachi variable-wavelength spectrophotometer (Model 155-40) was used as the detector. Samples were introduced by a Model 210 syringe-loading injector. Ultrasphere octadecylsilane (ODS, 5 μm) columns (4.6 mm $\times$ 250 mm) were used. A 0.5-μm pre-filter was always inserted before the column and careful attention was given to the removal of particulate matter from the samples and solvents. The flow rate of mobile phase was 1 ml min^{-1}.

Procedure. Samples that are liquid at room temperature were prepared as follows: 100 μl of benzene-d_6 was mixed with 75 μl of benzene-h_6 and 1 ml of methanol was added to the mixture; the mixture was vortexed and 1 μl was injected for the chromatographic separation. The mixtures of isotopic forms of toluene and nitrobenzene were prepared in exactly the same manner and again 1 μl was injected. For the solid hydrocarbons, a 1.0-mg amount proved adequate; naphthalene analogs were dissolved in 1.0 ml of methanol; isotopic forms of anthracene, phenanthrene, biphenyl and durene were prepared in 1.0 ml of tetrahydrofuran. All samples were vortexed. Unequal volumes of the solutions of the two isotopic forms were mixed to facilitate the identification of peaks in the chromatogram. Each sample (2 μl) was followed by a 5-μl flush of acetonitrile. Detection was at 254 nm with a chart speed of 1 cm min^{-1}.

Results and discussion

Table 1 lists the effects of mobile-phase composition on the chromatographic properties of the hydrocarbons. In all cases, the ^2H analog eluted more rapidly than the ^1H analog. Complete (baseline) separations of mixtures of ^1H- and ^2H-benzene, toluene, and naphthalene were accomplished, but at the expense of relatively long separation times. Resolution similar to that shown for toluene in Fig. 1 was obtained for hydrogen and deuterium analogs of biphenyl, anthracene, phenanthrene, and durene with a mobile phase rich in acetonitrile. The hydrogen and deuterium analogs of anthracene or phenanthrene were baseline-separated with a 30:70 water/aceto-

TABLE 1

Retention times and capacity factors for aromatic hydrocarbons[a]

Aromatic hydrocarbon	Mobile phase H_2O:CH_3CN	Retention time (min)		Capacity factor[b]	
		D	H	D	H
Benzene	70:30	43.7	45.7	14.60	15.32
Toluene	60:40	36.7	38.4	12.10	12.73
Naphthalene	55:45	39.6	41.7	12.91	13.63
Anthracene	30:70	16.4	17.3	4.77	5.10
Phenanthrene	30:70	15.2	16.1	4.35	4.64
Durene	30:70	17.4	18.4	4.35	4.66
Biphenyl	45:55	29.4	31.0	7.90	8.39
Nitrobenzene	85:15	64.5	66.8	22.05	22.85

[a]D, deuterium form; H, hydrogen form. [b]$k' = (t_r - t_0)/t_0$.

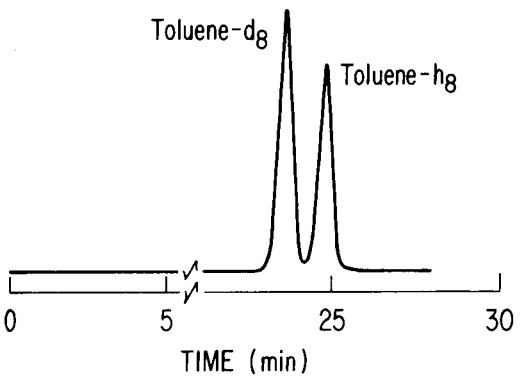

Fig. 1. Reversed-phase HPLC separation of toluene-d_8 and toluene-h_8; mobile phase, water/acetonitrile (60:40 v/v).

nitrile mobile phase (Table 1). Experiments in which heavy water (D_2O) was used instead of ordinary water showed that the deuterium compounds eluted ahead of their hydrogen analogs and that the retention times and capacity factors matched their respective values in water/acetonitrile. This is consistent with other studies [9].

Although the isotopic forms of durene and biphenyl were resolved with the mobile phases given in Table 1, it was not possible to separate the isotopes of nitrobenzene fully on a C_{18} column. No further studies were conducted with nitrobenzene.

For all the compounds tested, the deuterated form eluted first. This chromatographic behavior appears to be independent of the size of the molecule. Relatively greater solubility of the deuterium isotope in the mobile phase is apparently not a factor. There are two reasons for this conclusion. First, if solubility were a factor, then in some solvent systems it

would be expected that the deuterium compound would elute more slowly which is not the case. Second, if solubility were a factor, the deuterium analog should show a different retention time with a D_2O/CH_3CN than with a H_2O/CH_3CN mobile phase; this behavior was not observed.

The elution of the deuterium forms before their hydrogen analogs suggests that van der Waals forces are operational. It has been noted that the entire molecule need not be considered in dealing with isotope effects [10, 11]. The major contribution to such effects is essentially from isotopically participating bonds and not from vicinal bonds, i.e., the chromatographic behavior depends fundamentally on the interaction between the C—H or C—D bonds and the stationary phase. A C—H bond has a higher oscillation frequency (3300 cm^{-1}) than a C—D bond (2334 cm^{-1}). This oscillation frequency creates an electromagnetic field which in turn produces an induced field of opposite charge in surrounding molecules. The C—H bond induces greater forces of attraction between itself and the stationary phase than those generated between the C—D bond and the stationary phase, so that the deuterium compound moves ahead of the hydrogen compound.

Stable isotopes, particularly deuterium, are proving useful as tracers for studies of drug distribution and metabolism. A major deterrent to more extensive use of stable isotopes for tracer studies has been the lack of suitable analytical methods. It appears that HPLC should prove useful in these and other studies involving isotopic analogs.

The author thanks Dr. M. I. Blake (University of Illinois) and Dr. J. J. Katz (Argonne National Laboratory) for their suggestions, and Argonne National Laboratory for the Fellowship provided.

REFERENCES

1 J. Hofman, O. Tomanek, L. Vodicka and S. Landa, Collect. Czech. Chem. Commun., 34 (1969) 1042.
2 K. D. Bartle, M. L. Lee and S. A. Wise, Chem. Soc. Rev., 10 (1981) 113.
3 J. D. Suatoni and H. R. Garber, J. Chromatogr. Sci., 14 (1976) 546.
4 L. Nondek and J. Malek, J. Chromatogr., 15 (1978) 187.
5 B. P. Dunn and R. J. Armour, Anal. Chem., 52 (1980) 2027.
6 W. C. Eisenberg, J. Chromatogr. Sci., 16 (1978) 145.
7 A. F. Haeberer, M. E. Snook and O. T. Chortyk, Anal. Chim. Acta, 80 (1975) 303.
8 N. Tanaka and E. R. Thornton, J. Am. Chem. Soc., 98 (1976) 16/7.
9 S. Wal, J. Liq. Chromatogr., 8 (1985) 2003.
10 P. D. Klein, Advances in Chromatography, M. Dekker, New York, 1966, p. 3.
11 D. L. Hachey, K. Nakamura, M. J. Kreek and P. D. Klein, in H. L. Schmidt, H. Forstel and K. Heinzinger (Eds.), Stable Isotopes, Proceedings of the Fourth International Conference, Elsevier, Amsterdam, 1982, p. 235.

Analytica Chimica Acta, 192 (1987) 349—353
Elsevier Science Publishers B.V., Amsterdam — Printed in The Netherlands

Short Communication

INDIRECT DETERMINATION OF IRON IN A FLOW-INJECTION SYSTEM WITH AMPEROMETRIC DETECTION

LILIANA SILVA R., LUIS E. LEÓN* and ALFREDO CALVO C.

Departamento de Química, Universidad Simón Bolivar, Apartado 80659, Caracas 1080-A (Venezuela)

(Received 19th May 1986)

Summary. The change in peak current resulting from the reaction of Fe(II) with nitroso-*R* salt in a flow-injection system is used to quantify Fe(II) with either single- or dual-electrode amperometric detectors. The current change varies linearly with Fe(II) concentration from 0 to 200 mg l^{-1}. The relative standard deviation was about 5% with the single-electrode detector and about 10% with the dual-electrode detector. The method is evaluated for the determination of iron in dietary supplements.

Amperometric detectors are becoming increasingly popular in flow-injection systems and high-performance liquid chromatography [1—3]. In this communication, an indirect method is described for the determination of iron in pharmaceutical preparations using the nitroso-*R* salt (1-nitroso-2-naphthol-3,6-disulfonic acid, disodium salt; NRS). In acetate buffer at pH 4.7, NRS is reduced at —0.37 V vs. SCE to give the corresponding amine, which can be re-oxidized at +0.25 V [4]. Samples containing iron(II) are injected into a stream of NRS, and the change in uncomplexed NRS concentration is detected either directly with a single working electrode, or indirectly with a two-electrode system based on oxidation of the amine produced in the reduction step. The two-electrode approach may help to reduce effects of dissolved oxygen.

Experimental

Equipment. The electrochemical cell used was the combination of two previous designs [5, 6]. A saturated calomel electrode (SCE) with a Vycor tip was used as the reference electrode and the working and auxiliary electrodes were made of carbon paste (Metrohm EA-267-C). The diameters of the exposed circular surfaces of the working electrodes (WE_1 and WE_2) were 2.2 and 4.5 mm, respectively; the diameter of the exposed circular surface of the auxiliary electrode was 2.6 mm. The electrodes were mounted on Plexiglas blocks so they could be used in a two-electrode configuration. The reference and auxiliary electrodes were separated from the working electrodes by a 0.2-mm thick acetate film. The volume of the cell was about 6 μl.

Currents were measured with a bipotentiostat constructed in this labora-

0003-2670/87/$03.50

tory from an earlier design [7]. A three-electrode potentiostat (PAR 173 potentiostat/galvanostat with 175 universal programmer) was used for the cyclic voltammetric experiments as described elsewhere [4].

The flow system included a peristaltic pump (Pharmacia Model P-3) and a pulse damper between the pump and the injection valve. Samples were introduced with a Rheodyne 510 injection valve (with a sample loop of 20 μl). Polyethylene tubing (0.7-mm i.d.) was used throughout; the manifold tubing was 100-cm long. The flow rate was 3.5 ml min^{-1} and all experiments were done at 23 ± 1°C.

Reagents. Analytical-grade chemicals were used. Standard solutions of iron(II) were prepared as described before [4]. All studies were done with 1.0 M acetate buffer at pH 4.7. The nitroso-*R* salt (Riedel-de Haën) was used as received.

Preparation of samples. The proposed method was tested by determining the iron concentration of three pharmaceutical products used as iron supplement in normal human diet, namely Yectofer, Trinfer and Girard. The first preparation listed contains iron as the oxalate; the second contains iron as the sorbitol and citrate complexes with dextrin as a stabilizer; and the third contains iron(II) fumarate with ascorbic acid (38.1%) and several other components, including vitamin B_{12} (0.004%) thiamine mononitrate (0.9%), riboflavin (0.75%), nicotinamide (4.6%), vitamin B_6 (0.8%), and calcium pentothenate (1.7%). Yectofer ampules were dissolved in 50 ml of water that contained about 2 ml of concentrated sulfuric acid. Then, the final solution was diluted to 500 ml with water. Trinfer capsules or Girard powders were homogenized in an agate mortar and known amounts were placed in 250-ml beakers that contained 2 ml of concentrated sulfuric acid in 150 ml of distilled water. The mixtures were heated and stirred gently for about 15 min; after cooling to room temperature, the solutions were transferred to 500-ml volumetric flasks and diluted to volume with water. After these treatments, excipients in the formulations were not electroactive.

Procedure. Known volumes of sample solutions were placed in 25-ml volumetric flasks which contained 0.5 ml of 0.15 M hydroxylammonium chloride and diluted to volume with the acetate buffer. Then, known volumes of these solutions were injected into the flow system. Potentials applied to the detectors were −0.45 V at WE_1 and +0.25 V at WE_2 (when needed).

Results and discussion

The cyclic voltammogram of NRS under static conditions shows a reduction peak at −0.40 V and an oxidation peak at +0.15 V. These were the potentials used for the single- and dual-detector studies.

Previously established conditions [4] were used to confirm that the peak current with a single-electrode detector varied linearly with NRS concentration and that addition of iron(II) caused the current to decrease. Also, preliminary studies with Fe(II) showed that 2 mM NRS in the flow stream

was a suitable compromise between the smaller relative change in current at higher concentration (e.g., 3 mM), and the larger relative change but reduced linear range for Fe(II) at lower concentration (e.g., 1 mM).

Blank (buffer) samples intercalated into a stream of 2.1 mM NRS in the acetate buffer were used to evaluate effects of tube length and flow rate. Results are presented in Fig. 1. Conditions chosen (100 cm of 0.7-mm i.d. tubing and 3.5 ml min^{-1} flow rate) represents a compromise between higher sensitivity and larger dilution effects for iron(II) injections.

Figures 2 and 3 show the responses of the WE_1 and WE_2, respectively, when different amounts of Fe(II) were injected into the NRS stream. As expected, the peak current decreases at WE_1 and increases at WE_2; however, the sensitivity at WE_2 is only about 8% of that at WE_1, presumably because of incomplete re-oxidation of reduced NRS. In each case, the current change (Δi) varies linearly with Fe(II) concentration (Fig. 4). Both calibration plots have non zero intercepts as a result of dilution of the RNS in the flow stream by the samples. In Figs. 2 and 3, the peaks (recorded at slow chart speed) to the right of each detailed peak indicate the reproducibility of the signals. The signals at WE_2 were not affected by the reduction products formed from oxygen at WE_1, in accord with previous results [8].

Analytical applications. Results for the three pharmaceutical preparations are summarized in Table 1 together with results obtained by spectrophotometry [9]. Both calibration plots and a standard-addition method were

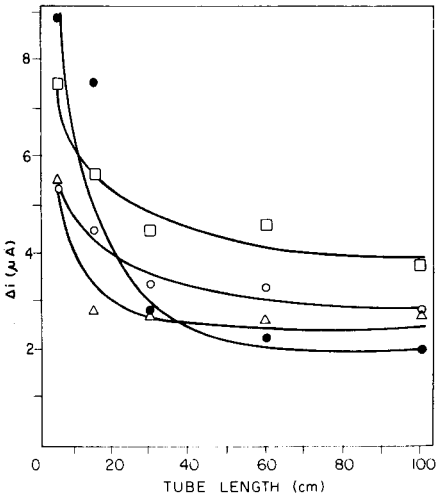

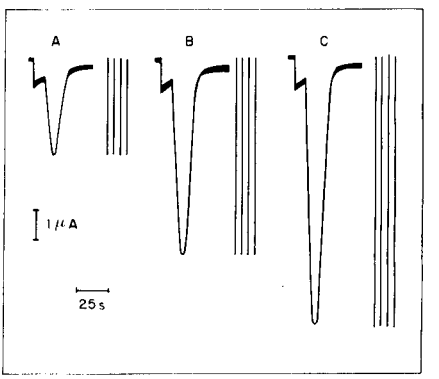

Fig. 1. Variation of change in current (Δi) with tube length after injection of blank solutions into 2.1 mM NRS. Flow rate (ml min^{-1}): (●) 0.5; (△) 1.2; (○) 2.7; (□) 3.5. Applied potential, −0.45 V.

Fig. 2. Amperometric response of the WE_1 (held at −0.45 V) to Fe(II): (A) 0.0; (B) 48.0; (C) 88.0 mg l^{-1}.

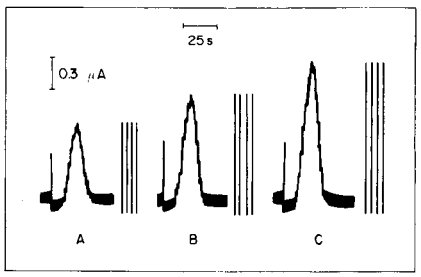

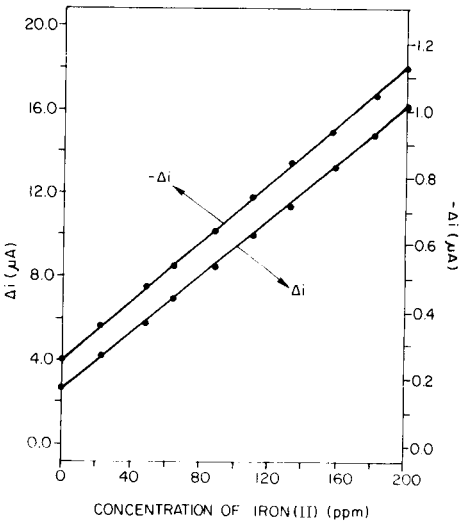

Fig. 3. Amperometric response of the WE_2 (held at +0.25 V) to Fe(II): (A) 88.0; (B) 132.8; (C) 200.0 mg l^{-1}

Fig. 4. Calibration curves for Fe(II) with single- and dual-electrode detection.

TABLE 1

Results for iron content of the Girard, Yectofer, and Trinfer products

Product[a]	Mode[b]	Iron content			
		Amperometry[c]		Spectrophot.[c]	Nominal
		Single electrode	Dual electrodes		
Girard[b]	Cal.	31.5 (2.0)	31.2 (4.6)	31.1 (1.3)	34.5
	S.a.	31.8 (4.5)	32.9 (5.0)	33.5 (2.3)	
Yectofer[c]	Cal.	100.7 (2.2)	101.8 (4.5)	99.8 (1.1)	100
	S.a.	100.1 (3.6)	105.0 (5.0)	104.3 (1.3)	
Trinfer[b]	Cal.	14.5 (3.4)	15.9 (8.0)	15.1 (2.6)	17.5
	S.a.	15.4 (4.8)	16.9 (9.3)	16.2 (2.5)	

[a]Results for the Girard and Trinfer products are given as %; those for Yectofer are given as mg ml^{-1}. [b]Cal., calibration plot; s.a., standard addition. [c]Each result is the average of nine determinations, with % relative standard deviation in parentheses.

used. There is reasonable agreement among the different methods. The imprecision of both amperometric methods is poorer than for the photometric method. The poorer imprecision of the dual-electrode method is attributed to the lower sensitivity noted earlier.

We thank CONICIT (Caracas, Venezuela) for partial financial support (Grant No. S1-1265) and Laboratorio Farmacológico Venezolano and Farma, S.A. for supplying the samples.

REFERENCES

1 W. L. Candill, J. O. Howell and R. M. Wightman, Anal. Chem., 54 (1982) 2532.
2 P. T. Kissinger, C. Refshange, R. Dreiling and R. N. Adams, Anal. Lett., 6 (1973) 465.
3 P. T. Kissinger, Anal. Chem., 49 (1977) 447.
4 A. Flores, L. E. Leόn and A. Calvo, Anal. Lett., 17 (1984) 1913.
5 R. Eggli and R. Asper, Anal. Chim. Acta, 101 (1978) 253.
6 J. W. Diecker and W. E. van der Linden, Anal. Chim. Acta, 114 (1980) 267.
7 S. A. McClintock and W. C. Purdy, Anal. Lett., 14 (1981) 791.
8 P. Maitoza and D. C. Johnson, Anal. Chim. Acta, 118 (1980) 233.
9 A. N. Ströhl and D. J. Curran, Anal. Chem., 51 (1979) 1045.

Analytica Chimica Acta, 192 (1987) 355—359
Elsevier Science Publishers B.V., Amsterdam — Printed in The Netherlands

Short Communication

FAST-RESPONSE SYSTEM FOR SIGNAL ACQUISITION AND PROCESSING IN ELECTROTHERMAL ATOMIC ABSORPTION SPECTROMETRY

EDWIN ALLEN and KENNETH W. JACKSON*

Department of Chemistry, University of Saskatchewan, Saskatoon, Sask., S7N 0W0 (Canada)

(Received 15th September 1986)

Summary. An electrothermal atomic absorption (a.a.) spectrometer is modified to allow accurate correlation of absorbance and pyrometrically measured temperature with time. To by-pass the slow electronics of the spectrometer, the signal is fed from the preamplifier immediately after the photomultipier tube to a 12-bit A/D converter mounted in a 320K IBM-PC microcomputer. The wall temperature of the graphite furnace, measured with an automatic optical pyrometer, is recorded simultaneously with absorbance by feeding the pyrometer output to a second channel of the A/D board. Fast deuterium-arc background correction is also done. Background-corrected absorbance, background absorbance and temperature are recorded at 60 Hz. A simple algorithm allowed experimental activation energies to be calculated automatically. All programming was in BASIC or PASCAL.

In recent years, improvements in electrothermal atomic absorption spectrometry (a.a.s.) have led to substantial reductions in interferences. Slavin and Carnrick [1] incorporated these improvements in their "stabilized-temperature platform furnace". They emphasised that several features need to be combined to minimize interferences. These include atomization from a L'vov platform inside the furnace tube [2], the use of matrix modifiers [3] (often needed to delay atomization until the vapour phase is nearly isothermal), effective background correction, the measurement of peak areas rather than heights, and fast digital electronics. With this technology, different workers could often obtain similar sensitivities for a given element [1].

The need for fast electronics in electrothermal a.a.s. was realized as early as 1975 [4]. More recently, it was shown [5] that the transient absorbance signal from an electrothermal atomizer is distorted if instrument response is slow, and the linear range of calibration curves is consequently reduced. The more expensive modern a.a. spectrometers usually have fast enough response, but older instruments and modern cheaper instruments are often too slow for use with an electrothermal atomizer. An additional highly desirable feature is an optical pyrometer to allow simultaneous high-speed monitoring of absorbance and temperature. This allows the operator to be sure that analyte vaporization does not occur before near-isothermal conditions are established.

0003-2670/87/$03.50

To date, no commercial instrument has this capability. Bayunov et al. [6] made optical temperature measurements directly by transmitting radiation from the atomizer into the spectrometer through a fibre-optic light guide. This avoided the use of an optical pyrometer, but required absorbance and temperature to be measured sequentially.

In this communication, a modification of a cheap commercial a.a. spectrometer is described, which allows the slow electronics to be by-passed, and which provides simultaneous background-corrected absorbance and pyrometric temperature measurements at a rate of 60 Hz.

Experimental

Instrumentation. A Perkin-Elmer Model 2280 a.a. spectrometer, equipped with deuterium-arc background correction, and a Perkin-Elmer HGA 500 atomizer were used. To obtain undistorted signals from the spectrometer at its modulation frequency (60 Hz), the signal-processing electronics were by-passed. The analog output signal from the preamplifier immediately following the photomultiplier tube was fed to one channel of an 8-channel differential input 12-bit analog-to-digital converter (ADC) board (Model DT2801, Data Translation, Marlborough, MA). This board was mounted in a 320K IBM-PC microcomputer with dual 360K floppy-disk drives, a 640 × 200 B/W graphics monitor and an Okidata Microline 92-dot matrix printer. The graphite-tube wall temperature was measured by focussing an optical pyrometer (Model 1100, Ircon, Niles, IL) either through the sample injection hole in the tube or on the outside wall. The output from the pyrometer was fed to an amplifier (fabricated from an Analog Devices AD524 IC chip) with appropriate offset and gain combinations needed to match the output to the ADC channels. This signal was fed to a second channel of the ADC board.

The synchronous timing of these analog signals, together with three digital control signals, is shown in Fig. 1. Signal D is the output from the a.a. preamplifier. It is a time-modulated composite of three analog signals: the hollow-cathode lamp signal (HCL), the dark current (DC), and the deuterium-lamp background signal (D_2). Signal E is the amplified output of the optical pyrometer. The timing of all signals inside the spectrometer is controlled by a 960-Hz master clock pulse train (signal C) which is phase-locked to 16 times the 60-Hz mains frequency. This was fed to the ADC board through a buffer amplifier, and alternately clocked in the conversions on the two signal channels. A trigger pulse was generated by combining two signals using a single 4011 CMOS quad NAND gate. The first signal was the READ pulse from the atomizer (signal A) which allowed data collection to be synchronized with the heating of the graphite furnace tube. This signal normally goes to the spectrometer to trigger integration at the instant the "atomize" stage of the furnace heating cycle is initiated. The second component of the trigger pulse was the SAMPLE BEAM DECODER (signal B), which is generated within the spectrometer and locked to the HCL component of the signal pulse train. This was clipped back from 3.6 ms to 6 μs. It ensured that data acquisition started when the hollow-cathode lamp pulsed on after the start of the atomize stage.

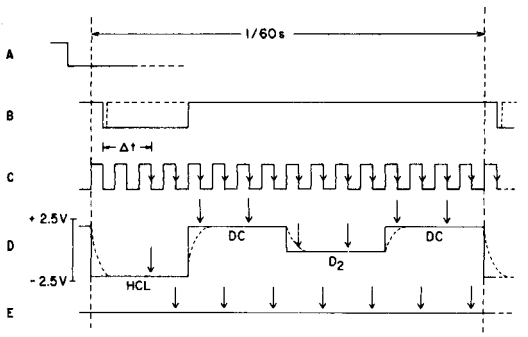

Fig. 1. The synchronous signals. A, Electrothermal atomizer read pulse; B, sample beam decoder; C, 960-Hz clock; D, spectrometer analog output; E, optical pyrometer analog output; HCL, hollow-cathode lamp; DC, dark current; D_2, deuterium lamp; Δt, time delay between triggering and the onset of data collection.

The first clock pulse received by the ADC board after the trigger pulse is used to synchronize the on-board circuitry. Hence, as shown in Fig. 1, data acquisition was initiated on the second clock pulse after the trigger pulse, resulting in the short time delay, Δt. The timing of alternate acquisition by the two ADC channels (signals D and E, respectively) is also shown in Fig. 1.

A useful feature of the ADC board is its operation in a direct-memory access mode. This allows the board to acquire a block of data and transfer it directly to the main computer memory without CPU intervention. Therefore, data was acquired at high rates even when a relatively slow, high-level interpreter language such as BASIC was used.

Software. Because of distortion at the leading edge of each pulse from the preamplifier (Fig. 1), the first reading on the pulse is discarded. One HCL intensity and one deuterium-lamp intensity are then calculated per cycle (16.7 ms) by subtracting the average of the two dark-current signals which bracket each lamp signal. This allows high-speed (60-Hz) background correction. The HCL and D_2-lamp intensities at the baseline level, i.e., before atomization has occurred, are each averaged to give an I_0 value. Then every HCL and D_2-lamp signal can be converted to absorbance. Similarly, a baseline for the optical pyrometer readings is established and each reading is converted to a percentage of the full-scale deflection (% FSD) of the pyrometer.

A routine was written to plot absorbances and optical pyrometer "% FSD" readings on the same time axis. The pyrometer has a number of modules which can be substituted to select different temperature ranges. Hence, in order to convert each reading to a temperature, it would be necessary to store in memory calibration data for all of the modules. It was more convenient to output the readings as "% FSD" and then convert selected readings (such as peak appearance) to temperatures afterwards. Depending on operator selection, the program will plot uncorrected absorbance, background-corrected absorbance, background absorbance, or any combination of these. The

completed graph is transferred automatically to the dot matrix printer. This requires the IBM graphics routine (on the system operating disk).

The total RAM requirement for reading, manipulating and outputting data is 320K.

Results and discussion

A typical graphics printout of transient absorbance and temperature vs. time is shown in Fig. 2. This was obtained from an aqueous slurry of the clay montmorillonite which contains traces of lead (0.8 ng of lead in this aliquot). For clarity of presentation, a simple (3-point) running average smoothing routine was applied to these data. However, all mathematical manipulation is performed on the unsmoothed data. Shown in the figure are the background-corrected absorbance of lead at 283.3 nm, the background (non-specific) absorbance from the clay matrix, and the tube-wall temperature curve from the optical pyrometer. This diagram shows clearly that all of the absorbance signal is in the near-isothermal region (after the temperature curve has reached a plateau). However, detailed information is obtained from the data printout which accompanies the graph. Appearance time is computed from an algorithm which detects a continuous change in the slope, and all three absorbance peak areas (as absorbance × seconds) are printed. Over an operator-selected time range, all three absorbances and the optical pyrometer reading are then printed at each 16.7-ms interval. Hence, it is possible to correlate absorbance with time and temperature to an accuracy of 16.7 ms. This has proved invaluable in work [7, 8] on the atomization of solid samples introduced as slurries. Of particular interest are the appearance temperature (T_{app}), peak-maximum temperature (T_{peak}), the integrated absorbance, and the shapes of the peaks. The Arrhenius relationship between ln k and $1/T$ for a first-order kinetic process can be used in electrothermal a.a.s. to enable energies of activation (E_a) to be calculated. Sturgeon et al. [9] showed that, for the initial part of the absorbance signal, a graph of ln A vs. $1/T$ is linear and E_a is derived from

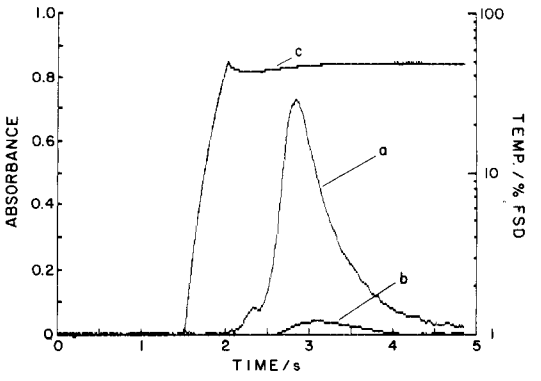

Fig. 2. A typical instrumental output for 0.8 ng of lead in a slurry of montmorillonite: (a) Background-corrected absorbance; (b) background absorbance; (c) pyrometer signal.

the slope. The presentation of data has allowed the easy preparation of Arrhenius plots by this method [8]. Alternatively, the method of Smets [10] has been used; the rate constant (k) is calculated from the ratio of the absorbance at time, t, to the integral of the remainder of the absorbance peak. A short subroutine allows this to be calculated easily. This facility was also available on the system described by Bayunov et al. [6].

Conclusions

This hardware/software system was designed specifically for research purposes where transient absorbance vs. temperature characteristics in electrothermal a.a.s. are used to study atomization behaviour. However, for routine work, it is important to ensure that atomization does not occur prior to near-isothermal conditions. Therefore, the ability to record pyrometric temperature data and absorbance simultaneously would be a highly desirable feature in all routine electrothermal a.a. spectrometers. Fast-response electronics are also important, and this system could be used to upgrade slower instruments. The ability to program in BASIC facilitates software modification for specific needs, but a disadvantage is the slow processing speed of BASIC. This does not affect data acquisition from the spectrometer, because the ADC board can be operated in the direct-memory access mode. However, the subsequent processing and plotting of data are quite slow. For research use, the processing time of several minutes is tolerable, but this would not be acceptable for routine work when large numbers of samples need to be analyzed. A much faster version of the software has been written in PASCAL. With this, complete data processing takes only a few seconds.

The ADC board and the BASIC or PASCAL software for data acquisition will operate in microcomputers compatible with the IBM-PC. The data-processing and graphics software will, with slight modification, be suitable for digital data collected by other hardware systems. More detailed information of the hardware and a complete listing of the software are available from the authors on request.

We are grateful to the Natural Sciences and Engineering Research Council of Canada for financial support of this work. Also, we thank M. W. Hinds who translated the BASIC program into PASCAL.

REFERENCES

1 W. Slavin and G. R. Carnrick, Spectrochim. Acta, Part B, 39 (1984) 271.
2 B. V. L'vov, Spectrochim. Acta, Part B, 33 (1978) 153.
3 R. D. Ediger, At. Absorpt. Newsl., 14 (1975) 127.
4 R. E. Sturgeon, C. L. Chakrabarti and P. C. Bertels, Anal. Chem., 47 (1975) 1250.
5 D. D. Siemer and J. M. Baldwin, Anal. Chem., 52 (1980) 295.
6 P. A. Bayunov, A. S. Savin and B. V. L'vov, At. Spectrosc., 3 (1982) 161.
7 R. Karwowska and K. W. Jackson, Spectrochim. Acta, Part B, 41 (1986) 947.
8 R. Karwowska and K. W. Jackson, J. Anal. At. Spectrom., in press.
9 R. E. Sturgeon, C. L. Chakrabarti and C. H. Langford, Anal. Chem., 48 (1976) 1792.
10 B. Smets, Spectrochim. Acta, Part B, 35 (1980) 33.

Analytica Chimica Acta, 192 (1987) 361—366
Elsevier Science Publishers B.V., Amsterdam — Printed in The Netherlands

Short Communication

DETERMINATION OF SULFUR, NICKEL AND VANADIUM IN FUEL AND RESIDUAL OILS BY X-RAY FLUORESCENCE SPECTROMETRY

ERIC R. DENOYER and LESTER A. SIEGEL
American Cyanamid Company, 1937 West Main Street, Stamford, CT 06904 (U.S.A.)
(Received 24th March 1986)

Summary. The determination of sulfur, nickel and vanadium in fuel and residual oils by wavelength-dispersive x-ray fluorescence spectrometry is reported. Calibration is initially established with matrix-matched synthetic standards, and maintained free of instrumental drift by daily normalization to a reference standard. An epoxy-cast reference standard pellet offers mechanical rigidity and chemical stability for at least nine months. Matrix effects of sulfur and carbon are studied and corrected. Results for NBS SRM oils fall within the NBS certified values, with imprecision (% RSD) for S, Ni, and V of 1.1, 1.5 and 1.0%, respectively. Detection limits (3 s.d.) are 20 $\mu g\ g^{-1}$ for sulfur and 0.8 $\mu g\ g^{-1}$ for Ni and for V.

In developing catalysts for the petroleum industry, a method for determining sulfur, nickel, and vanadium in fuel and residual oils is needed. Sulfur levels are used to monitor hydrotreating catalyst efficiency. Nickel and vanadium are monitored because these metals poison cracking catalysts, decreasing catalyst activity and selectivity.

X-ray fluorescence (x.r.f.), atomic absorption and plasma emission spectrometry have been used to quantify trace-element impurities in petroleum products [1—5]. In this work, x.r.f. was chosen primarily because of its high sensitivity for sulfur and because the x.r.f. measurement is made directly on the oil sample itself. This obviates any sample dilution, heating or digestion and avoids calibration problems associated with sample nebulization [3]. Analyses are possible with minimum support from operators, and can be done unattended with an autosampler and a computer-controlled spectrometer. This is important because the method reported here was developed to support a pilot-plant catalyst testing facility.

In this method, calibration is established with matrix-matched synthetic standards. Instrumental drift is corrected by daily normalization of the calibration curve to a reference normalization standard. If available, a stable natural oil sample can be used. Synthetic oil standards generally suffer from instability caused by precipitation of the organometallic species used in their preparation. Solid pellets offer the advantage of long-term chemical stability, and freedom from day-to-day signal fluctuations arising from variations in the preparation of liquid sample cells. However, preparing pressed or fused

0003-2670/87/$03.50

pellets with long-term mechanical stability can be difficult. In this communication, a simple approach for preparing a stable, mechanically rigid epoxy-cast standard pellet is described. Application to the x.r.f. determination of S, Ni and V in fuel and residual oils is demonstrated.

Experimental

Apparatus. All measurements were made with a Siemens SRS-200 wavelength-dispersive x-ray fluorescence spectrometer equipped with a PDP-11/03 computer (Digital Equipment Corporation), and an 80-position autosampler. Samples were held in standard 40-mm diameter cells with Mylar support film. Measurements were done under a helium atmosphere with a Cr-target side-window tube. The secondary fluorescent x-radiation was dispersed with a graphite crystal and detected with both a gas-flow proportional counter and a scintillation counter.

X-ray measurements. Sample cells were rotated during measurement. In the case of sulfur, counts were taken for 20 s at the peak and one background position. For Ni and V, counts were taken for 40 s at the peak and two background positions. In all cases, sample depth was maintained at or greater than about 1 cm This ensures infinite thickness (ca. 0.4 cm) for the most energetic x-ray (Ni K_α). Measurement conditions are listed in Table 1.

Chemicals. Reagent-grade xylene, vanadium oxide, nickel oxide and sodium sulfate were obtained from J. T. Baker Chemical Co. Bis(2-ethylhexyl)amine, 6-methyl-2,4 heptanedione and 2-ethylhexanoic acid were from Eastman Kodak Company. National Bureau of Standards Standard Reference Materials (SRM) 1065B (nickel cyclohexanebutyrate) and 1052E [bis(1-phenyl-1,3-butanediono)oxovanadium(IV)] were used to prepare standards for Ni and V. Di-n-butyl sulfide (Philips Petroleum Company) was used to prepare standards for sulfur. X-ray MIX polymeric pellet binder (Chemplex) and EPO-MIX epoxide (Buehler) were used to prepare the normalization pellet standard.

Standard solutions. Stock solutions containing 502.9 $\mu g\ g^{-1}$ nickel and 501.3 $\mu g\ g^{-1}$ vanadium were prepared with nickel cyclohexanebutyrate and bis(1-phenyl-1,3-butanediono)oxovanadium(IV), respectively, according to the procedure supplied with these SRM.

Standard solutions were prepared by weight with xylene, paraffin oil, di-n-butyl sulfide, and the nickel and vanadium organometallic stock solutions. The ranges of concentrations were 6—30 $\mu g\ g^{-1}$ for Ni, 20—100 $\mu g\ g^{-1}$ for V and 0.01—3% for S. The carbon content of the standard solutions was matched to that of the oil samples (86.8%) by adjusting the ratio of xylene and paraffin oil.

Test solutions. Several test solutions were prepared to study matrix effects. Di-n-butyl sulfide and the organometallic stock solutions were mixed with appropriate amounts of xylene and paraffin oil to contain 1% S, 25 $\mu g\ g^{-1}$ Ni and 25 $\mu g\ g^{-1}$ V, with carbon varying in the range 85—89%

TABLE 1

Conditions for x-ray fluorescence measurement at the K_α lines

Parameter	Sulfur	Nickel	Vanadium
Crystal	Graphite	LiF 200	LiF 200
Peak angle (°2θ)	106.4	48.66	76.95
High background (°2θ)	109	49.6	78.5
Low background angle (°2θ)	—	47.5	76.0
Counting time (s)	20	40	40
Detection[a]	FP	FP, S	FP, S
Tube voltage (kV)	50	50	50
Tube current (mA)	40	40	40

[a]FP, flow proportional to counter; S, scintillation counter.

Other solutions contained 86.8% C, 25 $\mu g\ g^{-1}$ V, and sulfur in the range 0.01—3%; and 86.8% C, 1% S, 25 $\mu g\ g^{-1}$ V, and nickel in the range 5.0—75.0 $\mu g\ g^{-1}$.

Normalization standard pellets. The normalization standard developed for this application was cast as an epoxy-resin pellet. Nickel oxide, vanadium trioxide and a polymeric x-ray pellet binder were mixed to achieve approximately 6000 $\mu g\ g^{-1}$ each of nickel and vanadium. The binding material was used as a convenient powder dilution medium for the Ni and V, owing to its purity and low x-ray absorption characteristics. A 0.5-g portion of this powder mixture was mixed, with grinding, with 1.3 g of anhydrous sodium sulfate. This was added with slow stirring to 28 g of pre-mixed epoxy resin. This addition was done directly in a 40-mm x-ray sample cell (without cover film) which had been glued onto a smooth layer of Teflon-coated aluminum foil laid on a glass plate. The epoxy composite was left to set at room temperature for 24 h. It should be noted that mixing the powder with the epoxy resin must be done slowly to minimize entrapment of air bubbles. After the epoxy had set, the pellet-cell system was snapped off from the Teflon-coated foil resulting in a smooth, hard surface. The pellet was stored under vacuum until use.

Results and discussion

Interelement effects. No significant effect of varying carbon content between 85 and 90% could be detected on the S, Ni, or V signals in the concentration ranges studied. The least-squares regression lines of analyte signal intensity as a function of carbon content had slopes and standard deviations (±1 s.d.) as follows: $(-0.11 \pm 0.16) \times 10^3$ cps/%C for S, $(0.009 \pm 0.01) \times 10^3$ cps/%C for Ni, and $(-0.009 \pm 0.01) \times 10^3$ cps/%C for V. Based on the Student t-test, neither of these slopes is different from zero at the 99% confidence level. The least-squares regression line of the vanadium signal intensity as a function of nickel content had a slope and standard deviation of -0.19 ± 0.15 cps/$\mu g\ g^{-1}$ Ni. From the t-test, this slope is also

not significantly different from zero at the 99% confidence level. However, sulfur was found to have a significant suppression effect on the signals of Ni and V (Fig. 1). Thus, an influence factor compensating for the effect of sulfur in the sample must be incorporated into the calibration scheme for Ni and V.

Calibration. Initial calibration of the spectrometer was done with the synthetically blended liquid standards. The calibration curve for sulfur, derived from a multiple-regression best fit to a second-order function relating net signal intensity to sulfur concentration, is shown in Fig. 2. Calibration for Ni and V was based on the model of Lucas-Tooth and Pyne [6]. This results in a calibration surface describing the dependence of analyte signal intensity on S K_α x-ray intensity (proportional to S concentration), as well as on analyte (Ni or V) concentration.

X-ray drift was corrected by daily normalization to the reference standard pellet. The x-ray intensity of each analyte in the standard pellet was measured initially at the time of calibration. Henceforth, for each sequence of samples, the intensity of the standard pellet was measured again, and ratioed to the original intensity at the time of initial calibration. This intensity ratio was then used to correct intensity measurements for instrumental drift.

Accuracy and precision. The stability of the standard pellet was investigated. The S K_α x-ray intensity was measured 21 times over a period of 34 days. Sulfur was chosen to study the stability of the standard pellet because it has the lowest x-ray energy of the three analytes. This means that the sulfur radiation is measured from a shallower depth than the Ni or V radiation, and is most sensitive to any possible degradation of the pellet surface. To compensate for daily instrumental drift, the S K_α x-ray intensity of a reference fuel oil, set aside for this purpose, was measured under the same conditions. The ratio of the S K_α intensity of the pellet to that of the fuel oil reference sample was then calculated. No significant change in this

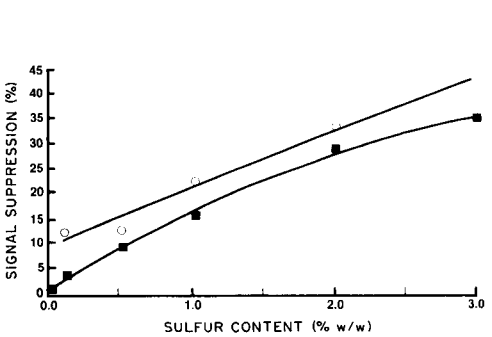

Fig. 1. Effect of sulfur content on the nickel (■) and vanadium (○) x-ray intensities.

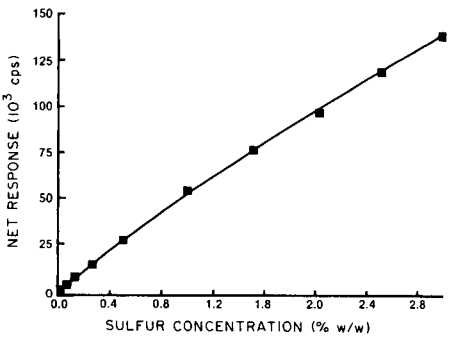

Fig. 2. Calibration curve for x.r.f. determination of sulfur in oil.

intensity ratio was observed over the 34-day period. The slope of the least-squares regression line relating the intensity ratio and time was not significantly different from zero at the 99% confidence level.

The stability of the pellet was investigated over a longer period of time (4 months) by measuring S, Ni and V in SRM 1634a Residual Oil. The results (Table 2) demonstrate the long-term stability of the pellet and the accuracy of the method. This was the only NBS SRM available which was certified for Ni and V content. The accuracy of the method for sulfur was further demonstrated by measuring sulfur in various other SRM. These results are summarized in Table 3. Again, the agreement with the certified values is good.

The precision of the method was estimated by means of the pooled standard deviation derived from the replicate runs with the SRM (Table 2). The imprecision (% RSD) was 1.1% for S, 1.5% for Ni, and 1% for V. The

TABLE 2

Results for S, Ni and V in NBS SRM 1634a

Date (Month-day-year)	No. of replicates	Concentration[a]		
		S (%, w/w)	Ni ($\mu g\ g^{-1}$)	V ($\mu g\ g^{-1}$)
6-25-85	5	2.83 ± 0.03	54.0 ± 1.7	28.5 ± 0.3
7-12-84	3	2.80 ± 0.04	53.1 ± 0.6	28.2 ± 0.4
7-24-84	4	2.87 ± 0.03	54.0 ± 0.6	28.4 ± 0.3
8-2-84	4	2.86 ± 0.02	53.8 ± 0.6	28.1 ± 0.3
10-25-84	4	2.85 ± 0.03	54.1 ± 0.5	27.9 ± 0.05
Certified value		2.85 ± 0.05	56 ± 2	29 ± 1

[a]Uncertainties are reported as 95% confidence limits.

TABLE 3

Results for sulfur in various oil standard reference materials

SRM	Sulfur concentration (%, w/w)[a]	
	Measured	Certified
1624a	0.144 ± 0.004	0.141 ± 0.002
1623a	0.242 ± 0.002	0.240 ± 0.003
1619	0.71 ± 0.01	0.719 ± 0.007
1621a	0.94 ± 0.02	0.950 ± 0.005
1622b	1.94 ± 0.04	1.982 ± 0.018

[a]Uncertainties reported as 95% confidence limits.

detection limits, based on 3 times the standard deviation of the background noise were 20 $\mu g\ g^{-1}$ for sulfur and 0.8 $\mu g\ g^{-1}$ each for nickel and vanadium.

REFERENCES

1 S. N. Sharma, J. Sci. Ind. Res., 42 (1983) 341.
2 J. V. Thomas and S. Ringer, Anal. Chem., 55 (1983) 478R.
3 J. L. Fabec and M. L. Ruschak, Anal. Chem., 57 (1985) 1853.
4 H. Kubo, R. Bernthal and T. R. Wildeman, Anal. Chem., 50 (1978) 899.
5 A. N. Yousif and H. Al-Sharistani, Int. J. Appl. Radiat. Isotop., 28 (1977) 759.
6 H. J. Lucas-Tooth and E. C. Pyne, Adv. X-ray Anal., 7 (1964) 523.

Analytica Chimica Acta, 192 (1987) 367—372
Elsevier Science Publishers B.V., Amsterdam — Printed in The Netherlands

Short Communication

IDENTIFICATION OF THE COMPOSITION OF OLIGOSACCHARIDES AND POLYSACCHARIDES BY PYROLYSIS/CAPILLARY GAS CHROMATOGRAPHY

R. J. HELLEUR[a], D. R. BUDGELL[b] and E. R. HAYES*
Department of Chemistry, Acadia University, Wolfville, Nova Scotia B0P 1X0 (Canada)
(Received 7th August 1986)

Summary. Pyrolysis/capillary gas chromatography is used for the characterization of the monomer composition of various oligosaccharides and polysaccharides including glucose-containing disaccharides, glucans, a galactomannan and an arabinogalactan. The chromatograms showed many common pyrolysis products, but also unique anhydrosugar products (e.g., 1,6-anhydroglucopyranose, 1,4-anhydroarabinopyranose, 2,6-anhydrofructofuranose) derived from each type of saccharide unit present in the samples. Reasonable values of the monomer composition of the polysaccharide can also be obtained from the pyrograms. The method is rapid and direct, requiring no sample preparation.

Pyrolysis in combination with gas chromatography (py./g.c.) has been used extensively to characterize biological and synthetic materials [1] by the distinctive gas chromatogram (pyrogram), or by specific volatile pyrolysis products which can be correlated with their chemical structure. Carbohydrates have occasionally been examined by py./g.c. but with limited success. Recently, promising results from a study involving the characterization of algal galactans and their saccharide compositions [2] prompted further exploration of the potential of py./g.c. for characterizing the saccharide composition of other types of carbohydrates. It has been shown [3] that py./g.c. of the monosaccharides can be used successfully to identify the structures of many of the stereoisomers of carbohydrates. Each monosaccharide (e.g., glucose, arabinose) produces its characteristic volatile anhydrosugar (i.e., 1,6-anhydroglucose, 1,4-anhydroarabinose, etc.) thus providing a basis for distinguishing among mixtures of saccharides and their isomers.

This study is part of a systematic investigation aimed at improving py./g.c. as a rapid technique for characterizing complex carbohydrates. In the study of anhydrosugars from hexoses and pentoses, pyrolysis products were identified by py./g.c./mass spectrometry [3]. In this communication, these

[a]Present address: Chemistry Department, Memorial University, St John's, Newfoundland, Canada.
[b]Present address: Chemistry Department, McGill University, Montreal, Canada.

0003-2670/87/$03.50

structural assignments of the pyrograms of the simple monosaccharides are used and the pyrolytic technique is applied to selected oligosaccharides and polysaccharides.

Experimental

Pyrograms were obtained with a Chemical Data Systems Pyroprobe 120 equipped with a coil filament that was interfaced to a Hewlett-Packard 5880A gas chromatograph equipped with a flame ionization detector and a fused silica capillary column (J&W, DB-1701 bonded phase, 1.0 μm thick, 30 m × 0.329 mm). More details about the experimental conditions are given in another paper [3]. Samples were powdered and weighed to 100—150 μg. It was noted that smaller samples (30 μg) could be used to obtain similar results. Each carbohydrate sample was processed in triplicate. Peak-height ratios of any sample varied by less than 10%.

The arabinogalactan which was isolated from larch wood was a gift from Dr. G. Hay, Queen's University, Ontario. All other samples listed in Table 1 were obtained from Sigma (St. Louis, MO). Amylose, isolated from potato cellulose material (Sigmacell), had a 50-μm particle size, and the dextran was grade no. D-6649.

Results and discussion

Carbohydrates were selected on the basis that their saccharide compositions and, in the case of the glucans, linkage types were different. The polysaccharides are all from plant sources. Table 1 lists the carbohydrates that were examined by py./g.c. Included were disaccharides having structures similar to those of the polysaccharides examined. Several fructose-containing oligosaccharides were pyrolyzed for the combination of ketohexose and aldohexose.

All samples gave pyrograms consisting of pyrolysis products common to their hexose/pentose compositions. More importantly, every pyrogram showed distinctive anhydrosugar products derived from each type of saccharide unit present in the sample. Discussion of the results will focus on a selected number of carbohydrates and their pyrograms, illustrating the usefulness of py./g.c. for characterizing the composition of higher-molecular-weight carbohydrates. The peaks of the pyrograms are labelled to indicate the type of saccharide unit from which the identified anhydrosugar product originated. In the case of the pyrolysis of glucose- and galactose-containing samples, two and three types of anhydrosugars were detected, respectively. The identities of the various anhydrosugar products were assigned by their retention times. Specific retention time data are reported in a previous paper [3]. More detailed discussion of the general study of carbohydrate pyrolysis and products observed in the programs is available [2, 3].

Pyrograms of glucose-containing disaccharides and polysaccharides. Glucose-containing polysaccharides, namely the glucans, are the most abundant biopolymers. The glucans, cellulose and dextran, and their respective

TABLE 1

List of oligosaccharides and polysaccharides examined by py./g.c.

Compound	Structure
Cellobiose[a]	4-*O*-β-D-glucopyranosyl-D-glucose
Isomaltose[a]	6-*O*-α-D-glucopyranosyl-D-glucose
Maltose	4-*O*-α-D-glucopyranosyl-D-glucose
Gentiobiose	6-*O*-β-D-glucopyranosyl-D-glucose
Sucrose[a]	*O*-β-D-fructofuranosyl-*O*-α-D-glucopyranoside
Lactulose	4-*O*-β-D-galactopyranosyl-D-fructose
Raffinose	*O*-α-D-galactopyranosyl-(1 → 6)-α-D-glucopyranosyl-(1 → 2)-β-D-fructofuranoside
Stachyose[a]	*O*-α-D-galactopyranosyl-(1 → 6)-*O*-α-D-galactopyranosyl-(1 → 6)-*O*-α-D-glucopyranosyl-(1 → 2)-β-D-fructofuranoside
Lactose	4-*O*-β-D-galactopyranosyl-D-glucose
Galactose-mannose[a]	4-*O*-β-D-galactopyranosyl-D-mannose
Galactose-arabinose[a]	3-*O*-β-D-galactopyranosyl-D-arabinose
Cellulose[a]	→ 4)-*O*-β-D-glucopyranosyl-(→ 4)-*O*-β-D-glucopyranosyl-(1-
Dextran[a]	→ 6)-*O*-α-D-glucopyranosyl-(→ 4)-*O*-α-D-glucopyranosyl-(1-
Amylose	→ 4)-*O*-α-D-glucopyranosyl-(→ 4)-*O*-α-D-glucopyranosyl-(1-
Guar gum[a]	A galactomannan (see Fig. 3B for complete structure)
Larch wood galactan[a]	An arabinogalactan (see Fig. 4B for complete structure)

[a]The carbohydrate and its pyrogram are discussed in this communication.

disaccharides (repeating units) cellobiose and isomaltose (see Table 1), respectively, were examined, first, to observe whether there is abundant formation of the anhydrosugar, 1,6-anhydro-D-glucopyranose from glucose, and second, to examine whether the pyrolytic technique affords discrimination among homopolysaccharides of different glycosidic linkage and/or configuration.

Figures 1 and 2 show the pyrograms of cellobiose and cellulose, and isomaltose and dextran, respectively. The 1,6-anhydro-D-glucopyranose (gluco) is clearly present in all four pyrograms, but to a lesser extent in the pyrolysis products of the disaccharides. Because the disaccharide contains one saccharide that is not glycosidically linked and because anhydrosugars are known to be formed through a transglycosidation step [4], the formation of other products such as 5-hydroxymethylfuraldehyde (largest peak) is very significant. Cellulose and dextran, in contrast, give primarily 1,6-anhydroglucopyranose. The amount of anhydrosugar produced from the pyrolysis of cellulose is 30% greater than that obtained from dextran. It is believed that because initial transglycosidation occurs more easily through the participation of the free 6-hydroxyl group, the (1 → 6) linkages in dextran have hampered the formation of the more stable 1,6-anhydrosugar product.

Pyrograms of galactopyranosylmannose and galactomannan. Pyrograms of 4-*O*-β-D-galactopyranosyl-D-mannose and the galactomannan guar gum are shown in Fig. 3. The guar gum is thought to have a trisaccharide repeating

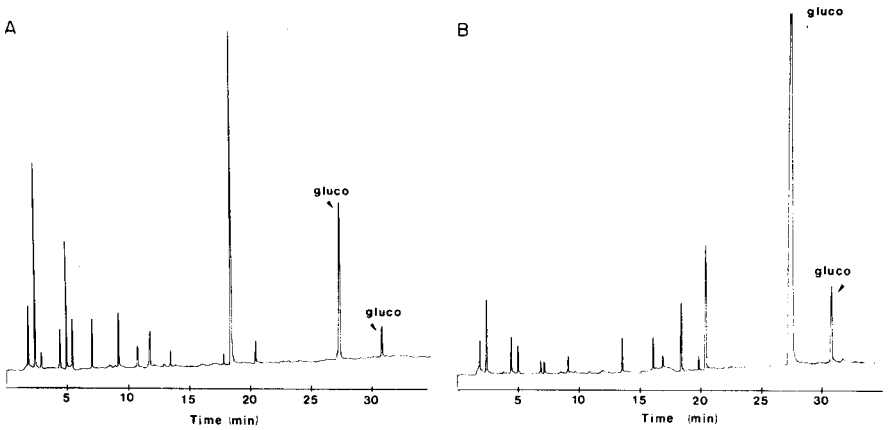

Fig. 1. Pyrograms of cellobiose (A) and cellulose (B).

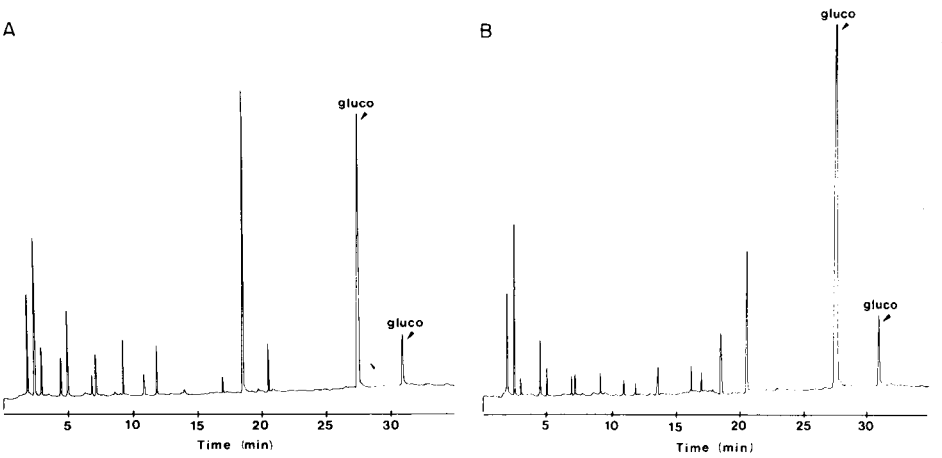

Fig. 2. Pyrograms of isomaltose (A) and dextran (B).

unit, a (1 → 4) linked -β-D-mannopyranosyl linear chain which contains one D-galactopyranosyl unit linked (1 → 6) to every second mannose unit. Both pyrograms in Fig. 3 exhibit the anhydrosugar products associated with galactose and mannose units, i.e., 1,6-anhydro-D-galactopyranose (and smaller amounts of 1,6-anhydro-D-galactofuranose and 1,4-anhydro-D-galactopyranose) (galacto) and 1,6-anhydro-D-mannopyranose (manno). It is worth noting that, although in the previous pyrolysis study [3] mannose gave about equal amounts of 1,6-anhydromannopyranose and 1,6-anhydromannofuranose products, the results of this study indicate that a glycosidically-linked mannose produces primarily its 1,6-anhydropyranose structure.

If only the yields of the respective 1,6-anhydrohexopyranose products are compared, the heights of the manno and galacto peaks are almost equal

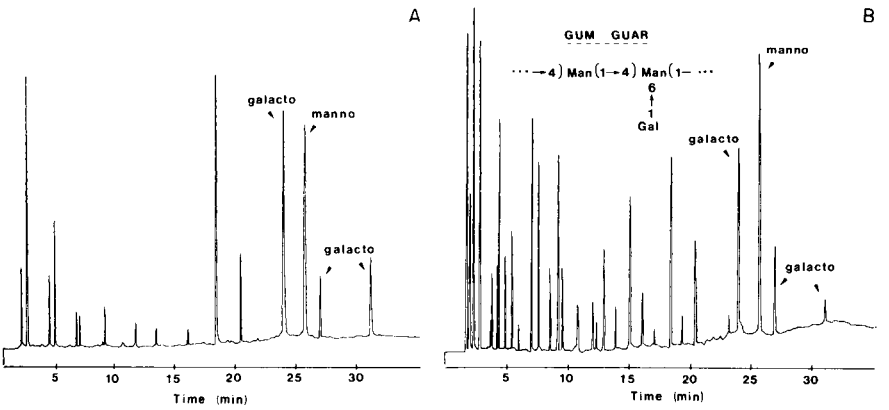

Fig. 3. Pyrograms of 4-*O*-β-D-galactopyranosyl-D-mannose (A) and the galactomannan, guar gum (B). In the structure, Man is *O*-β-D-mannopyranosyl and Gal is *O*-α-D-galactopyranosyl.

in the disaccharide pyrogram. This suggests that py./g.c. shows promise not only in identifying the nature of the saccharides present but also for quantitative work. The mannose/galactose ratio in guar gum, in general, has been found to be 2/1. Again, if only the 1,6-anhydrohexopyranose products are measured and compared, the pyrogram of guar gum shows that there is significantly more mannose in the sample. The composition of this sample of guar gum was not examined further. The significance of the formation of the two lesser anhydrosugars of galactose should be studied.

Pyrograms of galactopyranosylarabinose and arabinogalactan. The pyrograms of carbohydrates containing hexose-pentose, i.e., 3-*O*-β-D-galactopyranosyl-D-arabinose and a complex arabinogalactan (isolated from larch wood) are given in Fig. 4. The anhydrosugar associated with galactose units (galacto) is, again, clearly shown in both pyrograms. The product from arabinose, 1,4-anhydro-L-arabinopyranose (arabino), eluted sooner than its hexose counterpart. The ratio of galactose to arabinose in larch wood galactan is known to be approximately 6/1 (Fig. 4B). The pyrogram of the larch wood galactan (Fig. 4) reveals this saccharide composition.

Pyrograms of carbohydrates containing hexose-fructose. Pyrolysis yields of anhydrosugars from ketohexoses are very low [3]. The ketoses preferentially form the more stable furan pyrolysis products. The pyrolysis results of sucrose and stachyose show this to be true for fructose-linked sugars (see pyrograms in Fig. 5). Although the quantities of 2,6-anhydro-D-fructofuranose (fructo) are small, the anhydrosugar is clearly present in the pyrograms. All of the different anhydrosugars (6 in total) of the four saccharides of stachyose are well resolved in the pyrogram.

Conclusions

This study has shown that py./g.c. is a useful technique for identifying the composition of saccharides of low- and high-molecular-weight carbohydrates. The advantages of the method are that it is rapid, requires no sample prepara-

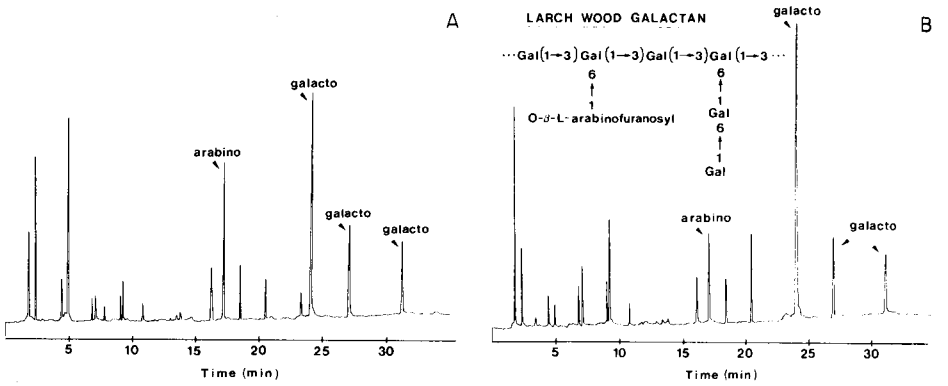

Fig. 4. Pyrograms of 3-*O*-β-D-galactopyranosyl-D-arabinose (A) and arabinogalactan from larch wood (B). In the structure, Gal is *O*-β-D-galactopyranosyl.

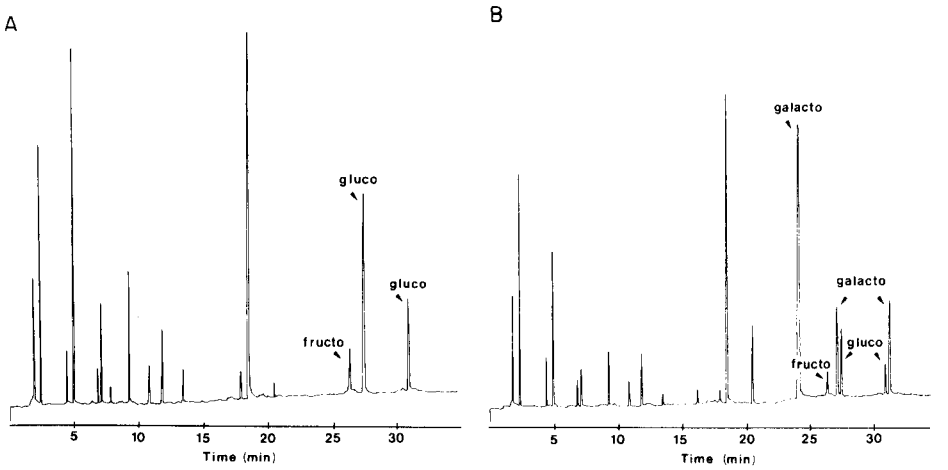

Fig. 5. Pyrograms of sucrose (A) and stachyose (B).

tion and is suitable for microscale samples. A promising feature is that quantitative measurements can be obtained directly from pyrograms. Quantitative examination of more complex polysaccharides (i.e., those containing uronic acids and aminosugars) by py./g.c. is in progress.

The authors thank the Atlantic Research Laboratory, NRC, Halifax for financial support.

REFERENCES

1 W. J. Irwin, Analytical Pyrolysis: A Comprehensive Guide, Dekker, New York, 1982.
2 R. J. Helleur, E. R. Hayes, W. E. Jamieson and J. S. Craigie, J. Anal. Appl. Pyrol., 8 (1985) 333.
3 D. R. Budgell, E. R. Hayes and R. J. Helleur, Anal. Chim. Acta, 192 (1987) 243.
4 F. Shafizadeh, J. Anal. Appl. Pyrol., 3 (1982) 283.

Analytica Chimica Acta, 192 (1987) 373—377
Elsevier Science Publishers B.V., Amsterdam — Printed in The Netherlands

Short Communication

SOLUBILITIES OF CHROMIUM(III) IN MOLTEN POTASSIUM HYDROGENSULFATE

L. DURAND-KEKLIKIAN*[a] and J. VEDEL

Laboratoire d'Electrochimie Analytique et Appliquée (Laboratoire Associé au C.N.R.S., n° 216), E.N.S.C.P., 11 Rue Pierre & Marie Curie, 75231 — Paris, Cedex — 05 (France)

(Received 14th July 1986)

Summary. The behavior of chromium(III) in molten potassium hydrogensulfate (220° C, $P(H_2O)$ = 0.04 atm) is reported. Chromium(III) exists as Cr^{3+} in acidic medium, and as chromium(III) sulfate, which is insoluble in neutral medium but soluble in basic medium as $Cr(SO_4)_2^-$. The values of acidity constants and the solubilities of Cr(III) are reported.

Previous studies [1] have shown that molten potassium hydrogensulfate undergoes self-dissociation characterized by the equilibrium $2\,HSO_4^- \rightleftharpoons H_2SO_4 + SO_4^{2-}$. The composition of the solvent depends on the vapor pressure of water because of the dehydration reaction $2\,HSO_4^- \rightleftharpoons S_2O_7^{2-} + H_2O$. At a fixed vapor pressure of water, the solvent composition is constant, as is the apparent autoprotolysis constant, $k_i = [H^+][SO_4^{2-}]$, which has the value $10^{-2.5}$ mol^2 kg^{-2} for potassium hydrogensulfate at 220° C and $P(H_2O)$ = 0.04 atm.

The measure of acidity was related to the quantity of dissolved sulfuric acid by the equation pH = $-\log [H_2SO_4]$, defining a pH scale which varies from zero (for 1 mol kg^{-1} sulfuric acid solution) to the value pH = $-\log (k_i/S)$ imposed by the solubility (S) of potassium sulfate [1]. Between these two values, the acidity of molten $KHSO_4$ can be modified, and therefore the nature and the properties of dissolved metal species in the solvent can also be changed.

Several studies of chromium compounds dissolved in molten hydrogensulfates have been reported [2—4]. Such studies are of interest because the electrodeposition of protective chromium coatings from molten salt baths [5—8] is used on a large scale industrially. Le Ber [2] reported high solubilities of Cr_2O_3 and CrO_3 in fused $NaHSO_4/KHSO_4$ at 160° C. He also showed, by voltammetric measurements, that chromium(VI) oxidizes vanadium(IV) to V(V). Spectral studies of chromium were done in $NH_4HSO_4/KHSO_4$ [3] and in $NaHSO_4/KHSO_4$ [4]. It was found that Cr(III) has

[a]Present address: Department of Chemistry, Clarkson University, Potsdam, NY 13676, U.S.A.

0003-2670/87/$03.50

maximum absorbance at 476 nm in $NH_4HSO_4/KHSO_4/H_2SO_4$ (molar fractions: 78.5:16.5:5.0), and maximum absorbance at 667 nm in $NaHSO_4/KHSO_4$. It was observed that the solvent decomposed Cr(VI) (introduced as CrO_3) to Cr(III). However, studies of chromium compounds in molten $KHSO_4$ appear to be non-existent.

The purpose of the present work therefore was to determine the solubilities of Cr(III) in molten $KHSO_4$ at 220°C and $P(H_2O)$ = 0.04 atm over a range of pH. In addition, the various acid—base species of Cr(III) in molten $KHSO_4$ were established. As in other molten hydrogensulfates [2—4], Cr(VI) behaves as a strong oxidizing agent in molten $KHSO_4$. It was observed that the latter solvent was oxidized by Cr(VI) (introduced as K_2CrO_4); it was not possible to show, by voltammetry, the oxidation of Cr(III) (introduced as $Cr_2(SO_4)_3 \cdot 8H_2O$) in acidic or basic media. Thus it was assumed that Cr(VI) can only exist in molten $KHSO_4$ if there is a high concentration of Cr(III). Therefore, the solubilities of Cr(III) vs. pH were evaluated spectrophotometrically rather than by potentiometric measurements.

Experimental

An excess of Cr(III) (as $Cr_2(SO_4)_3 \cdot 8H_2O$), enough to saturate the solution over the whole pH range, was introduced into molten $KHSO_4$ (220°C). The acidity was changed in the more acidic direction by addition of sulfuric acid (98%), and in the more basic direction by addition of potassium sulfate. Sulfate ions liberated by chromium(III) sulfate were neutralized by addition of sulfuric acid.

A partial water vapor pressure, $P(H_2O)$ = 0.04 atm, was applied to keep the solvent composition constant. The pH was calculated by means of the equation given above.

In the solubility measurements, the solution was agitated and aliquots (ca. 1.5 g) were taken from the molten salt every hour after the agitation had ceased for 15 min. These aliquots were taken by suction through a fritted glass filter (porosity 0) to avoid drawing off the precipitate. For each solubility value, several experiments were conducted (Table 1). In each experiment, which was done on a new solution, five consecutive samples were usually taken from the solution; about 250 g of $KHSO_4$ and 25 g of $Cr_2(SO_4)_3 \cdot 8H_2O$ were used. For the determination of Cr(III), the aliquots taken from the melt were dissolved in water. Chromium(III) was oxidized in very alkaline medium (pH > 9) to Cr(VI) with sodium peroxide solution [9], and quantified spectrophotometrically at 370 nm [10].

A least-squares fit of the data was used to evaluate the dependence of solubility on the acidity of the medium.

Results and discussion

The measured solubilities of Cr(III) are shown as a function of acidity in Table 1. These results indicate the formation of a species insoluble in neutral media but soluble in both highly acidic ad basic media. It is assumed that

TABLE 1

Solubility of chromium(III) in molten potassium hydrogensulfate at 220° C and $P(H_2O)$ = 0.04 atm

pH	Solubility[a] (10^{-2} mol kg^{-1})	pH	Solubility[a] (10^{-2} mol kg^{-1})
0	7.72 ± 2.25 (5)	0.6	4.58 ± 0.53 (5)
0.1	8.14 ± 1.41 (3)	1.6	12.60 ± 4.71 (5)
	7.64 ± 1.61 (5)	1.8	15.60 ± 2.08 (6)
	8.22 ± 2.07 (4)	2.0	20.86 ± 4.16 (5)
0.3	6.15 ± 0.077 (7)	2.1	25.28 ± 1.62 (5)
	6.16 ± 1.31 (3)		

[a]Mean with standard deviation; numbers of measurements are in parentheses.

$Cr_2(SO_4)_3$ is the insoluble species in neutral medium. The slope of the tangent to the curve, log S = f(pH) (Fig. 1), is 0.5 for pH = pK_i. This indicates that the dependence of Cr(III) solubility on the acidity is consistent with the reaction

$$Cr_2(SO_4)_3(s) + SO_4^{2-} \rightleftharpoons 2\,Cr(SO_4)_2^-$$

For an excess of $Cr_2(SO_4)_3$, d(log $[Cr(SO_4)_2^-]$)/d(—log $[H^+]$) = 0.5. The basic solute is believed to be $Cr(SO_4)_2^-$. It is considered that in acidic conditions, $Cr_2(SO_4)_3$ dissolves in $KHSO_4$ as $Cr_2SO_4^{4+}$ or as Cr^{3+}. The dominant acidic solute was ascertained from the absorption spectrum of Cr(III) in acidic media, which shows maxima at 463 and 650 nm (Fig. 2). The maximum absorptivity is ca. 120 kg mol^{-1} cm^{-1}. The spectrum recorded is similar to that obtained by Duffy and MacDonald [3] for the $NH_4HSO_4/KHSO_4/H_2SO_4$ melt. This indicates that the dominant acidic solute of $Cr_2(SO_4)_3$ is the Cr^{3+} ion.

On the basis of these measurements, the apparent solubility of Cr(III) in molten $KHSO_4$ can be written as

$$S = [Cr^{3+}] + [Cr_2(SO_4)_3] + [Cr(SO_4)_2^-] \quad (1)$$

The three concentrations occurring in Eqn. 1 are related to pH by means of the mass-action constants of the following acid—base equilibria:

$$2\,Cr^{3+} + 3\,SO_4^{2-} \rightleftharpoons Cr_2(SO_4)_3(s);\ K_3 = [H_2SO_4]^3/[Cr^{3+}]^2 K_i^3 \quad (2)$$

$$Cr_2(SO_4)_3(s) + SO_4^{2-} \rightleftharpoons 2\,Cr(SO_4)_2^-;\ K_2 = [Cr(SO_4)_2^-]^2[H_2SO_4]/K_i \quad (3)$$

and by the solubility of chromium(III) sulfate, S_{CS}. Equation 1 then becomes

$$S = ([H_2SO_4]^3/K_3K_i^3)^{1/2} + S_{CS} + (K_2K_i/[H_2SO_4])^{1/2} \quad (4)$$

If $(K_3K_i^3)^{1/2} = K_{a3}$ and $(K_2K_i)^{1/2} = K_{a2}$, S becomes equal to

$$S = 10^{(pK_{a3} - 3/2pH)} + S_{CS} + 10^{(1/2ph - pK_{a2})} \quad (5)$$

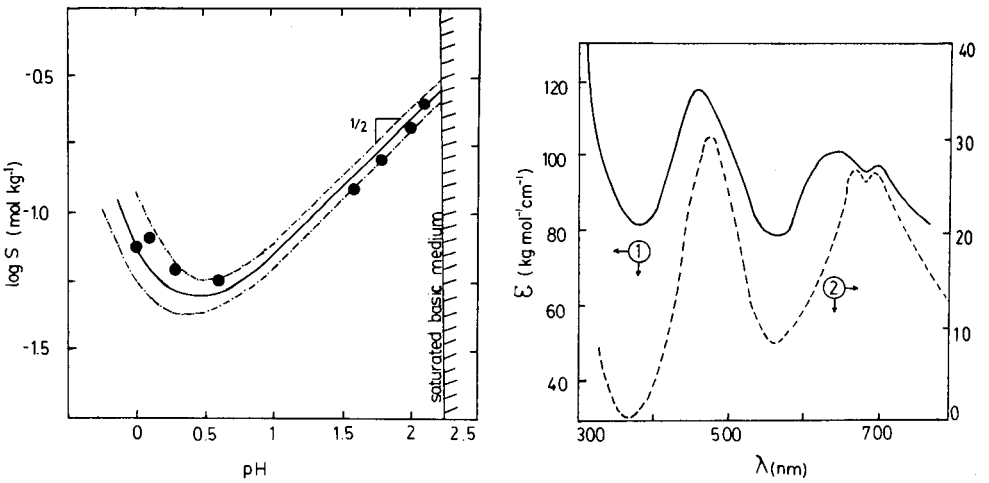

Fig. 1. Variation of chromium(III) solubility in molten potassium hydrogensulfate (220° C, $P(H_2O)$ = 0.04 atm), as a function of pH.

Fig. 2. Absorption spectra of Cr(III): (1) in molten $KHSO_4$ at 220° C with $P(H_2O)$ = 0.04 atm, in acid medium; (2) in molten $NH_4HSO_4/KHSO_4/H_2SO_4$ at 142° C [3].

The constants K_{a2}, K_{a3} and S_{CS} were evaluated from this relation which gives the theoretical values of the solubility in relation to pH, and also from the measured values of the solubility in relation to pH, by the least-squares method. The best fit between the calculated (Eqn. 5) and measured values of the solubility for each pH value was obtained for the following values: pK_{a2} = 1.66 ± 0.02; pK_{a3} = −1.22 ± 0.11 and S_{CS} = 0.

The apparent solubility, calculated with these constants, is shown as the continuous line in Fig. 1, and the area limited by the two dashed curves is the uncertainty domain of the solubility. The errors (±1 s.d.) about the constants pK_{a2} and pK_{a3} were evaluated by the pit-mapping technique [11]. The errors about pK_{a2}, pK_{a3} and S_{CS} allow determination of the error on the solubility S, by using the law of propagation of errors [12]. The calculation was also done assuming that the $Cr_2(SO_4)_3$ solubility is finite. The values obtained with the least-squares method were: pK_{a2} = 1.66 ± 0.02, pK_{a3} = −1.24 ± 0.16 and S_{CS} = (0.92 ± 5.1) × 10^{-3}. The good agreement between the two sets of constants and the very low value of the solubility show that it is not necessary to take the $Cr_2(SO_4)_3$ solubility into account.

The results reported here show the behavior of Cr(III) in molten $KHSO_4$. Chromium(III) exists as insoluble $Cr_2(SO_4)_3$ in acid medium (pH = 0.3), as Cr^{3+} in very strongly acidic medium and as $Cr(SO_4)_2^-$ in basic medium. Although the acidity variation in molten $KHSO_4$ is small, it undoubtedly has an important influence on the forms of dissolved species.

The authors thank Prof. Dr. B. Trémillon of the Universite Pierre et Marie Curie, Paris, for his helpful suggestions and encouragement.

REFERENCES

1 J. P. Vilaverde, G. Picard, J. Vedel and B. Trémillon, J. Electroanal. Chem., 54 (1974) 279.
2 F. Le Ber, Thèse 3ème Cycle, University of Paris VI, 1963.
3 J. A. Duffy and W. J. D. MacDonald, J. Chem. Soc. A (1970) 2066.
4 J. A. Duffy and W. J. D. MacDonald, J. Chem. Soc. A (1970) 977.
5 H. A. Laitinen and C. H. Liu, J. Am. Chem. Soc., 80 (1958) 1015.
6 D. Inman, J. C. L. Legey and R. Spencer, J. Electroanal. Chem., 61 (1975) 289.
7 F. L. Whiting, G. Mamantov and J. P. Young, J. Inorg. Nucl. Chem., 34 (1972) 2475.
8 C. L. Hussey, L. A. King and J. K. Erbacher, J. Electrochem. Soc.: Electrochem. Sci. Technol., 125 (1978) 561.
9 I. M. Kolthoff and P. J. Elving, Treatise on Analytical Chemistry, Interscience-Wiley, New York, 1963, Part II, Vol. 8.
10 G. Charlot, Chimie Analytique Quantitative, Masson, Paris, 1974.
11 L. G. Sillén, Acta Chem. Scand., 16 (1962) 159.
12 W. E. Demings, Statistical Adjustment of Data, Dover, New York, 1964.

ANALYTICA CHIMICA ACTA, VOL. 192 (1987)

AUTHOR INDEX

Optimization of Chromatographic Selectivity

A Guide to Method Development

by P. Schoenmakers, *Philips Research Laboratories, Eindhoven, The Netherlands*

(Journal of Chromatography Library, 35)

This is the first detailed description of method development in chromatography – the overall process of which may be summarized as: method selection, phase selection, selectivity optimization, and system optimization. All four aspects receive attention in this book.

Chapter 1 gives a short introduction, describes chromatographic theory and nomenclature, and outlines the method development process. Chapter 2 describes guidelines for method selection, and quantitative concepts for characterizing and classifying chromatographic phases. Selective separation methods, from both gas and liquid chromatography are given in Chapter 3; the main parameters of each method are identified and simple, quantitative relations are sought to describe their effects. Criteria by which to judge the quality of separation are discussed in Chapter 4 with clear recommendations for different situations. The specific problems involved in the optimization of chromatographic selectivity are explained in Chapter 5. Optimization procedures, illustrated by examples, are extensively described and compared on the basis of a number of criteria. Suggestions are made both for the application of different procedures and for further research. The optimization of programmed analysis receives special attention in Chapter 6, and the last chapter summarizes the optimization of the chromatographic system, including the optimization of the efficiency, sensitivity and instrumentation.

Those involved in developing chromatographic methods or wishing to improve existing methods will value the detailed, structured way in which the subject is presented. Because optimization procedures and criteria are described as elements of a complete optimization package, the book will help the reader to understand, evaluate and select current and future commercial systems.

1986 362 pages
US $ 93.25 / Dfl. 210.00
ISBN 0-444-42681-7

ELSEVIER SCIENCE PUBLISHERS

P.O. Box 211, 1000 AE Amsterdam, The Netherlands
52 Vanderbilt Avenue, New York, NY 10017, USA

7366A

ELECTROANALYSIS

Theory and Applications in Aqueous and Non-Aqueous Media and in Automated Chemical Control

by **E.A.M.F. DAHMEN,** *Emeritus Professor of Chemical Analysis, Twente University of Technology, Enschede, The Netherlands*

(Techniques and Instrumentation in Analytical Chemistry, 7)

Electroanalysis as a representative of the wet-chemical methods has many attractive advantages, such as: selectivity and sensitivity, notwithstanding its inexpensive equipment; ample choice of possibilities; and direct accessibility, especially to electronic and hence automatic control even at distance; automated data treatment; and simple insertion, if desirable, into a process-regulation loop. There may be circumstances in which an electroanalytical method, as a consequence of the additional chemicals required, has disadvantages in comparison with instrumental techniques of analysis; however the above-mentioned advantages often make electroanalysis the preferred approach for chemical control in industrial and environmental studies.

This book provides the reader with a full understanding of what electroanalysis can do in these fields, by presenting on the one hand a systematic treatment of the subject and its commonly used techniques on a more explanatory basis, and on the other hand by illustrating the practical applications of these techniques in chemical control in industry, health and environment. As such control today requires the increasing introduction of automation and computerization, electroanalysis with its direct input and/or output of electrical signals often has advantages over other techniques especially because recent progress in electronics and computerization have greatly stimulated new developments in the electroanalysis technique themselves.

Part A looks systematically at electro analysis while more attention is paid i Part B to electroanalysis in non-aqueou media in view of its growing importance The subject is rounded off in Part C b some insight into and examples c applications to automated chemic control.

CONTENTS: General Introduction. *Part A Electroanalysis (Systematic Treatment)* **1. Introduction.** Definitions and selecte bibliography. Systematics and standar abbreviations. Electrochemical cells. **2. Non faradaic Methods of Electrochemica Analysis.** Conductometric analysis. Potentio metric analysis. **3. Faradaic Methods o Electrochemical Analysis.** Pragmatic treat ment of the theory of electrolysis. Kineti treatment of the theory of electrolysis Voltammetry. Electrogravimetry. Coulometry *Part B. Electroanalysis in Non-Aqueou Media.* **4. Introduction.** Theory of electro chemistry in non-aqueous media. Practice c electroanalysis in non-aqueous media. *Pa C. Electroanalysis in Automated Chemica Control.* **5. Introduction.** Nature of chemica control. Character and degree of automatio in chemical control. Role of electroanalysi in automated chemical control. Automate electroanalysis in laboratory contro Automated electroanalysis in environmer control. (All chapters include References Appendix. Author Index. Subject Index.

1986 384 pages
US $ 166.75 / Dfl. 375.00
ISBN 0-444-42534-9

ELSEVIER SCIENCE PUBLISHERS

P.O. Box 211,
1000 AE Amsterdam,
The Netherlands

P.O. Box 1663,
Grand Central Station,
New York, NY 10163, U.S.A

tinued from back cover)

CONTENTS

(Abstracted, Indexed in: Anal. Abstr.; Biol. Abstr.; Chem. Abstr.; Curr. Contents Phys. Chem. Earth Sci.; Life Sci.; Index Med.; Mass Spectrom. Bull.; Sci. Citation Index; Excerpta Med.)

(continued on inside back cover)